Advances in Boundary Element Techniques X

Proceedings of the 10th International Conference
Athens, Greece
22-24 July 2009

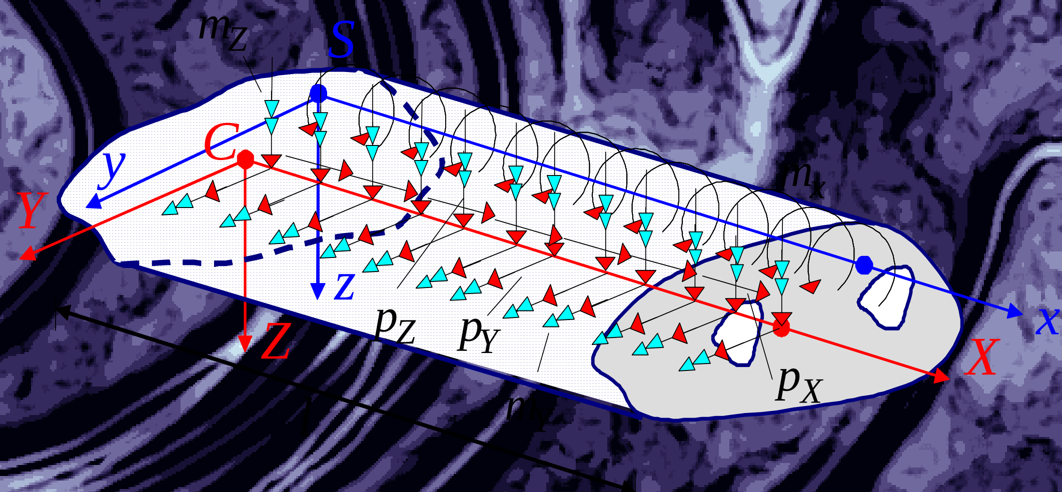

Edited by
E.J.Sapountzakis
M H Aliabadi

ECltd

Advances in Boundary Element Techniques X

ECltd

ISBN 978-0-9547783-6-1
Publish by EC Ltd, United Kingdom

Advances In Boundary Element Techniques X

Edited by

E.J.Sapountzakis
M H Aliabadi

EC ltd

Published by EC, Ltd. , UK

Phone (+44) 2380 260334

ISBN: 978-0-9547783-6-1

International Conference
on
Boundary Element Techniques X
22-24 July 2009, Athens, Greece

Organising Committee:

Assoc. Professor Evangelos J. Sapountzakis, Institute of Structural Analysis and Aseismic Research
School of Civil Engineering
National Technical University of Athens
Zografou Campus Gr-15780
Athens, GREECE

Professor Ferri M.H. Aliabadi
Department of Aeronautics
Imperial College London
South Kensington
London, SW7 2BY, UK

International Scientific Advisory Committee

PREFACE

The Conferences in Boundary Element Techniques are devoted to fostering the continued involvement of the research community in identifying new problem areas, mathematical procedures, innovative applications, and novel solution techniques in both boundary element methods (BEM) and boundary integral equation techniques (BIEM). Previous successful conferences devoted to Boundary Element Techniques were held in London, UK (1999), New Jersey, USA (2001), Beijing, China (2002), Granada, Spain (2003), Lisbon, Portugal (2004), Montreal, Canada (2005), Paris, France (2006), Naples, Italy (2007) and Seville, Spain (2008).

The present volume is a collection of edited papers that were accepted for presentation at the Boundary Element Techniques Conference held at the Amarilia Hotel, Vouliagmeni, Athens, Greece, during 22nd-24th July 2009. Research papers received from 18 counties formed the basis for the Technical Program. The themes considered for the technical program included solid mechanics, fluid mechanics, potential theory, composite materials, fracture mechanics, damage mechanics, contact and wear, optimization, heat transfer, dynamics and vibrations, acoustics and geomechanics. The Keynote Lectures were given by D.E.Beskos and J.T.Katsikadelis.

The Organizers are indebted to the School of Civil Engineering of the National Technical University of Athens, to the Attiko Metro S.A. and to the Greek Club of Imperial College Alumni for their support of the meeting. The organizers would also like to express their appreciation to the International Scientific Advisory Board for their assistance in supporting and promoting the objectives of the meeting and for their assistance in the form of reviews of the submitted papers.

Editors
July 2009

Contents

Boundary element analysis of 2-D and 3-D cracks in gradient elastic solids

G.F. Karlis [1], S.V. Tsinopoulos [2], D. Polyzos[3] and D. E. Beskos[4]

[1] Department of Mechanical and Aeronautical Engineering, University of Patras, GR-26500 Patras, Greece, gkarlis@mech.upatras.gr

[2] Department of Mechanical Engineering, Technological and Educational Institute of Patras, GR-26334, Patras, Greece, stsinop@teipat.gr

[3] Department of Mechanical and Aeronautical Engineering, University of Patras, GR-26500 Patras, Greece

and Institute of Chemical Engineering and High Temperature Chemical Process, GR-26504, Patras, Greece, Polyzos@mech.upatras.gr

[4] Department of Civil Engineering, University of Patras, GR-26500 Patras, Greece, d.e.beskos@upatras.gr

Keywords: boundary element method; gradient elasticity; fracture.

Abstract. A boundary element method based on the simplified version of Mindlin's Form II gradient elastic theory is presented for two- and three-dimensional gradient elastic solids containing cracks. A special crack element is described and employed to both, the 2D and the 3D cases. This element is of variable order of singularity, depending on the field it describes. It is placed near the crack in order to deal with the field singularities occurring at that location. 2D and 3D numerical problems are presented to demonstrate the effect of the microstructure on the stress and displacement distribution near the crack.

Introduction

It is well known that in classical elasticity theory all the fundamental quantities and material constants defined at any point of the analyzed elastic body are taken as mean values over very small volume elements the size of which must be sufficiently large in comparison with the material microstructure. Considering a very simple one dimensional example and taking Taylor expansions for displacements around the point of interest, Exadaktylos and Vardoulakis [1] explain that this assumption is possible only when displacements are constant or vary linearly throughout the aforementioned representative volume elements. In cases where non-linear variations of displacements are observed, higher order Taylor expansion terms and thus higher order gradients of displacements should be taken into account. Making use of higher Taylor terms, however, some new internal length scale constants correlating the microstructure with the macrostructure are introduced in the constitutive equations of the considered elastic continuum [2]. Thus, in fracture mechanics problems where near the tip of the crack abrupt changes of strains and stresses are observed, enhanced elastic theories that take into account higher order gradients of strains and stresses and introduce new internal length scale parameters to describe microstructural effects, should be applied.

Integral Representation of the Problem

Consider a linear gradient elastic body of volume V surrounded by a smooth surface S. The geometry of this body is described with the aid of the unit normal vector $\hat{\mathbf{n}}$ on S and a Cartesian coordinate system with its origin located interior to V. Considering isotropic material the stored potential energy-density has the form [2]

$$W = \tilde{\boldsymbol{\tau}} : \tilde{\mathbf{e}} + \tilde{\boldsymbol{\mu}} \vdots \nabla\tilde{\mathbf{e}} \tag{1}$$

where $\tilde{\boldsymbol{\tau}}$ is the Cauchy stress tensor being dual in energy with the macroscopic strain tensor $\tilde{\mathbf{e}}$, $\tilde{\boldsymbol{\mu}}$ is a third order tensor, called by Mindlin double stress tensor, which is dual to the strain gradient $\nabla\tilde{\mathbf{e}}$, while the two and three dots indicate inner product between tensors of second and third order, respectively. Considering zero body forces, taking the variation of the potential energy-density (1) over V and performing some algebra [4], one obtains the following gradient elastic equation of equilibrium

$$\nabla \cdot \left(\tilde{\boldsymbol{\tau}} - \nabla \cdot \tilde{\boldsymbol{\mu}} \right) = \mathbf{0} \tag{2}$$

accompanied by the classical and non-classical boundary conditions (3) and (4), respectively,

$$\mathbf{p}(\mathbf{x}) = \hat{\mathbf{n}} \cdot \tilde{\boldsymbol{\tau}} - (\hat{\mathbf{n}} \otimes \hat{\mathbf{n}}) : \frac{\partial \tilde{\boldsymbol{\mu}}}{\partial n} - \hat{\mathbf{n}} \cdot (\nabla_S \cdot \tilde{\boldsymbol{\mu}}) - \hat{\mathbf{n}} \cdot [\nabla_S \cdot (\tilde{\boldsymbol{\mu}})^{213}] + (\nabla_S \cdot \hat{\mathbf{n}})(\hat{\mathbf{n}} \otimes \hat{\mathbf{n}}) : \tilde{\boldsymbol{\mu}} - (\nabla_S \hat{\mathbf{n}}) : \tilde{\boldsymbol{\mu}} = \mathbf{p}_0 \quad \text{and/or} \quad \mathbf{u}(\mathbf{x}) = \mathbf{u_0} \tag{3}$$

$$\mathbf{R}(\mathbf{x}) = \hat{\mathbf{n}} \cdot \tilde{\boldsymbol{\mu}} \cdot \hat{\mathbf{n}} = \mathbf{R_0} \text{ and/or } \mathbf{q}(\mathbf{x}) = \frac{\partial \mathbf{u}(\mathbf{x})}{\partial n} = \mathbf{q_0} \tag{4}$$

where **p**, **R** represent the traction and double stresses traction vectors, respectively, **u** stands for displacements, **q** is the normal derivative of displacements, $\mathbf{u_0}$, $\mathbf{p_0}$, $\mathbf{R_0}$, $\mathbf{q_0}$ denote prescribed vectors and the symbols $\otimes$ and ∇_S indicate dyadic product and surface gradient, respectively.

According to [3], strains e_{ij}, double stresses μ_{ijk}, relative stresses s_{ij}, Cauchy stresses τ_{ij} and total stresses σ_{ij} are

$$\tilde{\boldsymbol{\sigma}} = \tilde{\boldsymbol{\tau}} + \tilde{\mathbf{s}}, \quad \tilde{\mathbf{s}} = -\nabla \cdot \tilde{\boldsymbol{\mu}} = -g^2 \nabla^2 \tilde{\boldsymbol{\tau}}, \quad \tilde{\boldsymbol{\mu}} = g^2 \nabla \tilde{\boldsymbol{\tau}} \tag{5}$$

$$\tilde{\boldsymbol{\tau}} = 2\mu \tilde{\mathbf{e}} + \lambda (\nabla \cdot \overline{\mathbf{u}}) \tilde{\mathbf{I}}, \quad \tilde{\mathbf{e}} = \frac{1}{2}[\nabla \mathbf{u} + \mathbf{u} \nabla] \tag{6}$$

where g^2 is the volumetric strain energy gradient coefficient, the only constant that relates the microstructure with the macrostructure and $\tilde{\mathbf{I}}$ is the unit tensor. Adopting the above simple strain gradient theory and inserting the constitutive eqs (5) and (6) into eq.(2) one obtains the equation of equilibrium of a gradient elastic continuum in terms of the displacement field **u**

$$\mu \nabla^2 \mathbf{u} + (\lambda + \mu) \nabla \nabla \cdot \mathbf{u} - g^2 \nabla^2 [\mu \nabla^2 \mathbf{u} + (\lambda + \mu) \nabla \nabla \cdot \mathbf{u}] = \mathbf{0} \tag{7}$$

As it is proved in [3], the integral representation of the above described problem is

$$\tilde{\mathbf{c}}(\mathbf{x}) \cdot \mathbf{u}(\mathbf{x}) + \int_S \left\{ \tilde{\mathbf{p}}^*(\mathbf{x},\mathbf{y}) \cdot \mathbf{u}(\mathbf{y}) - \tilde{\mathbf{u}}^*(\mathbf{x},\mathbf{y}) \cdot \mathbf{p}(\mathbf{y}) \right\} dS_{\mathbf{y}} = \int_S \left\{ \frac{\partial \mathbf{u}^*(\mathbf{x},\mathbf{y})}{\partial n_{\mathbf{y}}} \cdot \mathbf{R}(\mathbf{y}) - \tilde{\mathbf{R}}^*(\mathbf{x},\mathbf{y}) \cdot \mathbf{q}(\mathbf{y}) \right\} dS_{\mathbf{y}} \tag{8}$$

where $\tilde{\mathbf{u}}^*(\mathbf{x},\mathbf{y})$ is the fundamental solution of eq.(7) given in [3], $\tilde{\mathbf{p}}^*(\mathbf{x},\mathbf{y})$, $\tilde{\mathbf{R}}^*(\mathbf{x},\mathbf{y})$ are the fundamental traction and double stress traction tensors taken by inserting the fundamental displacement $\tilde{\mathbf{u}}^*(\mathbf{x},\mathbf{y})$ in relations (3)-(6), respectively and $\tilde{\mathbf{c}}(\mathbf{x})$ is the well-known jump tensor being equal to $1/2\tilde{\mathbf{I}}$ for $\mathbf{x} \in S$ and equal to $\tilde{\mathbf{I}}$ when $\mathbf{x} \in V \cap S$. All the kernels appearing in the integral equation (8) are given explicitly in [3]. Eq(8) contains four unknown fields **u(x)** ,**p(x)**, **R(x)** and **q(x)**. Thus, after the satisfaction of the classical and non-classical boundary conditions, one more equation is required. This equation is obtained by applying operator $\partial/\partial n_{\mathbf{x}}$ on eq(8) and reads

$$\tilde{\mathbf{c}}(\mathbf{x}) \cdot \frac{\partial \mathbf{u}(\mathbf{x})}{\partial n_{\mathbf{x}}} + \int_S \left\{ \frac{\partial \tilde{\mathbf{p}}^*(\mathbf{x},\mathbf{y})}{\partial n_{\mathbf{x}}} \cdot \mathbf{u}(\mathbf{y}) - \frac{\partial \tilde{\mathbf{u}}^*(\mathbf{x},\mathbf{y})}{\partial n_{\mathbf{x}}} \cdot \mathbf{p}(\mathbf{y}) \right\} dS_{\mathbf{y}} = \int_S \left\{ \frac{\partial^2 \tilde{\mathbf{u}}^*(\mathbf{x},\mathbf{y})}{\partial n_{\mathbf{x}} \partial n_{\mathbf{y}}} \cdot \mathbf{R}(\mathbf{y}) - \frac{\partial \tilde{\tilde{\mathbf{R}}}^*(\mathbf{x},\mathbf{y})}{\partial n_{\mathbf{x}}} \cdot \mathbf{q}(\mathbf{y}) \right\} dS_{\mathbf{y}} \tag{9}$$

The kernels of eq.(9) are given in [3]. Eqs (8) and (9) accompanied by the classical and non-classical boundary conditions form the integral representation of a gradient elastic boundary value problem obeying eqs (2)-(6).

Unified 2D and 3D discontinuous elements

Karlis, Tsinopoulos, Polyzos and Beskos [5] proposed a new variable singularity element suitable for representing fields developed near the crack tip of a 2D gradient elastic solid. In the present section a new 3D variable singularity element is proposed and 2D and 3D special elements are presented in a unified manner. According to [6-13], the fields **u**, **q**, **R** and **P** near the crack tip vary as $r^{3/2}, r^{1/2}, r^{-1/2}, r^{-3/2}$ respectively, with r being the distance from the tip. In the present work, adopting the idea of using variable order singularity boundary elements around the tip or the front of the crack for the description of the near tip behavior and the evaluation of the corresponding SIFs as described in [14,15], special variable order of singularity discontinuous line and quadrilateral boundary elements for 2D and 3D analyses, respectively, are proposed.

The crack side of the special elements is always discontinuous, having as main advantage that no functional nodes are located at the crack front and thus, despite the singularity of **R** and **P** there, the field nodal values are finite and can be computed.

2D discontinuous elements of variable-order of singularity

The local coordinates of the functional nodes of the special element are identical to those of a classical, partially or fully discontinuous, 3-noded, quadratic line element. The tip of the crack can be located either at $\xi = -1$ or at $\xi =$

1 for the special element being to the left or right of the tip. In order to unify these two possible cases a new variable p is introduced via the linear transformation

$$p = (1 + c\xi)/2 \tag{10}$$

with $c = \pm 1$ for the tip located at $\xi = \mp 1$, respectively. Thus, the tip of the crack is always located at $p=0$ and the interval $\xi \in [-1,1]$ is transformed into the interval $p \in [0,1]$.

After the transformation, the tip of the crack is located at $p=0$. Consider a point $\boldsymbol{x}(p)$ on the element and a point $y(0)$ located at the crack tip. The fields of interest $\mathbf{F}$ at the point $\mathbf{x}$, can be expressed in terms of the asymptotic solutions as

$$\mathbf{F} = \mathbf{K}r^{\lambda_1} + \mathbf{L}r^{\lambda_2} + \mathbf{C} \tag{11}$$

where $\mathbf{K}$, $\mathbf{L}$ and $\mathbf{C}$ are constant vectors to be determined. Vector $\mathbf{F}$ could represent $\mathbf{u}$, $\mathbf{q}$, $\mathbf{R}$ or $\mathbf{P}$ and λ_1 and λ_2 take the values displayed in Tab.1. Considering that interpolation functions N^i exist, field $\mathbf{F}$ can be approximated as

$$\mathbf{F} = N^i \mathbf{F}^i, \quad i = 1,2,3 \tag{12}$$

with $\mathbf{F}^i$ being the three nodal values of $\mathbf{F}$. In view of eq (11), N^i should have the form

$$N^i(r, p, \lambda_1, \lambda_2) = b^i r^{\lambda_1} + b^i r^{\lambda_2} + z^i \tag{13}$$

where $r = \left| x^j(p) - y(0) \right|$ is the distance of the functional node j from the crack tip, as illustrated in Fig. 1, while the vectors $\mathbf{K}$, $\mathbf{L}$, $\mathbf{C}$ of eq (11) are given by

$$\mathbf{K} = a^i \mathbf{F}^i, \quad \mathbf{L} = b^i \mathbf{F}^i, \quad \mathbf{C} = z^i \mathbf{F}^i \tag{14}$$

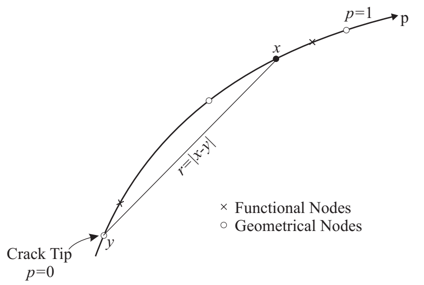

Figure 1 : A 2D, discontinuous, variable order of singularity element

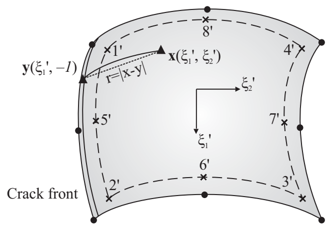

Figure 2 : Projection of point x to the crack front

The constants a^i, b^i, z^i can be obtained by solving three linear systems, of three equations each, arising from the requirement that each interpolation function must satisfy the relations

$$N^i(p \text{ corresponding to node } j) = \delta_{ij} \qquad i, j = 1,2,3 \tag{15}$$

It can be verified that $\sum N^i = 1$ for all the combinations of λ_1, λ_2 provided in Table 1.

3D discontinuous elements of variable-order of singularity

As in 2D, near the crack front, the fields $\mathbf{u}$, $\mathbf{q}$, $\mathbf{R}$ and $\mathbf{P}$ vary as $r^{3/2}$, $r^{1/2}$, $r^{-1/2}$ and $r^{-3/2}$ respectively, with r the distance from the crack front. Once more, adopting the idea of using variable-order continuous elements ([14,15]), a new discontinuous, quadrilateral, eight-nodded element with variable-order singularity is proposed for treating the fields around the crack front.

The local coordinates of the functional nodes are identical to those of a classical, partially or fully discontinuous, eight-noded, quadratic, quadrilateral element. In order to be able to deal with all the possible cases of the crack front location, the local numbering of the element nodes is changed, so that the crack front always resides on the first side of the element. The result of the local renumbering is described in Table 2 for all the possible cases. Consider a point $\mathbf{x}(\xi'_1, \xi'_2)$ on the element and a point $\mathbf{y}(\xi'_1, -1)$ located at the crack front having the same ξ_1-coordinate as $\mathbf{x}$, as shown in Fig. 2. The field of interest $\mathbf{F}$ at the point $\mathbf{x}$, can be expressed in terms of the asymptotic solutions as

$$\mathbf{F}(\xi'_1, r) = \mathbf{K}(\xi'_1) r^{\lambda_1} + \mathbf{L}(\xi'_1) r^{\lambda_2} + \mathbf{C}(\xi'_1) \tag{16}$$

where r is the distance $r = |\mathbf{x} - \mathbf{y}|$, the symbol $\mathbf{F}$ represents $\mathbf{u}$, $\mathbf{q}$, $\mathbf{R}$ and $\mathbf{P}$ and λ_1, λ_2 take the values from Table 1. In addition, the fields $\mathbf{F}$ can be approximated using the interpolation functions N^i and their corresponding nodal values $\mathbf{F}^i$ as follows:

$$\mathbf{F}\left(\xi'_1, r\right) = N^i\left(\xi'_1, r\right)\mathbf{F}^i,\ i = 1,\ldots 8 \tag{17}$$

Combining Eqs (16) and (17) and assuming a quadratic behavior for the functions $\mathbf{K}\left(\xi'_1\right)$, $\mathbf{L}\left(\xi'_1\right)$ and $\mathbf{C}\left(\xi'_1\right)$, the interpolation functions N^i should be of the form

$$N^i\left(\xi'_1, r\right) = \left(e_1^i + e_2^i \xi'_1 + e_3^i \xi'^2_1\right) r^{\lambda_1} + \left(e_4^i + e_5^i \xi'_1 + e_6^i \xi'^2_1\right) r^{\lambda_2} + e_7^i + e_8^i \xi'_1 + e_9^i \xi'^2_1 \tag{18}$$

where e_j^i, (j=1,…9) are constants to be determined. Since eight-noded elements are used, one of the nine terms of the above expression must be omitted. Here, having in mind that the coefficients of r^{λ_1} and r^{λ_2} will be used for the SIF calculation, this term is taken to be e_9^i. The remaining eight constants can be easily obtained by solving a set of eight linear systems, of eight equations each, which come from the delta property of the interpolation functions

$$N^i\left(\xi'^j_1, r^j\right) = \delta_{ij},\ i, j = 1,\ldots 8 \tag{19}$$

Where δ_{ij} is the Kronecker delta, $r^j = \left|\mathbf{x}\left(\xi'^j_1, \xi'^j_2\right) - y\left(\xi'^j_1, -1\right)\right|$ and $\left(\xi'^j_1, \xi'^j_2\right)$ are the local coordinates of the j functional node. It can be verified that $\sum N^i = 1$ for all the combination of λ_1, λ_2 provided in Table 2.

BEM Procedure and SIF Calculation

The goal of the BEM is to solve numerically the well-posed boundary value problem constituted by the system of two integral equations (8) and (9) and the boundary conditions (3) and (4). To this end the global boundary S is discretized into eight-nodded, quadratic, quadrilateral, continuous and discontinuous isoparametric boundary elements in the 3D case and into three noded quadratic line continuous and discontinuous isoparametric elements, while special variable-order singularity, discontinuous elements are placed around the crack front (or crack tip in 2D). Then, the integral eqs (8) and (9) for a node k are written as

$$\begin{aligned} &\frac{1}{2}\mathbf{u}^k + \sum_{\beta=1}^{M}\tilde{\mathbf{H}}_\beta^k \cdot \mathbf{u}^\beta + \sum_{\beta=1}^{M}\tilde{\mathbf{K}}_\beta^k \cdot \mathbf{q}^\beta = \sum_{\beta=1}^{M}\tilde{\mathbf{G}}_\beta^k \cdot \mathbf{p}^\beta + \sum_{\beta=1}^{M}\tilde{\mathbf{L}}_\beta^k \cdot \mathbf{R}^\beta \\ &\frac{1}{2}\mathbf{q}^k + \sum_{\beta=1}^{M}\tilde{\mathbf{S}}_\beta^k \cdot \mathbf{u}^\beta + \sum_{\beta=1}^{M}\tilde{\mathbf{T}}_\beta^k \cdot \mathbf{q}^\beta = \sum_{\beta=1}^{M}\tilde{\mathbf{V}}_\beta^k \cdot \mathbf{p}^\beta + \sum_{\beta=1}^{M}\tilde{\mathbf{W}}_\beta^k \cdot \mathbf{R}^\beta \end{aligned} \tag{20}$$

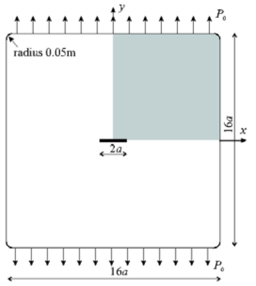

Figure 3 : Gradient elastic plate with a horizontal line crack

F	λ_1	λ_2
U	3/2	1
Q	1/2	1
R	-1/2	1
P	-3/2	-1/2

Table 1: Orders of magnitude of the asymptotic fields

Nodes	Crack on:			
	Side 1	Side 2	Side 3	Side 4
1′	1	2	3	4
2′	2	3	4	1
3′	3	4	1	2
4′	4	1	2	3
5′	5	6	7	8
6′	6	7	8	5
7′	7	8	5	6
8′	8	5	6	7
Coord. ξ'_1	ξ_1	ξ_2	$-\xi_1$	$-\xi_2$
Coord. ξ'_2	ξ_2	$-\xi_1$	$-\xi_2$	ξ_1

Table 2: The renumbering of the element nodes, so that the crack front always resides on the first side

where M is the total number of nodes. Explicit expressions for $\tilde{\mathbf{H}}_\beta^k, \tilde{\mathbf{K}}_\beta^k, \tilde{\mathbf{G}}_\beta^k, \tilde{\mathbf{L}}_\beta^k, \tilde{\mathbf{S}}_\beta^k, \tilde{\mathbf{T}}_\beta^k, \tilde{\mathbf{V}}_\beta^k$ and $\tilde{\mathbf{W}}_\beta^k$ are given in [4]. Collocating eqs (20) at all nodal points M and applying the boundary conditions (eqs (3),(4)) one produces the final linear system of the form $\tilde{\mathbf{A}} \cdot \mathbf{X} = \mathbf{B}$, with **X**, **B** containing all the unknown and known nodal components of the boundary fields, respectively. The singular and hypersingular integrals involved, are evaluated applying a methodology for direct treatment of CPV and hypersingular integrals [4], noting that an extra singularity due to the singular behaviour of the interpolation functions (12) near the front of the crack should be taken into account. Finally, the linear system is solved via a typical LU-decomposition.

Approaching the crack tip or front ($r \to 0$) the traction **p**, according to eq.(11) for the 2D case and eq.(16) for the 3D case, admits a representation of the form:

$$\mathbf{p} = \left[\mathbf{K}_1\left(\mathbf{p}_1,\ldots,\mathbf{p}_8\right)/\sqrt{2\pi}\right]\lim_{r\to 0} r^{-3/2} + \left[\mathbf{K}_2\left(\mathbf{p}_1,\ldots,\mathbf{p}_8\right)/\sqrt{2\pi}\right]\lim_{r\to 0} r^{-1/2} + \mathbf{C}\left(\mathbf{p}_1,\ldots,\mathbf{p}_N\right) \tag{21}$$

where $\left(\mathbf{p}_1,...,\mathbf{p}_8\right)$ are the tractions of the functional nodes and the components of the vectors $\mathbf{K_1}$ and $\mathbf{K_2}$ stand for the SIFs corresponding to *x*, *y* and *z* directions according to the following relations:

$$\mathbf{K}_1\left(\xi_1\right)=\sqrt{2\pi}\mathbf{K}=\sqrt{2\pi}a^j\mathbf{P}_j,\quad \mathbf{K}_2\left(\xi_1\right)=\sqrt{2\pi}\mathbf{L}=\sqrt{2\pi}b^j\mathbf{P}_j \tag{22}$$

and

$$\mathbf{K}_1\left(\xi_1\right)=\sqrt{2\pi}\left(\mathbf{D}_1+\xi_1\mathbf{D}_2+\xi_1^2\mathbf{D}_3\right),\quad \mathbf{K}_2\left(\xi_1\right)=\sqrt{2\pi}\left(\mathbf{D}_4+\xi_1\mathbf{D}_5+\xi_1^2\mathbf{D}_6\right) \tag{23}$$

with $j=1,..3$ for 2D, $\mathbf{D}_i=e_i^j\mathbf{P}_j, i=1,..6$ and $j=1,..8$ for 3D and a^j, b^j, e_i^j obtained by solving the systems (15), (19).

Mode-I Crack Problem

Two mode-I fracture problems are studied in this section. The first deals with a 2D crack, while the second concerns a rectangular 3D crack both subjected to a tensile loading. The obtained crack profiles as well as the corresponding SIFs are presented and compared against those of classical elasticity.

2D Mode-I crack problem

Consider a square gradient elastic plate with rounded corners of small radius of curvature (in order to have a smooth boundary) in a state of plane stress. The plate contains a central horizontal line crack and is subjected to a uniform tensile traction P_0 =100MPa normal to its top and bottom sides (Fig.3). The crack length is chosen to be equal to 2a = 1m and the side of the square plate is L = 16a. The Young modulus and the Poisson ratio of the gradient elastic plate are E =210GPa and ν = 0.2, respectively. Due to the problem symmetries, only one quarter of the plate is discretized, with the following boundary conditions along the axes of symmetry: P(0,y) = 0 and R(0,y) = 0 for $0 \le y < a$, $u_y(0,y) = 0$ and R(0,y) = 0 for $a \le y \le L/2$ and $u_x(x,0)=0$ and R(x,0)=0 for $0 \le x \le L/2$.
Fig. 4 displays the crack opening displacement obtained by the present BEM for four different values of the gradient coefficient g. In the same figure, the crack profile of the classical elasticity theory (g = 0) is also shown. The crack profile in the gradient elastic case remains sharp at the crack tip and is not blunted as in the classical case. This cusp type of profile is identical to the one coming out of Barenblatt's [18] cohesive zone theory. Also,

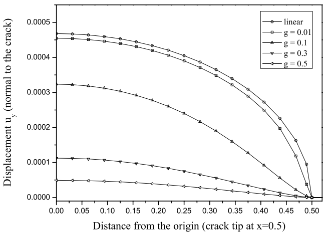

Figure 4 : Upper right quarter of the COD profile

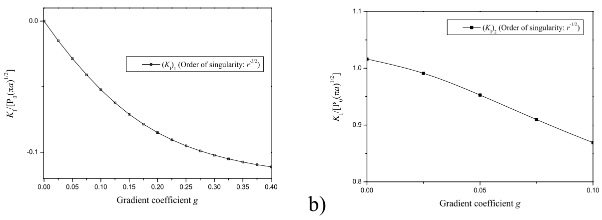

a) b)

Figure 5 : a) SIF $(K_I)_1$ and b) $(K_I)_2$ as function of the gradient coefficient *g*

it should be noticed that as the gradient coefficient g increases, the crack becomes stiffer. In Figs 5 (a) and (b) the two mode-I SIFs for the gradient elastic case, $(K_I)_1$ and $(K_I)_2$, are plotted versus the gradient coefficient g. The interesting remark here is that the SIF $(K_I)_1$ tends to zero as the gradient coefficient g tends to zero. As a result, eq(21) becomes $P_y=\left(K_I\right)_2\Big/\sqrt{2\pi}\lim\limits_{r\to 0}r^{-1/2}$,with $(K_I)_2$ being the mode-I SIF as defined in classical elasticity theory. Moreover, Fig. 5(b) shows the behavior of the SIF corresponding to $r^{-1/2}$ traction term as a function of the gradient coefficient g. It should be noted that for $g \ge 0.1$ the contribution of this term is much smaller than that of the term corresponding to $r^{-3/2}$. For small g it is apparent from Fig. 5(b) that as g approaches zero, $(K_I)_2$ becomes dominant and goes to the classical elastic case. However, the most important observation is that the SIF $(K_I)_1$ takes only negative values. This means that in gradient elasticity the stresses near the tip not only go to infinity with a different order ($r^{-3/2}$) than those of classical elasticity ($r^{-1/2}$), but are also compressive and not tensile. This explains the different shapes of the crack profile in gradient and classical elasticity theories, as shown in Fig. 4.

3D Mode-I crack problem

Consider a gradient elastic cube with rounded corners of small radius of curvature. The cube contains a horizontal

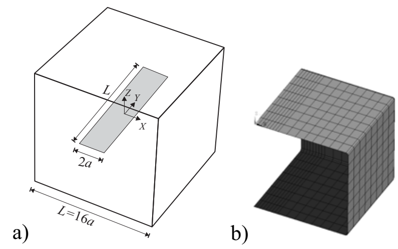

Figure 6 : a) The gradient elastic cube with a central horizontal rectangular crack b) the discretized domain

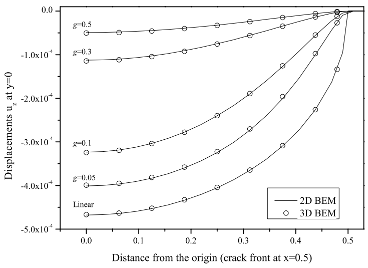

Figure 7 : Shape of mode-I crack for different values ofthe gradient coefficient g

rectangular crack and is subjected to a uniform tensile traction P_0 = 100MPa applied normal to its top and bottom sides (Fig. 6(a)). The material characteristics are the same as before. Due to the octant symmetry of the problem, the analysis is performed by taking into account two Cartesian symmetries with respect to the XZ and YZ planes, while on the XY symmetry plane the following boundary conditions are considered: P(x,y) = 0 and R(x,y)=0 for $0 \le x < a$ and $0 \le y < L/2$ and $u_z(x,y)=0$ and R(x,y)=0 for $a \le x \le L/2$ and $a \le y \le L/2$. The mesh used is shown in Fig. 6(b). Fig.7 displays the lower right of the crack opening displacement profile, at y = 0, obtained by the present 3D BEM for four different values of the gradient coefficient g, as well as the profile corresponding to the classical elastic case (g = 0). The profiles are compared to the 2D ones of Fig. 4 and found to be the same as expected.

References

[1] Exadaktylos, G., Vardoulakis, I., “Microstructure in linear elasticity and scale effects: a reconsideration of basic rock mechanics and rock fracture mechanics”, Technophysics 335, pp. 81- 109 (2001).

[2] Mindlin, R. D.: “Microstructure in linear elasticity”, Arch. Rat. Mech. Anal., Vol. 10, pp. 51-78 (1964).

[3] Polyzos D., Tsepoura K. G., Tsinopoulos S. V. and Beskos D. E., “A Boundary Element Method for solving 2-D and 3-D Static Gradient Elastic problems. Part I: Integral Formulation”, Comp. Meth. Appl. Mech. Engng., Vol. 192, Issue 26-27, pp. 2845-2873 (2003).

[4] Tsepoura K. G., Tsinopoulos S. V., Polyzos D. and Beskos D. E., “A Boundary Element Method for solving 2-D and 3-D Static Gradient Elastic problems. Part II: Numerical Implementation”, Comp. Meth. Appl. Mech. Engng., Vol. 192, Issue 26-27, pp. 2875-2907 (2003).

[5] G.F. Karlis, S.V. Tsinopoulos, D. Polyzos and D.E. Beskos, “Boundary element analysis of mode I and mixed mode (I and II) crack problems of 2-D gradient elasticity”, Comp. Meth. Appl. Mech. Engng., Vol. 196, pp. 5092-5103, 2007.

[6] I. Vardoulakis, G. E. Exadaktylos, E. D. Aifantis, “Gradient elasticity with surface energy: mode-III crack problem”, Int. J. Solids Struct., Vol. 33, pp.4531–4559, 1996.

[7] G. E. Exadaktylos, I. Vardoulakis, E. Aifantis, “Cracks in gradient elastic bodies with surface energy”, Int. J. Fract., Vol. 79, pp. 107–119, 1996.

[8] I. Vardoulakis, G. Exadaktylos, “The asymptotic solution of anisotropic gradient elasticity with surface energy for mode-II crack”. D. Durban (Ed.), Nonlinear Singularities in Deformation and Flow, Kluwer Academic Publishers, Dordrecht, pp. 87–98, 1997.

[9] G. E. Exadaktylos, “Gradient elasticity with surface energy: mode-I crack problem”, Int. J. Solids Struct., Vol. 35, pp. 421–456, 1998.

[10] L. Zhang, Y. Huang, J.Y. Chen, K.C. Hwang, “The mode III full-field solutions in elastic materials with strain gradient effects”, Int. J. Fracture, Vol. 92, pp. 325–348, 1998.

[11] M. X. Shi, Y. Huang, K.C. Hwang, “Fracture in a higher-order elastic continuum”, J. Mech. Phys. Solids, Vol. 48, pp. 2513–2538, 2000.

[12] A.C. Fannjiang, Y. S. Chan, G.H. Paulino, “Strain gradient elasticity for antiplane shear cracks: a hypersingular integrodifferential equation approach”, SIAM J. Appl. Math., Vol. 62, pp. 1066–1091, 2002.

[13] H.G. Georgiadis, “The mode III crack problem in microstructured solids governed by dipolar gradient elasticity: static and dynamic analysis”, J. Appl. Mech. ASME, Vol. 70, pp. 517–530, 2003.

[14] K.M. Lim, K.H. Lee, A.A.O. Tay, W. Zhou, “A new variable-order singular boundary element for two-dimensional stress analysis”, Int. J. Numer. Meth. Engng., Vol. 55, pp. 293–316, 2002.

[15] W. Zhou, K.M. Lim, K.H. Lee, A.A.O. Tay, “A new variable-order singular boundary element for calculating stress intensity factors in three-dimensional elasticity problems”, Int. J. Solids & Structures;42:159-185 (2005)

[16] G.I. Barenblatt,“Mathematical theory of equilibrium cracks in brittle fracture”,Adv.Appl.Mech.,Vol. 7, pp.55–129, 1962.

Nonlinear Vibrations of Viscoelastic Membranes of Fractional Derivative Type

John T. Katsikadelis

School of Civil Engineering, National Technical University of Athens

Athens, GR-15773, Greece, jkats@central.ntua.gr

Keywords: viscoelastic membranes, fractional derivatives, nonlinear vibrations, large deflections, analog equation method, boundary elements, non linear fractional differential equations

Abstract. The nonlinear dynamic response of viscoelastic membranes is investigated. The employed viscoelastic material is described with fractional order derivatives. The governing equations are derived by considering the equilibrium of the undeformed membrane element. They are three coupled second order nonlinear hyperbolic fractional partial differential equations in terms of the displacement components. Using the AEM, these equations are transformed into a system of three-term ordinary fractional differential equations (FDEs), which are solved using the numerical method for the solution of FDEs developed recently by Katsikadelis. A membrane of arbitrary shape is studied to illustrate the proposed method and demonstrate the efficiency of the solution procedure. The presented method provides a computational tool to analyze viscoelastic membranes enabling thus the investigator to have a better insight into this complicated but very interesting response of membrane structures.

Introduction

Membranes made of linear viscoelastic materials are extensively used in structural membranes in modern engineering applications. These materials exhibit both viscous and elastic behavior and various models have been proposed in order to describe the mechanical behavior of such materials (e.g. Maxwell, Voigt, Kelvin, Zener). Recently, many researchers have shown that viscoelastic models with fractional derivatives are in better agreement with the experimental results than the integer derivative models [1,2].

The dynamic response of viscoelastic membranes using integer order derivative models have been examined by many investigators. However, viscoelastic membranes of fractional type derivative have not been analyzed. The reason is that the response of such membrane is described by a system of nonlinear fractional partial differential equations, for which no analytical or numerical methods have been developed as yet. There are only some analytical methods for the analysis of linear response of viscoelastic beams.

Without excluding other models the employed herein viscoelastic material is described by the Voigt type model with fractional order derivative

$$\begin{Bmatrix} \sigma_x \\ \sigma_y \\ \tau_{xy} \end{Bmatrix} = \frac{E}{1-\nu^2} \begin{bmatrix} 1 & \nu & 0 \\ \nu & 1 & 0 \\ 0 & 0 & \dfrac{1-\nu}{2} \end{bmatrix} \begin{Bmatrix} \varepsilon_x + \eta D_c^a \varepsilon_x \\ \varepsilon_y + \eta D_c^a \varepsilon_y \\ \gamma_{xy} + \eta D_c^a \gamma_{xy} \end{Bmatrix} \tag{1}$$

where E, ν are the elastic material constants, η the viscoelastic parameter and D_c^a the Caputo fractional derivative of order α defined as

$$D_c^\alpha u(t) = \begin{cases} \left[\dfrac{1}{\Gamma(m-\alpha)} \displaystyle\int_0^t \dfrac{u^{(m)}(\tau)}{(t-\tau)^{\alpha+1-m}} d\tau \right], & m-1 < \alpha < m \\ \dfrac{d^m}{dt^m} u(t) & m = \alpha \end{cases} \tag{2}$$

where m is a positive integer. The advantage of this definition is that it permits the assignment of initial conditions which have direct physical significance [3]. Apparently, the classical derivatives result for integer values of α. An advantage of this two parameter viscoelastic model is that it can described more complicated models for appropriate values of the two parameters, namely α and η [4], besides the simplicity to formulate the equations of structural viscoelastic systems.

Problem Statement and Governing Equations

We consider a thin flexible initial flat [5] membrane of thickness h and mass density ρ consisting of homogeneous linearly viscoelastic material occupying the two-dimensional, in general multiply connected, domain Ω in x, y plane. The membrane is prestressed either by imposed displacement $\bar{u}_n, \bar{v}_t$ or by external forces N_n^*, N_t^* acting along the boundary Γ. Moderate large deflections result from nonlinear kinematic relations, which retain the square of the slopes of the deflection surface, while, the strain components remain still small compared with the unity. This theory is good for considerably large deflections with the exception in the vicinity of the boundary where the stress resultants of the finite deformation of membrane should be considered to satisfy the equilibrium and explain the folding near the edge. Thus, the strain components are given as [6]

$$\varepsilon_x = u,_x + \frac{1}{2} w,_x^2 \qquad \varepsilon_y = v,_y + \frac{1}{2} w,_y^2 \qquad \gamma_{xy} = u,_y + v,_x + w,_x w,_y \tag{3a,b,c}$$

where $u = u(x, y, t)$, $v = v(x, y, t)$ are the inplane displacement components and $w = w(x, y, t)$ the transverse displacement. The membrane is subjected to the transverse load $p_z = p_z(x, y, t)$ and the inplane loads $p_x = p_x(x, y, t)$ and $p_y = p_y(x, y, t)$.

On the basis of Eqs (1) and (3) the stress resultants are written as

$$\bar{N}_x = N_x + \eta D_c^\alpha N_x \qquad \bar{N}_y = N_y + \eta D_c^\alpha N_y \qquad \bar{N}_{xy} = N_{xy} + \eta D_c^\alpha N_{xy} \tag{4a,b,c}$$

where

$$N_x = C[u,_x + \nu v,_y + \frac{1}{2}(w,_x^2 + \nu w,_y^2) \tag{5a}$$

$$N_y = C[\nu u,_x + v,_y + \frac{1}{2}(\nu w,_x^2 + w,_y^2)] \tag{5b}$$

$$N_{xy} = C\frac{1-\nu}{2}(u,_y + v,_x + w,_x w,_y) \tag{5c}$$

with $C = Eh/(1-\nu^2)$ being the membrane stiffness.

The governing equations result by taking the equilibrium of the membrane element in the undeformed configuration. This yields

$$\bar{N}_x,_x + \bar{N}_{xy},_y - \rho h \ddot{u} = -p_x \tag{6a}$$

$$\bar{N}_{xy},_x + \bar{N}_y,_y - \rho h \ddot{v} = -p_y \tag{6b}$$

$$\bar{N}_x w,_{xx} + 2\bar{N}_{xy} w,_{xy} + \bar{N}_y w,_{yy} - p_x w,_x - p_y w,_y - \rho h \ddot{w} + \rho h \ddot{u} w,_x + \rho h \ddot{v} w,_y = -p_z \tag{6c}$$

Without restricting the generality, we consider displacement boundary conditions on Γ

$$u_n = \bar{u}_n, \qquad u_t = \bar{u}_t, \qquad w = \bar{w} \tag{7a,b,c}$$

Using Eqs (4) in Eqs (6) we obtain the membrane equations in terms of the displacements in Ω

$$\begin{aligned} &C\{[u,_x + \nu v,_y + \frac{1}{2}(w,_x^2 + \nu w,_y^2) + \eta D_c^\alpha [u,_x + \nu v,_y + \frac{1}{2}(w,_x^2 + \nu w,_y^2)\},_x \\ &C\frac{1-\nu}{2}\{(u,_y + v,_x + w,_x w,_y) + \eta D_c^\alpha (u,_y + v,_x + w,_x w,_y)\},_y - \rho h \ddot{u} = -p_x \end{aligned} \tag{8a}$$

$$\begin{aligned} &C\frac{1-\nu}{2}\{(u,_y + v,_x + w,_x w,_y) + \eta D_c^\alpha (u,_y + v,_x + w,_x w,_y)\},_x \\ &C\{[\nu u,_x + v,_y + \frac{1}{2}(\nu w,_x^2 + w,_y^2)] + \eta D_c^\alpha [\nu u,_x + v,_y + \frac{1}{2}(\nu w,_x^2 + w,_y^2)]\},_y - \rho h \ddot{v} = -p_y \end{aligned} \tag{8b}$$

$$\begin{aligned} &C\{[u_{,x}+\nu v_{,y}+\frac{1}{2}(w_{,x}^2+\nu w_{,y}^2)+\eta D_c^\alpha[u_{,x}+\nu v_{,y}+\frac{1}{2}(w_{,x}^2+\nu w_{,y}^2)\}w_{,xx} \\ &+C(1-\nu)\{(u_{,y}+v_{,x}+w_{,x}w_{,y})+\eta D_c^\alpha(u_{,y}+v_{,x}+w_{,x}w_{,y})\}w_{,xy} \\ &+C\{[\nu u_{,x}+v_{,y}+\frac{1}{2}(\nu w_{,x}^2+w_{,y}^2)]+\eta D_c^\alpha[\nu u_{,x}+v_{,y}+\frac{1}{2}(\nu w_{,x}^2+w_{,y}^2)]\}w_{,yy} \\ &-p_x w_{,x}-p_y w_{,y}-\rho h\ddot{w}+\rho h\ddot{u}w_{,x}+\rho h\ddot{v}w_{,y}=-p_z \end{aligned} \tag{8c}$$

Equations (8) are subjected to the boundary conditions (7) and initial conditions

$$u(x,y,0)=f_1(x,y)\,,\quad \dot{u}(x,y,0)=g_1(x,y) \tag{9a}$$

$$v(x,y,0)=f_2(x,y)\,,\quad \dot{v}(x,y,0)=g_2(x,y) \tag{9b}$$

$$w(x,y,0)=f_3(x,y)\,,\quad \dot{w}(x,y,0)=g_3(x,y) \tag{9c}$$

Obviously, the equation for the elastic membrane result for $\eta=0$ [7].

Equations (8) constitute a system of three coupled nonlinear fractional partial equations of hyperbolic type that are solved using the AEM as presented in the following sections.

The AEM Solution

Since Eqs (8) are of the second order with regard to the spatial derivatives, the analog equations will be

$$\nabla^2 u=b_1(\mathbf{x},t)\qquad \nabla^2 v=b_2(\mathbf{x},t)\qquad \nabla^2 w=b_3(\mathbf{x},t)\,,\qquad \mathbf{x}:\{x,y\}\in\Omega \tag{10a,b,c)}$$

where $b_i(\mathbf{x},t)$, $i=1,2,3$ represent in the first instance unknown time dependent fictitious sources. The solution of Eq. (10a) is given in integral form [8].

$$\varepsilon u(\mathbf{x},t)=\int_\Omega u^* b\,d\Omega-\int_\Gamma (u^* q-q^* u)ds \qquad \mathbf{x}\in\Omega\cup\Gamma \tag{11}$$

in which $q=u_{,n}$; $u^*=\ell nr/2\pi$ is the fundamental solution of Eq. (9a) and $q^*=u^*_{,n}$ its derivative normal to the boundary with $r=\|\boldsymbol{\xi}-\mathbf{x}\|$, $\mathbf{x}\in\Omega\cup\Gamma$ and $\boldsymbol{\xi}\in\Gamma$; ε is the free term coefficient ($\varepsilon=1$ if $\mathbf{x}\in\Omega$, $\varepsilon=a/2\pi$ if $\mathbf{x}\in\Gamma$ and $\varepsilon=0$ if $\mathbf{x}\notin\Omega\cup\Gamma$; a is the interior angle between the tangents of boundary at point $\mathbf{x}$; $\varepsilon=1/2$ for points where the boundary is smooth). Eq. (11) is solved numerically using the BEM. The boundary integrals are approximated using N constant boundary elements, whereas the domain integrals are approximated using M linear triangular elements. The domain discretization is performed automatically using the Delaunay triangulation. Since the fictitious source is not defined on the boundary, the nodal points of the triangles adjacent to the boundary are placed on their sides (Fig 1). Thus, after discretization and application of the boundary integral Eq. (11) at the N boundary nodal points we obtain

$$\mathbf{Hu}=\mathbf{Gq}+\mathbf{Ab}^{(1)} \tag{12}$$

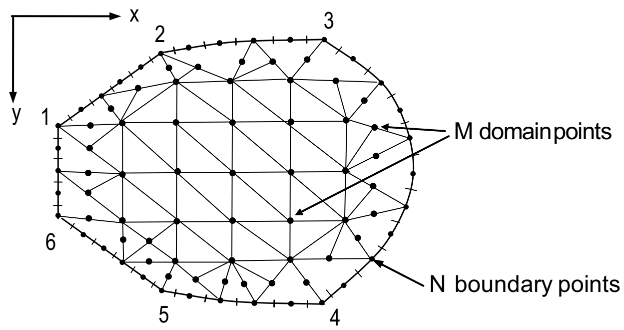

Figure 1. Boundary and domain discretization.

where $\mathbf{H}, \mathbf{G}$ are $N \times N$ known coefficient matrices originating from the integration of the kernel functions on the boundary elements and $\mathbf{A}$: is an $N \times M$ coefficient matrix originating from the integration of the kernel function on the domain elements; $\mathbf{u}, \mathbf{u}_n$ are the vectors of the nodal displacements and slopes and $\mathbf{b}^{(1)}$ the nodal values of the fictitious source at the M domain nodal points. Further application of Eq. (11) at the domain nodal points and use of Eq. (12) combined with the boundary conditions to eliminate the boundary quantities, we can express $\mathbf{u}$ and its derivatives at the domain nodal points in terms of the fictitious source

$$\mathbf{u}_{,pq}(t) = \mathbf{S}_{,pq}\, \mathbf{b}^{(1)}(t) + \mathbf{s}^{(1)}{}_{,pq}\,, \qquad p,q = 0,x,y \tag{13a}$$

Similarly, we obtain

$$\mathbf{v}_{,pq}(t) = \mathbf{S}_{,pq}\, \mathbf{b}^{(2)}(t) + \mathbf{s}^{(2)}{}_{,pq}\,, \qquad p,q = 0,x,y \tag{13b}$$

$$\mathbf{w}_{,pq}(t) = \mathbf{S}_{,pq}\, \mathbf{b}^{(3)}(t) + \mathbf{s}^{(3)}{}_{,pq}\,, \qquad p,q = 0,x,y \tag{13c}$$

For homogeneous boundary conditions we have $\mathbf{s}^{(i)}{}_{,pq} = 0$. Applying now Eqs (8) at the M domain nodal points and substituting the involved derivatives from Eqs (13) we obtain

$$\mathbf{F}_k(\ddot{\mathbf{b}}^{(i)}, D_c^{\alpha}\mathbf{b}^{(i)}, \mathbf{b}^{(i)}) = -\{p_x \quad p_y \quad p_z\}^T, \qquad i = 1,2,3 \ \text{ and } \ k = 1,2,\ldots,3M \tag{14}$$

where the functions F_k depend nonlinearly on the elements of the vector arguments. The initial conditions (9) for $\mathbf{b}^{(i)}$ become

$$\mathbf{b}^{(i)}(0) = \mathbf{S}^{-1}\mathbf{f}_i\,, \qquad \dot{\mathbf{b}}^{(i)}(0) = \mathbf{S}^{-1}\mathbf{g}_i \tag{15}$$

Equations (14) constitute a system of $3M$ three-term nonlinear FDEs, which are solved using the time step numerical procedure developed by Katsikadelis [9] and is presented below. The use however, of all the degrees of freedom may be computationally costly and in some cases inefficient due to the large number of coefficients $b_k^{(i)}(t)$. To overcome this difficulty in this investigation, the number of degrees of freedom is reduced using the Ritz transformation, namely

$$\mathbf{b}^{(i)} = \Psi^{(i)}\mathbf{z}^{(i)} \tag{16}$$

where $z_k^{(i)}(t)$, ($k = 1,..,L < M$) are new time dependent parameters and $\Psi^{(i)}$ are $M \times L$ transformation matrices. In this investigation the eigenmodes of the linear problem are selected as Ritz vectors [10].

Numerical Solution of the of the Nonlinear FDEs

We consider the system of the K nonlinear three-term FDEs

$$\mathbf{F}(D_c^{\beta}\mathbf{u}, D_c^{\alpha}\mathbf{u}, \mathbf{u}) = \mathbf{p}(t) \tag{17}$$

with $0 < \alpha < \beta \leq 2, \quad t > 0, \ \mathbf{a}_i \in \mathbb{R}, \ \det(\mathbf{a}_1) \neq 0$

under the initial conditions

$$\mathbf{u}(0) = \mathbf{u}_0, \quad \text{if } \beta \leq 1 \tag{18a}$$

or

$$\mathbf{u}(0) = \mathbf{u}_0, \ \dot{\mathbf{u}}(0) = \dot{\mathbf{u}}_0\,, \text{ if } 1 < \beta \leq 2 \tag{18b}$$

Let $\mathbf{u} = \mathbf{u}(t)$ be the sought solution of Eq. (17). Then, if the operator D_c^{β} is applied to $\mathbf{u}$ we have

$$D_c^{\beta}\mathbf{u} = \mathbf{q}(t), \quad 0 < \beta \leq 2, \quad t > 0 \tag{19}$$

where $\mathbf{q}(t)$ is a vector of unknown fictitious sources. Eq. (19) is the analog equation of (17). It indicates that the solution of Eq. (17) can be obtained by solving Eq. (19) with the initial conditions (18), if the $\mathbf{q}(t)$ is first established. This is achieved by working as following.

Using the Laplace transform method we obtain the solution of Eq. (19) as

$$\mathbf{u}(t)=\mathbf{u}_0+[\mathrm{ceil}(\beta)-1]\dot{\mathbf{u}}_0 t+\frac{1}{\Gamma(\beta)}\int_0^t \mathbf{q}(\tau)(t-\tau)^{\beta-1}d\tau \tag{20}$$

where $\mathrm{ceil}(\,)$ represents the ceiling function, e.g. $\mathrm{ceil}(\beta)$ yields the integer greater or equal to β. The use of this function permits to realize computationally the proper initial conditions prescribed by Eqs (18). Eq. (20) is an integral equation for $\mathbf{q}(t)$, which can be solved numerically within a time interval $[0,T]$ as following. The interval $[0,T]$ is divided into N equal intervals $\Delta t=h$, $h=T/N$, in which $\mathbf{q}(t)$ is assumed to vary according to a certain law, e.g. constant, linear etc. In this analysis $\mathbf{q}(t)$ is assumed to be constant and equal to the mean value in each interval h. Hence, Eq. (20) at instant $t=nh$ can be written as

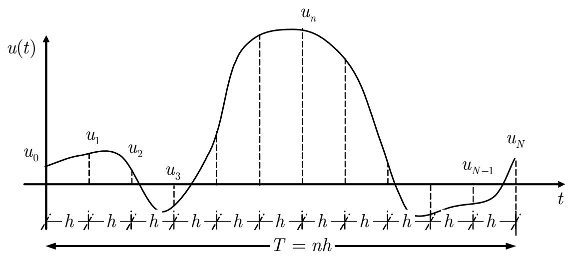

Fig. 2: Discretization of the interval $[0,T]$ into N equal intervals $h=T/N$.

$$\begin{aligned}\mathbf{u}_n&=\mathbf{u}_0+[\mathrm{ceil}(\beta)-1]nh\dot{\mathbf{u}}_0+\frac{1}{\Gamma(\beta)}\Big[\mathbf{q}_1^m\int_0^h(nh-\tau)^{\beta-1}d\tau\\&+\mathbf{q}_2^m\int_h^{2h}(nh-\tau)^{\beta-1}d\tau+\cdots+\mathbf{q}_n^m\int_{(n-1)h}^{nh}(nh-\tau)^{\beta-1}d\tau\Big]\end{aligned} \tag{21}$$

which after evaluation of the integrals yields

$$\begin{aligned}\mathbf{u}_n&=\mathbf{u}_0+[\mathrm{ceil}(\beta)-1]nh\dot{\mathbf{u}}_0\\&+c\sum_{r=1}^{n-1}\left[(n+1-r)^{\beta}-(n-r)^{\beta}\right]\mathbf{q}_r^m+\frac{c}{2}\left(\mathbf{q}_{n-1}+\mathbf{q}_n\right)\end{aligned} \tag{22}$$

where

$$c=\frac{h^{\beta}}{\beta\Gamma(\beta)},\qquad \mathbf{q}_r^m=\frac{1}{2}(\mathbf{q}_{r-1}+\mathbf{q}_r) \tag{23}$$

Eq. (22) can be further written as

$$\begin{aligned}-\frac{c}{2}\mathbf{q}_n+\mathbf{u}_n&=\mathbf{u}_0+[\mathrm{ceil}(\beta)-1]nh\dot{\mathbf{u}}_0\\&+c\sum_{r=1}^{n-1}\left[(n+1-r)^{\beta}-(n-r)^{\beta}\right]\mathbf{q}_r^m+\frac{c}{2}\mathbf{q}_{n-1}\end{aligned} \tag{24}$$

We now set

$$D_c^{\alpha}\mathbf{u}=\overline{\mathbf{q}}(t) \tag{25}$$

where $\overline{\mathbf{q}}(t)$ is another unknown vector. We can establish a relation between $\mathbf{q}(t)$ and $\overline{\mathbf{q}}(t)$ by considering the Laplace transform of Eqs (19) and (25). Thus, we can write

$$\mathbf{U}(s)=\mathbf{u}_0\frac{1}{s}+[\mathrm{ceil}(\beta)-1]\dot{\mathbf{u}}_0\frac{1}{s^2}+\frac{1}{s^{\beta}}\mathbf{Q}(s) \tag{26a}$$

$$\mathbf{U}(s)=\mathbf{u}_0\frac{1}{s}+[\mathrm{ceil}(\alpha)-1]\dot{\mathbf{u}}_0\frac{1}{s^2}+\frac{1}{s^{\alpha}}\overline{\mathbf{Q}}(s) \tag{26b}$$

Equating the right-hand sides of the above equations we have

$$\bar{\mathbf{Q}}(s) = ([\mathrm{ceil}(\beta) - \mathrm{ceil}(\alpha)])\,\dot{\mathbf{u}}_0\,\frac{1}{s^{2-\alpha}} + \frac{1}{s^{\beta-\alpha}}\mathbf{Q}(s)\,, \qquad \alpha \neq \beta \tag{27}$$

Taking the inverse Laplace transform of Eq. (27) we obtain

$$\bar{\mathbf{q}} = ([\mathrm{ceil}(\beta) - \mathrm{ceil}(\alpha)])\,\dot{\mathbf{u}}_0\,\frac{t^{1-\alpha}}{\Gamma(2-\alpha)} + \frac{1}{\Gamma(\beta-\alpha)}\int_0^t \mathbf{q}(\tau)(t-\tau)^{\beta-\alpha-1}d\tau \tag{28}$$

Using the same disctetization of the interval $[0,T]$ to approximate the integral in Eq. (28), we obtain

$$\begin{aligned}\bar{\mathbf{q}}_n &= ([\mathrm{ceil}(\beta) - \mathrm{ceil}(\alpha)])\,n^{1-\alpha}d\dot{\mathbf{u}}_0 \\ &\quad + \bar{c}\sum_{r=1}^{n}\left[(n+1-r)^{\beta-\alpha} - (n-r)^{\beta-\alpha}\right]\mathbf{q}_r^m\end{aligned} \tag{29}$$

where

$$\bar{c} = \frac{h^{\beta-\alpha}}{(\beta-\alpha)\Gamma(\beta-\alpha)}, \qquad d = \frac{h^{1-\alpha}}{\Gamma(2-\alpha)}, \qquad \mathbf{q}_r^m = \frac{1}{2}(\mathbf{q}_{r-1} + \mathbf{q}_r) \tag{30}$$

Eq. (29) can be further written as

$$\begin{aligned}-\frac{\bar{c}}{2}\bar{\mathbf{q}}_n + \mathbf{q}_n &= [\mathrm{ceil}(\beta) - \mathrm{ceil}(\alpha)]nd\dot{\mathbf{u}}_0 \\ &\quad + \bar{c}\sum_{r=1}^{n-1}\left[(n+1-r)^{\beta-\alpha} - (n-r)^{\beta-\alpha}\right]\mathbf{q}_r^m + \frac{\bar{c}}{2}\mathbf{q}_{n-1}\end{aligned} \tag{31}$$

Applying Eq. (17) for $t = t_n$ we have

$$\mathbf{F}(\mathbf{q}_n, \bar{\mathbf{q}}_n, \mathbf{u}_n) = \mathbf{p}_n \tag{32}$$

Eqs (24), (31) and (32) are algebraic equations and they can be combined and solved successively for $n = 1, 2, \ldots$ to yield the solution $\mathbf{u}_n$ and the fractional derivatives $\mathbf{q}_n, \bar{\mathbf{q}}_n$ at instant $t = nh \le T$. For $n = 1$, the value $\mathbf{q}_0$ appears in the right hand side of Eqs (24) and (31). This value can be evaluated as following.

Equation (27) for $t = 0$ gives

$$\mathbf{F}(\mathbf{q}_0, \bar{\mathbf{q}}_0, \mathbf{u}_0) = \mathbf{p}_0 \tag{33}$$

The above equation includes two unknowns, $\mathbf{q}_0, \bar{\mathbf{q}}_0$. These values can be expressed in terms of the known initial conditions using the relations below (see Appendix).

$$\left.\begin{aligned}\bar{\mathbf{q}}_0 &= \left[\mathbf{a}_1\frac{\Gamma(2-\alpha)\left(2-2^{1-\beta}\right)}{\Gamma(2-\beta)\left(2-2^{1-\alpha}\right)}h^{\alpha-\beta} + \mathbf{a}_2\right]^{-1}\left(\mathbf{p}_0 - \mathbf{a}_3\mathbf{u}_0\right) \\ \mathbf{q}_0 &\cong \frac{\Gamma(2-\alpha)}{\Gamma(2-\beta)}\frac{\left(2-2^{1-\beta}\right)}{\left(2-2^{1-\alpha}\right)}h^{\alpha-\beta}\bar{\mathbf{q}}_0\end{aligned}\right\}\ \text{if } 0<\alpha<\beta\le 1 \tag{34a}$$

$$\left.\begin{aligned}\bar{\mathbf{q}}_0 &= \left[\mathbf{a}_1\frac{\Gamma(3-\alpha)\left(2-2^{2-\beta}\right)}{\Gamma(3-\beta)\left(2-2^{2-\alpha}\right)}h^{\alpha-\beta} + \mathbf{a}_2\right]^{-1}\left(\mathbf{p}_0 - \mathbf{a}_3\mathbf{u}_0\right) \\ \mathbf{q}_0 &\cong \frac{\Gamma(3-\alpha)}{\Gamma(3-\beta)}\frac{\left(2-2^{2-\beta}\right)}{\left(2-2^{2-\alpha}\right)}h^{\alpha-\beta}\bar{\mathbf{q}}_0\end{aligned}\right\}\ \text{if } 1<\alpha<\beta\le 2 \tag{34b}$$

$$\left.\begin{aligned}\bar{\mathbf{q}}_0 &= \frac{1}{\Gamma(2-a)}h^{1-a}\left(2-2^{1-\alpha}\right)\dot{\mathbf{u}}_0 \\ \mathbf{q}_0 &= \mathbf{a}_1^{-1}(\mathbf{p}_0 - \mathbf{a}_3\mathbf{u}_0 - \mathbf{a}_2\bar{\mathbf{q}}_0)\end{aligned}\right\}\ \text{if } 0<\alpha\le 1 \text{ and } 1<\beta\le 2 \tag{34c}$$

Examples

The viscoelastic membrane shown in Fig. 3 has been studied. The boundary of the domain is defined by the curve $r=(ab)^{1/2}/\left[(\cos\theta/a)^2+(\sin\theta/b)^2\right]^{(1/4)}\left[(\cos\theta/b)^2+(\sin\theta/a)^2\right]^{(1/4)}$, $0\le\theta\le 2\pi$. The membrane is prestressed by $u_n=0.2\,m$ in the direction normal to the boundary and $u_t=0\,m$ in the tangential direction. The employed data are: $a=3$, $b=1.3$; $h=0.002\,\mathrm{m}$, $\rho/h=5000\,\mathrm{kg/m^3}$, $E=1.1\times10^5\,\mathrm{kN/m^2}$, $\nu=0.3$. The results were obtained using $N=210$ boundary elements and $M=106$ internal collocation points. The membrane is subjected to a transverse load $p_z=2H(t)\,\mathrm{kN/m^2}$. Firstly, the influence of the membrane inertia forces is investigated when the membrane is purely elastic. Fig. 4a,b,c present the time history of the transverse displacement at the center of the membrane, the inplane displacement u and the membrane force at point A(-1.741,0) respectively, taking into account and neglecting the membrane inertia forces. Apparently, the influence of the membrane inertia forces is negligible. Moreover, Fig. 5a,b show the deflection at the center and the membrane displacement u at point A for various number of Ritz vectors employed for reduction of the degrees of freedom and are compared with the results of the unreduced system. The use of more than 20 modes changes the results negligibly.

Next, the free vibrations of the elastic ($\eta=0$) and the viscoelastic membrane ($\eta=0.2$) are studied. The initial conditions are $w(x,y,0)=$ the deflection of the membrane for a static load $p_z=1\,kN/m^2$ and $\dot{w}(x,y,0)=0$. The results were obtained using 20 linear modes for reduction. Fig. 6 presents the response of the membrane. Finally, the forced vibrations of the viscoelastic membrane are studied. The membrane is subjected to a transverse load $p_z=H(t)\,\mathrm{kN/m^2}$. The results were obtained using 20 linear modes as Ritz vectors for the reduction of the degrees of freedom. Fig. 7 presents the time history of the membrane for various values of the order of the fractional derivative of the Voigt type model. Fig. 8b shows the phase plane of the deflection at the center for $\alpha=0.5$, $\eta=0.5$.

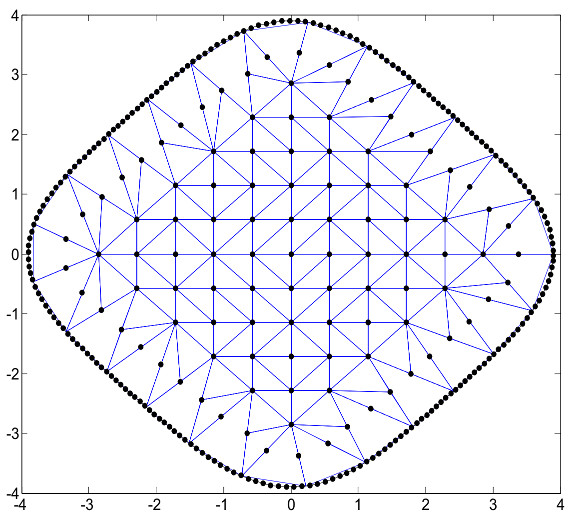

Fig. 3: Boundary and domain nodal points of the membrane

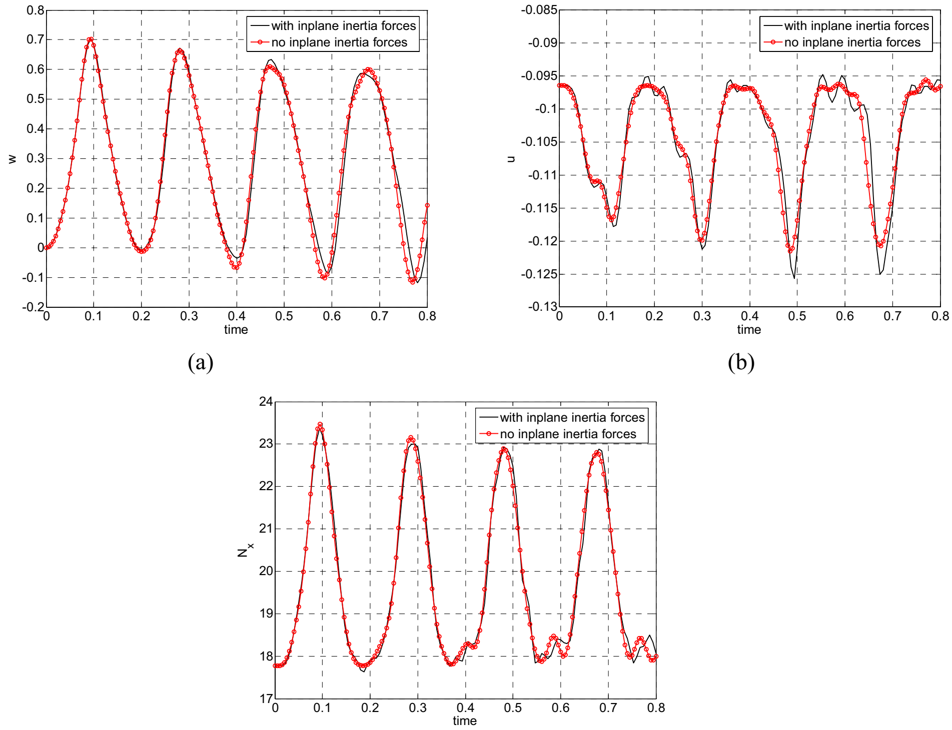

(c)
Fig. 4: Time history of (a) transverse displacement at the center of the membrane (b) inplane displacement u and (c) membrane force N_x at point (-1.741,0).

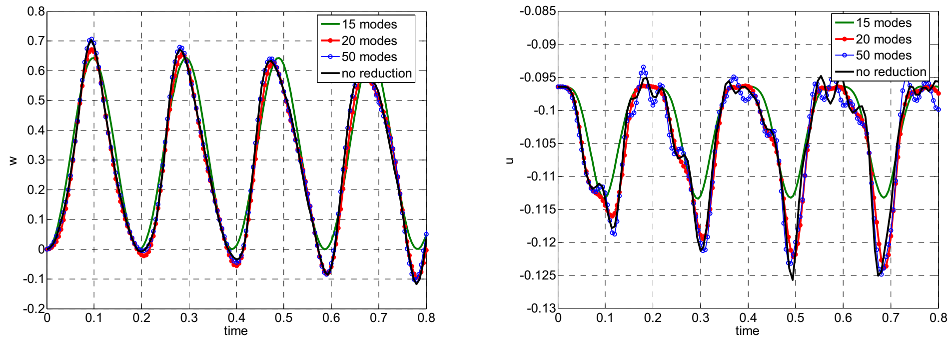

(a) (b)
Fig. 5: Time history of (a) transverse displacement at the center of the membrane and (b) inplane displacement u at point (-1.741,0) with different number of the linear modes used for reduction.

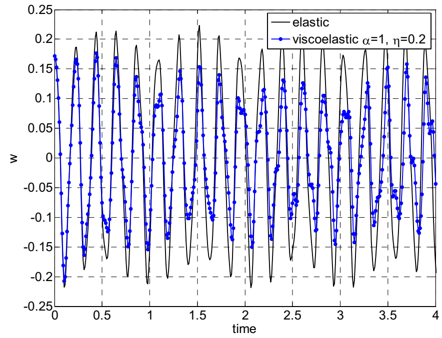

(a)

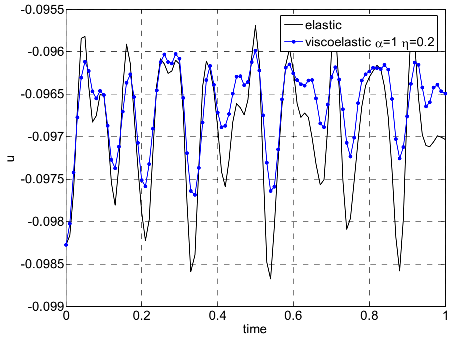

(b)

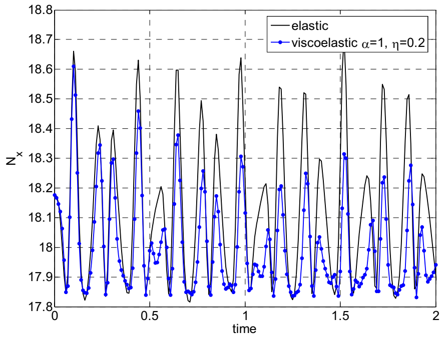

(c)

Fig. 6: Time history of (a) transverse displacement at the center of the membrane (b) inplane displacement u and (c) membrane force N_x at point (-1.741,0) for elastic and viscoelastic material.

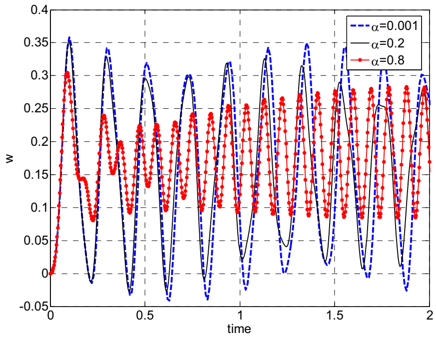

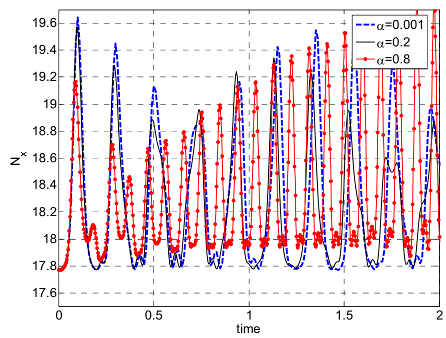

(a) (b)

Fig. 7: Time history of (a) transverse displacement at the center of the membrane (b) membrane force N_x at point (-1.741,0) for various values of the order α ($\eta = 0.5$)

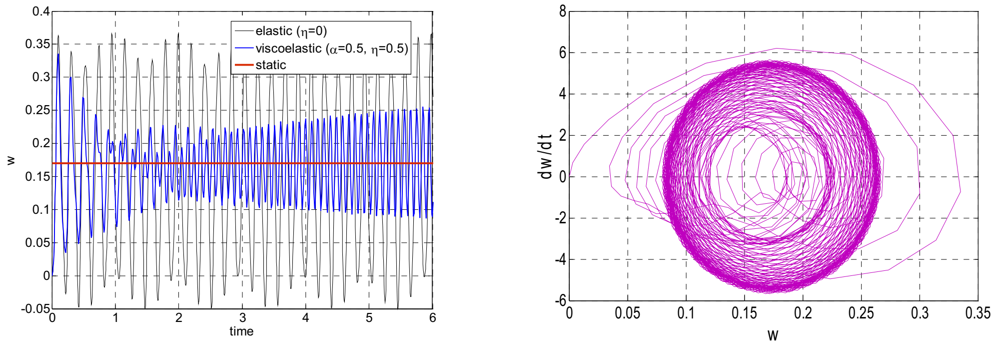

(a) (b)

Fig. 8: (a) transverse displacement at the center of the membrane and (b) phase plane for $\alpha = 0.5$, $(\eta = 0.5)$

Conclusions

The governing equations describing the nonlinear dynamic response of viscoelastic membranes made of fractional type derivative viscoelastic materials are derived and a BEM method based on the concept of the analog equation is developed for solving the coupled nonlinear partial fractional differential equations. The system of the nonlinear fractional ordinary differential equations resulting after domain discretization is solved by a new recently developed method for solving multi-term FDEs. The membrane may have arbitrary shape and it can be prestressed. The obtained results show that the membrane inertia forces have a negligible effect. In absence of damping the membrane under a suddenly applied load vibrates about the static equilibrium configuration with the maximum amplitude reaching asymptotically constant value much smaller than the elastic.

In closing, the presented method provides an efficient computational tool to analyse nonlinear viscoelastic membranes described by realistic models and enables the investigator to understand their complicated dynamic response.

References

[1] M. Stiassnie, On the application of fractional calculus for the formulation of viscoelastic models, *Appl. Math. Modeling*, **3**, 300-302, 1979.

[2] G. Haneczok, M. Weller, A fractional model of viscoelastic relaxation, *Materials Science and Engineering A*, **370**, 209-212, 2004.

[3] I. Podlubny, *Fractional differential equations*, Academic Press, New York, 1999.

[4] A. Schmidt and L. Gaul, Finite Element Formulation of Viscoelastic Constitutive Equations using Fractional Time Derivatives, *Nonlinear Dyn*amics, **29**(1-4), 37-55, 2002.

[5] G.C. Tsiatas and J.T. Katsikadelis, Large Deflection Analysis of Elastic Space Membranes, *International Journal for Numerical Methods in Engineering*, **65**, 264-294, 2006.

[6] J.T. Katsikadelis, M.S. Nerantzaki and G.C. Tsiatas, The Analog Equation Method for Large Deflection Analysis of Membranes. A Boundary Only Solution, *Computational Mechanics*, **27**, 513-523, 2001.

[7] Nonlinear Dynamic Analysis of Heterogeneous Orthotropic Membranes, *Engineering Analysis with Boundary Elements*, **27**, 115-124, 2003.

[8] J.T. Katsikadelis, The BEM for Non-homogeneous Bodies, *Archive of Applied Mechanics*, **74**, 780-789, 2005.

[9] J.T. Katsikadelis, Numerical Solution of Multi-term Fractional Differential Equations, 2009 (to be published).

[10] J.T. Katsikadelis, N.G. Babouskos, Nonlinear flutter instability of thin damped plates. An AEM solution, *Journal of Mechanics of Materials and Structures* (accepted).

Appendix: Approximation of $D_c^\alpha u(0)$

The function $u(t)$ is expanded in Taylor series

$$u(t) = u_0 + \dot{u}_0 t + \frac{1}{2!}\ddot{u}_0 t^2 + \frac{1}{3!}\dddot{u}_0 t^3 \cdots \tag{A1}$$

(i) $0 < \alpha \le 1$.
We have

$$\left.\begin{aligned} &D_c^\alpha(1) = 0 \\ &D_c^\alpha(t) = \frac{\Gamma(2)}{\Gamma(2-a)} t^{1-a} \\ &D_c^\alpha(t^2) = \frac{\Gamma(3)}{\Gamma(3-a)} t^{2-a} \\ &\vdots \\ &D_c^\alpha(t^n) = \frac{\Gamma(n+1)}{\Gamma(n+1-a)} t^{n-a} \end{aligned}\right\} \tag{A2}$$

then

$$D_c^\alpha u(t) = \dot{u}_0 \frac{\Gamma(2)}{\Gamma(2-a)} t^{1-a} + \frac{1}{2}\ddot{u}_0 \frac{\Gamma(3)}{\Gamma(3-a)} t^{2-a} + \cdots \tag{A3}$$

from which we obtain

$$D_c^\alpha u(h) = \dot{u}_0 \frac{\Gamma(2)}{\Gamma(2-a)} h^{1-a} + \frac{1}{2}\ddot{u}_0 \frac{\Gamma(3)}{\Gamma(3-a)} h^{2-a} + \cdots \tag{A4}$$

$$D_c^\alpha u(2h) = \dot{u}_0 \frac{1}{\Gamma(2-a)} (2h)^{1-a} + \ddot{u}_0 \frac{1}{\Gamma(3-a)} (2h)^{2-a} + \cdots \tag{A5}$$

linear extrapolation yields

$$D_c^\alpha u(0) = 2D_c^\alpha u(h) - D_c^\alpha u(2h) \tag{A6}$$

or after neglecting terms of $O(h^{2-\alpha})$

$$D_c^\alpha u(0) \simeq \frac{1}{\Gamma(2-a)} h^{1-a} (2 - 2^{1-a})\, \dot{u}_0 \tag{A7}$$

(ii) $1 < \alpha \le 2$
We have

$$\left.\begin{aligned} &D_c^\alpha(1) = 0 \\ &D_c^\alpha(t) = 0 \\ &D_c^\alpha(t^2) = \frac{\Gamma(3)}{\Gamma(3-a)} t^{2-a} \\ &\vdots \\ &D_c^\alpha(t^n) = \frac{\Gamma(n+1)}{\Gamma(n+1-a)} t^{n-a} \end{aligned}\right\} \tag{A8}$$

then

$$u(t) = u_0 + \dot{u}_0 t + \frac{1}{2!}\ddot{u}_0 t^2 + \frac{1}{3!}\dddot{u}_0 t^3 \cdots \tag{A9}$$

$$D_c^\alpha u(t) = \ddot{u}_0 \frac{1}{\Gamma(3-a)} t^{2-a} + \dddot{u}_0 \frac{1}{\Gamma(4-a)} t^{3-a} + \cdots \tag{A10}$$

Using Eq. A4 and neglecting $O(h^{3-\alpha})$ we take

$$D_c^\alpha u(0) \simeq \frac{1}{\Gamma(3-a)} h^{2-a} \left(2 - 2^{2-a}\right) \ddot{u}_0 \tag{A11}$$

Note that Eqs A7 and A11 yield

$$D_c^1 u(0) = \dot{u}_0 \,, \qquad D_c^2 u(0) = \ddot{u}_0 \tag{A12}$$

Fast Solution of 3D Elastodynamic Boundary Element Problems by Hierarchical Matrices

I. Benedetti[1], M.H. Aliabadi[2]

[1] On leave from DISAG – Dipartimento di Ingegneria Strutturale Aerospaziale e Geotecnica, Università di Palermo, Viale delle Scienze, Edificio 8, 90128, Palermo, Italy, i.benedetti@unipa.it

[2] Department of Aeronautics, Imperial College London, South Kensington Campus, Roderic Hill Building, Exhibition Road, SW72AZ, London, UK, m.h.aliabadi@imperial.ac.uk

Keywords: Elastodynamic BEM, Laplace Transform Method, Adaptive Cross Approximation, Hierarchical Matrices, Fast BEM solvers

Abstract. In this paper a fast solver for three-dimensional elastodynamic BEM problems formulated in the Laplace transform domain is presented, implemented and tested. The technique is based on the use of hierarchical matrices for the representation of the collocation matrix for each value of the Laplace parameter of interest and uses a preconditioned GMRES for the solution of the algebraic system of equations. The preconditioner is built exploiting the hierarchical arithmetic and taking full advantage of the hierarchical format. An original strategy for speeding up the overall analysis is presented and tested. The reported numerical results demonstrate the effectiveness of the technique.

Introduction

The analysis of elastic dynamic problems through reliable numerical techniques is a subject of great relevance in many fields of science and engineering. The Boundary Element Method (BEM) has been effectively employed for the analysis of dynamic problems using several different strategies, like the time domain formulation, the Fourier and Laplace transform techniques or the dual reciprocity method [1-3].

In the context of Fracture Mechanics, to mention a field of interest to the authors, dynamic crack problems have been successfully solved using the Dual Boundary Element Method in the time domain [4] (Time Domain Method, TDM), in the Laplace transform domain [5,6] (Laplace Transform Method, LTM) and in conjunction with the dual reciprocity method [7] (Dual Reciprocity Method, DRM) and the performances of the three approaches have been compared, in terms of analysis time and memory consumption, for both two-dimensional [8] and three-dimensional [9] cases.

In these works it was found that the Laplace Transform Method, although very accurate, is computationally expensive, in terms of computational time, in comparison to the other techniques. Moreover, although the storage memory required for the analysis in the transform domain is less than that required by the other strategies for dynamics, it is however larger than that needed by the corresponding static problem. On the other hand, it is well known that the BEM produces fully populated matrices whose storage and direct solution are of order $O\left(n^2\right)$ and $O\left(n^3\right)$ respectively, if n is the order of the problem. Such considerations limit the size of the problems that can be effectively tackled on common computers using the standard BEM. This circumstance hindered for many years the industrial development of the method and has limited its use to the analysis of small or medium size problems.

However, in the recent years, a considerable effort has been devoted to the development of strategies aimed at reducing the computational complexities of the BEM, reducing both memory requirements and time consumption.

Many investigations have been carried out to overcome such limitations and different techniques have been developed such as the fast multipole method (FMM) [10,11], the panel clustering method [12], the mosaic-skeleton approximation [13] and the methods based on the use of hierarchical matrices [14]. The general aim of such techniques is to reduce the computational complexity of the matrix-vector multiplication which is the core operation in iterative solvers for linear systems. However while FMMs and panel clustering tackle the problem from an analytical point of view and require the knowledge of some kernel expansion in advance to carry out the integration, mosaic-skeleton approximations and hierarchical matrices provide purely algebraic tools for the approximation of the boundary element matrices, thus proving particularly suitable for problems where analytic closed form expressions of the kernels are not available or difficult to expand.

The analysis of elastodynamic problems through FMM BEM has been addressed both in the time[15] and frequency domain [16-18], with a special attention to seismology and soil-structure interaction problems. Although the reported results show a noticeable reduction in both memory and time requirements, the implementation of FM strategies requires heavy and *ad hoc* recoding of available packages. On the other hand, fewer works have been devoted to the use of hierarchical matrices for the analysis of elastodynamic problems. In particular, the authors are aware of only one application of the Adaptive Cross Approximation (ACA) to a symmetric elastodynamic Galerkin boundary element formulation [19].

In this work the use of hierarchical matrices for the rapid solution of 3D BEM elastodynamic problems in the Laplace transform domain is presented and investigated for the first time, extending the work previously developed by the authors for the fast solution of 3D static Dual BEM problems [20,21]. To obtain an accurate solution through any inverse transform technique, the solution in the transform domain for a sufficient number of Laplace parameters has to be computed. The hierarchical format is used for representing and storing the collocation matrix for each value of the Laplace parameter. The coefficient matrices are built by Adaptive Cross Approximation (ACA) and the final system for each parameter is solved through a preconditioned GMRES iterative solver, in which the matrix-vector product is sped up by the hierarchical representation itself. Also the preconditioner is built taking advantage of the hierarchical format and an original strategy to further speed up the overall analysis is presented an tested.

Elastodynamic BEM in the Laplace transform domain

The boundary integral equation governing the dynamic behavior of an elastic body in the Laplace transform domain can be written

$$c_{ij}(\boldsymbol{x}_0)\tilde{u}_j(\boldsymbol{x}_0)+\fint_\Gamma \tilde{T}_{ij}(\boldsymbol{x}_0,\boldsymbol{x},s)\tilde{u}_j(\boldsymbol{x})\,d\Gamma = \int_\Gamma \tilde{U}_{ij}(\boldsymbol{x}_0,\boldsymbol{x},s)\tilde{t}_j(\boldsymbol{x})\,d\Gamma \tag{1}$$

where the tilde indicates transformed quantities and s is the Laplace parameter. The boundary integral representation of the elastodynamic problem in the Laplace domain has the same form as that of the elastostatic problem. Eq.(1) is to be used in conjunction with the transformed boundary conditions to solve any specific problem.

The form of the elastodynamic fundamental solutions in the Laplace domain allows to write each of them as the sum of two contributions: the first term does not depend on s and contains the same singularities as those present in the elastostatic 3D fundamental solutions; the second term depends on s, but contain only weak singularities. This circumstance leads, after the classical boundary elements discretization procedure, to a linear system of the form

$$\left[\mathbf{A}+\tilde{\mathbf{A}}(s)\right]\tilde{\mathbf{x}}(s)=\tilde{\mathbf{y}}(s) \tag{2}$$

where $\mathbf{A}$ is the matrix stemming from the integration of the terms containing the singularities and needs to be computed only once in advance, while $\tilde{\mathbf{A}}(s)$ stems from the integration of the terms depending on s and has to be computed for each value of the Laplace parameter.

To analyze a general elastodynamic problem by using the Laplace transform technique, one has generally to compute the solution of the system (2) for a set of Laplace parameters s_k, with $k=1,\dots,L$, in order to calculate the time-dependent values of any relevant variable by means of some Laplace inverse transformation technique. Wen et al. [6] obtained for example accurate results for long durations in the time domain by using

$$s_k=\sigma+\frac{2\pi k i}{T} \qquad k=0,\dots,25 \tag{3}$$

with $\sigma T = 5$ and $T/t_0 = 20$, where t_0 is the unit time. In this work, the solution for the previous set of Laplace points will be computed for some elastodynamic problems and the performance of the hierarchical BEM in terms of memory and time requirements will be compared to that of the standard BEM.

Hierarchical matrices for elastodynamic BEM in the Laplace domain

To improve both storage memory and time required by the elastodynamic BEM analysis in the Laplace domain, system (2) is represented in *hierarchical format* for each value of the Laplace parameter.

The hierarchical or *low rank* representation of a BEM matrix is built by generating the matrix itself as a collection of sub blocks, some of which admit a special *approximated* and *compressed* format. Such blocks, referred to as *low rank blocks*, can be stored in the form

$$\mathbf{B} \cong \mathbf{B}_k = \sum_{i=1}^{k} \mathbf{u}_i \cdot \mathbf{v}_i^T = \mathbf{U} \cdot \mathbf{V}^T \tag{4}$$

The block **B** of order $m \times n$ is approximately generated through the product of **U,** of order $m \times k$, and $\mathbf{V}^T$, of order $k \times n$. If *k*, i.e. the *rank* of the block, is *low* then the representation (4) allows to reduce both memory storage and the computational cost of the matrix-vector multiplication, which is the bottleneck of any iterative solver.

The approximation of the low rank blocks (4) is built by computing only *some* of the entries of the original blocks through adaptive algorithms known as Adaptive Cross Approximation (ACA) [22,23], that allow to reach an initially selected accuracy ε. Low rank blocks represent the numerical interaction, through *asymptotic smooth* kernels, between sets of collocation points and clusters of integration elements which are sufficiently far apart from each other. The distance between clusters of elements enters a certain admissibility condition of the form

$$min\left(diam\ \Omega_{coll}, diam\ \Omega_{int}\right) \leq \eta\ dist(\Omega_{coll}, \Omega_{int}) \tag{5}$$

where Ω_{coll} *and* Ω_{int} are clusters of elements and $\eta > 0$ is a parameter influencing the number of admissible blocks on one hand and the convergence speed of the adaptive approximation of the low rank blocks on the other hand [24]. The blocks that do not satisfy such condition are called *full rank blocks* and they need to be computed and stored entirely, without approximation. Once low and full rank blocks have been generated, some recompression techniques can be used to further reduce the storage memory and computational complexity of the single blocks and of the overall hierarchical matrix (reduced SVD [25] and *coarsening* [26]).

As an almost optimal representation is obtained, the solution of the system can be tackled either directly, through hierarchical matrix inversion [27], or indirectly, through iterative methods [28]. In both cases, the efficiency of the solution relies on the use of a special arithmetic, i.e. a set of algorithms that implement the operations on matrices represented in hierarchical format, such as addition, matrix-vector multiplication, matrix-matrix multiplication, inversion and hierarchical LU decomposition. A collection of algorithms that implement many of such operations is given in [24] while the hierarchical LU decomposition is discussed in [28].

The use of iterative methods takes full advantages of the hierarchical representation, exploiting the efficiency of the low-rank matrix-vector multiplication. The convergence of iterative solvers can be improved by using suitable preconditioners. In this work a hierarchical LU preconditioner is built starting from a coarse approximation of accuracy ε_p of the collocation matrix. An iterative GMRES algorithm is eventually used in conjunction with such preconditioner for solving the system for each value of the Laplace parameter of interest.

Selecting the accuracy ε_c for the collocation matrix, the hierarchical counterpart of system (2) is written

$$\left[\mathscr{A}\left(\varepsilon_c\right) + \tilde{\mathscr{A}}\left(s_k, \varepsilon_c\right)\right]\tilde{\mathbf{x}}\left(s_k\right) = \tilde{\mathbf{y}}\left(s_k\right) \tag{6}$$

The LU preconditioner $\mathbf{P}(s_k)$ is generated in hierarchical format as well, selecting a reduced accuracy ε_p. The preconditioned final system has the form

$$\mathscr{P}\left(s_k,\varepsilon_p\right)\left[\mathscr{A}\left(\varepsilon_c\right)+\tilde{\mathscr{A}}\left(s_k,\varepsilon_c\right)\right]\tilde{\mathbf{x}}\left(s_k\right)=\mathscr{P}\left(s_k,\varepsilon_p\right)\tilde{\mathbf{y}}\left(s_k\right) \tag{7}$$

Even using the hierarchical format, the setup of a preconditioner is an expensive procedure. In the previous scheme a new preconditioner should be built for each value s_k of the Laplace parameter. To further speed up the overall dynamic analysis, an idea is put forward here and it is validated through numerical investigation. The preconditioner set up by using the hierarchical format can be thought of as a coarse approximation of the inverse of the system matrix for a given value s_k. If two subsequent values s_k and s_{k+j} of the Laplace parameter are *close* to each other, the preconditioner set up for s_k could constitute an approximation of the inverse of the system matrix set for s_{k+j}. This idea configures the use of *local preconditioners*, in the sense introduced above, and will be investigated in the next section.

Numerical experiments

Let us consider the bar depicted in Fig. 1, subjected to impact traction load $\sigma(t)=10\cdot\delta(t)$ on the (grey) superior base and constrained in correspondence of the thick points of the inferior base. The bar has square cross section $a\times a$, with $a=1$ and height $h=4$. A representative material with $E=1000$ and $\nu=0.3$ has been considered (all the quantities are non-dimensionalized). To test the performance of the hierarchical solver at varying mesh sizes, three different meshes have been considered, as shown in Table 1.

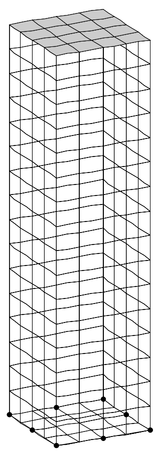

Figure 1 Analyzed configuration.

	Elements	*Nodes*
Mesh 1	288	866
Mesh 2	450	1352
Mesh 3	648	1946

Table 1 Analyzed meshes.

The parameters for the hierarchical analysis have been set to the following values: cardinality of the leaf $C_{leaf}=36$, admissibility parameter $\eta=3$, collocation matrix accuracy $\varepsilon_c=10^{-5}$, preconditioner accuracy $\varepsilon_p=10^{-1}$, GMRES tolerance $\varepsilon_{GMRES}=10^{-6}$.

The preset required accuracy has been obtained for all the preformed computations, confirming the effectiveness of ACA in the approximation of the low rank block stemming form elastodynamic kernels.

The memory storage required by the hierarchical collocation matrix and by the hierarchical preconditioner for each Laplace parameter and for various mesh sizes is then analyzed and results are reported in Fig.2. Also the memory requirement for the elastostatic counterpart of the analyzed problem is reported in the same figure, for the sake of comparison, as the first value of the plotted curves ($k=-1$). As it can be noted, the amount of required memory increases when the imaginary part of the Laplace parameter increases, due to the behavior of ACA with oscillatory kernels. It is to be noted that the strategy of the *local preconditioners* has been used and this explains the memory trends for the preconditioner. Moreover, for a given Laplace parameter, analogously to what happens in the static case, the storage memory, expressed as percentage of the full rank storage, decreases when the mesh size increases.

Figure 3 reports the assembly speed up ratio for various Laplace parameters and various mesh sizes. Also in this case the value corresponding to the static case is reported as the first value of the curves. The speed up ratio is defined as the ratio between the time necessary to perform an operation in hierarchical format and the corresponding classical time. It is to be noted that the classical assembly of the matrix contributions

$\tilde{\mathbf{A}}(s_k)$ requires less time in comparison to the classical assembly of the contribution $\mathbf{A}$, that stems from the integration of the singular integrals. On the other hand, ACA converges with an average rank which is greater or equal than the average rank in the static case. This consideration explains the jump with respect to the static case in the assembly speed up ratios depicted in Fig.3. It can be noted how the assembly speed up ratios grow with the Laplace parameter. This growth is considerable and can lead to assembly times greater than the full rank assembly time. This behavior is a direct consequence of the performance of ACA with the considered elastodynamic kernels and it is related to the growth of the average rank of the approximated blocks.

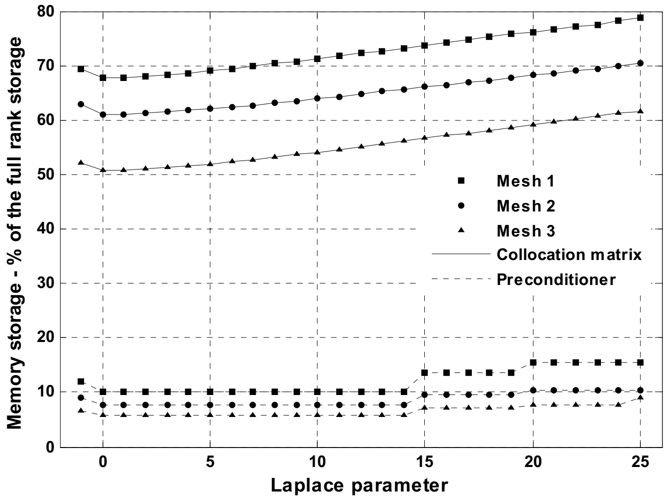

Figure 2 Memory requirements for various Laplace parameters and mesh sizes.

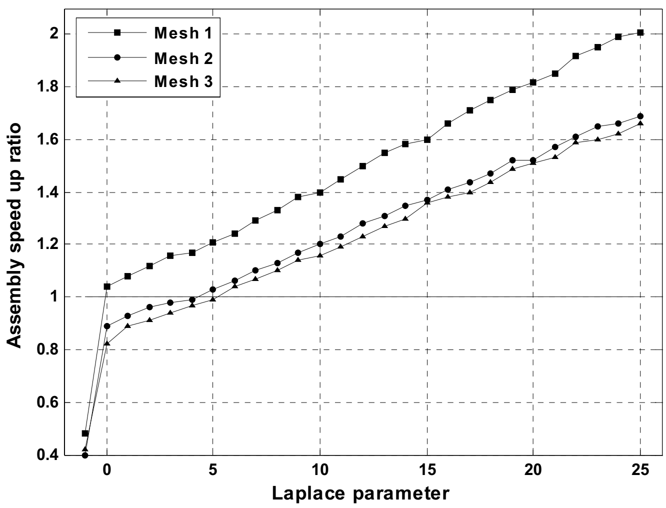

Figure 3 Assembly speed up ratio for various Laplace parameters and mesh sizes.

However, even when the hierarchical assembly times are higher than the full rank assembly times, the advantages in terms of *solution* time can be considerable and allow actual savings in terms of *total* (assembly plus solution) analysis time, as shown in Figs. 4 and 5. These figures demonstrate the effectiveness of the strategy of the *local preconditioners* introduced in the previous section, as well as the noticeable speed up ratios obtained for the three different meshes for various Laplace parameters.

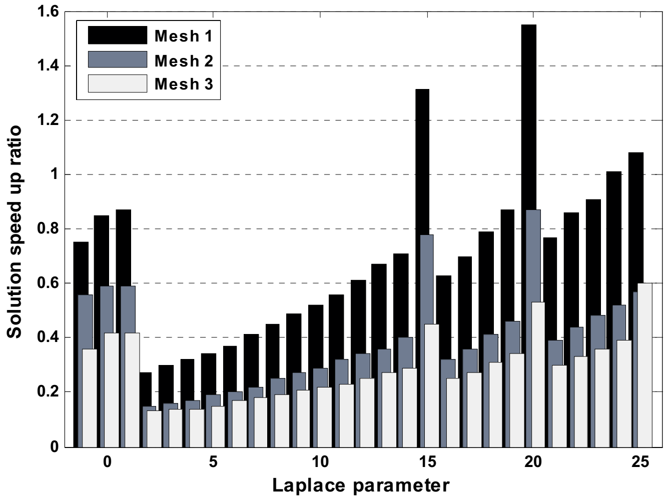

Figure 4 Solution speed up ratios for various Laplace parameters and mesh sizes.

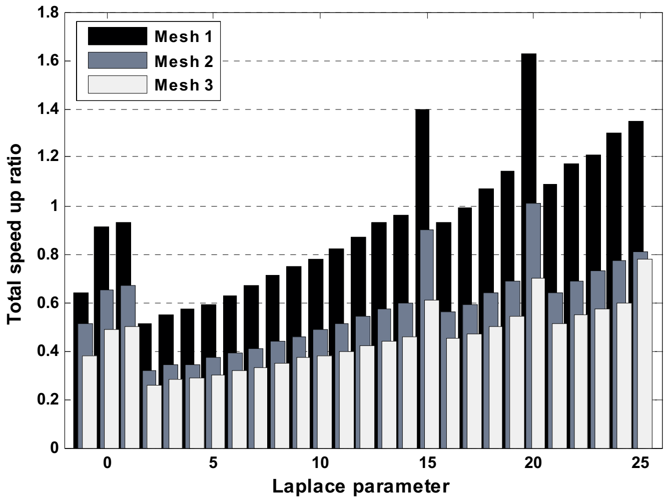

Figure 5 Total speed up ratios for various Laplace parameters and mesh sizes.

The idea of local preconditioners is further clarified by the number of GMRES iterations to convergence reported in Fig. 6 for the various Laplace parameters and different mesh sizes. When the preconditioner is computed for a certain value s_k, the number of iterations to convergence is relatively low. A given computed preconditioner is then used for the following values of the Laplace parameter and demonstrates to be able to precondition the system effectively. The number of GMRES iterations grows when the preconditioner is used *far* from the parameter for which it was computed. When the number of iterations overcomes a prefixed threshold, 140 in the figure, a new preconditioner is computed. The trends in terms of GMRES iterations confirm the effectiveness of the idea.

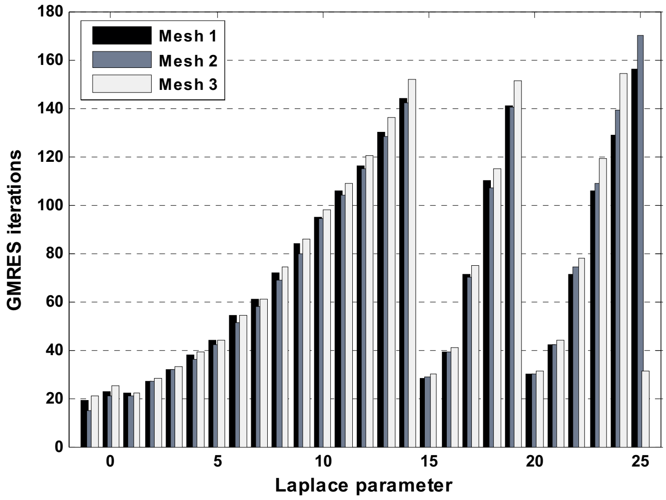

Figure 6 Number of GMRES iterations for various Laplace parameters and mesh sizes.

Summary

In this work a fast solution strategy for 3D elastodynamic BEM problems in the Laplace transform domain has been presented, implemented and tested. The strategy is based on the use of hierarchical matrices for the representation of the collocation matrix in the Laplace domain and uses a GMRES iterative solver for the solution of the final system. The hierarchical format allows to reduce the storage memory necessary for the representation of the system and speeds up the performance of the solver enhancing the speed of the matrix-vector product, which is the core and the bottleneck of any iterative solver for large systems. A coarse hierarchical LU preconditioner is used to improve the convergence of the iterative solution. Moreover, to further speed up the overall analysis in the Laplace domain, the idea of *local preconditioners* is presented and successfully assessed.

Acknowledgements

This work was partially funded within the European research project SEAT (Smart tEchnologies for stress free Air Travel) AST5-CT-2006-030958.

References

[1] G.D. Manolis and D.E. Beskos, *Boundary element methods in elastodynamics*, Unwin Hyman, London (1988).

[2] J. Dominguez, *Boundary elements in dynamics*, Computational Mechanics Publications, Elsevier Applied Science", London", (1993).

[3] M.H. Aliabadi, *The Boundary Element Method: Applications in Solids and Structures*, vol. 2. John Wiley & Sons Ltd (2002).

[4] P. Fedelinski, M.H. Aliabadi and D.P. Rooke, *Int J Sol Struct*, **32**, 3555-3571, (1995).

[5] P. Fedelinski, M.H. Aliabadi and D.P. Rooke, *Comp & Struct*, **59**(6), 1021-1031", (1996).

[6] P.H. Wen, M.H. Aliabadi and D.P. Rooke, *Comp Meth App Mech Eng*, **167**, 139-151, (1998).

[7] P.H. Wen, M.H. Aliabadi and D.P. Rooke, *Comp Meth App Mech Eng*, **173**, 365-374, (1999).

[8] P. Fedelinski, M.H. Aliabadi and D.P. Rooke, *Eng Anal Bound El*, **17**, 45-56, (1996).

[9] P.H. Wen, M.H. Aliabadi and A. Young, *J Strain Anal Eng Design*, **34**(6), 373-394", (1999).

[10] H. Rokhlin, *J Comp Phys*, **60**, 187-207, (1985).

[11] V. Popov, H. Power, *Eng. An. Bound. Elem.*, **25**, 7–18 (2001).

[12] W. Hackbusch and Z.P. Nowak, *Numerische Mathematik*, **73**, 207-243, (1989).

[13] E. E. Tyrtyshnikov, *Calcolo*, **33**, 47-57, (1996).

[14] W. Hackbusch, *Computing*, **62**, 89-108, (1999).

[15] T. Takahashi, N. Nishimura and S. Kobayashi, *Eng Anal Bound El*, **27**, 491-506, (2003).

[16] H. Fujiwara, *Geophys J Int*, **133**, 773-782, (1998).

[17] H. Fujiwara, *Geophys J Int*, **140**, 198-210, (2000).

[18] S. Chaillat, M. Bonnet and J-F. Semblat, J-F, *Comp Meth App Mech Eng*, **197**, 4233-4249, (2008).

[19] M. Messner and M. Schanz, *PAMM Proc App Math Mech*, **8**, 10309-10310, (2008).

[20] I. Benedetti, M.H. Aliabadi, G.Davì, *Int. J. Solids Structures*, **45**, 2355-2376 (2008).

[21] I. Benedetti, A. Milazzo, M.H. Aliabadi, "A fast Dual Boundary Element Method for 3D Anisotropic Crack Problems", *Int J Num Meth Eng*, Accepted for pubblication

[22] M. Bebendorf, *Numerische Mathematik*, **86**, 565-589, (2000).

[23] M. Bebendorf, S. Rjasanow, *Computing*, **70**, 1-24, (2003).

[24] S. Börm, L. Grasedyck and W. Hackbusch, *Eng. An. Bound. Elem.*, **27**, 405–422, (2003).

[25] M. Bebendorf, Effiziente numerische Lösung von Randintegralgleichungen unter Verwendung von Niedrigrang-Matrizen, Ph.D. Thesis, Universität Saarbrücken, 2000. dissertation.de, Verlag im Internet, ISBN 3-89825-183-7, (2001)

[26] L. Grasedyck, *Computing*, **74**, 205-223, (2005).

[27] L. Grasedyck, W. Hackbush, *Computing*, **70**, 295-334, (2003).

[28] M. Bebendorf, *Computing*, **74**, 225-247, (2005).

The BEM for optimum design of plates

Nick G. Babouskos and J.T. Katsikadelis

Institute of Structural Analysis, School of Civil Engineering, National Technical University of Athens, Zografou Campus, GR-15773 Athens, Greece,
babouskosn@yahoo.gr, jkats@central.ntua.gr

Keywords: shape optimization; boundary element method; Analog equation method; thin plate with variable thickness

Abstract. The thickness shape optimization is used to optimize the performance of a Kirchhoff plate having constant volume. The plate has arbitrary shape and any type of admissible boundary conditions. The objective function can be the stiffness of the plate, the buckling load, the maximum stresses or the regulation of the frequencies. The plate optimization problems are solved efficiently thanks (a) to developing an AEM solution for the bending and plane stress problem of the plate with variable stiffness and mass properties and (b) to appropriate selection of the design parameters. The validity of the Kirchhoff plate theory is ensured by imposing certain inequality constraints regarding the thickness variation. Thus realistic solutions are obtained. The introduced design parameters are the coefficients of the interpolation functions series which approximate the variable thickness within the plate domain and on its boundary. The presented plate optimization method overcomes the basic shortcoming of a possible FEM solution, which would require resizing of the elements and re-computation of their stiffness properties during the optimization process. Besides, upper and lower bounds of thickness are imposed dictated by serviceability reasons. Several plate optimization problems are solved, which give realistic solutions for plate design.

Introduction

Thin plates of variable thickness are used as structural components in many engineering applications. In most cases it is very useful to optimize the thickness variation of the plate in order to reduce the cost, increase the strength and improve the quality and the reliability of the structure. The problem consists in finding the thickness distribution of a plate with constant volume that minimizes or maximizes an objective function under some inequality constraints on the thickness variation dictated by serviceability reasons and at the same time ensure the validity of the thin plate theory with variable thickness. The objective function may be the stiffness of the plate, the buckling load, the maximum stresses, the frequencies of the dynamic response and others.

The evaluation of the objective function requires the solution of the problem of a plate with variable thickness. This problem has been solved using analytic and approximate techniques such as the Galerkin and the Rayleigh-Ritz method [1-3] and numerical methods like the FEM and the BEM [4-7]. Many researchers have studied the thickness optimization of rectangular and circular plates to maximize the lower natural frequency [8,9]. The buckling load for circular and annular plates has been optimized using Rayleigh-Ritz method [10] and FEM [11]. The stiffness of rectangular plates has been also maximized in [12]. In the previous papers and some others [13-16] the optimization problem is unconstrained or is subjected on upper and lower bounds on thickness. These studies usually lead to complicated shapes with discontinuous thickness variation for which the thin plate theory is not applicable. Niordson [17] introduced a constraint on the slope of the thickness function in order to obtain designs with slowly varying thickness. In the examined cases, the researchers study plates with simple geometries and inplane boundary conditions and the obtained results depend on the discretization of the plate. Furthermore, in the reported buckling optimization solutions the assumption of uniform membrane forces is adopted to avoid solving the plane stress problem arising simultaneously with the bending problem in each optimization step. Apparently, this gives unrealistic design solutions.

In this paper we consider the problem of determining the optimum thickness of the plate with a given volume in order to maximize the stiffness or the buckling load. It is a nonlinear optimization problem under equality and inequality constraints. The thickness function is approximated by polynomials of certain degree or by radial basis functions series. The parameters of the approximating functions are the design variables of the optimization. The shape optimization problem is solved using a general nonlinear minimization algorithm under linear and nonlinear inequalities. The bending problem of the plate variable thickness combined with membrane forces as well as the simultaneous plane stress problem is solved efficiently using the AEM of Katsikadelis [18, 19]. According to this method the original equations are converted into three uncoupled linear equations, namely a linear plate (biharmonic) equation for the transverse deflection and two linear membrane (Poisson) equations for the inplane deformation under unknown fictitious loads. The plate may have arbitrary geometry and any type of admissible bending and inplane boundary conditions. The resulting boundary value problems are solved with the D/BEM. Several plates with various shapes, boundary conditions and loads have been optimized, which illustrate the method and demonstrate its applicability and efficiency.

Statement of the problem

The shape optimization problem

We consider a thin elastic plate with a given volume occupying the two-dimensional domain Ω. Our problem is to establish the thickness variation so that:

a) The stiffness of the plate becomes a maximum when it is subjected to a transverse load.
b) The buckling load reaches its maximum value when it is subjected to inplane forces.

It is a nonlinear optimization problem under equality and inequality constraints. The equality constraint results from the condition that the volume of the material is kept constant, while the inequality constraints are imposed on the thickness variation to ensure validity of Kirchhoff plate theory and satisfy serviceability requirements.

The problem of plate with variable thickness

The evaluation of the objective function requires the solution of the plate bending problem combined with membrane forces as well as the plane stress problem. In both cases the thickness of the plate is variable. These problems are stated as follows.

(i) *For the transverse displacement* $w = w(x,y)$:

$$\begin{aligned} D\nabla^4 w + 2D_{,x}\,\nabla^2 w_{,x} + 2D_{,y}\,\nabla^2 w_{,y} + \nabla^2 D \nabla^2 w - (1-\nu)\left(D_{,xx}\,w_{,yy} - 2D_{,xy}\,w_{,xy} + D_{,yy}\,w_{,xx}\right) \\ - N_x w_{,xx} - 2N_{xy} w_{,xy} - N_y w_{,yy} + b_x w_{,x} + b_y w_{,y} = f \end{aligned} \quad \text{in } \Omega \quad (1)$$

$$\tilde{V}w + N_n^* w_{,n} + N_t^* w_{,t} + k_T w = V^* \text{ or } w = w^* \text{ on } \Gamma \quad (2a)$$

$$Mw + k_R w_{,n} = M^* \text{ or } w_{,n} = w_{,n}^* \text{ on } \Gamma \quad (2b)$$

$$k_T^{(k)} w^{(k)} - [\![Tw]\!]_k = R^* \text{ or } w^{(k)} = w_k^* \text{ at corner point k} \quad (2c)$$

where $D = Eh^3/12(1-\nu^2)$ is the variable flexural rigidity of the plate, with E,ν being the modulus of elasticity and Poisson's ratio, respectively, and $h = h(x,y)$, is the variable thickness; $f(x,y)$ and $b_x(x,y), b_y(x,y)$ are the transverse and the inplane loads; $[\![Tw]\!]_k$ is the discontinuity jump of the twisting moment at the corner, while $\tilde{V}w$ is the equivalent shear force of a plate with variable thickness, Mw is the normal bending moment and Tw the twisting moment on the boundary. The operators producing these quantities are given as [4]

$$\tilde{V} = V + 2\frac{\partial D}{\partial s}(\nu-1)\left(\frac{\partial^2}{\partial s \partial n} - \kappa\frac{\partial}{\partial s}\right) - \frac{\partial D}{\partial n}\left(\nabla^2 + (1-\nu)\left(\frac{\partial^2}{\partial s^2} + \kappa\frac{\partial}{\partial n}\right)\right) \quad (3a)$$

$$M = -D\left[\nabla^2 - (1-\nu)\left(\frac{\partial^2}{\partial s^2} + \kappa\frac{\partial}{\partial n}\right)\right] \quad (3b)$$

$$T = D(1-\nu)\left(\frac{\partial^2}{\partial s \partial n} - \kappa\frac{\partial}{\partial s}\right) \quad (3c)$$

where $\kappa = \kappa(s)$ is the curvature of the boundary and V is the operator of the equivalent shear force of a plate with constant thickness, given as [20]

$$V = -D\left[\frac{\partial}{\partial n}\nabla^2 + (1-\nu)\frac{\partial}{\partial s}\left(\frac{\partial^2}{\partial s \partial n} - \kappa\frac{\partial}{\partial s}\right)\right] \tag{4}$$

(ii) *For the membrane displacements* $u = u(x,y)$ *and* $v = v(x,y)$*:*

$$\left.\begin{aligned} &\mu h\nabla^2 u + (\lambda+\mu)h(u,_{xx} + v,_{xy}) + h,_x[\lambda(u,_x + v,_y) + 2\mu u,_x] + h,_y\,\mu(u,_y + v,_x) + b_x = 0 \\ &\mu h\nabla^2 v + (\lambda+\mu)h(u,_{xy} + v,_{yy}) + h,_x\,\mu(u,_y + v,_x) + h,_y[\lambda(u,_x + v,_y) + 2\mu v,_y] + b_y = 0 \end{aligned}\right\} \text{ in } \Omega \tag{5}$$

$$u_n = u_n^* \text{ or } N_n = N_n^* \quad \text{on } \Gamma \tag{6a}$$

$$u_t = u_t^* \text{ or } N_t = N_t^* \quad \text{on } \Gamma \tag{6b}$$

where $\lambda = E\nu/(1-\nu^2)$ and $\mu = E/2(1+\nu)$ are the Lamé constants and N_n^*, N_t^*, are inplane loads acting on boundary Γ. The membrane forces are given as

$$N_x = C(u,_x + \nu v,_y) \qquad N_{xy} = C\frac{1-\nu}{2}(u,_y + v,_x) \qquad N_y = C(\nu u,_x + v,_y) \tag{7}$$

The AEM for the plate bending problem

The boundary value problem (1)-(2) for the transverse deflection of the plate is solved using the AEM [18]. The analog equation for the problem at hand is

$$\nabla^4 w = b(\mathbf{x}), \quad \mathbf{x} = \{x,y\} \in \Omega \tag{8}$$

where $b(\mathbf{x})$ represents a fictitious load, unknown in the first instance. Eq. (8) under the boundary conditions (2) is solved using the BEM. Thus, the solution at a point $\mathbf{x} \in \Omega$ is obtained in integral form as

$$\begin{aligned} w(\mathbf{x}) = \int_\Omega w^* b\, d\Omega + \int_\Gamma (w^* Vw + w,_n Mw^* - w^*,_n Mw - wVw^*)ds \\ - \sum_k \left(w^* [\![Tw]\!] - w[\![Tw^*]\!]\right)_k \end{aligned} \tag{9}$$

which for $\mathbf{x} \in \Gamma$ yields the following two boundary integral equations

$$\begin{aligned} \frac{a}{2\pi}w(\mathbf{x}) = \int_\Omega w^* b\, d\Omega + \int_\Gamma (w^* Vw + w,_n Mw^* - w^*,_n Mw - wVw^*)ds \\ - \sum_k \left(w^* [\![Tw]\!] - w[\![Tw^*]\!]\right)_k \end{aligned} \tag{10}$$

$$\begin{aligned} a_x w,_x(\mathbf{x}) + a_y w,_y(\mathbf{x}) = \int_\Omega w_1^* b\, d\Omega + \int_\Gamma (w_1^* Vw + w,_n Mw_1^* - w_1^*,_n Mw - wVw_1^*)ds \\ - \sum_k \left(w_1^* [\![Tw]\!] - w[\![Tw_1^*]\!]\right)_k \end{aligned} \tag{11}$$

in which $w^* = w^*(\mathbf{x},\mathbf{y})$, $\mathbf{x},\mathbf{y} \in \Gamma$, is the fundamental solution and w_1^* its normal derivative at point $\mathbf{x} \in \Gamma$, i.e.

$$w^* = \frac{1}{8\pi}r^2 \ln r \qquad w_1^* = \left(\frac{1}{8\pi}r^2 \ln r\right),_\nu = \frac{1}{8\pi}rr,_\nu(2\ln r + 1) \tag{12a,b}$$

$\boldsymbol{\nu}$ is the unit normal vector to the boundary at point $\mathbf{x}$, whereas $\mathbf{n}$ is the unit normal vector to the boundary at the integration point $\mathbf{y}$ and $r = \|\mathbf{x} - \mathbf{y}\|$ (see Fig. 2a). Moreover $a = \theta_1 - \theta_2$ is the angle between the tangents at point $\mathbf{x} \in \Gamma$ and

$$a_x = \frac{a}{2\pi}\nu_x + \frac{\nu}{2\pi}\left[\frac{1}{2}\nu_x \sin 2\theta + \nu_y \sin^2\theta\right]_{\theta_1}^{\theta_2}, \quad a_y = \frac{a}{2\pi}\nu_y + \frac{\nu}{2\pi}\left[\nu_x \sin^2\theta - \frac{1}{2}\nu_y \sin 2\theta\right]_{\theta_1}^{\theta_2} \tag{13a,b}$$

For points where the boundary is smooth we have $a=\pi$ and $a_x w_{,x}(\mathbf{x})+a_y w_{,y}(\mathbf{x})=w_{,\nu}(\mathbf{x})/2$. Eqs (10) and (11) can be used to establish the not specified boundary quantities. They are solved numerically using the BEM. The boundary is approximated with N line segments on which the deflection w is approximated using a Hermit interpolation function while the other boundary quantities are approximated with piecewise linear interpolation functions [21]. The domain integrals are approximated using M linear triangular elements. The domain discretization is performed automatically using the Delaunay triangulation. Since the fictitious source is not defined on the boundary, the nodal points of the triangles adjacent to the boundary are placed on their sides (Fig. 2b).

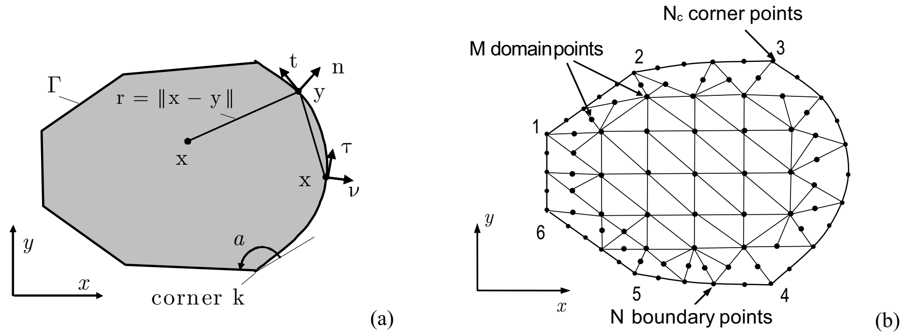

Figure 2: (a) BEM notation (b) boundary and domain discretization

At the N_c corner points on the boundary, the normal slope, the bending moment and the equivalent shear force may have discontinuity and a concentrated force may exist. Introducing the double node concept, $4N_c$ boundary values are introduced, which require $4N_c$ independent relations. These additional relations are given in [19]. Thus, after discretization and application of the boundary integral Eqs (10) and (11) at the N boundary nodal points we obtain

$$\mathbf{H}\begin{Bmatrix}\mathbf{w}\\ \mathbf{w}_{,n}\end{Bmatrix}=\mathbf{G}\begin{Bmatrix}\mathbf{V}\\ \mathbf{R}\\ \mathbf{M}\end{Bmatrix}+\mathbf{Ab} \tag{14}$$

where

- $\mathbf{H},\mathbf{G}$: are $2N\times(2N+N_c)$ and $2N\times(2N+3N_c)$, respectively, known coefficient matrices originating from the integration of the kernel functions on the boundary elements.
- $\mathbf{A}$: is a $2N\times M$ coefficient matrix originating from the integration of the kernel function on the domain elements.
- $\mathbf{w}$, $\mathbf{w}_{,n}$: are the vectors of the N boundary nodal displacements and $N+N_c$ boundary nodal normal slopes, respectively.
- $\mathbf{V}$, $\mathbf{R}$, $\mathbf{M}$: are the vectors of the $N+N_c$ nodal values of the effective shear force, N_c concentrated corner forces and $N+N_c$ nodal values of the normal bending moment.
- $\mathbf{b}$: is the vector of the M nodal values of the fictitious source.

Eq. (14) constitutes a system of $2N$ equations for $4N+4N_c$ unknowns. Additional $2N$ equations are obtained from the boundary conditions. Thus, the BCs (2a)-(2b), when applied at the N boundary nodal points yield the set of equations

$$\boldsymbol{\alpha}_1\mathbf{w}+\boldsymbol{\alpha}_2\mathbf{w}_{,n}+\boldsymbol{\alpha}_3\mathbf{V}+\boldsymbol{\alpha}_4\mathbf{M}=\boldsymbol{\alpha}_5 \qquad \boldsymbol{\beta}_1\mathbf{w}_{,n}+\boldsymbol{\beta}_2\mathbf{M}=\boldsymbol{\beta}_3 \tag{15a,b,c}$$

where $\boldsymbol{\alpha}_1,\boldsymbol{\alpha}_2,\boldsymbol{\alpha}_3,\boldsymbol{\alpha}_4,\boldsymbol{\alpha}_5,\boldsymbol{\beta}_1,\boldsymbol{\beta}_2,\boldsymbol{\beta}_3$ are known coefficient matrices. Note that Eq. (15a) has resulted after approximating the derivatives $w_{,t}$, $w_{,nt}=w_{,sn}-\kappa w_{,n}$ and $D_{,t}$ in Eq. (2a) with a finite difference scheme.

Equations (14) and (15) and the $4N_c$ additional equations can be combined and solved for the boundary quantities $\mathbf{w}, \mathbf{w}_{,n}, \mathbf{V}, \mathbf{R}, \mathbf{M}$ in terms of the fictitious load $\mathbf{b}$. Subsequently, these expressions are used to eliminate the boundary quantities from the discretised counterpart of Eq. (9). Thus we obtain the following representation for the deflection

$$w(\mathbf{x},t) = \sum_{k=1}^{M} b_k(t) W_k(\mathbf{x}) + W_0(\mathbf{x}) \qquad \mathbf{x} \in \Omega \tag{16}$$

The derivatives of $w(\mathbf{x})$ at points $\mathbf{x}$ inside Ω are obtained by direct differentiation of Eq. (9). Thus, we obtain after elimination of the boundary quantities

$$w_{,pqr}(\mathbf{x},t) = \sum_{k=1}^{M} b_k(t) W_{k,pqr}(\mathbf{x}) + W_{0,pqr}(\mathbf{x}), \qquad p,q,r = 0,x,y \qquad \mathbf{x} \in \Omega \tag{17}$$

where $W_{k,pqr}$, $W_{0,pqr}$ are known functions. $W_{0,pqr}$ result from nonhomogeneous boundary conditions. Note that the above notation implies $w_{,000} = w$, $w_{,0y0} = w_{,y}$, etc.

The AEM for the plane stress problem

Noting that Eqs (5) are of the second order their analog equations are obtained using the Laplace operator. This yields

$$\nabla^2 u = b_1(\mathbf{x},t) \qquad\qquad \nabla^2 v = b_2(\mathbf{x},t) \tag{18a,b}$$

The integral representation of the solution of Eq. (18a) is

$$\varepsilon u(\mathbf{x}) = \int_\Omega v^* b_1 d\Omega - \int_\Gamma (v^* q - q^* u) ds \qquad \mathbf{x} \in \Omega \cup \Gamma \tag{19}$$

in which $q = u_{,n}$; $v^* = \ell n r / 2\pi$ is the fundamental solution to Eq. (18a) and $q^* = v^*_{,n}$ its derivative normal to the boundary; $r = \|\mathbf{y} - \mathbf{x}\|$ $\mathbf{x} \in \Omega \cup \Gamma$ and $\mathbf{y} \in \Gamma$; ε is the free term coefficient ($\varepsilon = 1$ if $\mathbf{x} \in \Omega$, $\varepsilon = 1/2$ if $\mathbf{x} \in \Gamma$ and $\varepsilon = 0$ if $\mathbf{x} \notin \Omega \cup \Gamma$). Using the BEM with constant boundary elements and linear triangular domain elements and following the same procedure applied for the plate equation, we obtain the following representation for the inplane displacement u and its derivatives

$$u_{,pq}(\mathbf{x},t) = \sum_{k=1}^{M} b_k^{(1)}(t) U_{k}^{(1)}{}_{,pq}(\mathbf{x}) + \sum_{k=1}^{M} b_k^{(2)}(t) U_{k}^{(2)}{}_{,pq}(\mathbf{x}) + U_{0,pq}(\mathbf{x}) \qquad p,q = 0,x,y \qquad \mathbf{x} \in \Omega \tag{20}$$

Similarly, we obtain for the displacement v

$$v_{,pq}(\mathbf{x},t) = \sum_{k=1}^{M} b_k^{(1)}(t) V_{k}^{(1)}{}_{,pq}(\mathbf{x}) + \sum_{k=1}^{M} b_k^{(2)}(t) V_{k}^{(2)}{}_{,pq}(\mathbf{x}) + V_{0,pq}(\mathbf{x}) \qquad p,q = 0,x,y \qquad \mathbf{x} \in \Omega \tag{21}$$

$U_k^{(1)}, U_k^{(2)}, V_k^{(1)}, V_k^{(2)}, U_0, V_0$ are known functions. Note that U_0, V_0 result from the nonhomogeneous boundary conditions.

The final step of the AEM

Collocating the equation for the transverse deflection Eq. (1) and the equations for plane stress problem Eqs (5) at the M internal nodal points and substituting the expressions for the displacements w, u, v and their derivatives from Eqs (17),(20) and (21), we finally obtain the following linear system of equations for the fictitious loads $b_i, b_i^{(1)}, b_i^{(2)}$

$$(\mathbf{K} + \mathbf{S})\mathbf{b} = \mathbf{G} \tag{22a}$$

$$\mathbf{A}_1 \mathbf{b}^{(1)} + \mathbf{B}_1 \mathbf{b}^{(2)} = \mathbf{G}_1 \tag{22b}$$

$$\mathbf{A}_2\mathbf{b}^{(1)} + \mathbf{B}_2\mathbf{b}^{(2)} = \mathbf{G}_2 \tag{22c}$$

where $\mathbf{K}$ is the bending stiffness matrix, $\mathbf{S}$ is the geometric stiffness matrix which depends on the membrane forces; $\mathbf{A_1}, \mathbf{A_2}, \mathbf{B_1}, \mathbf{B_2}$ are known matrices and $\mathbf{G}, \mathbf{G_1}, \mathbf{G_2}$ known vectors.

For the buckling problem the plate is subjected only to inplane loads and Eq. (22a) leads to the following eigenvalue problem

$$(\mathbf{K} - \eta\mathbf{S})\,\mathbf{b} = 0 \tag{23}$$

where η is the load factor.

Optimization procedure

The shape optimization problem is solved using a FORTRAN nonlinear minimization algorithm with linear and nonlinear inequalities. At each step of the iterative procedure the thickness variation law is required in order to solve Eqs (1), (5) and evaluate the objective function and the equality and inequality constraints. This can be established by its approximation with the design parameters. In this investigation the following approximations have been considered :

a) polynomial of certain degree :

$$h(\mathbf{x}) = a_0 + a_2 x + a_2 y + a_3 x^2 + a_5 xy + a_4 y^2 + \ldots \tag{24}$$

where $a_k, (k = 0,1,2,..)$ are the design variables.

b) radial basis functions series

$$h(\mathbf{x}) = \sum_{k=1}^{M_1} \alpha_k f_k(r) \tag{25}$$

where $f(r)$ are the radial basis functions of polynomial type $f(r) = 1 + r + r^3$ or multiquadrics $f(r) = \sqrt{r^2 + c^2}$; $r = \|\mathbf{x} - \mathbf{x}_k\|$ with $\mathbf{x}_k$ being M_1 collocation points inside Ω and c is an arbitrary shape parameter; a_k are the design variables

The maximum stiffness is achieved by minimizing the compliance [12], which is defined as

$$C = \int_\Omega wf d\Omega \tag{26}$$

In this investigation the requirement of slowly varying thickness is achieved by introducing a constraint on the magnitude of the principal curvatures of the thickness function. The principal curvatures $\kappa_{1,2}$ are given by the equation

$$\left(1 + h_{,x}^2 + h_{,y}^2\right)\kappa^2 + \frac{\left[\left(1 + h_{,x}^2\right)h_{,yy} - 2h_{,x}\,h_{,y}\,h_{,xy} + \left(1 + h_{,y}^2\right)h_{,xx}\right]}{\sqrt{1 + h_{,x}^2 + h_{,y}^2}}\kappa + \frac{h_{,xx}\,h_{,yy} - h_{,xy}^2}{1 + h_{,x}^2 + h_{,y}^2} = 0 \tag{27}$$

where h,qq , ($p,q = 0,x,y$) are the derivatives of the thickness function.

Numerical examples

Example 1

The square plate of Fig. 3 has been optimized in order to maximize the stiffness and the buckling load. The employed data are $E = 21 \times 10^6$ kN/m^2, $\nu = 0.3$. The inplane boundary conditions are shown in Fig. 3. The results were obtained using $N = 196$ boundary nodes and $M = 89$ internal collocation points. The thickness is approximated first by polynomial function of degree $n = 2$ and $n = 4$, then by radial basis function using $M_1 = 41$ nodal points. The inequality constraints were $0.05 < h < 0.25$ and $\lfloor \kappa_{\max} \rfloor < 0.1$. The buckling load and the compliance of the plate with uniform thickness $h = 0.1$ are employed as starting values at the optimization procedure. Tables 1 and 2 present the optimum values for compliance and buckling load for the simply supported and clamped plate. Fig. 4 shows the optimum thickness variation for maximum buckling load for the two cases of the boundary conditions. The optimum shapes are in agreement with that found by other researchers [Ref. 12].

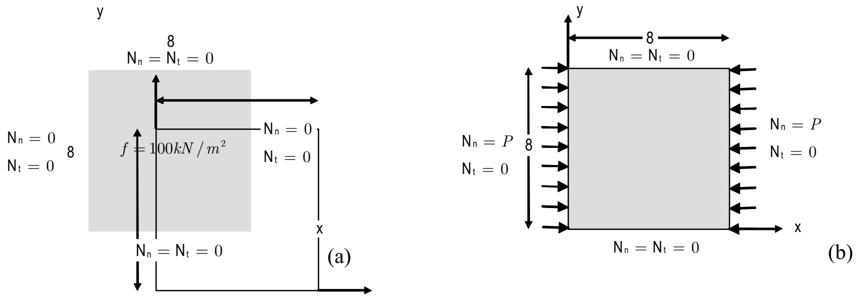

Figure 3: Plate geometry in example 1 (a) for maximum stiffness and (b) for maximum buckling load

Boundary conditions	Starting buckling load value ($h = 0.1$)	Approximating function		
		Polynomial		RBF
		$n = 2$	$n = 4$	$\sqrt{r^2 + c^2}$
Simply supported	1209	1259 (4.13%)	1483 (22.6%)	1489 (23.1%)
clamped	3082	4062 (31.2%)	4997 (62%)	4815 (56.2%)

Table 1. Optimum values of buckling loads in example 1. Lower values : percentage increases in buckling loads.

Boundary conditions	Starting value of compliance ($h = 0.1$)	Approximating function		
		Polynomial		RBF
		$n = 2$	$n = 4$	$1 + r + r^3$
Simply supported	2266	2215 (2.2%)	1739 (23.2%)	1882 (16.9%)
clamped	509	504 (0.98%)	292 (42.6%)	361 (29%)

Table 2. Minimum values of compliance in example 1. Lower values : percentage decreases in compliance.

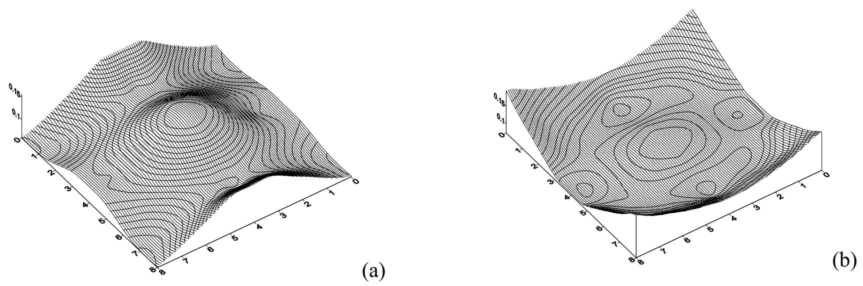

Figure 4: Optimum thickness for maximum buckling load of (a) a clamped plate and (b) a simply supported plate.

Example 2

A clamped circular plate with radius $r = 1\text{m}$, subjected to an inplane radial load N_n along the boundary, has been studied in order to increase the buckling load. The employed data are $E = 21 \times 10^6$ kN/m^2, $\nu = 0.25$ and the results were obtained with $N = 160$ boundary elements and $M = 166$ internal collocation points. The inequality constraints were $0.01 < h < 0.03$ and $\lfloor \kappa_{\max} \rfloor < 0.15$. Fig. 5a presents the optimum thickness for axisymmetric thickness variation using polynomial approximation of certain degree. Fig. 5b shows the optimum thickness for non axisymmetric variation using MQs for thickness approximation with $M_1 = 57$ nodal points ($N_{cr} = 271 kN/m$).

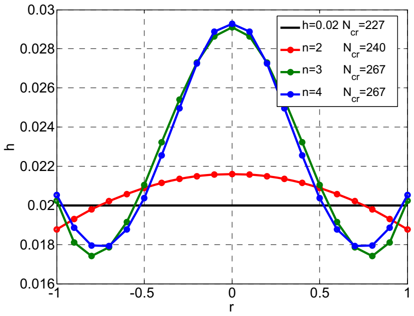

(a)

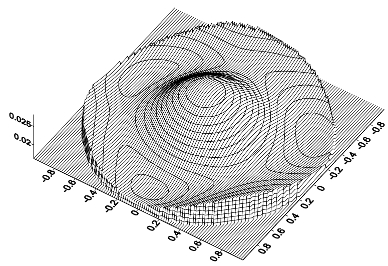

(b)

Figure 5: Optimum thickness for maximum buckling load (a) for polynomial axisymmetric thickness variation and (b) for non-axisymmetric variation.

Example 3

The simply supported triangular plate of Fig. 6a has been optimized in order to maximize the stiffness. The employed data are $E = 21 \times 10^6$ kN/m^2, $\nu = 0.3$ and the results were obtained using $N = 160$ boundary nodes and $M = 92$ internal collocation points. The inequality constraints were $0.02 < h < 0.3$ and $\lfloor \kappa_{\max} \rfloor < 0.3$. The compliance was reduced to $C_{\min} = 0.038$ ($C = 0.0456$ for uniform thickness $h = 0.2m$) and the optimum thickness variation is shown in Fig. 6b.

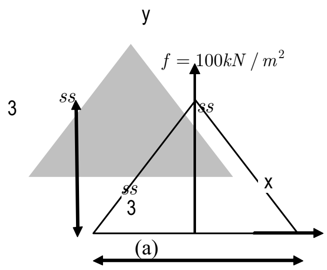

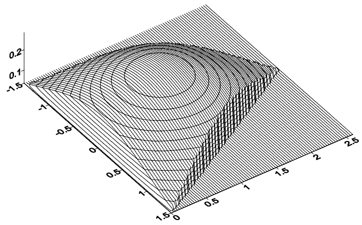

(b)

Figure 6: (a) triangular simply supported plate and (b) optimum thickness for maximum stiffness.

Example 4

The simply supported plate shown in Fig. 7a, which is subjected to a uniform surface transverse load $f = 100$ kN/m^2, has been optimized in order to maximize the stiffness. The employed data are $E = 21 \times 10^6$ kN/m^2, $\nu = 0.3$ and the results were obtained using $N = 252$ boundary nodes and $M = 132$ internal collocation points. The inequality constraints were $0.02 < h < 0.3$ and $\lfloor \kappa_{\max} \rfloor < 0.3$.

The compliance has been reduced to $C_{\min} = 22.32$ for the plate with the thickness distribution shown in Fig. 7b ($C = 29.05$ for uniform thickness $h = 0.2m$) .

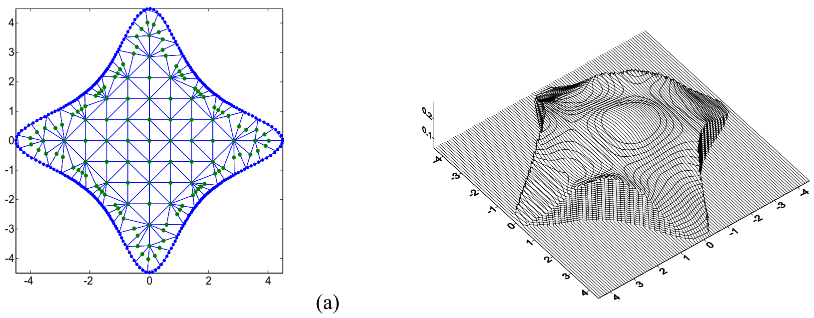

(a) (b)

Figure 7: (a) boundary and domain discretization for the plate in example 4 and (b) optimum thickness for maximum stiffness.

Conclusions

In this paper the thickness shape optimization is used to maximize the buckling load and the stiffness of a thin plate of arbitrary geometry having constant volume under any type of boundary conditions and loads. The problem is reduced to a nonlinear optimization problem under equality and inequality constraints. In each iteration of the optimization procedure, the plate bending and the plane stress problem with variable thickness are solved using the AEM. The advantages of the presented method can be summarized as :

1. The optimum design remains within the limits of the Kirchhoff plate theory by imposing restrictions on the curvature of the thickness function in order to obtain slowly varying thickness. Otherwise the optimization leads to thickness distributions with abrupt changes and discontinuities that result in unrealistic design solutions.
2. The AEM solution is efficient, accurate and overcomes the shortcoming of element resizing that is required in a possible FEM solution.
3. The inplane boundary conditions and the actual membrane forces due to thickness variation are taken into account in the buckling optimization problem.
4. The thickness distribution is approximated by appropriate RBF series, which can be used in the optimization of plates with complicated geometries. Moreover, the thickness optimization does not depend on the number of collocation points that is used for the RBF approximation in contrast to other methods, which depend on the plate discretization (FDM, FEM).
5. The optimum buckling load can be increased up to 62% while the compliance can be reduced to 42% in comparison to a plate with constant thickness and equal volume.

References

[1] M. Eisenberger and A. Alexandrov Buckling loads of variable thickness thin isotropic plates. *Thin-Walled Structures* **41,** 871–889 (2003).

[2] Y.-P. Xu and D. Zhou Three-dimensional elasticity solution for simply supported rectangular plates with variabl thickness. *J. Strain Analysis* **43,** 165–176 (2007).

[3] C.M. Wang, G. M. Hong and T. J. Tan Elastic buckling of tapered circular plates. *Computer & Structures* **55(6)**, 1055–1061 (1995).

[4] E.J. Sapountzakis and J.T. Katsikadelis Boundary element solution for plates of variable thickness. *Journal for Engineering Mechanics* **117(6),** 1241–1256 (1991).

[5] E.W.V. Chaves, G.R. Fernandes and W.S. Venturini Plate bending boundary element formulation considering variable thickness. *Engineering Analysis with Boundary Elements* **23,** 405–418 (1999).

[6] M.S. Nerantzaki and J.T. Katsikadelis Buckling of plates with variable thickness-an analog equation solution. *Engineering Analysis with Boundary Elements* **18,** 149–154 (1997).

[7] A. Mukherjee and M. Mukhopadhyay Finite element free flexural vibration analysis of plates having various shapes and varying rigidities. *Computer & Structures* **23(6)**, 807–812 (1986).

[8] N. Olhoff Optimal design of vibrating circular plates. *Int. J. Solids Structures* **6**, 139–156 (1970).

[9] N. Olhoff Optimal design of vibrating rectangular plates. *Int. J. Solids Structures* **10**, 93–109 (1974).

[10] R. Levy and A. Ganz Analysis of optimized plates for buckling. *Computer & Structures* **41(6)**, 1379–1385 (1991).

[11] M. Ozakca, N. Taysi and F. Kolcu Buckling analysis and shape optimization of elastic variable thickness circular and annular plates-II. Shape optimization. *Engineering Structures* **25**, 193–199 (2003).

[12] K.-T. Cheng and N. Olhoff An investigation concerning optimal design of solid elastic plates. *Int. J. Solids Structures* **17**, 305–323 (1981).

[13] D. Lamblin and G. Guerlement Finite element iterative method for optimal elastic design of circular plates. *Computer & Structures* **12**, 85-92 (1980).

[14] B. Bremec and F. Kosel Thickness optimization of circular and annular plates at buckling. *Thin-Walled Structures* **44**, 74–81 (2006).

[15] W.R. Spillers and R. Levy Optimal design for plate buckling. *Journal for Structural Engineering* **116(3)**, 850–858 (1990).

[16] D. Manickarajah, Y.M. Xie and G.P. Steven An evolutionary method for optimization of plate buckling resistance. *Finite Elements in Analysis and Design* **29**, 205–230 (1998).

[17] F. Niordson Optimal design of elastic plates with a constraint on the slope of the thickness function. *Int. J. Solids Structures* **19(2)**, 141–151 (1983).

[18] J.T. Katsikadelis The Analog Boundary integral Equation Method for nonlinear static and dynamic problems in continuum mechanics. *Journal of Theoretical and Applied Mechanics* **40**, 961-984 (2002).

[19] J.T.Katsikadelis and A.J. Yiotis The BEM for plates of variable thickness on nonlinear biparametric elastic foundation. An analog equation method. *Journal of Engineering Mathematics* **46,** 313-330 (2003).

[20] J.T.Katsikadelis and A.E.Armenakas New boundary equation solution to the plate problem. *J. Appl. Mech.-T. ASME* **56**, 364-374 (1989).

[21] J.T.Katsikadelis *Boundary Elements: Theory and Applications*. Elsevier, Amsterdam-London (2002).

Rapid Acoustic Boundary Element Method for Solution of 3D Problems using Hierarchical Adaptive Cross Approximation GMRES Approach

A. Brancati[1], M. H. Aliabadi[2] and I. Benedetti[3]

[1] Department of Aeronautics, Imperial College London, South Kensington Campus, SW7 2AZ London, UK, a.brancati@imperial.ac.uk

[2] Department of Aeronautics, Imperial College London, South Kensington Campus, SW7 2AZ London, UK, m.h.aliabadi@imperial.ac.uk

[3] On leave from DISAG Dip. Ing. Strutturale Aerospaziale Geotecnica, Università degli Studi di Palermo, Palermo, Italy

Keywords: Rapid Acoustic Boundary Element Method, Adaptive Cross Approximation, Hierarchical Approach, GMRES, speed-up ratio, large scale problems, high frequency range.

Abstract. This paper presents a new solver for 3D acoustic problems called RABEM (Rapid Acoustic Boundary Element Method). The Adaptive Cross Approximation and a Hierarchical GMRES solver are used to generate both the system matrix and the right hand side vector by saving storage requirement, and to solve the system solution. The potential and the particle velocity values at selected internal points are evaluated using again the Adaptive Cross Approximation (ACA). A GMRES without preconditioner and with a block diagonal preconditioner are developed and tested for low and high frequency problems. Different boundary conditions (i.e. Dirichlet, Neumann and mixed Robin) are also implemented. Herein the problem of engine noise emanating from the Falcon aircraft is presented. The tests demonstrated that the new solver can achieve CPU times of almost O(N) for low frequency and O($NlogN$) for high frequency problems.

Introduction

The need of faster solver for three dimension acoustic simulations is encouraged by required solution in higher frequency range, for large scale and more accurate geometries.
One of the most general and efficient numerical technique for solving acoustic problems is the Boundary Element Method (BEM) [1]. The boundary element discretisation of the surface of the problem leads to a non-symmetric and fully populated system matrix. Both the memory storage and the setting up of the system matrices for a standard BEM formulation are of O(N^2), where N denotes the degree of freedom. Moreover, direct solvers require O(N^3) operations while iterative solvers O(kN^2), where k is the number of iterations.
The ACA is an effective method for solving non-symmetric and fully populated matrices and decreases the CPU time significantly [2] and has been applied to the Helmholtz equation by, for example, [3]. The solution of linear system of equations is accelerated by calculating only few entries of the original matrix. The whole matrix is divided into two rank (low and full rank) blocks based on size and distance between a group of collocation points and a group of boundary elements. The ACA algorithm has been applied to the low rank blocks achieving approximately O(N) for both storage and matrix-vector multiplication [4].
Herein a solver for 3D boundary element solution of Helmholtz problems that uses a new hierarchical adaptive cross approximation technique coupled with GMRES is presented. Implementing different types of boundary conditions (i.e. Dirichlet, Neumann and mixed Robin) into the ACA solution algorithm is widely considered. The constant elements are utilized to discretize the problem. The test carried out show that the new assembly and solution technique can achieve CPU times of almost O(N) for low frequency and O($N\backslash log\ N$) for high frequency problems.

Hierarchical BEM for Acoustics

The BEM system of equations was represented using the hierarchical matrices in conjunction with Krylov subspace methods by, for example [5, 6], and herein is extended to BEM acoustic problems with different boundary conditions. This technique speeds up the computation, whilst maintaining the required accuracy and saving on the memory storage.

Matrix Assembly using the Collocation Method. In a hierarchical representation the boundary element matrix is subdivided by a collection of two groups of blocks called *low rank blocks*, that have a compressed representation, and *full rank blocks*, that are represented in their entirety. The classification of the blocks is achieved subdividing the whole mesh into cluster of closed elements. A block populated by integrating over a cluster of elements whose distance, suitably defined, from the cluster of collocation nodes is above a certain threshold is called admissible and it can be represented in the low rank format. The remaining *full rank blocks* are generated and stored in their entirety.

A preliminary hierarchical partition of the matrix index set is the basis of the process for the subdivision and classification of the blocks. Contiguous elements are detected on the basis of some computationally efficient geometrical criterion. The process starts from the complete set of indices $I=\{1,2...n\}$ where n denotes the number of collocation points. This initial set constitutes the root of the tree node. Each cluster in the tree is split into two subsets, called *sons*, on the basis of the longest extended dimension of the whole geometry or of the geometry of each cluster *son* (see Fig.1).

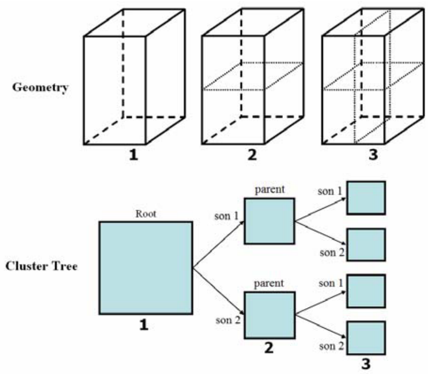

Fig. 1: A schematic of the first two iterations of the cluster tree creation: 1) the whole geometry is divided 2) into two parts, each of which is then subdivided again 3) into two parts.

The tree node that generates two sets of tree nodes is called the *parent*. The tree nodes that cannot be further split are called *leaves* of the tree. A leave of the tree is a tree node that cannot be further split because it contains a number of indices equal to or less than a minimum number n_{min}, called *cardinality* of the tree. This is a previously fixed value. This partition creates a binary tree of index subsets, or cluster tree, that constitutes the basis for the subsequent construction of the hierarchical block subdivision that will be stored in a quaternary *block tree*.

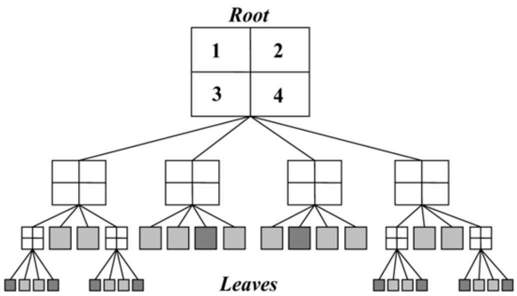

Fig. 2: A schematic presentation of the first three iterations that form the block tree. The light grey stands for low rank blocks, while the dark grey for full rank blocks.

The generation of the block tree is based on the previous found cluster tree and is created starting from the complete index $I \times I$ (both rows and columns) of the collocation matrix. The goal of this process is to split hierarchically the matrix into sub-blocks until that are classified as *leaves* of the tree (see Fig. 2). A *low-rank block* and a *full-rank block* are leaves that satisfy and not satisfy, respectively, an admissible criterion, based on a geometrical consideration related directly to the boundary mesh (see for example [7, 8]).
The admissible criterion can be written as

$$\min(diam\{\Omega_{x_0}\}, diam\{\Omega_x\} \le \eta \cdot dist(\Omega_{x_0}, \Omega_x) \tag{1}$$

where Ω_{x_0} and Ω_x denote the cluster of the row and the column elements, respectively, and η is a positive parameter influencing the number of admissible blocks and the convergence speed of the adaptive approximation of low rank blocks.
Let C be an $m \times n$ admissible block. It admits the low rank representation

$$C \approx C_k = A \cdot B^T = \sum_{i=1}^{k} a_i \cdot b_i^T \tag{2}$$

where *A* is of order $m \times k$ and *B* is of order $n \times k$, with *k* being the *rank* of the new representation. Sometimes it is useful to represent the matrix using the alternative sum representation, where a_i and b_i are the *i-th* columns of *A* and *B*, respectively. The approximate representation allows storage savings with respect to the full rank representation and speeds up the matrix-vector product [9].

Boundary Conditions and Right Hand Side Setting The actual setting of the final system for a problem where different boundary conditions are specified requires some additional considerations when ACA is applied. Different types of boundary conditions are here considered in such a way that rigid, soft and absorbing surfaces can all be studied in order to simulate a real situation and to perform an eventual parametric analysis.
The ACA algorithm is applied to one or both of the matrices **G** and **H** depending upon the boundary conditions that are predominant for each block matrix. Particular care must be taken when not pure Dirichlet, Neumann or mixed Robin conditions are applied. There may be four different cases that require different approaches [10]:

- BCs mainly in terms of flux (or potential) except for the k^{th} value expressed in terms of potential (or flux);
- BCs mainly in terms of flux except for the k^{th} value expressed in terms of impedance;
- BCs mainly in terms of potential except for the k^{th} value expressed in terms of impedance;
- BCs mainly in terms of impedance except for the k^{th} value expressed in terms of potential (or flux).

Additional considerations for the setting up of the right hand side vector are now explained. When the ACA algorithm is applied, the routine that calculates the i^{th} row of one of the block matrices **G** or **H** also calculates the i^{th} row of the other block matrix. Thus, the right hand side contribution of that row for the block matrix analyzed is directly calculated. Now, there are two main cases to analyze.

1. BCs mainly in terms of flux (or potential).
   The ACA algorithm is applied again on the matrix **G** (or **H**). A frequent occurrence is when all the boundary conditions are zero. In this case there is no need to calculate the contribution of the block matrix to the final right hand side and another block matrix can be analyzed. Moreover, owing to the fact that the number of entries needed for the ACA is, in most the cases, equal for both the block matrix **G** or **H**, may be convenient to calculate the contribution to the right hand side with a standard procedure.

2. BCs mainly in terms of admittance.
   Once the ACA as been applied to the block matrix **H**, the possible contribution to the right hand side vector **F**, due to the presence of the k^{th} value of the boundary conditions expressed in terms of potential, is easily calculated by multiplying each column of the ACA to the k^{th} value of each row with opposite sign. Finally, if the ACA algorithm applied to the block matrix **G** is also successful reached, the contribution to the right hand side of the eventual presence of the boundary condition expressed in terms of flux is clearly calculated.

System Solution The solution of the system can be computed through iterative solvers with or without preconditioners, once the system matrix has been represented in the hierarchical form.
In this study the value of the parameter η is 10 and the cardinality is set to 22. These values are chosen because they give the best performances. Being more specific, the value of the cardinality is quite restricted. As this value decreases, many blocks that satisfy the admissible criterion need, in fact, a bigger storage memory than if the same block is considered to be full rank. A direct consequence of it is a higher value of the CPU time. Nevertheless, the value of the parameter η can be modified between 1 and 1000 without loss of accuracy and resulting in a 5% CPU time acceleration. Furthermore, the optimum value of this parameter depends upon the geometry and the elements of the mesh.
Fig (3) shows the block-wise storage requirements of the collocation matrix generated by the ACA algorithm for four different values of η (1, 2, 4 and 10). The tone of grey is proportional to the ratio between the memory required for the low rank representation and the memory required for a standard format. Hence black blocks stand for the full rank block matrix, while almost white blocks are those for which the ACA compression works better.

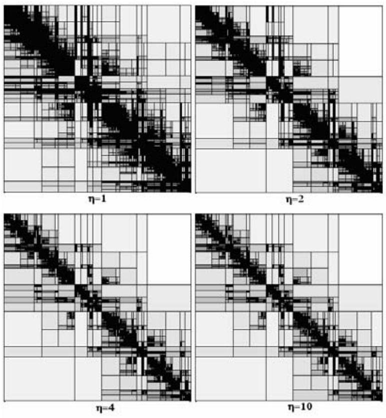

Fig. 3: Block-wise representation of the ACA generated matrix for η=1, η=2, η=4 and η=10.

Results

The simulation of a 53,074 elements mesh (see Fig. 4) of a model representing the Dassault Falcon airplane is presented.

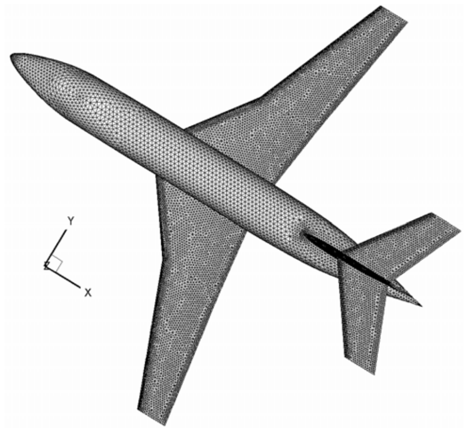

Fig. 3: Block-wise representation of the ACA generated matrix for η=1, η=2, η=4 and η=10.

The total length of the aircraft is 18.5m and the wing extension is 22.46m. The highest frequency applied was 100 Hz. The sizes of the smallest and the largest triangles are 8.73E-03 and 0.19 millimeter, respectively, so the maximum frequency that can be applied is around 250 Hz. In the simulation performed all the surfaces has been set as hard and two monopole sources with unit complex potential amplitude have been inserted where the two engines are generally located in this airplane. The CPU time ratio, obtained by dividing the CPU time for different frequencies and preconditioners with the frequency of 25Hz for the unpreconditioned GMRES, is shown in Fig. 5 for three frequencies (25, 50 and 100 Hz). Finally, Fig. 6 shows the Sound Pressure Level (SPL) at 100Hz. It is important to point out that a standard BEM code cannot solve such a simulation because the storage required is around 45 Gb whereas the limit for a medium desktop is 2Gb. Moreover, the speed up ratio, defined as the ratio between the CPU time of the standard code and the CPU time of the RABEM code, would be more than 350!

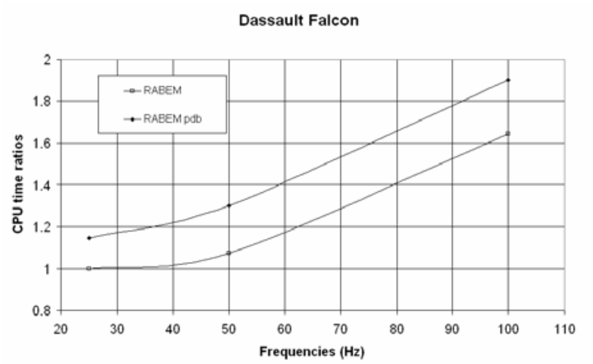

Fig. 4: Comparison between the unpreconditioned and block diagonal preconditioned GMRES for a Dassault Falcon meshed with 53,074 triangular elements.

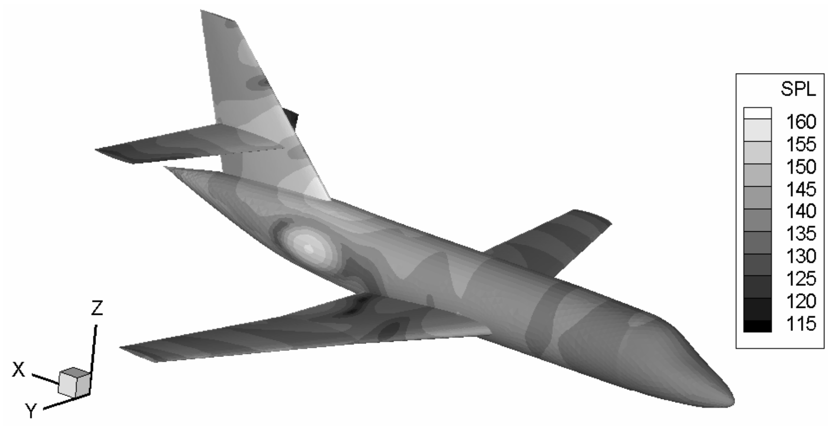

Fig. 4: Sound Pressure Level for a Falcon geometry with two monopoles at 100 Hz.

Conclusion

A new Rapid Acoustic BEM solver (RABEM) for 3D numerical simulation using the ACA algorithm in conjunction with GMRES has been herein presented. This study demonstrates that the new approach reduces significantly the storage and the solution time. Moreover, the simulation shown that the new solver can achieve CPU times of almost O(N) for low frequency and O($N \cdot \log N$) for high frequency problems.

Acknowledgment

This work was carried out with the support of European research project (SEAT: Smart tEchnologies for stress free Air Travel) AST5-CT-2006-030958. The authors are especially grateful to Dr. Vincenzo Mallardo for our many and always fruitful conversations. We wish to thank Dr. Joaquim Peiro for the Falcon mesh.

References

[1] L.C.Wrobel and M.H Aliabadi *The Boundary Element Method, Vol1 :Applications in Thermo-Fluids and Acoustics, Vol2: Applications in Solids and Structures,* Wiley (2002).

[2] M. Bebendorf and S. Rjasanow *Adaptive low-rank approximation of collocation matrices. Computing*, **70** (1), 1-24 (2003).

[3] O. Von Estorf, S. Rjasanow, M. Stolper and O. Zalesk *Two efficient methods for a multifrequency solution of the Helmholtz equation: Computing and Visualization in Science*,

8, 159-167 (2005).

[4] I. Benedetti, M. H. Aliabadi and G. Daví *A fast 3D dual boundary element method based on hierarchical matrices: International Journal of Solids and Structures*, **45 (**7-8), 2355-2376 (2007).

[5] C. Y. Leung and S. P. Walker *Iterative solution of large three dimensional BEM elastostatic analyses using the GMRES technique: International Journal for Numerical Methods in Engineering*, **40**, 2227-2236 (1997).

[6] M. Merkel, V. Bulgakov, R. Bialecki and G. Kuhn *Iterative solution of large-scale 3D-BEM industrial problems: Engineering Analysis with Boundary Elements*, **2**, 183-197(1998).

[7] M. Bebendorf and S. Rjasanow *Adaptive low-rank approximation of collocation matrices: Computing*, **70 (**1), 1-24 (2003).

[8] M. Bebendorf *Approximation of boundary element matrices: Numerische Mathematik*, **86**, 565-589 (2000).

[9] L. Grasedyck and W. Hackbusch *Construction and arithmetics of H-matrices: Computing*, vol **70**, 295-334 (2003).

[10] A. Brancati, M. H. Aliabadi and I. Benedetti. *Hierarchical Adaptive Cross Approximation GMRES Technique for Solution of Acoustic Problems Using the Boundary Element Method: CMES: Computer Modeling in Engineering & Sciences*. Accepted for publication in 2009.

Analysis of composite bonded joints using the 3D boundary element method

Souza, C. A. O.[1]; Sollero, P.[2]; Santiago, A. G.[3]; Albuquerque, E. L.[4]
Faculty Mechanical Engineering, State University of Campinas
13083-970, Campinas, Brazil
[caos[1], sollero[2], gsantiago[3], ederlima[4]]@fem.unicamp.br

Keywords: Bonded joints; composite material; boundary element; sub-regions; 3D anisotropy

Abstract

Bonded, riveted and bolted joints are frequently used in aeronautic industries. With recent development of new materials and new manufacturing techniques, bonded joints have been increasingly used due to some distinct advantages over traditional riveted and bolted ones, namely: more efficient load transfer, better sealing, better finishing and, most important for aeronautical applications, less weight. The design of bonded joints is based upon analyses to estimate peeling and shear stresses in the adhesive and the displacement field along the bonded region.

This paper describes an application of 3D boundary element method to bonded joints through the development of a computational tool for analysis of bonded joints in composite materials for aeronautical structures.

Introduction

The use of bonded, riveted and bolted joints to assemble components or structural parts is increasing in aeronautic industries. The design of bonded joints is based upon analyses to estimate peeling and shear stresses in the adhesive and the displacement field along the bonded region. The boundary element method (BEM) has proven to have good aproximation of high stress gradients such as those found in the overlap region of bonded joints or in regions of stress concentrations. Given the fact that the design of bonded joints are a critical technology in modern design and the stresses in the bonded region have steep gradients, one would expect a frequent use of BEM in the analysis of bonded joints. A previous application of BEM to bonded joints was presented by [1].

This paper presents an application of 3D boundary element method through the development of a computational tool for analysis of composite bonded joints.

Numerical results of lap joints show the potential of the boundary element method in the analysis of bonded joints.

Boundary element formulation for 3D anisotropic materials

The weighted residual technique may be used to derive the boundary integral equation. The basic equations of solid mechanics yield the following integral equation for elastostatics problems, named *Somigliana's identity* [2]:

$$c(\xi)u_i(\xi) = \int_\Gamma t_j(\xi)u_{ij}^*(\xi,x)d\Gamma - \int_\Gamma u_j(\xi)t_{ij}^*(\xi,x)d\Gamma \tag{1}$$

The coefficient $c(\xi)$ depends on the position of the source point ξ in relation to the boundary which is being integrated, $t_j(\xi)$ and $u_j(\xi)$ are tractions and displacements of the system, $t_{ij}^*(\xi,x)$ and $u_{ij}^*(\xi,x)$ are fundamental solutions for tractions and displacements.

In this work the composite adherends of the bonded joints are considered as transversely isotropic materials. Because this, the 3D anisotropic fundamental solution is used. The derivation of the anisotropic fundamental solution is carried out using the Radon transform, which is defined by [3]:

$$\hat{f}(\alpha,z_i) \equiv \Re\left\{f(x_i)\right\} = \int_\Omega f(x_i)\delta(\alpha - z_i x_i)d\Omega \tag{2}$$

where the integration is performed over the plane $z_i x_i = \alpha$, which is filtered out from the full-space by the Dirac function, as shown in Fig. 3. The inverse transform is given by:

$$f(x_i) = \Re^{-1}\left\{\hat{f}(\alpha,z_i)\right\} = -\frac{1}{8\pi^2}\int_{z_i z_i = 1}\left[\frac{\partial^2 \hat{f}}{\partial \alpha^2}\right]_{\alpha = z_i x_i} d\Gamma(z_i) \tag{3}$$

where the integration is carried out over the surface of a unit sphere, also shown in Fig. 1.

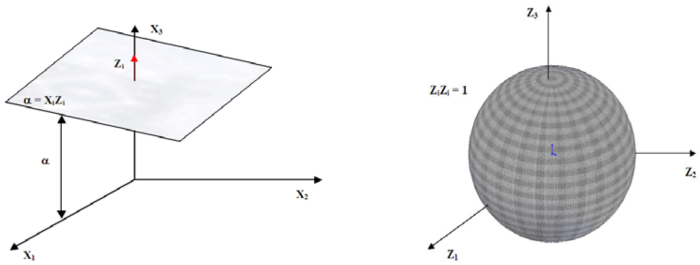

Fig. 1 – Radon transform and inverse Radon transform.

The fundamental solution of anisotropic elastostatics, u^*_{mk}, is defined by:

$$C_{ijkl}u^*_{mk,lj}(x,\xi) = -\delta_{im}\delta(x,\xi) \tag{4}$$

This yields:

$$u^*_{jm} = \frac{1}{8\pi^2 r}\oint_{\varphi}(M^{zz}_{jm}(z_i(\varphi)))^{-1}d\varphi \tag{5}$$

where the tensors that appear in the integrands are given in the z_i-space of the Radon transform by:

$$M^{ab}_{ik} = C_{ijkl}a_j b_l \tag{6}$$

Multi-region technique

The multi-region technique is employed in problems where the material properties change for different materials in the structure [4]. This work uses a model with three multi-regions, one for the upper adherend, one for the layer adhesive an one for the bottom adherend. A generic model of this type can be illustrated as shown in Fig. 2, where the domain is divided into three sub-domains.

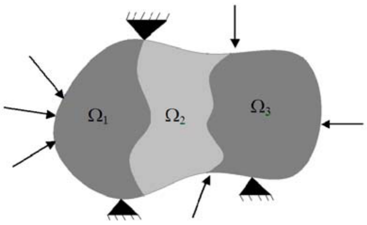

Fig. 2 - Body composed by three sub-domains

Suppose, that the model is be discretized by constants elements, according [5], the matrices $H]$ and $[G]$ can be written for each domain individually. The final matrix systens becomes:

$$\begin{bmatrix} G_E^1 & G_E^{1N} & G_I^1 & 0 & 0 & 0 & 0 & 0 \\ 0 & 0 & -G_I^1 & G_E^{2N} & G_E^2 & 0 & 0 & 0 \\ 0 & 0 & 0 & G_E^2 & G_E^{2N} & G_I^2 & 0 & 0 \\ 0 & 0 & 0 & 0 & 0 & -G_I^3 & G_E^{3N} & G_E^3 \end{bmatrix} \begin{Bmatrix} t_E^1 \\ t_E^{1N} \\ t_I \\ t_I \\ t_I \\ t_I \\ t_E^{3N} \\ t_E^3 \end{Bmatrix} = \begin{bmatrix} H_E^1 & H_E^{1D} & H_I^1 & 0 & 0 & 0 & 0 & 0 \\ 0 & 0 & H_I^2 & H_E^{2D} & H_E^2 & 0 & 0 & 0 \\ 0 & 0 & 0 & H_E^2 & H_E^{2D} & H_I^2 & 0 & 0 \\ 0 & 0 & 0 & 0 & 0 & H_I^3 & H_E^{3D} & H_E^3 \end{bmatrix} \begin{Bmatrix} u_E^1 \\ u_E^{1D} \\ u_I \\ u_I \\ u_I \\ u_I \\ u_E^{3D} \\ u_E^3 \end{Bmatrix} \qquad (7)$$

where the superscripts 1, 2 and 3 referred to sub regions 1, 2 and 3 respectively, and superscripts N and D referred to Neumann and Dirichlet boundary conditions.

Numerical results

The simulation was made for transversely isotropic material (composite). Fig. 3 shows the geometric model:

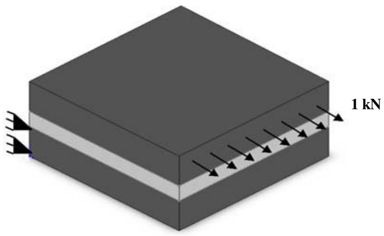

Dimensions	Values (mm)
Overlap length	10
Overlap width	10
Adherend thickness	2
Adhesive thickness	1

Fig. 3 – Geometric model considered in analysis

Table 1 lists the material properties for the transversely isotropic simulation:

Table 1 - Properties for the Trans. Iso adherends and adhesive

Propertie	Adherend Trans. Iso	Adhesive
E_1	2 GPa	4.82 GPa
E_2	1 GPa	
ν_1	0.3	0.4
ν_2	0.2	
Rotation	30º	

Figure 4 shows the shear stress along the overlap region through the middle of the adhesive layer. The results are compared with the analytic solution from [6], for isotropic material. Note that for transversely isotropic adherend, the shear stress in the adhesive, reach lower levels that the isotropic adherend.

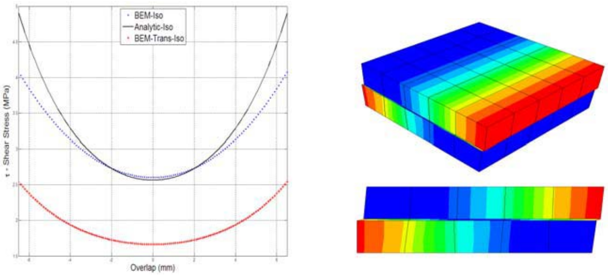

Fig. 4 – Shear stress distribution in the adhesive for Trans. Iso. Adherends.

Conclusions

This paper shows that the BEM can be used effectively in stress analysis of bonded joints. The results show that BEM has the potential of producing good resolution of stress gradient and robust enough for parametric study of bonded joints. The anisotropic fundamental solution was adequate to simulate composite materials. Finally, the sub region technique was also appropriate in the analysis of bonded joints, considering that in this type of problem there are at least, two materials involved.

Acknowledgments

The authors would like to thanks FAPESP (The State of São Paulo Research Foudation) and AFOSR (Air Force Office of Scientific Research) for the financial support of this work.

References

[1] Vable, M. & Maddi, J. R. (2004). *Boundary element analysis of adhesively bonded joints*. International Journal of Adhesion & Adhesives. Elsevier.

[2] Kane, J. H. (1994). *Boundary Element Analysis in Engineering Continuum Mechanics*. Prentice-Hall, Inc.

[3] Gaul, L., Kögl, M. & Wagner, M. (2003). *Boundary Element Methods for Engineers and Scientists: An Introductory Course with Advanced Topics*. Springer.

[4] Beer, G. (2001). *Programing the Boundary Element Method - An Introduction to Engineers*. John Wiley & Sons.

[5] Aliabadi, M. H. (2002). *The Boundary Element Method - Vol. 2 - Aplications in Solids and Structures*. John Wiley & Sons.

[6] Goland, M. & Reissner, E. *The stresses in cemented joints*. J. Appl. Mech., Trans. ASME., 1944, 66, A17–A27.

Conceptual Completion of the Simplified Hybrid Boundary Element Method

Maria F. F. de Oliveira[1*] and Ney A. Dumont[2]

[1] Computer Graphics Technology Group (Tecgraf), Pontifical Catholic University of Rio de Janeiro, 22453 900, Brazil. e-mail: mariafer@tecgraf.puc-rio.br

[2] Department of Civil Engineering, Pontifical Catholic University of Rio de Janeiro, 22453 900, Brazil. e-mail: dumont@puc-rio.br

Keywords: Hybrid boundary element method, spectral properties, elasticity problems.

Abstract. The paper outlines the basic features of a method that, although extremely economical in terms of mathematical concepts, code implementation and overall computation costs, leads to numerical results that are as accurate as in the variational and the conventional boundary element methods, as shown in an example.

Introduction

The hybrid boundary element method (HBEM) was introduced about two decades ago on the basis of the Hellinger-Reissner potential, as a generalization of Pian's hybrid finite element method [1, 3, 4]. The formulation requires evaluation of integrals only along the boundary and makes use of fundamental solutions (Green's functions) to interpolate fields in the domain. Accordingly, an elastic body of arbitrary shape may be treated as a single finite macro-element with as many boundary degrees of freedom as desired. In the meantime, the formulation has evolved to several application possibilities, including time-dependent problems, fracture mechanics, and non-homogeneous materials [6, 8, 12]. The original method makes use of a flexibility matrix **F**, for which evaluation of integrals along the entire boundary is required.

A simplified, although equally accurate, version of the HBEM was proposed about a decade ago [5, 11]. This simplified hybrid boundary element method (SHBEM) makes use of a displacement matrix that is obtained directly from the fundamental solution, with which the time-consuming evaluation of **F** is circumvented. In either formulation, submatrices about the main diagonal cannot be obtained by mathematical means: their evaluation requires the use of spectral properties that are directly or indirectly related to rigid-body displacements, for a bounded domain (or for the complementary domain, in case of an unbounded region) [3, 4]. For some specific topological configurations, however, as in case of notches, for axisymmetric problems or for some spectral abnormalities related to material non-homogeneity, this procedure may lead to local mathematical indefinitions (approximate zero by zero divisions) [13] and the diagonal submatrices can only — if ever — be obtained by interpolation of values from adjacent coefficients.

This paper presents new theoretical developments that provide a definitive solution to the issue [14]. The SHBEM relies basically on a virtual work statement and on a displacement compatibility equation. The key improvement consists in correctly applying a contragradient theorem to derive simple relations that are generally valid and can successfully substitute for the spectral properties, as it is required for the numerical solution to improve with mesh refinement. Actually, an underlying hybrid virtual work principle had been identified since the onset of the SHBEM, but its application was precluded by some until recently not well understood theoretical subtleties. Now, once some simple stress or strain cases are identified as inherent to a given problem, it is always possible to find a set of linearly independent analytical solutions to provide sufficient equations for the evaluation of the diagonal submatrices, regardless of topology and spectral properties.

Numerical results are consistent with the ones obtained in terms of spectral properties, whenever available, and also pass convergence tests. The new theoretical improvements are validated by a numerical example for an axisymmetric problem, which is among the most critical ones in terms of topological properties [14].

Problem Formulation

Let an elastic body be submitted to tractions $\bar{t}_i$ on part Γ_σ of the boundary Γ and to displacements $\bar{u}_i$ on the complementary part Γ_u. For the sake of brevity, body forces are not included [10]. One is attempting to find the best approximation for stresses and displacements, σ_{ij} and u_i, such that

$$\sigma_{ji,j} = 0 \quad \text{in the domain} \quad \Omega, \tag{1}$$

$$u_i = \bar{u}_i \quad \text{along} \quad \Gamma_u \quad \text{and} \quad t_i = \sigma_{ij}\,\eta_j = \bar{t}_i \quad \text{along} \quad \Gamma_\sigma \tag{2}$$

in which η_j is the outward unit normal to the boundary. Indicial notation is used.

Stress and Displacement Assumptions. Two independent trial fields are assumed, according to the hybrid methodology proposed by Pian [1]. The displacement field is explicitly approximated along the boundary by u_i^d, where $(\,)^d$ means *displacement assumption*, in terms of polynomial functions u_{im} with compact support and nodal displacement parameters $\mathbf{d} = [d_m] \in \mathbb{R}^{n^d}$, for n^d displacement degrees of freedom of the discretized model. An independent stress field σ_{ij}^s, where $(\,)^s$ stands for *stress assumption*, is given in the domain in terms of a series of fundamental solutions σ^*_{ijm} with global support, multiplied by point force parameters $\mathbf{p}^* = [p^*_m] \in \mathbb{R}^{n^*}$ applied at the same boundary nodal points m to which the nodal displacements d_m are attached ($n^* = n^d$). Displacements u_i^s are obtained from σ^s_{ij}. Then,

$$u_i^d = u_{im}\,d_m \quad \text{on} \quad \Gamma \quad \text{such that} \quad u_i^d = \bar{u}_i \quad \text{on} \quad \Gamma_u \quad \text{and} \tag{3}$$

$$\sigma^s_{ij} = \sigma^*_{ijm}\,p^*_m \quad \text{such that} \quad \sigma^*_{jim,j} = 0 \quad \text{in} \quad \Omega \tag{4}$$

$$\Rightarrow \quad u_i^s = u^*_{im}\,p^*_m + u^r_{is}\,C_{sm}\,p^*_m \quad \text{in} \quad \Omega \tag{5}$$

where u^*_{im} are displacement fundamental solutions corresponding to σ^*_{ijm}. Rigid body motion is included in terms of functions u^r_{is} multiplied by arbitrary constants C_{sm} [9, 10]. For convenience, u^r_{is} is normalized so as to yield, when evaluated at the nodal points m, the orthogonal matrix $\mathbf{W} = [W_{ms}] \in \mathbb{R}^{n^d \times n^r}$ with n^r columns of nodal rigid body displacements introduced in eq. (9) as $u^r_{is} = u_{in} W_{ms}$ on Γ [10].

Governing Matrix Equations

The Hellinger-Reissner potential, based on the two-field assumptions of the latter section, as implemented by Pian [1] and generalized by Dumont [4], leads to two matrix equations that express nodal equilibrium and compatibility requirements. In the following simplified developments, the same equilibrium matrix equation is obtained in terms of virtual work (which is a variational approach), but the set of compatibility equations is obtained by direct evaluation of displacements at the boundary nodal points (which is non-variational).

Displacement Virtual Work. In the absence of body forces, equilibrium is weakly enforced by

$$\int_\Omega \sigma_{ij}\,\delta u_{i,j}\,\mathrm{d}\Omega = \int_{\Gamma_\sigma} \bar{t}_i\,\delta u_i\,\mathrm{d}\Gamma \tag{6}$$

for $\sigma_{ij} = \sigma_{ji}$. Assuming that σ_{ij} is approximated according to eq. (4) and that δu_i is given by eq. (3), integration by parts of the term at the left-hand side of eq. (6) and application of Green's theorem yield

$$\delta d_n \left[\int_\Gamma \sigma^*_{ijm}\,\eta_j\,u_{in}\,\mathrm{d}\Gamma - \int_\Omega \sigma^*_{ijm,j}\,u_{in}\,\mathrm{d}\Omega \right] p^*_m = \delta d_n \left[\int_\Gamma t_i\,u_{in}\,\mathrm{d}\Gamma \right] \tag{7}$$

Then, for arbitrary nodal displacements δd_n one obtains the matrix equilibrium equation

$$H_{mn}\,p^*_m = p_n \quad \text{or} \quad \mathbf{H}^{\mathrm{T}}\,\mathbf{p}^* = \mathbf{p} \tag{8}$$

in which $\mathbf{H} = [H_{nm}] \in \mathbb{R}^{n^d \times n^*}$, given by the first expression in brackets in eq. (7), is the same double layer potential matrix of the collocation boundary element method [7], and $\mathbf{p} = [p_n] \in \mathbb{R}^{n^d}$, given as the second term in brackets in eq. (7), are equivalent nodal forces obtained as in the displacement finite element method. The domain integral of eq. (7) is actually void, since σ^*_{ijm} are fundamental solutions. Singular integration issues of H_{mn} for m and n referring to the same nodal point are solved according to standard mathematical means [7].
In eq. (8), $\mathbf{H}^{\mathrm{T}}$ is an equilibrium matrix that transforms forces $\mathbf{p}^*$ of the stress reference system into equivalent nodal forces $\mathbf{p}$ obtained according to the boundary displacement assumptions. For a finite domain, $\mathbf{H}$ is singular

and its null space is spanned by the nodal rigid body displacements, given for convenience as an orthogonal matrix $\mathbf{W} = [W_{ms}] \in \mathbb{R}^{n^d \times n^r}$ with n^r columns as

$$\mathbf{W} = N(\mathbf{H}) \quad \Rightarrow \quad \mathbf{V} = N(\mathbf{H}^{\mathrm{T}}) \tag{9}$$

One uses the equation above to introduce a (for convenience) orthogonal basis $\mathbf{V} = [V_{ms}] \in \mathbb{R}^{n^* \times n^r}$, which has played a major role in the development of the hybrid boundary element method [4] and, differently from $\mathbf{W}$, has properties that are intrinsically correlated with the topology of the problem one is attempting to analyze [13]. For the moment, one checks that, for consistency of eq. (8),

$$\mathbf{W}^{\mathrm{T}}\,\mathbf{p} = \mathbf{0} \quad \text{and} \quad \mathbf{V}^{\mathrm{T}}\,\mathbf{p}^* = \mathbf{0} \tag{10}$$

Nodal Displacement Compatibility. Application of the Hellinger-Reissner potential leads to, besides eq. (6), a stress virtual work statement that enables writing a set of compatibility equations between the nodal displacements $\mathbf{d}$ and equivalent nodal displacements $\mathbf{d}^*$ that are related to the stress reference system given in terms of fundamental solutions [4, 9]. This set of equations relies on the evaluation of a flexibility matrix $\mathbf{F}^*$ that transforms $\mathbf{d}^* = \mathbf{F}^*\mathbf{p}^*$ and such that, for consistency, $\mathbf{F}^*\mathbf{V} = \mathbf{0}$, when dealing with a finite domain. Application of the formulation to the complementary unbounded domain leads to the conclusion that, in a fully variational framework, but not as the direct result of a variational statement, one is entitled to transform point forces p^*_m into nodal displacements d_n by directly using the fundamental solution u^*_{im}, according to the following eq. (11). This has led to the *simplified* hybrid boundary element method [5, 10], in which the time-consuming evaluation of the flexibility matrix $\mathbf{F}^*$ of the firstly developed, fully variational hybrid formulation [3, 4] could be circumvented.

Actually, one may dispense with any reference to the Hellinger-Reissner potential and just establish that both eqs. (3) and (5) apply to the boundary nodal points, that is,

$$d_n = U^*_{nm}\,p^*_m + W_{ns}\,C_{sm}\,p^*_m \quad \text{or} \quad \mathbf{d} = \mathbf{U}^*\,\mathbf{p}^* + \mathbf{W}\,\mathbf{C}\,\mathbf{p}^* \tag{11}$$

where $\mathbf{U}^* = [U^*_{nm}] \in \mathbb{R}^{n^d \times n^*}$ corresponds to the fundamental solution u^*_{im} measured as d_n at the nodal degree of freedom n for a unit point force p^*_m applied at the nodal degree of freedom m. For singular fundamental solutions, the coefficients of $\mathbf{U}^*$ cannot be directly measured if m and n refer to the same nodal point, as the singularity points are excluded from the domain Ω. This feature is consistent with the requirement that u^*_{im} be analytical in Ω. Then, the coefficients of $\mathbf{U}^*$ about its main diagonal can only be obtained by means of a global, problem-dependent, assessment of the linear algebra properties of eq. (11) in conjunction with eq. (8).

Assuming for the moment that $\mathbf{U}^*$ is completely known, one may pre-multiply eq. (11) by $\mathbf{W}^{\mathrm{T}}$ and arrive at

$$\mathbf{C}\,\mathbf{p}^* = \mathbf{W}^{\mathrm{T}}(\mathbf{d} - \mathbf{U}^*\,\mathbf{p}^*) \tag{12}$$

which, applied to eq. (11), leads to

$$\mathbf{P}^{\perp}_{W}\,\mathbf{U}^*\,\mathbf{p}^* = \mathbf{P}^{\perp}_{W}\,\mathbf{d} \tag{13}$$

where $\mathbf{P}^{\perp}_{W} = \mathbf{I} - \mathbf{P}_W = \mathbf{I} - \mathbf{W}\,\mathbf{W}^{\mathrm{T}}$ is an orthogonal projector [2]. For a finite domain, only displacements that are orthogonal to rigid body motions can be transformed between the stress and displacement reference systems.

A Hybrid Virtual Work Statement

In the initial formulation of the SHBEM, the unevaluated submatrices about the main diagonal of $\mathbf{U}^*$ were obtained by applying to eq. (11) a spectral property related to the basis $\mathbf{V}$ defined in eq. (9), which requires the solution of a small system of equations for each node, similarly to the procedure described using eq. (16) [5, 10, 11]. However, the coefficients of $\mathbf{V}$ are intrinsically related to the topology of the problem under analysis. For some specific topological configurations, as in case of notches or for material non-homogeneity, the procedure using $\mathbf{V}$ may eventually lead to local mathematical indefinitions [13], which, although not incorrect, may turn out useless. There is a mechanical explanation for such an impasse, as the problem occurs when the stress gradient around a nodal point has a local character and therefore cannot be represented in terms of some global

spectral property. Such a lack of generality of the SHBEM became critical when the first author of the present paper tried to implement it to several types of axisymmetric problems [14].
The solution of the impasse was ultimately found in the frame of a hybrid virtual work principle, which may be stated as in the following [14]. In the present two-field formulation, $\mathbf{d}$ and $\mathbf{p}^*$ are the primary unknowns of the problem, to which correspond equivalent nodal forces and displacements $\mathbf{p}$ and $\mathbf{d}^*$, respectively. Since one is dealing with linear, elastic deformation, the energy $U(\mathbf{d})$ represented by the pair $(\mathbf{d}, \mathbf{p})$ must be equal to the complementary energy $U^c(\mathbf{p}^*)$ represented by the pair $(\mathbf{p}^*, \mathbf{d}^*)$. Let an admissible, virtual deformed state be represented by $\delta\mathbf{p}^*$ and $\delta\mathbf{d}$, which are interrelated by eq. (13) . Then, since $\delta U(\mathbf{d}) = \delta U^c(\mathbf{p}^*)$,

$$\delta\mathbf{p}^{*\mathrm{T}}\,\mathbf{P}_V^\perp\,\mathbf{d}^* = \delta\mathbf{d}^\mathrm{T}\,\mathbf{P}_W^\perp\,\mathbf{p} \quad \Rightarrow \quad \delta\mathbf{p}^{*\mathrm{T}}\,\mathbf{P}_V^\perp\,\mathbf{d}^* = \delta\mathbf{p}^{*\mathrm{T}}\,\mathbf{U}^{*\mathrm{T}}\mathbf{P}_W^\perp\,\mathbf{p} \tag{14}$$

where $\mathbf{P}_V^\perp = \mathbf{I} - \mathbf{P}_V = \mathbf{I} - \mathbf{V}\,\mathbf{V}^\mathrm{T}$ is an orthogonal projector [2]. $\mathbf{P}_W^\perp$ and $\mathbf{P}_V^\perp$ enter the equation above to ensure that only deformation-related equivalent nodal forces and displacements $\mathbf{p}$ and $\mathbf{d}^*$ take part in the statement. The expression on the right of eq. (14) is obtained from the first expression by substituting for $\delta\mathbf{d}^\mathrm{T}\,\mathbf{P}_W^\perp$ according to eq. (13). Then, since this expression is valid for any $\delta\mathbf{p}^*$, one arrives at the hybrid contragradient expression

$$\mathbf{U}^{*\mathrm{T}}\,\mathbf{P}_W^\perp\,\mathbf{p} = \mathbf{d}^* \quad \text{or} \quad \mathbf{U}^{*\mathrm{T}}\,\mathbf{P}_W^\perp\,\mathbf{p} = \mathbf{H}\,\mathbf{d} \tag{15}$$

as derived from eq. (13). One writes on the right a more convenient expression, already substituting for $\mathbf{d}^*$ with $\mathbf{H}$ as a kinematic transformation matrix — the contragradient of eq. (8).

Evaluation of the Coefficients about the Main Diagonal of $\mathbf{U}^*$

Equation (15) must apply to any admissible deformed configuration regardless of topological configurations. Let $(\mathbf{D}, \mathbf{P})$ be nodal displacements and equivalent forces corresponding to the simplest set of deformed configurations conceivable, as in a patch test for finite elements. Moreover, let $\mathbf{U}^*$ be formed by two parts, $\mathbf{U}^* = \mathbf{U}^*_{diag} + \bar{\mathbf{U}}^*$, in which $\mathbf{U}^*_{diag}$ contains the coefficients that still remain to be evaluated. Then, one may rewrite eq. (15) as

$$\mathbf{U}^{*\mathrm{T}}_{diag}\,\mathbf{P} = \mathbf{H}\,\mathbf{U} - \bar{\mathbf{U}}^{*\mathrm{T}}\,\mathbf{P} \tag{16}$$

and always guarantee a sufficient number of adequate simple deformed configurations to render eq. (16) uncoupled in small sets of well-conditioned equation systems with the submatrices comprised by $\mathbf{U}^{*\mathrm{T}}_{diag}$ as unknowns [14]. For two-dimensional elasticity, for instance, three simple deformed configurations,

$$u_{1x} = \frac{1-\nu}{2\mu}\,x, \quad u_{1y} = -\frac{\nu}{2\mu}\,y, \quad t_{1x} = \eta_x, \quad t_{1y} = 0; \tag{17}$$

$$u_{2x} = -\frac{\nu}{2\mu}\,x, \quad u_{2y} = \frac{1-\nu}{2\mu}\,y, \quad t_{2x} = 0, \quad t_{2y} = \eta_y \quad \text{and} \tag{18}$$

$$u_{3x} = \frac{2y - \nu\,x}{2\mu}, \quad u_{3y} = -\frac{\nu}{2\mu}\,y, \quad t_{3x} = \eta_y, \quad t_{3y} = \eta_x \tag{19}$$

where μ is the shear modulus and ν is the Poisson's ratio, enable well-conditioning of eq. (16) for any combination of coordinates and outward normals.
$\mathbf{U}^*$ is symmetric for the coefficients referring to different nodal points. However, there is no theoretical reasoning why the submatrices about its main diagonal should be symmetric, as a result from eq. (16). It has been observed that these submatrices tend to be symmetric as the mesh discretization becomes more refined.

Stiffness-type Matrix

Equations (8) and (13) were the governing equations of the SHBEM in its original version [5, 10, 11]. In the present framework, one makes use of eq. (15) for deriving a stiffness-type matrix, whenever required, as

$$\mathbf{K} = (\mathbf{U}^{*\mathrm{T}}\,\mathbf{P}_W^\perp)^{(-1)}\,\mathbf{H} \quad \text{in} \quad \mathbf{K}\,\mathbf{d} = \mathbf{p} \tag{20}$$

where, for a constant λ of order $1/\mu$ to keep the term to be inverted well conditioned [2, 14],

$$(\mathbf{U}^{*\mathrm{T}}\,\mathbf{P}_W^\perp)^{(-1)} = \mathbf{P}_W^\perp\,(\mathbf{U}^{*\mathrm{T}}\,\mathbf{P}_W^\perp + \lambda\,\mathbf{P}_W)^{-1} \tag{21}$$

Since eq. (20) is formulated on the basis of a non-variational approach, $\mathbf{K}$ is not necessarily symmetric. However, it tends to become symmetric with increasing mesh refinement.

Evaluation of Displacements and Stresses in the Domain

Stresses and displacements are evaluated in the domain Ω by eqs. (5) and (4) directly from the force parameters $\mathbf{p}^*$, which are obtained in either eq. (8) or (13) in terms of generalized inverses [2, 14]. The rigid body amount of displacements, represented in eq. (4) by the constant C_{sm}, is obtained from eq. (12) in terms of $\mathbf{p}^*$ and $\mathbf{d}$. Results close to or at nodal points may be obtained in a straightforward way and as accurately as possible, given mesh refinement limitations, if the stress gradient has no local characteristics, by using spectral properties related to $\mathbf{V}$ [10, 14]. However, when the stress gradient has some local property, as in case of notches or cracks, the local effects must be dealt with adequately.

Numerical Example

For an axisymmetric problem, a ring of unitary point force (MNm) is applied at coordinates (10,-5) for each coordinate direction of the elastic medium, with $\mu = 10$ MPa and $\nu = 0.3$, thus generating displacements and stresses given as in eqs. (5) and (4), respectively. Next, one cuts out an irregular contour, as depicted in Fig. 1, and applies to its boundary the traction effects of the stress field. Moreover, one prescribes the vertical displacement $u_z(C) = 0.4356\ 10^{-3}$ m at point C. For the numerical analysis, the boundary is discretized with quadratic elements in a total of 64 nodes. The problem was solved by the conventional boundary element method (BEM), the BEM by means of a stiffness-type matrix (KBEM) [7] and the simplified hybrid boundary element method (SHBEM). Results along the boundary ABCDEF and at 10 points along the line segment A'B' are presented in Fig. 2 and the corresponding global errors are presented in Table 1 [14].

	ABCDEFA		A'B'	
(%)	u_r	u_z	u_z	σ_{zz}
BEM	0.57	0.40	0.10	0.11
KBEM	0.82	0.21	0.11	0.12
SHBEM	1.53	0.12	0.02	0.24

Table 1: Global error for some results along the boundary ABCDEFA and the line segment A'B'.

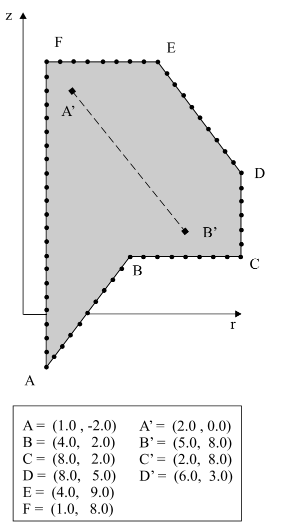

Figure 1: Cutout test of an irregular contour ABCDEFA.

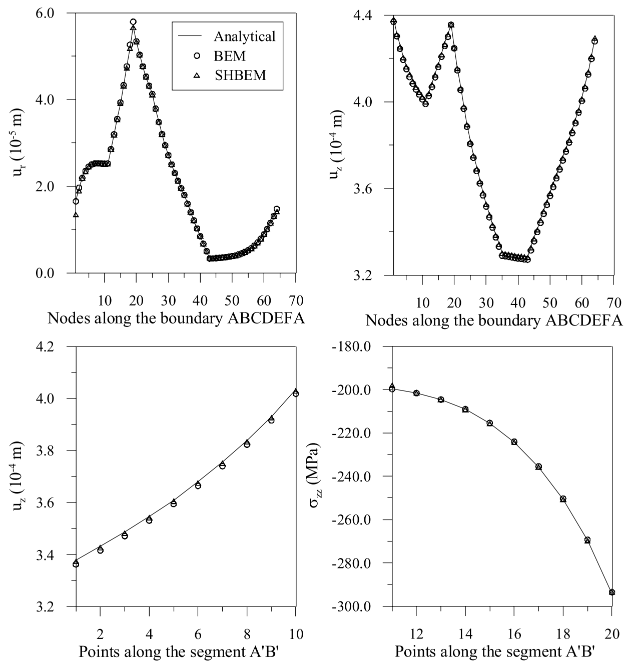

Figure 2: Results along the boundary ABCDEFA and the line segment A'B'.

Conclusions

The main contribution of the present paper is the introduction of a novel hybrid virtual work principle in relation to the simplified hybrid boundary element method, which enables the application of the method to problems of any topology. It is shown that, for singular fundamental solutions, it is mechanically impossible to evaluate coefficients of a displacement matrix $\mathbf{U}^*$ for results related to the same node of application of the point forces. However, enforcing that simple deformed configurations, as in a patch test, be represented in the frame of a hybrid virtual work principle, these results become available. The cutout test of Fig. 1 is a simple, although evident illustration of the capabilities of the present method, as it deals efficiently with an axisymmetric, multiply-connected problem. The proposed method is a simplification of the conventional, collocation boundary element method, as well, since only one matrix, related to the double-layer potential, requires evaluation via integration along the boundary. Moreover, results at internal point are evaluated directly, thus circumventing any computationally demanding integration.

Acknowledgments

This project was supported by the Brazilian agencies CAPES, CNPq and FAPERJ.

References

[1] T. H. H. Pian In: *Proc. Conf. on Matrix Meths. in Struct. Mech.*, AFFDL–TR–60–88, 457–477, Wright Patterson Air Force Base (1966).
[2] A. Ben-Israel and T. N. E. Greville *Generalized Inverses: Theory and Applications*, Krieger (1980).
[3] N. A. Dumont In: C. A. Brebbia and W. Venturini (Eds) *Boundary Element Techniques: Applications in Fluid Flow and Computational Aspects*, 225–239, Adlard and Son Ltd. (1987).
[4] N. A. Dumont *Applied Mechanics Reviews*, **42**, S54–S63 (1989).
[5] N. A. Dumont and R. A. P. Chaves In: *Proceedings of 20th Iberian Latin American Congress on Computational Methods in Engineering — XX CILAMCE*, 20 pp in CD, Brazil (1999).
[6] N. A. Dumont and R. Oliveira *International Journal of Solids and Structures*, **38**, 1813–1830 (2001).
[7] M. H. Aliabadi *The Boundary Element Method — Vol. 2: Applications in Solids and Structures*, John Wiley & Sons, Ltd. (2002).
[8] N. A. Dumont and A. A. O. Lopes *Fatigue & Fracture of Engineering Materials & Structures*, **26**, 151–161 (2003).
[9] N. A. Dumont *Computer Assisted Mechanics and Engineering Sciences*, **10**, 407–430 (2003).
[10] N. A. Dumont and R. A. P. Chaves *Computer Assisted Mechanics and Engineering Sciences*, **10**, 431–452 (2003).
[11] R. A. P. Chaves *The Simplified Hybrid Boundary Element Method Applied to Time-Dependent Problems*, PhD Thesis (in Portuguese), PUC-Rio (2003).
[12] N. A. Dumont, R. A. P. Chaves and G. H. Paulino. *International Journal of Computational Engineering Science*, **5**, 863–894 (2004).
[13] N. A. Dumont In: *Proceedings of Multiscale and Functionally Graded Materials Conference 2006 — FGM 2006*, 6 pp (2006).
[14] M. F. F. Oliveira *Conventional and simplified-hybrid boundary element methods applied to axisymmetric elasticity problems in fullspace and halfspace*, PhD Thesis, PUC-Rio (2009).

International Conference on Boundary Element Techniques
22 – 24 July, 2009
Athens, Greece

Enrichment of the Boundary Element Method through the Partition of Unity Method for Mode I and II fracture analysis

*** R. Simpson[1] and J. Trevelyan[2]**

[1] Durham University
School of Engineering
South Road
Durham DH1 3LE, UK
robert.simpson2@durham.ac.uk

[2] Durham University
School of Engineering
South Road
Durham DH1 3LE, UK
jon.trevelyan@durham.ac.uk

Key Words: *BEM, PUM, fracture, enrichment*

SUMMARY

The present method offers an approach to 2D fracture problems where certain basis functions that are known to capture the required crack tip displacement field are incorporated in a boundary element formulation through the Partition of Unity Method. The same basis functions that were used by Moës et al. in the implementation of the Extended Finite Element Method (XFEM) [1] for fracture analysis are used. It is found, in the simple case of a straight crack, that these reduce to rather simple expressions for the boundary element implementation. With the introduction of these basis functions, additional unknown coefficients are produced which are accommodated by providing additional collocation points. To allow the evaluation of asymmetric crack problems, enrichment was applied to the Dual Boundary Element Method (DBEM) [2] with certain modifications made to the Displacement and Traction Boundary Integral Equations. With the inclusion of enrichment functions, analytical expressions can no longer be used for the evaluation of the strongly singular and hypersingular terms and instead a specially adapted numerical quadrature routine is used. The method was tested on both Mode I and Mode II problems where substantial increases in accuracy were gained for a small increase in degrees of freedom (DOF).

INTRODUCTION

Fracture problems, in which a singular stress field is encountered at the crack tip, present difficulties when modelled with conventional piecewise polynomial elements. The stress field exhibits a singularity of $O(1/\sqrt{\rho})$ (where ρ is the distance from the crack tip) while displacements are of the form $\sqrt{\rho}$. Unless extremely refined meshes are used in the vicinity of the crack tip, conventional elements fail to capture the required singular field. This is a well-known problem, with many techniques and methods available to overcome this difficulty such as quarter-point elements, special crack tip shape functions and the Subtraction of Singularity Technique. Instead, the present work captures the singular field by enriching elements that lie within a certain region around the crack tip, in a very similar manner to that of the Extended Finite Element Method.

ENRICHMENT

To allow enrichment of displacements in elements surrounding the crack tip, the Partition of Unity Method [3] is employed which states that an arbitrary basis can be included within the approximation. If this basis is chosen to correspond to a discontinuity or singularity from *a priori* knowledge, then higher accuracies should be expected. In this way, enriched displacements can be expressed as

$$u_j^n(\xi) = \sum_{a=1}^{M} N_a(\xi) u_j^{na} + \sum_{a=1}^{M} \sum_{l=1}^{4} N_a(\xi) \psi_l^U(\xi) A_{jl}^{na}, \quad j = x, y \tag{1}$$

where $\xi \in (-1, 1)$ is the local coordinate, n is the element number, N_a is the conventional Lagrangian shape function for local node a, ψ_l^U is the lth term in the vector ψ^U of enrichment functions, A_{jl}^{na} is the enrichment coefficient associated with basis function l and node a and M is the number of nodes per element. In the case of a crack the choice of basis functions is obtained by inspecting the expressions for displacements around a crack tip as derived by Williams, where it can be shown that the following provides a complete basis

$$\psi^U(\rho, \theta) = \left\{ \sqrt{\rho} \cos\left(\frac{\theta}{2}\right), \sqrt{\rho} \sin\left(\frac{\theta}{2}\right), \sqrt{\rho} \sin\left(\frac{\theta}{2}\right) \sin(\theta), \sqrt{\rho} \cos\left(\frac{\theta}{2}\right) \sin(\theta) \right\}^{\mathbf{T}} \tag{2}$$

where θ is the angle made from the crack tip. These are the same basis functions as used in the implementation of the XFEM in [1].

To apply enrichment to the BEM, expression (1) is substituted into the Displacement Boundary Integral Equation (DBIE) which is stated here (in its unenriched form) for clarity.

$$C_{ij}(\mathbf{x}')u_j(\mathbf{x}') + \fint_{\Gamma} T_{ij}(\mathbf{x}', \mathbf{x}) u_j(\mathbf{x}) d\Gamma(\mathbf{x}) = \int_{\Gamma} U_{ij}(\mathbf{x}', \mathbf{x}) t_j(\mathbf{x}) d\Gamma(\mathbf{x}) \tag{3}$$

where $\mathbf{x}'$ and $\mathbf{x}$ denote the source and field points on the boundary Γ respectively. After discretisation, this can be written as

$$C_{ij}(\mathbf{x}')u_j(\mathbf{x}') + \sum_{n=1}^{N_e} \sum_{a=1}^{M} P_{ij}^{na} u_j^{na} = \sum_{n=1}^{N_e} \sum_{a=1}^{M} Q_{ij}^{na} t_j^{na} \tag{4}$$

where the terms P_{ij}^{na} and Q_{ij}^{na} are conventional integral expressions which contain a fundamental solution, shape function and Jacobian of Transformation. Now, if the expression for enriched displacements is inserted into (4), the enriched discretised DBIE can be written as

$$\begin{aligned} C_{ij}(\mathbf{x}') \left(\sum_{a=1}^{M} N_a(\xi_p) u_j^{\bar{n}a} + \sum_{a=1}^{M} \sum_{l=1}^{4} N_a(\xi_p) \psi_l^U(\xi_p) A_{jl}^{\bar{n}a} \right) + \sum_{n=1}^{N_e} \sum_{a=1}^{M} P_{ij}^{na} u_j^{na} + \sum_{n=1}^{N_e} \sum_{a=1}^{M} \sum_{l=1}^{4} P_{ijl}^{na} A_{jl}^{na} \\ = \sum_{n=1}^{N_e} \sum_{a=1}^{M} Q_{ij}^{na} t_j^{na} \end{aligned} \tag{5}$$

where $\bar{n}$ is the number of the element containing $\mathbf{x}'$ and ξ_p refers to the local coordinate of the source point. The jump term is now distributed over element $\bar{n}$ to allow the source point to lie at any general position on the boundary. This technique, successfully implemented by Perry-Debain et al. [4], is crucial for the use of additional collocation points which is described later in the implementation of the method. The second and fourth terms are unchanged from (4) while the third is new. It is given by

$$P_{ijl}^{na} = \int_{-1}^{1} N_a(\xi) T_{ij}[\mathbf{x}', \mathbf{x}(\xi)] \psi_l^U(\xi) J^n(\xi) d\xi \tag{6}$$

where the enrichment function ψ_l^U is incorporated within the boundary integral.

The DBEM, which allows coincident crack surfaces to be modelled, makes use of an independent Boundary Integral Equation known as the Traction Boundary Integral Equation given by

$$\frac{1}{2}t_j(\mathbf{x}') + n_i(\mathbf{x}') \,=\!\!\!\!\!\!\int_\Gamma S_{kij}(\mathbf{x}', \mathbf{x}) u_k(\mathbf{x}) d\Gamma(\mathbf{x}) = n_i(\mathbf{x}') -\!\!\!\!\!\!\int_\Gamma D_{kij}(\mathbf{x}', \mathbf{x}) t_k(\mathbf{x}) d\Gamma(\mathbf{x}) \tag{7}$$

In a similar manner to the DBIE, the Traction Boundary Integral Equation (TBIE) can also be enriched by inserting expression (1) into the discretised form of the equation. Once again, for clarity, the unenriched form of the Boundary Integral Equation is stated

$$\frac{1}{2}t_j(\mathbf{x}') + n_i(\mathbf{x}') \sum_{n=1}^{N_e} \sum_{a=1}^{M} E_{kij}^{na} u_k^{na} = n_i(\mathbf{x}') \sum_{n=1}^{N_e} \sum_{a=1}^{M} F_{kij}^{na} t_k^{na} \tag{8}$$

where E_{kij}^{na} and F_{kij}^{na} are integral expressions which are hypersingular and strongly singular respectively. The enriched form of the TBIE is then given by

$$\frac{1}{2}\left(\sum_{a=1}^{M} N_a(\xi_p) t_j^{\bar{n}a} \right) + n_i(\mathbf{x}') \sum_{n=1}^{N_e} \sum_{a=1}^{M} E_{kij}^{na} u_k^{na} + n_i(\mathbf{x}') \sum_{n=1}^{N_e} \sum_{a=1}^{M} \sum_{l=1}^{4} E_{kijl}^{na} A_{kl}^{na}$$
$$= n_i(\mathbf{x}') \sum_{n=1}^{N_e} \sum_{a=1}^{M} F_{kij}^{na} t_k^{na} \tag{9}$$

where the new enriched integral term E_{kijl}^{na} is expressed as

$$E_{kijl}^{na} = \int_{-1}^{1} N_a(\xi) S_{kij}[\mathbf{x}', \mathbf{x}(\xi)] \psi_l^U(\xi) J^n(\xi) d\xi \tag{10}$$

By using the Boundary Integral expressions (5) and (9) enrichment can be applied to problems containing any general crack configuration. However, before this can be done, a method for solving the introduced enrichment coefficients along with a strategy for enrichment is required.

IMPLEMENTATION

When the enriched BIEs are applied to a fracture problem the introduction of each basis function leads to an additional unknown in each direction. A solution to this problem was presented in a similiar scheme to introduce enrichment to the BEM by Watson [5] who used additional BIEs derived by differentiating the DBIE. However, each of these require a rather complicated procedure to calculate the singular integral terms making the method rather cumbersome. Instead, the present approach is to use a technique demonstrated by Perry-Debain et al.[4] which utilises additional collocation points spread evenly throughout enriched elements. In the case of a flat crack where the basis functions reduce to simply $\sqrt{\rho}$, the number of additional unknowns is reduced to simply two per enriched node. Therefore, if a discontinuous quadratic element is used for enrichment (which greatly simplifies the implementation of the TBIE), three additional points will be required. This is illustrated in Figure 1 where the crack is depicted as having a finite opening to illustrate collocation on the upper and lower surfaces. In reality these surfaces are coincident.

It is well known in fracture that only a certain region surrounding the crack tip is dominated by the singularity. Therefore, only those elements that lie within the singular region are required to be enriched.

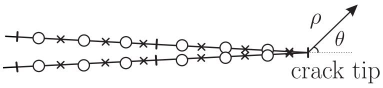

Figure 1: Additional collocation points on enriched flat crack elements

Of course, with each additional enriched element a corresponding increase in the number of system unknowns occurs requiring a balance to be struck between accuracy and efficiency. The present strategy enriches only those elements that lie on the crack surfaces with an expected increase in accuracy for each additional enriched element.

In the conventional BEM singular integral terms are usually computed using rigid-body motion while all others are evaluated using numerical quadrature. In the implementation of the DBEM Portela et al. explained that rigid-body motion could no longer be used but instead analytical expressions were given for singular terms, with the assumption that flat crack elements are used. However, when enrichment is applied to the DBEM these expressions are no longer valid and a numerical scheme that is capable of evaluating strongly singular and hypersingular integrals is required. A subtraction of singularity scheme, illustrated by Guiggiani [6], is used which relies on a Taylor series approximation about the source point. Once this is determined, the singular components are removed leaving a regular integral which can be evaluated using a conventional quadrature routine. Then, the singular components are re-introduced through analytical expressions. The expression used for the evaluation of enriched hypersingular integrals is given by

$$I = \int_{-1}^{+1} \left[F(\xi_p, \xi) - \left(\frac{F_{-2}(\xi_p)}{(\xi - \xi_p)^2} + \frac{F_{-1}(\xi_p)}{\xi - \xi_p} \right) \right] d\xi + F_{-1}(\xi_p) \ln \left| \frac{1 - \xi_p}{-1 - \xi_p} \right| + F_{-2}(\xi_p) \left(-\frac{1}{1 - \xi_p} + \frac{1}{-1 - \xi_p} \right) \quad \xi_p \in (-1, 1) \tag{11}$$

where $F_{-2}(\xi_p)$ and $F_{-1}(\xi_p)$ are regular functions determined by a Taylor series expansion of the integrand about the source point. Expression (11) can also be used for strongly singular singular integrals $O(\frac{1}{r})$ where it is found that the term F_{-2} vanishes.

Finally, to allow the evaluation of both Mode I and Mode II stress intensity factors (SIFs), a decomposed J-integral routine as implemented by Aliabadi [7] is used. A series of internal points located symmetrically around the crack is used which allow the integral to be split into Mode I and II components.

RESULTS

An edge crack was used to illustrate the improvements obtained by enriching elements along the crack faces. Accurate results for Mode I stress intensity factors (SIFs) are given for this problem [8] while it was also analysed by Portela et al. using the DBEM. In the convergence study a uniform mesh grading was used throughout (in contrast to the implementation of [2]) with additional elements added to each line in each step of mesh refinement. Figure 2(a) illustrates the edge crack problem along with an example mesh used for analysis. By varying the number of enriched elements lying on the crack faces it was found that results improved considerably when the elements adjacent to the crack were enriched, while any further enrichment had little effect on the accuracy. This strategy was used to study errors on normalised K_I while comparisons were made with the DBEM. Figure 2(b) illustrates a log-log plot of errors in normalised K_I for each method; it can be clearly seen that an improvement of almost an order of magnitude is achieved.

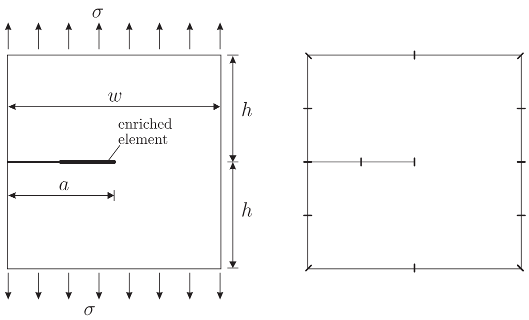

(a) Edge crack problem with example mesh

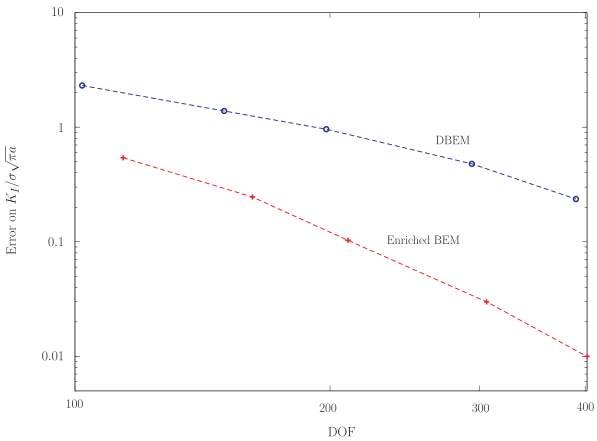

(b) Comparison of errors between DBEM and the enriched BEM

Figure 2: Edge crack results

A mixed-mode fracture problem in the form of an inclined edge crack was also considered with accurate results published by Wilson [9] using the boundary collocation technique. Figure 3(b) shows that for various crack angles and crack lengths the enriched BEM shows excellent agreement with Wilson for both Mode I and II SIFs.

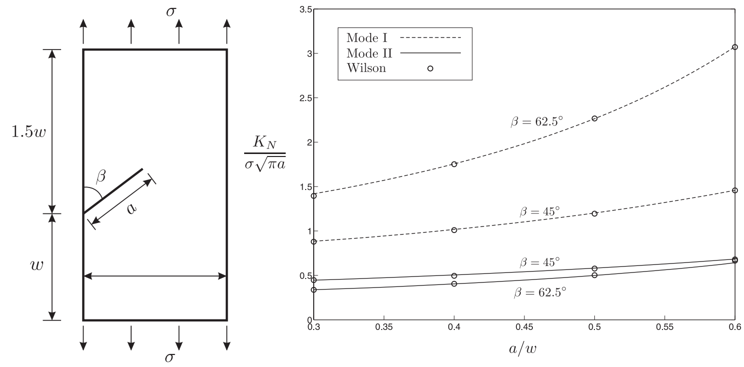

(a) Inclined edge crack geometry

(b) Comparison of normalised SIFs

Figure 3: Inclined edge crack results

CONCLUSIONS

A method has been presented for the enrichment of the BEM (and DBEM) for analysis of 2D cracks. An outline of how enrichment is implemented is given with particular attention paid to the use of additional collocation points and a numerical integration scheme that allows the evaluation of strongly singular and hypersingular integrals. Results show that, in comparison to the unenriched DBEM, an increase in accuracy of almost an order of magnitude is seen. A mixed mode problem was also analysed to verify the accuracy of both Mode I and II SIFs.

REFERENCES

[1] N. Moës, J. Dolbow and T. Belytschko. "A finite element method for crack growth without remeshing". *International Journal for Numerical Methods in Engineering*, Vol. **46**, 131–150, 1999.

[2] A. Portela, M.H. Aliabadi and D.P. Rooke "The dual boundary element method - effective implementation for crack problems". *International Journal for Numerical Methods in Engineering*, Vol. **33**, 1269–1287, 1992.

[3] J. Melenk and I. Babuška. ”The partition of unity finite element method: Basic theory and applications”. *Computer Methods in Applied Mechanics and Engineering*, Vol. **139**, 289–314, 1996.

[4] E. Perrey-Debain, J. Trevelyan and P. Bettess ”New special wave boundary elements for short wave problems”. *Communications in Numerical Methods in Engineering*, Vol. **18**, 259–268, 2002.

[5] J.O. Watson ”Singular boundary elements for the analysis of cracks in plane-strain”. *International Journal for Numerical Methods in Engineering*, Vol. **38**, 2389–2411, 1995.

[6] M. Guiggiani ”Hypersingular formulation for boundary stress evaluation”. *Engineering Analysis With Boundary Elements*, Vol. **13**, 169–179, 1994.

[7] M.H. Aliabadi ”Evaluation of mixed mode stress intensity factors using path independent integral”. *Proc. 12th Int. Conf. on Bound. Element Methods*, Computational Mechanics Publications, Southampton, 281–292, 1990.

[8] M.B. Civelek and F. Erdogan ”Crack problems for a rectangular plate and an infinite strip”. *International Journal of Fracture*, Vol. **19**, 139–159, 1982.

[9] W.K. Wilson. Research Report 69-IE7-FMECH-RI, Westinghouse research laboratory, Pittsburg, 1969.

Fracture Mechanics Analysis of Multilayer Metallic Laminates by BEM

P. M. Baiz[1], Z. Sharif Khodaei[2] and M. H. Aliabadi[3]

Department of Aeronautics, Imperial College London, London SW7 2AZ, UK
[1]p.m.baiz@imperial.ac.uk, [2]z.sharif-khodaei@imperial.ac.uk, [3]m.h.alibadi@imperial.ac.uk

Keywords: Shear Deformable Plates, Fracture Mechanics, Multilayer Structures.

Abstract. This paper presents an application of the Dual Boundary Element Method (DBEM) for fracture mechanics analysis of multilayer metallic laminate structures. The metal layers are modelled by coupling two-dimensional plane stress elasticity and shear deformable (Reissner) plate bending. Adhesive layers are modelled as a distribution of forces which include in-plane, out-of-plane and two moment body forces which are transfered to the boundary by the Dual Reciprocity Method (DRM). Stress intensity factors, three for the bending problem and two for the membrane problem, are evaluated from crack opening displacements. The accuracy of the proposed method is assessed by comparison with results from a commercial FEM software (ABAQUS).

Introduction

The quest for lighter, more affordable high performance airframes has accelerated demand for new advanced concepts. In recent years a number of new metal and hybrid technologies have been investigated. For instance, Fibre Metal Laminates (FMLs) have been developed in the past to increase the fatigue characteristics of laminated metal structures by adding fibres in the bond line. The fibres are insensitive to the occurring fatigue stresses in FMLs and bridge the fatigue cracks in the metal layers by restraining the crack opening. These metal laminate parts are constructed and repaired using mostly conventional metal material techniques. Alderliesten [2] presents an overview of relevant approaches (phenomenological, analytical and FEM) for fatigue crack propagation prediction in composite metallic laminates; outlining the need of further developments for accurate description of fatigue crack growth in FML.

Modelling of adhesively patched cracked sheets has been studied by several authors using the boundary element method. Young *et al.* [3] presented a two dimensional BEM model of the patch and cracked sheet. The adhesive layer was modelled using shear springs and treating the adhesive shear stresses as body forces acting on the patch and the sheet. Salgado *et al.* [4] used the dual reciprocity method (DRM) to transform the domain integrals from the adhesive patch to the boundary and the dual boundary element method (DBEM) to model the crack. This formulation was later extended to flat and curved plate bending analysis by Wen *et al.* [9, 10]. In this plate/shell formulation the interaction between the plate and the patch on a repaired sheet is modelled as a distribution of forces which include in-plane, out-of-plane and two moment body forces (shear deformable theory).

More recently, Sekine *et al.* [7] presented a combined detailed 3D boundary element method and finite element method to investigate the fatigue crack growth behavior of cracked aluminum panels repaired with an adhesively bonded composite patch. The detailed numerical simulation provide crack front profiles of the cracked panel during fatigue crack growth and the distributions of stress intensity factors along crack fronts. Useche *et al.* [6] presented a plate boundary element formulation for the analysis of isotropic cracked sheets, repaired with adhesively bonded anisotropic patches and Alaimo *et al.* [5] presented a 2D boundary integral formulation based on the multidomain technique to model cracks and assemble the multi-layered piezoelectric patches to the host damaged structure.

This paper aims to investigate fatigue crack propagation in multilayer metal laminates by a multi region shear deformable plate bending DBEM model. A coupled boundary integral formulation of shear deformable plate bending and two-dimensional plane stress elasticity are used to determine bending and membrane forces along the adhesive layer.

Governing Equations

Strain tensors in shear deformable linear elastic plate theories can be derived from the deformation pattern of a differential element. The membrane strain resultant tensor can be expressed as follows:

$$\varepsilon_{\alpha\beta} = \frac{1}{2}\left(u_{\alpha,\beta} + u_{\beta,\alpha}\right) \tag{1}$$

Transverse shear strain resultant can be expressed as:

$$\gamma_{\alpha 3} = w_{\alpha} + w_{3,\alpha} \tag{2}$$

And the flexural strain resultant can be written as:

$$\kappa_{\alpha\beta} = 2\chi_{\alpha\beta} = w_{\alpha,\beta} + w_{\beta,\alpha} \tag{3}$$

where u_α denotes in-plane displacements and w_i denotes out-of-plane displacement and rotations. In this paper Roman indices vary from 1 to 3 and Greek indices vary from 1 to 2.

The relationships between stress resultants and strains for plate bending were derived by Reissner, and are given as:

$$M_{\alpha\beta} = D\frac{1-\nu}{2}\left(2\chi_{\alpha\beta} + \frac{2\nu}{1-\nu}\chi_{\gamma\gamma}\delta_{\alpha\beta}\right) \tag{4}$$

for components of bending moment and,

$$Q_\alpha = C\gamma_{\alpha 3} \tag{5}$$

for components of out-of-plane shear. Membrane stress resultants are given as:

$$N_{\alpha\beta} = B\frac{1-\nu}{2}\left(2\varepsilon_{\alpha\beta} + \frac{2\nu}{1-\nu}\varepsilon_{\gamma\gamma}\delta_{\alpha\beta}\right) \tag{6}$$

where $B(=Eh/\left(1-\nu^2\right))$ is known as the tension stiffness; $D(=Eh^3/\left[12\left(1-\nu^2\right)\right])$ is the bending stiffness; $C(=\left[D\left(1-\nu\right)\lambda^2\right]/2)$ is the shear stiffness; $\lambda_s = \sqrt{10}/h$ is called the shear factor and $\delta_{\alpha\beta}$ is the Kronecker delta function.

Finally, the equilibrium equations for shear deformable plate bending can be written as follows:

$$M_{\alpha\beta,\beta} - Q_\alpha + q_\alpha = 0 \tag{7}$$

for summatory of moments around the center of gravity of a plate element,

$$Q_{\alpha,\alpha} + q_3 = 0 \tag{8}$$

for summatory of forces along the x_3 direction and,

$$N_{\alpha\beta,\beta} + f_\alpha = 0 \tag{9}$$

for summatory of forces on the $x_1 - x_2$ directions.

Metal Layers (DBEM formulation)

Lets consider flat isotropic sheets of thickness h^m, Young's modulus E^m, Poisson's ratio ν^m with a boundary Γ. The two-dimensional boundary integral equation for displacements at the boundary point $\mathbf{x}' \in \Gamma$ can be written as,

$$c_{\alpha\beta}(\mathbf{x}')u^m_\beta(\mathbf{x}') = \int_\Gamma U^*_{\alpha\beta}(\mathbf{x}',\mathbf{x})t^m_\beta(\mathbf{x})d\Gamma - \fint_\Gamma T^*_{\alpha\beta}(\mathbf{x}',\mathbf{x})u^m_\beta(\mathbf{x})d\Gamma + \frac{1}{h_m}\sum_{n=1}^{N}\int_{A_n} U^*_{\alpha\beta}(\mathbf{x}',\mathbf{x})f^m_\beta(\mathbf{x})dA \tag{10}$$

where $⨍$ denotes a Cauchy principal-value integral and $c_{\alpha\beta}(\mathbf{x}')$ is a function of the geometry at the collocation points equal to 1/2 for a smooth boundary. The boundary displacements and tractions for sheet m are denoted by u_α^m and t_α^m respectively; displacement and traction fundamental solutions for the plane stress condition are $U^*_{\alpha\beta}(\mathbf{x}',\mathbf{x})$ and $T^*_{\alpha\beta}(\mathbf{x}',\mathbf{x})$, respectively [1]. $f_\beta^m(\mathbf{x})$ denotes the two-dimensional body forces per unit area over a region A_n of adhesive and N represents the total number of bonding areas.

The boundary integral formulation presented by Wen *et al.* [9] can be rewritten as,

$$c_{ik}(\mathbf{x}')w_k^m(\mathbf{x}') = \int_\Gamma W^*_{ik}(\mathbf{x}',\mathbf{x})p_k^m(\mathbf{x})d\Gamma(\mathbf{x}) - ⨍_\Gamma P^*_{ik}(\mathbf{x}',\mathbf{x})w_k^m(\mathbf{x})d\Gamma(\mathbf{x}) + \sum_{n=1}^{N}\int_{A_n} W^*_{ik}(\mathbf{x}',\mathbf{x})q_k^m(\mathbf{x})dA \tag{11}$$

where p_k^m denotes boundary tractions, $W^*_{ij}(\mathbf{x}',\mathbf{x})$ and $P^*_{ij}(\mathbf{x}',\mathbf{x})$ are the fundamental solutions for rotations and out-of-plane displacements and bending and shear tractions, respectively [1]. $q_\beta^m(\mathbf{x})$ is the distribution of body forces in moment per unit area and $q_3^m(\mathbf{x})$ the out-of-plane body force in the adhesive area A_n.

Using the stress and strain relationships in equations (7)-(9), the traction integral equations for a source point on a smooth boundary can be obtained as [9, 1]:

$$\begin{aligned}
&\frac{1}{2}p_\alpha^m(\mathbf{x}') + n_\beta(\mathbf{x}')\,⨎_\Gamma P^*_{\alpha\beta\gamma}(\mathbf{x}',\mathbf{x})w_\gamma^m(\mathbf{x})d\Gamma(\mathbf{x}) + n_\beta(\mathbf{x}')\,⨍_\Gamma P^*_{\alpha\beta 3}(\mathbf{x}',\mathbf{x})w_3^m(\mathbf{x})d\Gamma(\mathbf{x})\\
&= n_\beta(\mathbf{x}')\,⨍_\Gamma W^*_{\alpha\beta\gamma}(\mathbf{x}',\mathbf{x})p_\gamma^m(\mathbf{x})d\Gamma(\mathbf{x}) + n_\beta(\mathbf{x}')\int_\Gamma W^*_{\alpha\beta 3}(\mathbf{x}',\mathbf{x})p_3^m(\mathbf{x})d\Gamma(\mathbf{x})\\
&\quad + n_\beta(\mathbf{x}')\sum_{n=1}^{N}\int_{A_n} W^*_{\alpha\beta k}(\mathbf{x}',\mathbf{x})q_k^m(\mathbf{x})dA
\end{aligned} \tag{12}$$

$$\begin{aligned}
&\frac{1}{2}p_3^m(\mathbf{x}') + n_\beta(\mathbf{x}')\,⨍_\Gamma P^*_{3\beta\gamma}(\mathbf{x}',\mathbf{x})w_\gamma^m(\mathbf{x})d\Gamma(\mathbf{x}) + n_\beta(\mathbf{x}')\,⨎_\Gamma P^*_{3\beta 3}(\mathbf{x}',\mathbf{x})w_3^m(\mathbf{x})d\Gamma(\mathbf{x})\\
&= n_\beta(\mathbf{x}')\int_\Gamma W^*_{3\beta\gamma}(\mathbf{x}',\mathbf{x})p_\gamma^m(\mathbf{x})d\Gamma(\mathbf{x}) + n_\beta(\mathbf{x}')\,⨍_\Gamma W^*_{3\beta 3}(\mathbf{x}',\mathbf{x})p_3^m(\mathbf{x})d\Gamma(\mathbf{x})\\
&\quad + n_\beta(\mathbf{x}')\sum_{n=1}^{N}\int_{A_n} W^*_{3\beta k}(\mathbf{x}',\mathbf{x})q_k^m(\mathbf{x})dA
\end{aligned} \tag{13}$$

and,

$$\begin{aligned}
&\frac{1}{2}t_\alpha^m(\mathbf{x}') + n_\beta(\mathbf{x}')\,⨎_\Gamma T^{(i)*}_{\alpha\beta\gamma}(\mathbf{x}',\mathbf{x})u_\gamma^m(\mathbf{x})d\Gamma(\mathbf{x}) = n_\beta(\mathbf{x}')\,⨍_\Gamma U^*_{\alpha\beta\gamma}(\mathbf{x}',\mathbf{x})t_\gamma^m(\mathbf{x})d\Gamma(\mathbf{x})\\
&\quad + n_\beta(\mathbf{x}')\sum_{n=1}^{N}\int_{A_n} U^*_{\alpha\beta\gamma}(\mathbf{x}',\mathbf{X})f_\gamma^m(\mathbf{x})dA
\end{aligned} \tag{14}$$

where $⨎$ denotes a Hadamard principal-value integral. Equations (12-14) represent five integral equations in terms of boundary tractions, and can be used together with the five displacement integral equations to form the plate bending dual boundary integral formulation.

Adhesive Layers

In the present shear deformable plate formulation there are five force distributions on the middle plane of the metal sheets (i.e. $f_\alpha^m(\alpha = 1,2), q_k^m(k = 1,2,3)$). From equilibrium conditions, the body forces can be expressed as:

$$\begin{aligned}
\bar{f}_\alpha^m + f_\alpha^m = 0, &\qquad \bar{q}_3^m + q_3^m = 0\\
\bar{q}_\alpha^m + q_\alpha^m + \left(h_a + \frac{h + h_m}{2}\right)\bar{f}_\alpha^m = 0, &\quad \alpha = 1,2
\end{aligned} \tag{15}$$

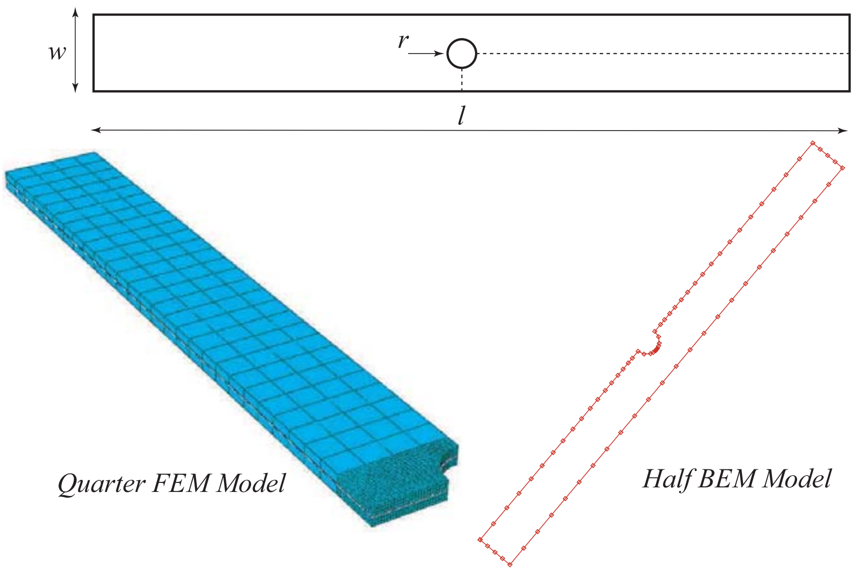

Figure 1: Open Hole Specimen Dimensions

Additionally, there are five corresponding displacement compatibility conditions,

$$\left(u_\alpha^m - \frac{h_m}{2} w_\alpha^m\right) - \left(u_\alpha + \frac{h_m}{2} w_\alpha\right) = \frac{h_a}{G_a} \bar{f}_\alpha^m, \quad \alpha = 1, 2$$

$$w_k = w_k^m, \quad k = 1, 2, 3 \quad \mathbf{X}' \in A_m \tag{16}$$

where $\bar{()}$ denotes the adjacent sheet and G_a and h_a are the shear modulus and thickness of the adhesive layer, respectively.

Numerical Implementation

To solve these boundary integral equations (10)-(14), the boundaries of metal layers are discretized into continuous quadratic elements, and the cracks into discontinuous quadratic elements. Domain integrals in equations (10)-(14) are transferred to the boundary by the dual reciprocity method [8, 9], therefore domain points as shown in Figure 2 are also necessary.

Numerical Results

The present approach was validated by comparing stress intensity factors from a cracked two layers open hole specimen, see Figure 1. For the maximum crack size, the FE model has a total of 19335 nodes with 3345 solid elements (C3D20R) and 228 cohesive elements (COH3D8). The boundary element model has a total of 192 nodes for the metal layers and 178 DRM points for the adhesive layer. Figure 2 shows mesh details of the cracked metal layer and adhesive layer.

The plate is under uniformly uni-axial tension and it has both ends simply supported. Normalized stress intensity factors are presented in Figure 3. As expected, stress intensity factors along the crack front vary from a minimum close to the bonded surface to a maximum on the free surface. The simplified plate bending BEM model is able to capture the maximum values of the SIF obtained with the detailed 3D FEM model. Stress plots of the BEM and FEM models are shown in Figure 4. The difference between mesh densities and similarity between stress contours is evident from this figure.

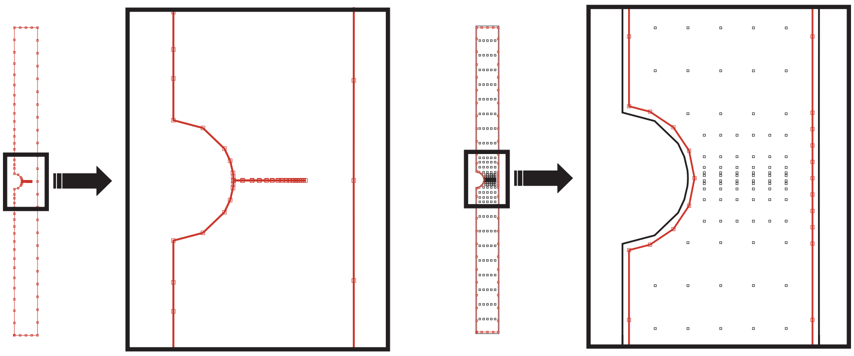

Figure 2: BEM mesh on Cracked Metal layer and Adhesive layer.

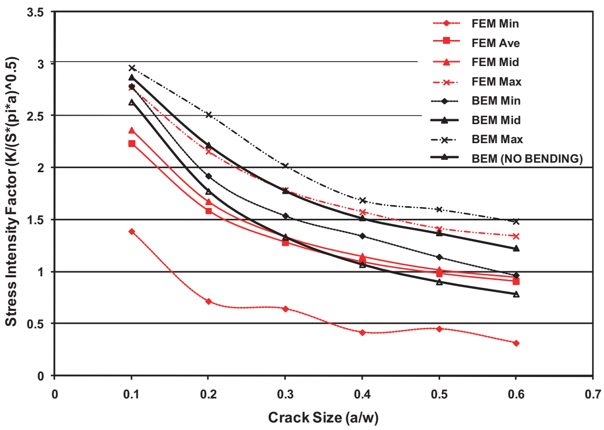

Figure 3: SIF vs. Crack Size in a metallic laminate structure.

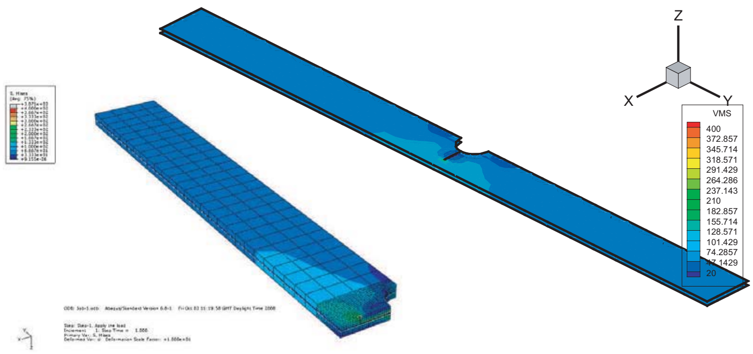

Figure 4: Stress Plot on the FEM and BEM Models.

Conclusions

This paper presented an application of the dual boundary element method for fracture mechanics analysis of multilayer metallic structures. Results from simplified 2D and 2.5D (shear deformable plate theory) Boundary Element formulations were compared with 3D FEM models. Results show the capabilities of a BEM formulation. The reduction of modelling and simulation times in the BEM formulation represents an attractive alternative to the 3D ABAQUS Model.

Acknowledgment

The authors would like to thanks AIRBUS UK and TSB for their financial support (Project No: TP/5/MAT/6/S/H0644G).

References

[1] Aliabadi M.H.,*The Boundary Element Method, vol II: Application to Solids and Structures*, Chichester, Wiley (2002).

[2] Alderliesten R.C., On the available relevant approaches for fatigue crack propagation prediction in Glare, *International Journal of Fatigue*, **29**, 289-304 (2007).

[3] Young A., Rooke D.P., Cartwright D.J., The boundary element method for analysing repair patches on cracked finite sheets, *Aero J*, **92**, 416421 (1988).

[4] Salgado N.K., Aliabadi M.H., The boundary element analysis of cracked stiffened sheets, reinforced by adhesively bonded patches, *Int J Numer Meth Eng*, **42**, 195217 (1998).

[5] Alaimo A., Milazzo A., Orlando C., Boundary elements analysis of adhesively bonded piezoelectric active repair, *Engineering Fracture Mechanics*, **76**, 500511 (2009).

[6] Useche J.F., Sollero P., Albuquerque E.L., Boundary element analysis of cracked sheets repaired with bonded anisotropic patches, *Key Engineering Materials*, **383**, 97-108 (2008).

[7] Sekine H., Yan B., Yasuho T., Numerical simulation study of fatigue crack growth behavior of cracked aluminum panels repaired with a FRP composite patch using combined BEM/FEM, *Engineering Fracture Mechanics*, **72**, 25492563 (2005).

[8] Wen P.H., Aliabadi M.H., Young A., Transformation of domain integrals to boundary integrals in BEM analysis of shear deformable plate bending problems, *Comput Mech*, **24(4)**, 304309 (1999).

[9] Wen P.H., Aliabadi M.H., Young A., Boundary element analysis of flat cracked panels with adhesively bonded patches, *Engineering Fracture Mechanics*, **69**, 21292146 (2002).

[10] Wen P.H., Aliabadi M.H., Young A., Boundary element analysis of curved cracked panels with adhesively bonded patches, *Int. J. Numer. Meth. Engng*, **58**, 4361 (2003).

Warping Shear Stresses in Nonlinear Nonuniform Torsional Vibrations of Bars by BEM

E.J.Sapountzakis[1] and V.J.Tsipiras[2]

[1,2]School of Civil Engineering, National Technical University, Zografou Campus, GR-157 80 Athens, Greece

Keywords: shear stresses, warping, bar, beam, boundary element method, nonuniform torsion, nonlinear vibrations, torsional vibrations

Abstract. In this paper a boundary element method is developed for the evaluation of warping shear stresses of bars of arbitrary doubly symmetric constant cross section undergoing nonuniform torsional vibrations taking into account the effect of geometrical nonlinearity. The bar is subjected to arbitrarily distributed or concentrated conservative dynamic twisting and warping moments along its length, while its edges are supported by the most general torsional boundary conditions. The transverse displacement components are expressed so as to be valid for large twisting rotations (finite displacement – small strain theory), thus the arising governing differential equations and boundary conditions are in general nonlinear. Employing a variational approach, a coupled nonlinear initial boundary value problem with respect to the main unknown kinematical components and two boundary value problems with respect to the primary and secondary warping functions are formulated. The solution of the last two problems is performed by a pure BEM approach requiring exclusively boundary discretization of the bar's cross section and leading to the evaluation of the warping shear stresses. The arising linear system of equations related to the secondary warping function is singular and a special technique is used to perform its regularization. The validity of negligible axial inertia assumption is examined for the problem at hand.

1. Introduction

When arbitrary torsional boundary conditions are applied either at the edges or at any other interior point of the bar due to construction requirements, this bar under the action of general twisting loading is leaded to nonuniform torsion. Besides, since weight saving is of paramount importance, frequently used thin-walled open sections have low torsional stiffness and their torsional deformations can be of such magnitudes that it is not adequate to treat the angles of cross-section rotation as small. In these cases, the study of nonlinear effects on these members becomes essential, where this non-linearity results from retaining the nonlinear terms in the strain–displacement relations (finite displacement – small strain theory). When finite twist rotation angles are considered, the nonuniform torsional dynamic analysis of bars becomes much more complicated, leading to the formulation of coupled and nonlinear torsional and axial equilibrium equations. In this case, accounting for the axial loading and boundary conditions becomes essential to perform a rigorous dynamic analysis of the bar.

While stress analysis of bars subjected to axial and/or bending stress resultants is elementary after the evaluation of the kinematical components, however this is not the case for torsional loading. St. Venant was the first to establish a boundary value problem to evaluate shear stresses for the case of uniform torsion. The solution of this problem has been extensively studied and solved by various analytical and numerical methods. In the case of nonuniform torsion, both normal and warping shear stresses arise and the St. Venant (primary) shear stress distribution is no longer valid. Vlasov proposed an approximate solution of the bar's stress field which is applicable to thin-walled beams of open cross section, while Sapountzakis & Mokos [1] formulated a boundary value problem with respect to the secondary warping function, to compute warping shear stresses of bars of arbitrary cross section. However, this formulation does not account either for dynamic loading or for geometrical nonlinearity while general axial loading and boundary conditions are also not included in the analysis. It is worth here noting that up-to-date Civil Engineering codes and regulations [2] indicate that warping shear stresses should be taken into account in torsional analysis of bars. In all of the research efforts in the literature, the evaluation of the warping shear stress distribution is not discussed.

In this paper a boundary element method is developed for the evaluation of warping shear stresses of bars of arbitrary doubly symmetric constant cross section undergoing nonuniform torsional vibrations taking into account the effect of geometrical nonlinearity. The bar is subjected to arbitrarily distributed or concentrated conservative dynamic twisting and warping moments along its length, while its edges are supported by the most general torsional boundary conditions. The transverse displacement components are expressed so as to be valid for large twisting rotations (finite displacement – small strain theory), thus the arising governing differential equations and boundary conditions are in general nonlinear. Employing a variational approach, a coupled nonlinear initial boundary value problem with respect to the main unknown kinematical components and two boundary value problems with respect to the primary and secondary warping functions are formulated. The solution of the last two problems is performed by a pure BEM approach requiring exclusively boundary discretization of the bar's cross section and leading to the evaluation of the warping shear stresses. The arising linear system of equations related to the secondary warping function is singular and a special technique [3] is used to perform its regularization. The essential features and novel aspects of the present formulation are summarized as follows.

i. The cross section is an arbitrarily shaped doubly symmetric thin or thick walled one. The formulation does not stand on the assumption of a thin-walled structure and therefore the cross section's torsional and warping rigidities are evaluated "exactly" in a numerical sense.
ii. The beam is supported by the most general boundary conditions including elastic support or restraint.
iii. For the first time in the literature, a boundary value problem for the evaluation of the warping shear stresses is formulated and numerically solved. Warping shear stresses alter the original St. Venant shear stress distribution and in up-to-date Civil Engineering codes and regulations [2] it is indicated that they should be taken into account in torsional analysis of bars.
iv. For the first time in the literature, the influence of the axial inertia term on warping shear stresses of bars under nonlinear torsional vibrations is investigated.
v. The proposed method employs a pure BEM approach (requiring exclusively boundary discretization for the cross sectional analysis) resulting in line or parabolic elements, while only a small number of line elements are required to achieve high accuracy.

Numerical examples are worked out to illustrate the efficiency and the range of applications of the developed method. The validity of negligible axial inertia assumption is examined for the problem at hand.

2. Statement of the Problem

2.1. Displacements, strains, stresses

Let us consider a prismatic beam of length l (Fig.1), of constant arbitrary doubly symmetric cross-section of area A. The homogeneous isotropic and linearly elastic material of the beam cross-section, with modulus of elasticity E, shear modulus G and mass density ρ occupies the two dimensional multiply connected region Ω of the y,z plane and is bounded by the $\Gamma_j\left(j=1,2,...,K\right)$ boundary curves, which are piecewise smooth, i.e. they may have a finite number of corners. In Fig. 1b Syz is the principal bending coordinate system through the cross section's shear center. The bar is subjected to the combined action of the arbitrarily distributed or concentrated time dependent conservative axial load $n\left(x,t\right)$, twisting $m_t=m_t\left(x,t\right)$ and warping $m_w=m_w\left(x,t\right)$ moments acting in the x direction (Fig. 1a).

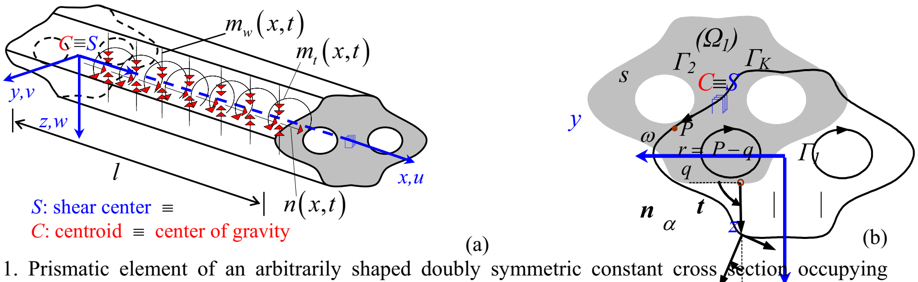

Fig. 1. Prismatic element of an arbitrarily shaped doubly symmetric constant cross section occupying region Ω (a) subjected to axial & torsional loading (b).

Under the aforementioned loading, the displacement field of the bar for large twisting rotations is given as

$$u(x,y,z,t) = u_m(x,t) + \theta'_x(x,t)\cdot\phi_S^P(y,z) + \phi_S^S(x,y,z,t) \tag{1a}$$

$$v(x,y,z,t) = -z\cdot \sin\theta_x(x,t) - y\cdot\left(1-\cos\theta_x(x,t)\right) \tag{1b}$$

$$w(x,y,z,t) = y\cdot \sin\theta_x(x,t) - z\cdot\left(1-\cos\theta_x(x,t)\right) \tag{1c}$$

where u, v, w are the axial and transverse bar displacement components with respect to the Syz system of axes; $\theta'_x(x,t)$ denotes the rate of change of the angle of twist $\theta_x(x,t)$ regarded as the torsional curvature; ϕ_S^P, ϕ_S^S are the primary and secondary warping functions with respect to the shear center *S*, respectively [1] and $u_m(x,t)$ is an "average" axial displacement of the cross section of the bar, the physical meaning of which is explained in [4].

Employing the strain-displacement relations of the three - dimensional elasticity for moderate displacements, the following strain components can be easily obtained

$$\varepsilon_{xx} = \frac{\partial u}{\partial x} + \frac{1}{2}\cdot\left[\left(\frac{\partial v}{\partial x}\right)^2 + \left(\frac{\partial w}{\partial x}\right)^2\right] \tag{2a}$$

$$\gamma_{xy} = \frac{\partial u}{\partial y} + \frac{\partial v}{\partial x} + \frac{\partial v}{\partial y}\cdot\frac{\partial v}{\partial x} + \frac{\partial w}{\partial y}\cdot\frac{\partial w}{\partial x} \tag{2b}$$

$$\gamma_{xz} = \frac{\partial w}{\partial x} + \frac{\partial u}{\partial z} + \frac{\partial v}{\partial z}\cdot\frac{\partial v}{\partial x} + \frac{\partial w}{\partial z}\cdot\frac{\partial w}{\partial x} \tag{2c}$$

where it has been assumed that for moderate displacements $\left(\partial u/\partial x\right)^2 \ll \partial u/\partial x$, $\left(\partial u/\partial x\right)\left(\partial u/\partial y\right) \ll \left(\partial v/\partial x\right) + \left(\partial u/\partial y\right)$, $\left(\partial u/\partial x\right)\left(\partial u/\partial z\right) \ll \left(\partial w/\partial x\right) + \left(\partial u/\partial z\right)$. Substi-tuting the displacement components (1) to the strain-displacement relations (2), the nonvanishing strain resultants are obtained as

$$\varepsilon_{xx} = u_m{}' + \theta''_x\cdot\phi_S^P(y,z) + \frac{1}{2}\cdot\left(y^2+z^2\right)\cdot\left(\theta'_x\right)^2 \tag{3a}$$

$$\gamma_{xy} = \theta'_x\cdot\left(\frac{\partial\phi_S^P}{\partial y} - z\right) + \frac{\partial\phi_S^S}{\partial y} \tag{3b}$$

$$\gamma_{xz} = \theta'_x\cdot\left(\frac{\partial\phi_S^P}{\partial z} + y\right) + \frac{\partial\phi_S^S}{\partial z} \tag{3c}$$

where the second-order geometrically nonlinear term in the right hand side of eqn (3a) $\left(y^2+z^2\right)\cdot\left(\theta'_x\right)^2/2$ is often described as the "Wagner strain". It is worth here noting that in obtaining eqn.(3a) the rate of change of the secondary warping function ϕ_S^S, that is the arising normal strain due to the secondary shear ones due to warping [5], has been ignored.

Considering strains to be small, employing the second Piola – Kirchhoff stress tensor, assuming a zero Poisson ratio and exploiting the Hooke's law of elasticity, the non vanishing stress components are defined in terms of the strain ones as

$$\begin{Bmatrix} S_{xx} \\ S_{xy} \\ S_{xz} \end{Bmatrix} = \begin{bmatrix} E & 0 & 0 \\ 0 & G & 0 \\ 0 & 0 & G \end{bmatrix} \begin{Bmatrix} \varepsilon_{xx} \\ \gamma_{xy} \\ \gamma_{xz} \end{Bmatrix} \tag{4}$$

or employing eqns (3) as

$$S_{xx} = E\left[u_m{}' + \theta_x'' \cdot \phi_S^P\left(y,z\right) + \frac{1}{2}\left(y^2+z^2\right)\cdot\left(\theta_x'\right)^2 \right] \tag{5a}$$

$$S_{xy} = G\cdot\theta_x'\cdot\left(\frac{\partial\phi_S^P}{\partial y} - z\right) + G\cdot\frac{\partial\phi_S^S}{\partial y} \tag{5b}$$

$$S_{xz} = G\cdot\theta_x'\cdot\left(\frac{\partial\phi_S^P}{\partial z} + y\right) + G\cdot\frac{\partial\phi_S^S}{\partial z} \tag{5c}$$

where the first terms in the right hand side of eqns (5b, c) represent the St. Venant (primary) shear stresses and the second terms the warping (secondary) shear ones.

2.2. Equations of local equilibrium

In order to establish local equilibrium equations, the principle of virtual work

$$\delta W_{int} + \delta W_{mass} = \delta W_{ext} \tag{6}$$

where

$$\delta W_{int} = \int_V \left(S_{xx}\delta\varepsilon_{xx} + S_{xy}\delta\gamma_{xy} + S_{xz}\delta\gamma_{xz} \right) dV \tag{7a}$$

$$\delta W_{mass} = \int_V \rho\cdot\left(\ddot{u}\delta u + \ddot{v}\delta v + \ddot{w}\delta w\right) dV \tag{7b}$$

$$\delta W_{ext} = \int_F \left(t_x\cdot\delta u + t_y\cdot\delta v + t_z\cdot\delta w \right) dF \tag{7c}$$

under a Total Lagrangian formulation, is employed. In the above equations, $\delta(\cdot)$ denotes virtual quantities, $(\dot{\ })$ denotes differentiation with respect to time, V, F are the volume and the surface of the bar, respectively, at the initial configuration and $t_x,\ t_y,\ t_z$ are the components of the traction vector with respect to the undeformed surface of the bar.

Neglecting virtual terms of the secondary warping function ϕ_S^S, the primary warping function's ϕ_S^P virtual components of eqn. (7a) are given as

$$I_1 = \int_V S_{xx}\theta_x''\delta\phi_S^P dV + \int_V \theta_x'\cdot\left(S_{xy}\frac{\partial\delta\phi_S^P}{\partial y} + S_{xz}\frac{\partial\delta\phi_S^P}{\partial z} \right) dV \tag{8}$$

Following the technique presented in [6], integration by parts is carried out on the first term of eqn. (8) with respect to the longitudinal variable x, thus obtaining

$$\int_{x=0}^{l}\int_{\Omega}\left(\theta_x'\right)'\cdot\left(S_{xx}\delta\phi_S^P\right)d\Omega dx = -\int_{x=0}^{l}\int_{\Omega}\theta_x'\cdot\frac{\partial}{\partial x}\left(S_{xx}\delta\phi_S^P\right)d\Omega dx + \left[\int_{\Omega}\left(\theta_x'\right)\cdot\left(S_{xx}\delta\phi_S^P\right)d\Omega\right]_{x=0}^{l} \tag{9}$$

Integrating by parts with respect to the cross-sectional variables y, z, the second term of eqn. (8) can be written as

$$\int_{x=0}^{l}\int_{\Omega}\theta_x' \cdot \left(S_{xy}\frac{\partial \delta\phi_S^P}{\partial y} + S_{xz}\frac{\partial \delta\phi_S^P}{\partial z} \right) d\Omega dx = \int_{x=0}^{l}\left[-\theta_x' \cdot \int_{\Omega}\left(\frac{\partial S_{xy}}{\partial y} + \frac{\partial S_{xz}}{\partial z} \right)\delta\phi_S^P d\Omega + \right.$$
$$\left. + \theta_x' \cdot \int_{\Gamma}\left(S_{xy}n_y + S_{xz}n_z \right)\delta\phi_S^P ds \right] dx \tag{10}$$

where $n_y = cos\beta$, $n_z = sin\beta$ are the direction cosines of the normal vector $\boldsymbol{n}$ to the boundary Γ, with $\beta = \widehat{\mathbf{y}\boldsymbol{n}}$ (see Fig.1). Substituting eqns (9), (10) into eqn (8) gives

$$I_1 = \int_{x=0}^{l}\left[-\theta_x' \cdot \int_{\Omega}\left(\frac{\partial S_{xx}}{\partial x} + \frac{\partial S_{xy}}{\partial y} + \frac{\partial S_{xz}}{\partial z} \right)\delta\phi_S^P d\Omega + \theta_x' \cdot \int_{\Gamma}\left(S_{xy}n_y + S_{xz}n_z \right)\delta\phi_S^P ds \right] dx +$$
$$+ \left[\theta_x' \cdot \int_{\Omega} S_{xx}\delta\phi_S^P d\Omega \right]_{x=0}^{l} \tag{11}$$

Neglecting virtual terms of the secondary warping function ϕ_S^S, the primary warping function's ϕ_S^P virtual components of eqns (7b), (7c) are given as

$$I_2 = \int_V \rho\ddot{u} \cdot \theta_x'\delta\phi_S^P dV = \int_{x=0}^{l}\left(\theta_x' \cdot \int_{\Omega}\rho\ddot{u}\delta\phi_S^P d\Omega \right) dx \tag{12a}$$

$$I_3 = \int_F t_x \cdot \theta_x'\delta\phi_S^P dF = \int_{\Omega_0} t_x \cdot \theta_x'\delta\phi_S^P d\Omega + \int_{\Omega_l} t_x \cdot \theta_x'\delta\phi_S^P d\Omega + \int_{F_{lat}} t_x \cdot \theta_x'\delta\phi_S^P dF \tag{12b}$$

where Ω_0, Ω_l are the bar's two dimensional regions of the end cross-sections and F_{lat} is the lateral surface of the bar. Having in mind that the traction vector with respect to the undeformed surface of the bar is expressed by the first Piola – Kirchhoff stress tensor, eqn (12b) is written as

$$I_3 = \left[\theta_x' \cdot \int_{\Omega} P_{xx} \cdot \delta\phi_S^P d\Omega \right]_0^l + \int_{x=0}^{l}\left[\theta_x' \cdot \int_{\Gamma}\left(P_{xy}n_y + P_{xz}n_z \right)\delta\phi_S^P ds \right] dx \tag{13}$$

where P_{xx}, P_{xy}, P_{xz} are components of the first Piola – Kirchhoff stress tensor. Employing the identity relating the first and second Piola – Kirchhoff stress tensors, eqn (13) is written as

$$I_3 = \left[\theta_x' \cdot \int_{\Omega} P_{xx}\delta\phi_S^P d\Omega \right]_0^l + \int_{x=0}^{l} \theta_x' \cdot \left[\int_{\Gamma}\left(1 + \frac{\partial u}{\partial x} \right) \cdot \left(S_{xy}n_y + S_{xz}n_z \right)\delta\phi_S^P ds \right] dx \tag{14}$$

Knowing that the primary warping function's ϕ_S^P virtual components cannot vanish and that deformation cannot be constant ($\frac{\partial u}{\partial x} \neq 0$), eqns (11), (12a), (14) lead to the following local equilibrium equation

$$\frac{\partial S_{xx}}{\partial x} + \frac{\partial S_{xy}}{\partial y} + \frac{\partial S_{xz}}{\partial z} - \rho\ddot{u} = 0 \text{ in } \Omega, \ \forall x \in (0,l) \tag{15}$$

along with its corresponding boundary condition

$$S_{xy}n_y + S_{xz}n_z = 0 \text{ on } \Gamma\,,\ \forall x \in (0,l) \tag{16}$$

In eqns (11), (14), the terms related to the bar's end cross sections insert an inconsistency into the present formulation, which is local and does not affect the overall behavior of the bar. Having in mind that a nonuniform torsion theory is formulated, such an inconsistency is expected, while in some cases (uniform torsion, fully restrained warping boundary conditions at the bar ends) the aforementioned terms vanish and equilibrium equations are exact.

Requiring both the primary and the secondary due to warping parts of eqns (15), (16) to vanish and ignoring the term $\ddot{\phi}_S^S$, the following governing equation for the secondary ϕ_S^S warping function is obtained as

$$\nabla^2\phi_S^S = \left(-\frac{E}{G}u_m''' + \frac{\rho}{G}\ddot{u}_m\right) - \left(\frac{E}{G}\theta_x'''' - \frac{\rho}{G}\ddot{\theta}_x'\right)\cdot\phi_S^P(y,z) - \frac{E}{G}\theta_x'\theta_x''\cdot\left(y^2+z^2\right) \qquad \text{in } \Omega \tag{17}$$

along with its corresponding boundary condition

$$\frac{\partial\phi_S^S}{\partial n} = 0 \qquad \text{on } \Gamma_j \tag{18}$$

where $\nabla^2 = \partial^2/\partial x^2 + \partial^2/\partial y^2$ is the Laplace operator and $\partial/\partial n$ denotes the directional derivative normal to the boundary Γ, while as expected, the governing equation related to the primary ϕ_S^P warping function is found to be coincident with the well known St. Venant's corresponding boundary value problem [1].

Thus, the secondary ϕ_S^S warping function will be evaluated from the solution of the Poisson problem described by the governing equation (17) inside the two dimensional region Ω, subjected to the boundary condition (18) on its boundary Γ. Since the boundary value problem at hand has Neumann type boundary condition, the evaluated warping function contains an integration constant (parallel displacement of the cross section along the bar axis). This integration constant is evaluated by inducing a suitable constraint to the Neumann problem (17-18) so that the problem at hand possesses a unique solution. This constraint is given from

$$\int_\Omega \phi_S^S \, d\Omega = 0 \tag{19}$$

and arises from the request that the torsional terms of the displacement field do not result any axial forces. It is worth pointing out that any other constraint could be used, although the use of eqn (19) decouples the governing equations of the torsional problem at the greatest extent.

2.3. Equations of global equilibrium

Substituting the stress components (eqns (5)), the strain ones (eqns (3)) and the displacement components (eqns (1)) to the principle of virtual work (eqn (6)), the governing partial differential equations of the bar are obtained after some algebra as

$$\rho A\cdot\ddot{u}_m - EA\cdot u_m'' - EI_P\cdot\theta_x'\theta_x'' = n(x,t) \tag{20a}$$

$$\begin{aligned}\rho I_P\cdot\ddot{\theta}_x - \rho C_S\cdot\ddot{\theta}_x'' - GI_t\theta_x'' + EC_S\theta_x'''' - \frac{3}{2}EI_{PP}\cdot\left(\theta_x'\right)^2\theta_x'' - EI_P\cdot u_m'\theta_x'' - EI_P\cdot u_m''\theta_x' = \\ = m_t(x,t) + \frac{\partial}{\partial x}\left[m_w(x,t)\right]\end{aligned} \tag{20b}$$

subjected to the initial conditions ($x \in (0,l)$)

$$u_m(x,0) = \bar{u}_{m0}(x) \qquad \dot{u}_m(x,0) = \dot{\bar{u}}_{m0}(x) \tag{21a,b}$$

$$\theta_x(x,0) = \bar{\theta}_{x0}(x) \qquad \dot{\theta}_x(x,0) = \dot{\bar{\theta}}_{x0}(x) \tag{21c,d}$$

together with the boundary conditions at the bar ends $x = 0,l$

$$a_1 N + \alpha_2 u_m = \alpha_3 \tag{22a}$$

$$\beta_1 M_t + \beta_2 \theta_x = \beta_3 \qquad \bar{\beta}_1 M_w + \bar{\beta}_2 \theta_x' = \bar{\beta}_3 \tag{22b,c}$$

where N, M_t, M_w are the axial force, the twisting and warping moments at the bar ends given in [4].

The expressions of the externally applied loads appearing in the right hand side of eqns (20) with respect to the first Piola-Kirchhoff stress components can be easily deduced by virtue of eqn (7c). It is worth here noting that in deriving the governing equations of the bar, the secondary shear stress distribution has been ignored [5], while damping could also be included without any special difficulty. The geometric cross sectional properties appearing in eqns (20) are also given in [4].

The solution of the initial boundary value problem described by eqns (20-22), for the evaluation of the unknown kinematical components $u_m(x,t)$, $\theta_x(x,t)$ assumes that the warping C_S and the torsion I_t constants are already established, the evaluation of which presumes that the primary warping function φ_S^P at any interior point of the domain Ω of the cross section of the bar is evaluated [1]. Once these components are established, the secondary warping function φ_S^S at any interior point of the domain Ω of the cross section of the bar is evaluated after solving the boundary value problem described by eqns (17-18). Subsequently the second Piola – Kirchhoff stress components are evaluated employing eqns (5), completing the computation of the stress field.

A significant reduction on both the set of the governing differential equations and the boundary value problem related to the secondary warping function φ_S^S can be achieved by neglecting the axial inertia term $\rho A \cdot \ddot{u}_m$ of eqn (20a), an assumption which is common among various dynamic beam formulations. Ignoring this term, a single partial differential equation along with a single unknown kinematical component (the angle of twist $\theta_x(x,t)$) is obtained, which is further simplified in the case of vanishing distributed axial load along the bar. In what follows, this procedure is described in detail for the cases of axially immovable ends and constant axial load along the bar, which are of great practical interest. The aforementioned axial inertia term will be taken into account in the section of numerical examples, for the first time in the literature for the stress analysis of bars under nonlinear nonuniform torsional vibrations, investigating the influence of its ignorance.

2.4. Reduced problems for special cases of axial boundary conditions

For the case of axially immovable ends, it is easily proved that [4]

$$u_m'' = -\frac{I_P}{A} \cdot \theta_x' \theta_x'' \ , \ \forall x \in (0,l) \tag{23}$$

which after subsequent integration yields

$$u_m' = -\frac{1}{2} \cdot \frac{I_P}{A} \cdot (\theta_x')^2 + \frac{\tilde{N}}{EA} \ , \ \forall x \in [0,l] \tag{24}$$

where $\tilde{N}$ is a time-dependent tensile axial load induced by the geometrical nonlinearity given as

$$\tilde{N} = \frac{1}{2} \cdot \frac{EI_P}{l} \cdot \int_0^l (\theta_x')^2 \, dx \tag{25}$$

For the case of constant along the bar axial load eqns (23-24) hold by setting $\tilde{N} = \bar{N}(l,t)$, where $\bar{N}(l,t)$ is the externally applied axial force at the bar's right end. Substituting eqns (23-24) into eqns (20) the reduced initial boundary value problem is established as

$$\rho I_P \cdot \ddot{\theta}_x - \rho C_S \cdot \ddot{\theta}''_x - \left(GI_t + \frac{I_P}{A} \cdot \tilde{N} \right) \theta''_x + EC_S \theta''''_x - \frac{3}{2} EI_n \cdot \left(\theta'_x\right)^2 \theta''_x = \\ = m_t(x,t) + \frac{\partial}{\partial x}\left[m_w(x,t) \right] \tag{26}$$

where the pertinent initial and boundary conditions are appropriately modified, while the boundary value problem related to the secondary warping function φ_S^S (eqns (17-18)) is accordingly modified to

$$\nabla^2 \phi_S^S = \frac{E}{G} \theta'_x \theta''_x \cdot \left[\frac{I_P}{A} - \left(y^2 + z^2\right) \right] - \left(\frac{E}{G} \theta'''_x - \frac{\rho}{G} \ddot{\theta}'_x \right) \cdot \phi_S^P(y,z) \qquad \text{in } \Omega \tag{27a}$$

$$\frac{\partial \phi_S^S}{\partial n} = 0 \qquad \text{on } \Gamma_j \tag{27b}$$

It is worth here noting that I_n in eqn.(26) is a nonnegative geometric cross sectional property, related to the geometrical nonlinearity, defined as

$$I_n = I_{PP} - \frac{I_P{}^2}{A} \tag{28}$$

The linear part of the secondary warping function ϕ_S^S, that is $\phi_{S\,lin}^S$, arising from a geometrically linear analysis can be retrieved by solving the boundary value problem

$$\nabla^2 \phi_{S\,lin}^S = -\left(\frac{E}{G} \theta'''_x - \frac{\rho}{G} \ddot{\theta}'_x \right) \cdot \phi_S^P(y,z) \qquad \text{in } \Omega \tag{29a}$$

$$\frac{\partial \phi_{S\,lin}^S}{\partial n} = 0 \qquad \text{on } \Gamma_j \tag{29b}$$

The influence of the geometrical nonlinearity on the secondary warping function and on the warping shear stresses will be investigated in the section of numerical examples.

3. Integral Representations – Numerical Solution

3.1. For the axial displacement u_m and the angle of twist θ_x

Both the complete and the reduced initial boundary value problems formulated in the previous section are nonlinear and cannot be solved analytically. Thus, an efficient numerical scheme must be employed requiring both longitudinal and time discretization. In this study the Analog Equation Method [7], as it is developed for hyperbolic differential equations [8] is used to approximate the displacement $u_m(x,t)$ and the angle of twist $\theta_x(x,t)$ along the bar. The arising semidiscretized nonlinear equations of motion are then solved employing the Petzold-Gear time discretization scheme [9].

3.2. For the primary warping function ϕ_S^P

The evaluation of the axial displacement u_m and the angle of twist θ_x assume that the warping C_S and the torsion I_t constants [1] are already established. The evaluation of these constants presumes that the primary warping function ϕ_S^P at any interior point of the domain Ω of the cross section of the bar is known.

Once ϕ_S^P is established, C_S and I_t constants are evaluated by converting the domain integrals into line integrals along the boundary using the corresponding relations presented in Sapountzakis and Mokos [1].

Moreover, the evaluation of the primary warping function ϕ_S^P with respect to the shear center *S* and of its derivatives with respect to y and z at any interior point for the calculation of the stress components (eqns (5)) is accomplished using BEM as this is presented in [1].

3.3. For the secondary warping function ϕ_S^S

The numerical solution of the boundary value problem described by eqns (17-18) or that of eqns (27a-b) for the evaluation of the secondary warping function ϕ_S^S will be accomplished using BEM [10]. This method is applied for the aforementioned problem using the formulation presented in [1]. The boundary conditions of each boundary value problem are of Neumann type, thus the arising linear systems of equations are singular and cannot be directly solved. In this study, the regularization technique proposed by Lutz et. al. [3], as this is employed for 2D potential problems [11], is used to eliminate the singularities of the problems of eqns (17-18), (27a-b). It is pointed out that other techniques proposed in the literature ([10], [12]) lead to completely erroneous results for the problem at hand. To employ the aforementioned technique, the Poisson equations (17), (27a) are transformed to Laplace ones, which is performed by using particular solutions of the Poisson equations [10]. After the resolution of ϕ_S^S, its derivatives with respect to y,z are computed in Ω so that the warping shear stresses (i.e. the last terms of eqns (5b, c)) are evaluated.

4. Numerical Examples

$A\left(m^2\right)$	$5,800\times 10^{-3}$
$I_P\left(m^4\right)$	$5,434\times 10^{-5}$
$I_{PP}\left(m^6\right)$	$6,722\times 10^{-7}$
$I_n\left(m^6\right)$	$1,631\times 10^{-7}$
$I_t\left(m^4\right)$	$2,080\times 10^{-7}$
$C_S\left(m^6\right)$	$1,200\times 10^{-7}$

Table 1. Geometric constants of the bar

$u_m'''\left(m^{-1}\right)$	$1,199\times 10^{-3}$
$\ddot{u}_m\left(m\cdot sec^{-2}\right)$	$-1,530\times 10^{4}$
$\theta_x'\left(rad\cdot m^{-1}\right)$	$0,237$
$\theta_x''\left(rad\cdot m^{-2}\right)$	$-0,803$
$\theta_x'''\left(rad\cdot m^{-3}\right)$	$-0,842$
$\ddot{\theta}_x'\left(rad\cdot m^{-1}\cdot sec^{-2}\right)$	$-1,585\times 10^{6}$

Table 2. Kinematical components used to resolve the secondary warping function.

An I-shaped cross-section bar ($E=2,1\times 10^8 kN/m^2$, $G=8,1\times 10^7 kN/m^2$, $\rho=8,002kN\,sec^2/m^4$) of length $l=4,0m$, having flange and web width $t_f=t_w=0,01m$, total height and total width $h=b=0,20m$ has been analyzed, while the numerical results have been obtained employing 21 nodal points (longitudinal discretization) and 600 boundary elements (cross section discretization). The geometric constants of the bar are given in Table 1. The bar is simply supported (according to its torsional boundary conditions) and subjected to a moving concentrated twisting moment. All of the initial conditions are zero, except for the initial axial displacements, which are given from $\bar{u}_{m0}(x)=\left[\bar{N}(l,0)/(EA)\right]\cdot x$, while the bar has an immovable left and free right end subjected to constant axial load $\bar{N}(l,t)=-2500kN$, according to its axial boundary conditions. The concentrated twisting moment has a constant numerical value $M_t=20,0kNm$ and "travels" with a constant velocity $\upsilon=40m/sec$, thus the bar is subjected to free vibrations after $t=0,1sec$.

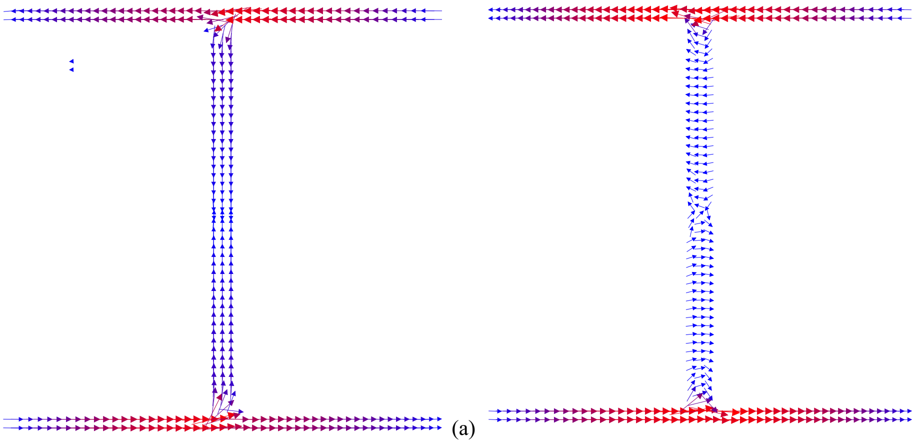

Fig. 2. Warping shear stress distributions arising from ϕ_S^S (a) and its linear part $\phi_{S\,lin}^S$ (b).

$max\,\theta'_x\phi_S^P\,(m)$	$2{,}344\times10^{-3}$
$min\,\theta'_x\phi_S^P\,(m)$	$-2{,}344\times10^{-3}$
$max\,\phi_S^S\,(m)$	$5{,}330\times10^{-5}$
$min\,\phi_S^S\,(m)$	$-7{,}338\times10^{-5}$
$max\,\phi_{S\,lin}^S\,(m)$	$6{,}823\times10^{-5}$
$min\,\phi_{S\,lin}^S\,(m)$	$-6{,}823\times10^{-5}$
$max\,S_{xn}^S\,(MPa)$	$96{,}971$
$max\,S_{xnlin}^S\,(MPa)$	$81{,}106$
$max\,S_{xn}^P\,(MPa)$	$191{,}346$
$max\,S_{xn}\,(MPa)$	$244{,}468$

Table 3. Extreme values of various kinematical and stress components at $x=1{,}905m$, $t=0{,}0588\,sec$ of the bar of example 1.

The evaluation of the secondary warping function precedes the solution of the initial boundary value problem of eqns (20) in order to obtain the kinematical components u_m, θ_x along with their derivatives (at the bar's nodal points) in the time domain. In Table 2, the obtained results at a cross section (slightly) at the left of the midpoint of the bar ($x=1{,}905m$) are presented for $t=0{,}0588\,sec$, that is the instant at which the angle of twist at the midpoint of the bar $\theta_x(l/2,t)$ becomes maximum ($max\,\theta_x(l/2,t)=1{,}181\mathrm{rad}$, for $0{,}0\le t\le0{,}15\,(sec)$). Using these results, the boundary value problems of eqns (17-18) and (26a, b) are solved to obtain the secondary warping function ϕ_S^S and its linear part $\phi_{S\,lin}^S$. In Fig. 2 the warping shear stress distributions arising from ϕ_S^S (denoted as S_{xn}^S) and their linear part $\phi_{S\,lin}^S$ (denoted as S_{xnlin}^S) are presented demonstrating the great discrepancy between them in the web area. A slight difference is also observed near the flange-web intersections. Finally, in Table 3 the extreme values of various kinematical and stress components are presented showing the efficiency of the proposed method. For comparison reasons, the extreme values of $\theta'_x\cdot\phi_S^P$ and the maximum values of the St. Venant (primary) shear stress vector S_{xn}^P and of the total shear stress vector $S_{xn} = S_{xn}^P + S_{xn}^S$ are also included, indicating that the warping shear stresses should not be neglected in nonuniform nonlinear torsional vibrations of bars.

5. Concluding remarks

The main conclusions that can be drawn from this investigation are

a. The numerical technique presented in this investigation is well suited for computer aided analysis of cylindrical bars of arbitrarily shaped doubly symmetric cross section, supported by the most general boundary conditions and subjected to the combined action of arbitrarily distributed or concentrated time dependent conservative axial and torsional loading.
b. Geometrical nonlinearity, dynamic loading and axial boundary conditions influence the warping shear stress distribution and magnitude of bars undergoing twisting deformations.
c. Warping shear stresses should not be neglected in nonuniform nonlinear torsional vibrations of bars.
d. The developed procedure retains the advantages of a BEM solution over a FEM approach since it requires exclusively boundary discretization of the bar's cross section.

Acknowledgements

The authors would like to thank the Senator Committee of Basic Research of the National Technical University of Athens, Programme "PEVE-2008", R.C. No: 65 for the financial support of this work.

References

[1] E.J.Sapountzakis and V.G.Mokos Warping shear stresses in nonuniform torsion by BEM, *Computational Mechanics*, **30,** 131-142, 2003.
[2] European Committee for Standardisation (CEN), *Eurocode 3: Design of Steel Structures - Part 1-1: General Rules and Rules for Buildings*, 2003.
[3] E.Lutz, Y.Wenjing and S.Mukherjee Elimination of rigid body modes from discretized boundary integral equations, *International Journal of Solids and Structures* **35,** 4427-4436, 1998.
[4] E.J.Sapountzakis and V.J.Tsipiras Nonlinear Elastic Torsional Vibrations of Bars by BEM, *Proc. of the Computational Methods in Structural Dynamics and Earthquake Engineering - COMPDYN 2009*, Island of Rhodes, Greece, 22-24 June, 2009.
[5] V.G.Mokos *Contribution to the Generalized Theory of Composite Beams Structures by the Boundary Element Method,* PhD Thesis, National Technical University of Athens (in Greek), 2007.
[6] K.Washizu *Variational Methods in Elasticity and Plasticity*, Pergamon Press, Oxford, 1975.
[7] J.T.Katsikadelis The analog equation method. A boundary-only integral equation method for nonlinear static and dynamic problems in general bodies, *Theoretical and Applied Mechanics*, **27,** 13-38, 2002.
[8] E.J.Sapountzakis and J.T.Katsikadelis Analysis of plates reinforced with beams, *Computational Mechanics*, **26,** 66-74, 2000.
[9] K.E.Brenan, S.L.Campbell and L.R.Petzold, *Numerical Solution of Initial-Value Problems in Differential-Algebraic Equations*, North-Holland, Amsterdam, 1989.
[10] J.T.Katsikadelis, *Boundary Elements: Theory and Applications*, Elsevier, Amsterdam-London, 2002.
[11] A.Aimi and M.Diligenti Numerical integration schemes for Petrov-Galerkin infinite BEM, *Applied Numerical Mathematics*, **58,** 1084-1102, 2008.
[12] H.Strese Remarks concerning the boundary element method in potential theory, *Applied Mathematical Modelling*, **8,** 40-44, 1984.

Secondary Torsional Moment Deformation Effect by BEM

E.J. Sapountzakis[1] and V.G.Mokos[2]

[1,2]School of Civil Engineering, National Technical University, Zografou Campus, GR-157 80 Athens, Greece

Keywords: Nonuniform torsion, Shear Deformation, Secondary Torsion Constant, Boundary Element Method.

Abstract. In this paper a boundary element method is developed for the nonuniform torsion of simply or multiply connected prismatic bars of arbitrary cross section, taking in to account secondary torsional moment deformation effect. The bar is subjected to an arbitrarily distributed twisting moment, while its edges are restrained by the most general linear torsional boundary conditions. To account for secondary shear deformation a secondary torsion constant is used, while the first derivative of the angle of twist is split in to a primary and a secondary part due to the bimoment and the secondary twisting moment, respectively. Three boundary value problems with respect to the variable along the bar angle of twist and to the primary and secondary warping functions are formulated and solved employing a pure BEM approach, that is only boundary discretization is used. From the aforementioned primary and secondary warping functions the warping and the primary torsion constant are evaluated using only boundary integration, while the secondary torsion constant is computed employing an effective domain integration. Numerical examples with great practical interest are worked out to illustrate the efficiency and the range of applications of the developed method. The influence of the secondary torsional moment deformation effect of closed-shaped cross sections is verified.

1. Introduction

In engineering practice we often come across the analysis of members of structures subjected to twisting moments. Curved bridges, beams subjected to eccentric loading or columns laid out irregularly in the interior of a plate due to functional requirements are most common examples. When the warping of the cross section of a member is not restrained the applied twisting moment is undertaken from the Saint–Venant shear stresses. In this case the angle of twist per unit length remains constant along the bar (uniform torsion). However, in most cases arbitrary torsional boundary conditions are applied either at the edges or at any other interior point of the bar due to construction requirements. This bar under the action of general twisting loading is leaded to nonuniform torsion (warping torsion), while the angle of twist per unit length is no longer constant along it. It is worth here noting that the effect of torsional warping has to be considered not only for bars with open shaped cross sections, but with closed shaped ones as well.

The nonuniform torsion problem of prismatic bars has been widely studied from both the analytical and numerical point of view. For bars with thin walled profiles the “Vlasov Theory” [1] is mentioned among the extended analytical studies. For bars with arbitrary cross section (thin and/or thick walled) the existing analytical solutions are limited to symmetric cross sections of simple geometry, loading and boundary conditions. Thus, over the past twenty years, numerical methods have been used for the analysis of the aforementioned problem. Among these methods the majority of researchers have employed the Finite Element Method (FEM) [2] or the Boundary Element Method (BEM) [3].

However, to the authors knowledge relatively little work has been done on the corresponding problem of nonuniform torsion of bars, considering the secondary torsional moment deformation effect. In the pioneer work of Heilig [4] a theoretical formulation of the problem is presented. Later, Roik and Sedlacek [5] presented an analytical solution applying the Force Method (Flexibility Method) and using the analogy between 2nd order beam theory (with tensional axial force) and torsion with warping. Rubin [6] using the same analogy gives a modified Three-Moment Equation for continuous prismatic bars. Recently, Murín and Kutiš [7] using also the aforementioned analogy presented a new beam finite element for nonuniform torsion with secondary shear deformation. In all of the aforementioned studies only bars with thin walled cross section are investigated, since the torsional cross section parameters (warping constant, primary and secondary torsion constant) are evaluated employing the thin tube theory. Finally, Kraus [8] presented a FEM solution for the calculation of the secondary torsion constant of bars with arbitrary cross section. Nevertheless, to the authors’ knowledge, the boundary element method has not yet been used for the solution of the nonuniform torsion problem considering secondary shear deformation.

In this paper a boundary element method is developed for the nonuniform torsion of simply or multiply connected prismatic bars of arbitrary cross section, taking into account secondary torsional moment deformation effect. The bar is subjected to an arbitrarily distributed twisting moment, while its edges are restrained by the most general linear torsional boundary conditions. To account for secondary shear deformation a secondary torsion constant is used, while the first derivative of the angle of twist is split in to a primary and a secondary part due to the bimoment and the secondary twisting moment, respectively. Three boundary value problems with respect to the variable along the bar angle of twist and to the primary and secondary warping functions are formulated and solved employing a pure BEM approach, that is only boundary discretization is used. From the aforementioned primary and secondary warping functions the warping and the primary torsion constant are evaluated using only boundary integration, while the secondary torsion constant is computed employing an effective domain integration. Numerical examples with great practical interest are worked out to illustrate the efficiency and the range of applications of the developed method. The influence of the secondary torsional moment deformation effect of close-shape cross sections is verified, while the accuracy of the proposed secondary torsion constant compared with those obtained from a FEM solution is noteworthy.

2. Statement of the Problem

Consider a prismatic bar with modulus of elasticity E and shear modulus G of length l with a cross section of arbitrary shape, occupying the two dimensional multiply connected region Ω of the y,z plane bounded by the $K+1$ curves $\Gamma_1, \Gamma_2, ..., \Gamma_K, \Gamma_{K+1}$ as shown in Fig.1. When the bar is subjected to the arbitrarily distributed twisting moment $m_t = m_t(x)$ its angle of twist $\theta_x = \theta_x(x)$ taking into account secondary torsional moment deformation effect is governed by the following boundary value problem

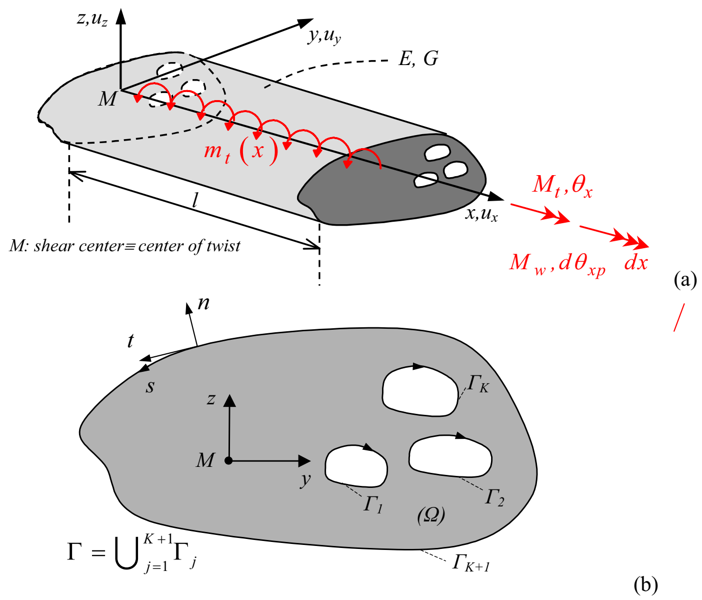

Fig. 1. Prismatic bar subjected to twisting loading (a) with a cross section of arbitrary shape occupying the two dimensional region Ω (b).

$$E\bar{C}_M \frac{d^4\theta_x}{dx^4} - GI_{tp}\frac{d^2\theta_x}{dx^2} = m_t - \frac{E\bar{C}_M}{GI_{tp}}\frac{d^2 m_t}{dx^2}(1-\kappa) \qquad \text{inside the bar} \tag{1}$$

$$\alpha_1\theta_x + \alpha_2 M_t = \alpha_3 \tag{2a}$$

at the bar ends $x = 0,l$

$$\beta_1 \frac{d\theta_{xp}}{dx} + \beta_2 M_w = \beta_3 \tag{2b}$$

where

$$\bar{C}_M = \frac{C_M}{\kappa} \tag{3}$$

$$\kappa = \frac{I_{tp}}{I_{tp} + I_{ts}} \tag{4}$$

In the aforementioned relations C_M, I_{tp} and I_{ts} are the warping constant, the primary torsion constant and the secondary torsion constant of the bar cross section, respectively. Moreover, M_t is the total torsional moment and M_w is the bimoment resulting from the normal stress distribution due to warping given as

$$M_t = M_{tp} + M_{ts} \tag{5}$$

$$M_w = -E\bar{C}_M \frac{d^2\theta_x}{dx^2} - \frac{E\bar{C}_M}{GI_{tp}} m_t \left(1-\kappa\right) \qquad \text{inside the bar} \tag{6a}$$

$$M_w = -E\bar{C}_M \frac{d^2\theta_x}{dx^2} \qquad \text{at the bar ends } x = 0,l \tag{6b}$$

In eqn (5) M_{tp} is the primary torsional moment resulting from the primary shear stress distribution due to twisting loading, while M_{ts} is the secondary torsional moment resulting from the secondary shear stress distribution due to warping given as

$$M_{tp} = GI_{tp} \frac{d\theta_x}{dx} \tag{7}$$

$$M_{ts} = -E\bar{C}_M \frac{d^3\theta_x}{dx^3} - \frac{E\bar{C}_M}{GI_{tp}} \frac{dm_t}{dx} \left(1-\kappa\right) \qquad \text{inside the bar} \tag{8a}$$

$$M_{ts} = -E\bar{C}_M \frac{d^3\theta_x}{dx^3} \qquad \text{at the bar ends } x = 0,l \tag{8b}$$

To account for secondary shear deformation the first derivative of the angle of twist is split into a primary and a secondary part due to the bimoment and the secondary twisting moment, respectively. Thus, the total first derivative of the angle of twist $d\theta_x/dx$ can be written as

$$\frac{d\theta_x}{dx} = \frac{d\theta_{xp}}{dx} + \frac{d\theta_{xs}}{dx} \tag{9}$$

where $d\theta_{xp}/dx$ represents the primary torsional curvature arising from the warping normal stresses, while $d\theta_{xs}/dx$ represents the secondary torsional curvature due to the warping shear stresses given as [5]

$$\frac{d\theta_{xs}}{dx} = \frac{M_{ts}}{GI_{ts}} \tag{10}$$

Employing eqns. (4), (9) and (10) the primary torsional curvature with respect to the total first derivative of the angle of twist can be written as

$$\frac{d\theta_{xp}}{dx} = \frac{d\theta_x}{dx} - \frac{M_{ts}}{GI_{tp}}\frac{1-\kappa}{\kappa} \tag{11}$$

Moreover, in eqns. (2) a_i, β_i $(i = 1,2,3)$ are functions specified at the boundary of the bar. The boundary conditions (2a,b) are the most general linear torsional boundary conditions for the bar problem including also elastic support. It is apparent that all types of the conventional torsional boundary conditions (clamped, simply supported, free or guided edge) can be derived from these equations by specifying appropriately the functions a_i and β_i (e.g. for a clamped edge it is $a_1 = \beta_1 = 1$, $a_2 = a_3 = \beta_2 = \beta_3 = 0$). It is worth here noting that in the case of negligible secondary shear deformations $I_{ts}{}^{-1} = 0 \rightarrow \kappa = 1$ and $d\theta_{xp}/dx = d\theta_x/dx$. This assumption is usually employed in the case of open formed cross sections.

The solution of the boundary value problem given from eqns (1), (2a,b) presumes the evaluation of the warping and the primary and secondary torsion constants C_M, I_{tp} and I_{ts}, respectively, which are given as

$$C_M = \int_\Omega \left(\varphi_M^P\right)^2 d\Omega \tag{12a}$$

$$I_{tp} = \int_\Omega \left(y^2 + z^2 + y\frac{\partial\varphi_M^P}{\partial z} - z\frac{\partial\varphi_M^P}{\partial y} \right) d\Omega \tag{12b}$$

$$I_{ts} = \frac{1}{\int_\Omega \left(\frac{\partial\tilde{\varphi}_M^S}{\partial z}\frac{\partial\tilde{\varphi}_M^S}{\partial y} + \frac{\partial\tilde{\varphi}_M^S}{\partial z}\frac{\partial\tilde{\varphi}_M^S}{\partial z} \right) d\Omega} \tag{12c}$$

where $\varphi_M^P(y,z)$ and $\tilde{\varphi}_M^S(y,z)$ are the primary (main) and secondary (unit) warping functions with respect to the shear center M [3] of the cross section of the bar, respectively, which can be establish by solving independently the following Neumann problems

$$\nabla^2\varphi_M^P = 0 \quad \text{in } \Omega \tag{13a}$$

$$\frac{\partial\phi_M^P}{\partial n} = zn_y - yn_z \quad \text{on } \Gamma \tag{13b}$$

$$\nabla^2\tilde{\varphi}_M^S = \frac{\varphi_M^P}{C_M}\frac{1}{\kappa} \quad \text{in } \Omega \tag{14a}$$

$$\frac{\partial\tilde{\phi}_M^S}{\partial n} = 0 \quad \text{on } \Gamma \tag{14b}$$

where $\nabla^2 = \partial^2/\partial y^2 + \partial^2/\partial z^2$ is the Laplace operator; $\partial/\partial n$ denotes the directional derivative normal to the boundary Γ and n_y, n_z are the direction cosines. Finally, it is worth here noting that the secondary torsion constant I_{ts} given from eqn. (12c) is evaluated equating the approximate energy of the secondary shear strain with the exact one [5].

3. Integral Representations – Numerical Solution

3.1. For the angle of twist $\theta_x(x)$

The evaluation of the angle of twist θ_x is accomplished using the Analog Equation Method (AEM) [9], a BEM-based method, as this is applied in Sapountzakis and Mokos [10].

3.2. For the primary and secondary warping functions $\varphi_M^P(y,z)$, $\tilde{\varphi}_M^S(y,z)$

The evaluation of the primary and secondary warping functions φ_M^P, $\tilde{\varphi}_M^S$ are accomplished using a pure BEM [11], as this is presented in Sapountzakis and Mokos [3], while from the aforementioned functions the warping and the primary torsion constant are evaluated using only boundary integration [3]. Finally, the secondary torsion constant is computed employing an automatic domain integration using the Advancing Front Method (AFM) [12].

4. Numerical examples

4.1. Example 1

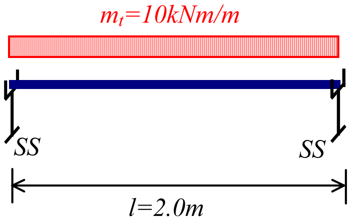

(a)

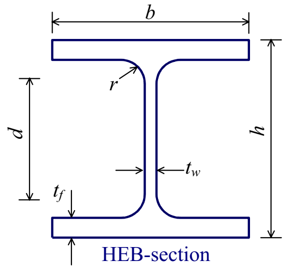

(b)

Fig. 2. Simply supported bar (a) of a steel HEB-section (b) of example 1.

A simply supported bar ($x=0,l$: $a_1=\beta_2=1$, $a_2=a_3=\beta_1=\beta_3=0$) of a steel ($E=2.1\times10^9\,kPa$, $G=8.0769\times10^8\,kPa$) HEB-section (open hot rolled I-section) of length $l=2.0m$, loaded by a uniformly distributed twisting moment $m_t=10kNm/m$, as shown in Fig.2, has been studied.

	BEM			FEM [8]
κ	$\bar{C}_M\left(m^6\right)$	$I_{tp}\left(m^4\right)$	$I_{ts}\left(m^4\right)$	$I_{ts}\left(m^4\right)$
HEB 100 $\left(h=100mm, b=100mm, t_w=6mm, t_f=10mm, r=12mm, d=56mm\right)$				
9.7447E-01	3.3139E-09	9.3916E-08	3.5854E-06	3.5790E-06
HEB 200 $\left(h=200mm, b=200mm, t_w=9mm, t_f=15mm, r=18mm, d=134mm\right)$				
9.8675E-01	1.6908E-07	6.0649E-07	4.5183E-05	4.5050E-05
HEB 300 $\left(h=300mm, b=300mm, t_w=11mm, t_f=19mm, r=27mm, d=208mm\right)$				
9.9046E-01	1.6645E-06	1.9173E-06	1.9917E-04	1.9845E-04

Table 1. Warping constant $\bar{C}_M$, primary I_{tp} and secondary I_{ts} torsion constants of the HEB-sections of example 1.

In Table 1 the computed torsional cross section parameters (κ, $\bar{C}_M$, I_{tp}, I_{ts}) for various HEB-sections are presented, while the secondary torsion constant I_{ts} is compared with that obtained from a FEM solution for arbitrary cross section [8]. From this table the accuracy of the proposed method is verified. Moreover, in

Table 2 the obtained results of the bar with HEB-100 cross section taking into account or ignoring the secondary shear deformation effect are presented, concluding that for this open formed cross section the secondary torsional moment deformation effect has not significant influence.

$max\, M_w$ at the midspan (kNm^2)	$max\, M_t$ at the edges (kNm)	$max\, M_{tp}$ at the edges (kNm)	$max\, M_{ts}$ at the edges (kNm)	$max\, \theta_x$ at the midspan (rad)	$max\, d\theta_{xp}/dx$ at the edges (rad/m)
Considering Secondary Torsional Moment Deformation Effect (κ=9.7447E-01)					
8.73381E-01	10.0000	6.97935	3.02065	5.47100E-02	9.09765E-02
Ignoring Secondary Torsional Moment Deformation Effect (κ=1.0)					
8.31025E-01	10.0000	7.01748	2.98252	5.49596E-02	9.25106E-02

Table 2. Stress resultants, angle of twist and primary torsional curvature of the bar of example 1 with HEB-100 cross section.

4.2. Example 2

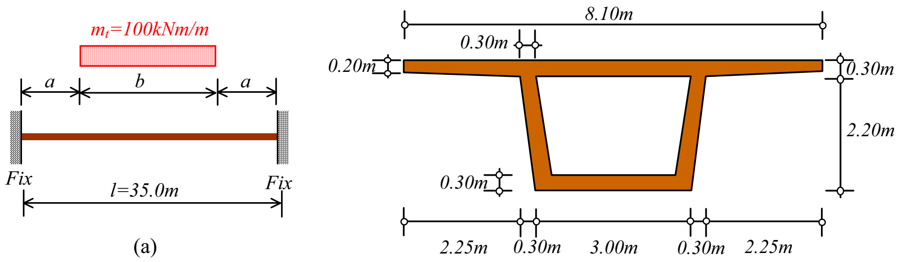

(a) (b)

Fig. 3. Clamped bar (a) of a concrete bridge box shaped cross section (b) of example 2.

To demonstrate the necessity of including the deformation effect of the secondary torsional moment in the nonuniform torsion analysis of bars with closed shaped cross section and especially for the calculation of the bimoment, as a second example a clamped bar of a concrete ($E = 3.00 \times 10^7\, kPa$, $G = 1.50 \times 10^7\, kPa$) bridge box shaped cross section of length $l = 35.0m$, loaded by a uniformly distributed twisting moment $m_t = 100kNm/m$, as this is shown in Fig.3, has been studied.

In Table 3 the computed maximum values of the bimoment ($max\, M_w$) of the bar for various values of the constants a, b are shown, while in Figs.4, 5 the variation of the bimoment along the bar axis for two cases of these constants, namely $a = 0.0m, b = 35.0m$ and $a = 15.0m, b = 5.0m$, respectively, are presented. Finally, in Fig.6 the distribution of the normal stress σ_{xx} due to warping along the boundary of the cross section for $a = 15.0m, b = 5.0m$ is shown ($max\, \sigma_{xx} = \pm 680.355$kPa, at the midspan considering secondary torsional moment deformation effect, $max\, \sigma_{xx} = \pm 265.407$kPa, at the edges ignoring it).

	$max\, M_w\, (kNm)$ at the edges		$max\, M_w\, (kNm)$ at the midspan	
	Considering	Ignoring	Considering	Ignoring
$a = 0.0m, b = 35.0m$	156.625	963.126	411.917	32.2227
$a = 5.0m, b = 25.0m$	263.985	715.245	411.870	32.2227
$a = 10.0m, b = 15.0m$	165.263	435.152	410.613	32.2226
$a = 15.0m, b = 5.0m$	55.178	145.051	371.830	31.8653

Table 3. Maximum values of the bimoments ($max\, M_w$) of the bar of example 2 considering ($\kappa = 0.14509$) or ignoring (κ=*1.0*) secondary torsional moment deformation effect.

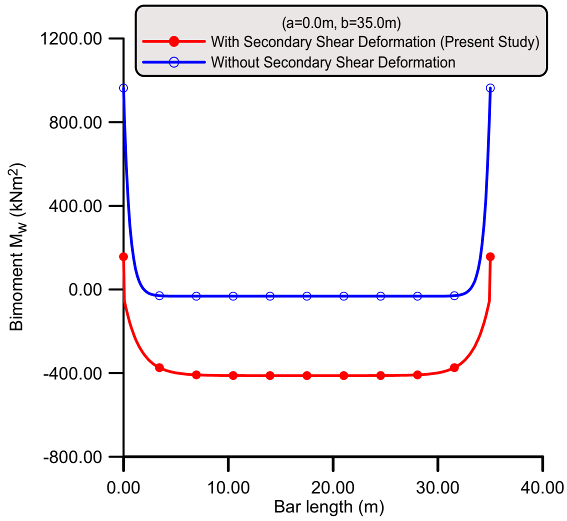

Fig. 4. Variation of the bimoment $M_w(kNm^2)$ for $a = 0.0m$ along the bar of example 2.

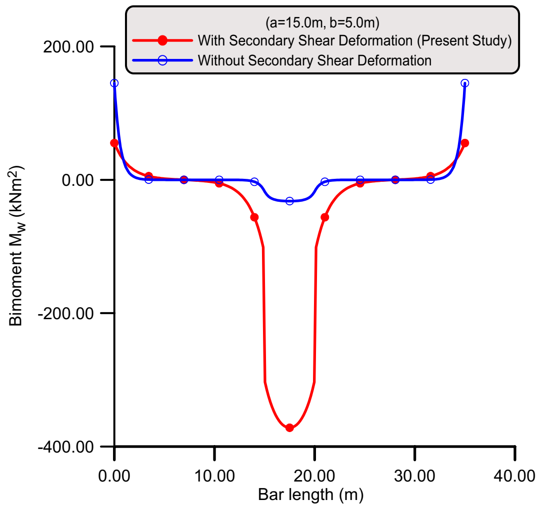

Fig. 5. Variation of the bimoment $M_w(kNm^2)$ for $a = 15.0m$ along the bar of example 2.

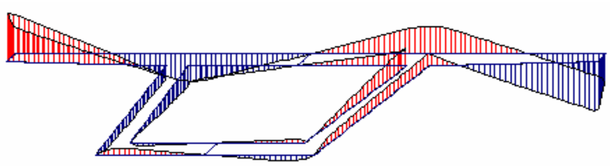

$$\sigma_{xx} = -\frac{M_w}{\bar{C}_M}\varphi_M^P \frac{1}{\kappa}$$

$a = 15.0m$

Fig. 6. Distribution of the normal stress due to warping σ_{xx} for $a = 15.0m$ along the boundary of the cross section of example 2.

From the aforementioned table and figures it is concluded that for bars with closed shaped cross sections the secondary torsional moment deformation effect has a significant influence in the results and especially when subjected to concentrated twisting loading, leading to the fact that this effect should be considered in the nonuniform torsion analysis, especially for the calculation of the bimoments.

5. Concluding Remarks

The main conclusions that can be drawn from this investigation are

a. The numerical technique presented in this investigation is well suited for computer aided analysis for bars of arbitrary cross section, subjected to any linear torsional boundary conditions and to an arbitrarily distributed twisting moment.
b. The magnitude of the evaluated warping normal stresses due to restrained warping necessitates the consideration of these additional normal stresses near the restrained edges.
c. The effect of torsional warping has to be considered not only for bars with open shaped cross sections, but with closed shaped ones as well.
d. The accuracy of the results compared with those obtained from a FEM solution is remarkable.
e. The inaccuracy of the thin tube theory in calculating the secondary torsion constant even for thin-walled sections is noteworthy.
f. For bars with open shaped cross section the secondary torsional moment deformation effect has not significant influence. However, the inclusion of this additional effect in the calculation makes the results more accurate.
g. For bars with closed shaped cross sections the secondary torsional moment deformation effect has an important influence in the results, especially when the bar is subjected to concentrated twisting loading, and should be considered in the analysis especially for the calculation of the bimoments.

References

[1] V.Z. Vlasov *Thin-Walled Elastic Beams*, Israel Program for Scientific Translations, Jerusalem, (1961).
[2] M.Kraus *Computerorientierte Berechnungsmethoden für beliebige Stabquerschnitte des Stahlbaus*, von der Fakultät für Bauingenieurwesen der Ruhr–Universität Bochum genehmigte Dissertation zur Erlangung des Grades Doktor–Ingenieur, (2005).
[3] E.J.Sapountzakis and V.G.Mokos, Warping Shear Stresses in Nonuniform Torsion by BEM, *Computational Mechanics,* **30**(2), 131-142, (2003).
[4] R.Heilig, Der Schubverformzugseinfluss auf die Wölbkrafttorsion von Stäben mit offenem Profil, *Stahlbau*, **30**, 97, (1961).
[5] K. Roik and G. Sedlacek Theorie der Wölbkrafttorsion unter Berücksichtigung der sekundären Schubverformungen – Analogiebetrachtung zur Berechnung des querbelasteten Zugstabes, *Stahlbau*, **35**, 43–52, (1966).
[6] H.Rubin, Wölbkrafttorsion von Durchlaufträgern mit konstantem Querschnitt unter Berücksichtigung sekundärer Schubverformungen, *Stahlbau*, **74**, 826–842, (2005).
[7] J.Murín and V.Kutiš An effective finite element for torsion of constant cross-sections including warping with secondary torsion moment deformation effect, *Engineering Structures*, **30**, 2716–2723, (2008).
[8] M.Kraus *Computerorientierte Bestimmung der Schubkorrekturfaktoren gewalzter I-Profile*, Festschrift Rolf Kindmann, Shaker Verlag, Aachen, 81-98, (2007).
[9] J.T.Katsikadelis The Analog Equation Method: A Boundary–only Integral Equation Method for Nonlinear Static and Dynamic Problems in General Bodies, *Theoretical and Applied Mechanics*, 27, 13−38, (2002).
[10] E.J.Sapountzakis and V.G.Mokos Nonuniform Torsion of Bars of Variable Cross Section, *Computers and Structures*, **82**(9-10), 703-715, (2004).
[11] J.T Katsikadelis *Boundary Elements*: *Theory and Application*, Elsevier, Amsterdam-London, (2002).
[12] S.H.Lo, A new mesh generation scheme for arbitrary planar domains, *Int. J. Num. Meth. Engng.*, **21**, 1403–1426, (1985).

Lateral Buckling Analysis of Beams of Arbitrary Cross Section by BEM

E.J. Sapountzakis[1] and J.A. Dourakopoulos[2]

[1,2]School of Civil Engineering, National Technical University,
Zografou Campus, GR-157 80 Athens, Greece

Keywords: Nonlinear Analysis; Large Deflections; Lateral Buckling; Shear center; Boundary element method

Abstract. In this paper, the lateral buckling analysis of beams of arbitrary cross section is presented taking into account moderate large displacements and employing nonlinear relationships between bending moments and curvatures. The beam is supported by the most general boundary conditions including elastic support or restraint. Starting from a displacement field without any simplifying assumptions about the angle of twist amplitude and based on the total potential energy principle, four highly coupled nonlinear governing differential equations are derived taking into account the shortening and warping effects, the prebuckling displacements and the Wagner's coefficients due to the asymmetric character of the cross section. The arising four boundary value problems with respect to the transverse displacements, to the axial displacement and to the angle of twist are solved using the Analog Equation Method, a BEM based method. The instability criterion is based on the positive definiteness of the second variation of the total potential energy. The proposed formulation does not stand on the assumption of a thin-walled structure and therefore the cross section's torsional rigidity is evaluated exactly without using the so-called Saint –Venant's torsional constant. Numerical examples are worked out to illustrate the efficiency, the accuracy and the range of applications of the developed method. The effects of both the load height and warping as well as the discrepancy of the Eurocode 3 standard solutions are discussed.

1. Introduction

Lateral buckling behaviour of beams is of fundamental importance in the design of structures subjected to heavy transverse loading. This beam lateral buckling analysis becomes much more complicated in the case the cross section's centroid does not coincide with its shear center (monosymmetric or asymmetric beams), leading to the formulation of a highly nonlinear flexural-torsional postbuckling problem. The nonlinearities involved (of geometrical nature) are due to the nonlinear kinematic relations and/or to the nonlinear bending moment - curvature relationship.

In this paper, the lateral buckling analysis of beams of arbitrary cross section is presented taking into account moderate large displacements and employing nonlinear relationships between bending moments and curvatures. Starting from a displacement field without any simplifying assumptions about the angle of twist amplitude and based on the total potential energy principle, four highly coupled nonlinear governing differential equations are derived. The arising four boundary value problems with respect to the transverse displacements, to the axial displacement and to the angle of twist are solved using the Analog Equation Method [1], a BEM based method. The instability criterion is based on the positive definiteness of the second variation of the total potential energy. The essential features and novel aspects of the present formulation compared with previous ones are summarized as follows.

i. The present formulation is applicable to arbitrarily shaped symmetric, monosymmetric or asymmetric thin or thick walled cross sections occupying simple or multiple connected domains.
ii. The proposed method can be employed to beams supported by the most general boundary conditions including elastic support or restraint.
iii. The beam is subjected to an arbitrarily distributed or concentrated transverse loading as well as to axial loading.
iv. The proposed formulation does not stand on the assumption of a thin-walled structure and therefore the cross section's torsional rigidity is evaluated exactly without using the so-called Saint –Venant's torsional constant.
v. The developed method takes into account nonlinear relationships between bending moments and curvatures.
vi. Both the Wagner's coefficients and the shortening effect are taken into account.

vii. The proposed method employs a BEM approach (requiring boundary discretization) resulting in line or parabolic elements instead of area elements of the FEM solutions (requiring the whole cross section to be discretized into triangular or quadrilateral area elements), while a small number of line elements are required to achieve high accuracy.

Numerical examples are worked out to illustrate the efficiency, the accuracy and the range of applications of the developed method. The effects of both the load height and warping as well as the discrepancy of the Eurocode 3 standard solutions are discussed.

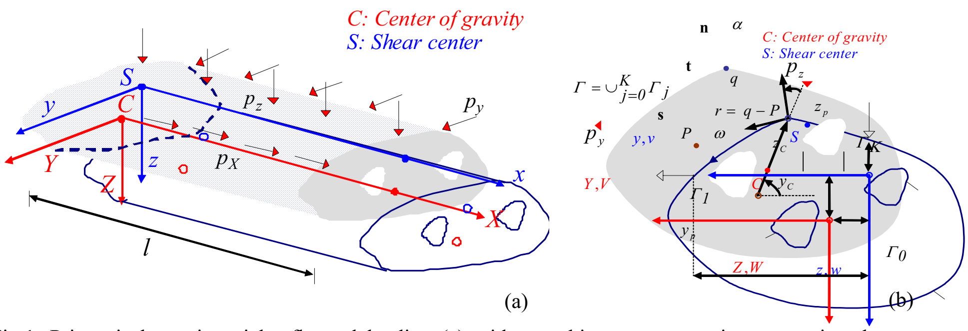

Fig.1. Prismatic beam in axial - flexural loading (a) with an arbitrary cross-section occupying the two dimensional region Ω (b).

2. Statement of the Problem

Let us consider a prismatic beam of length l (Fig.1), of constant arbitrary cross-section of area A. The homogeneous isotropic and linearly elastic material of the beam's cross-section, with modulus of elasticity E, shear modulus G and Poisson's ratio v occupies the two dimensional multiply connected region Ω of the y,z plane and is bounded by the $\Gamma_j\left(j=1,2,...,K\right)$ boundary curves, which are piecewise smooth, i.e. they may have a finite number of corners. In Fig. 1 CYZ is the principal bending coordinate system through the cross section's centroid C, while y_C, z_C are its coordinates with respect to the Syz shear system of axes through the cross section's shear center S, with axes parallel to those of the CYZ system. The beam is subjected to the combined action of the arbitrarily distributed or concentrated axial loading $p_X=p_X(X)$ along the centroid axis CX and transverse loading $p_y=p_y(x)$, $p_z=p_z(x)$ acting in the y and z directions, respectively, passing through the shear center S and applied at distances y_p, z_p from it. (Fig. 1a).

Under the action of the aforementioned loading, the displacement field of an arbitrary point of the cross section can be derived with respect to those of the shear center as

$$\bar{u}(x,y,z)=u(x)-(y-y_C)\theta_Z(x)+(z-z_C)\theta_Y(x)+\theta_x'(x)\varphi_S^P(y,z) \tag{1a}$$

$$\bar{v}(x,y,z)=v(x)-z\,sin\left(\theta_x(x)\right)-y\left[1-cos\left(\theta_x(x)\right)\right] \tag{1b}$$

$$\bar{w}(x,y,z)=w(x)+y\,sin\left(\theta_x(x)\right)-z\left[1-cos\left(\theta_x(x)\right)\right] \tag{1c}$$

$$\theta_Y(x)=v'(x)sin\left(\theta_x(x)\right)-w'(x)cos\left(\theta_x(x)\right) \tag{1d}$$

$$\theta_Z(x)=v'(x)cos\left(\theta_x(x)\right)+w'(x)sin\left(\theta_x(x)\right) \tag{1e}$$

where $\bar{u}$, $\bar{v}$, $\bar{w}$ are the axial and transverse beam displacement components with respect to the Syz shear system of axes; $u=u(x)$, $v=v(x)$, $w=w(x)$ are the corresponding components of the shear center S; θ_Y, θ_Z are the angles of rotation due to bending of the cross-section with respect to its centroid; $\theta_x'(x)$

denotes the rate of change of the angle of twist θ_x regarded as the torsional curvature and ϕ_S^P is the primary warping function with respect to the shear center S [2].

Employing the strain-displacement relations of the three - dimensional elasticity for moderate large displacements, the following strain components can be easily obtained

$$\varepsilon_{xx} = \frac{\partial \overline{u}}{\partial x} + \frac{1}{2}\left[\left(\frac{\partial \overline{u}}{\partial x}\right)^2 + \left(\frac{\partial \overline{v}}{\partial x}\right)^2 + \left(\frac{\partial \overline{w}}{\partial x}\right)^2\right] \approx \frac{\partial \overline{u}}{\partial x} + \frac{1}{2}\left[\left(\frac{\partial \overline{v}}{\partial x}\right)^2 + \left(\frac{\partial \overline{w}}{\partial x}\right)^2\right] \tag{2a}$$

$$\gamma_{xz} = \frac{\partial \overline{w}}{\partial x} + \frac{\partial \overline{u}}{\partial z} + \left(\frac{\partial \overline{u}}{\partial x}\frac{\partial \overline{u}}{\partial z} + \frac{\partial \overline{v}}{\partial x}\frac{\partial \overline{v}}{\partial z} + \frac{\partial \overline{w}}{\partial x}\frac{\partial \overline{w}}{\partial z}\right) \approx \frac{\partial \overline{w}}{\partial x} + \frac{\partial \overline{u}}{\partial z} + \left(\frac{\partial \overline{v}}{\partial x}\frac{\partial \overline{v}}{\partial z} + \frac{\partial \overline{w}}{\partial x}\frac{\partial \overline{w}}{\partial z}\right) \tag{2b}$$

$$\gamma_{xy} = \frac{\partial \overline{v}}{\partial x} + \frac{\partial \overline{u}}{\partial y} + \left(\frac{\partial \overline{u}}{\partial x}\frac{\partial \overline{u}}{\partial y} + \frac{\partial \overline{v}}{\partial x}\frac{\partial \overline{v}}{\partial y} + \frac{\partial \overline{w}}{\partial x}\frac{\partial \overline{w}}{\partial y}\right) \approx \frac{\partial \overline{v}}{\partial x} + \frac{\partial \overline{u}}{\partial y} + \left(\frac{\partial \overline{v}}{\partial x}\frac{\partial \overline{v}}{\partial y} + \frac{\partial \overline{w}}{\partial x}\frac{\partial \overline{w}}{\partial y}\right) \tag{2c}$$

$$\varepsilon_{yy} = \varepsilon_{zz} = \gamma_{yz} = 0 \tag{2d}$$

where it has been assumed that for moderate large displacements $\left(\partial \overline{u}/\partial x\right)^2 << \partial \overline{u}/\partial x$, $\left(\partial \overline{u}/\partial x\right)\left(\partial \overline{u}/\partial z\right) << \left(\partial \overline{u}/\partial x\right) + \left(\partial \overline{u}/\partial z\right)$, $\left(\partial \overline{u}/\partial x\right)\left(\partial \overline{u}/\partial y\right) << \left(\partial \overline{u}/\partial x\right) + \left(\partial \overline{u}/\partial y\right)$. Substitu-ting the displacement components (1a-1e) to the strain-displacement relations (2), the strain components can be written as

$$\begin{aligned} \varepsilon_{xx} = {} & u' + \left(z - z_C\right)\left(v'' \sin\theta_x - w'' \cos\theta_x\right) - \left(y - y_C\right)\left(v'' \cos\theta_x + w'' \sin\theta_x\right) + \\ & + \theta_x'' \phi_S^P - \theta_x' \left(z_C\left(v' \cos\theta_x + w' \sin\theta_x\right) + y_C\left(v' \sin\theta_x - w' \cos\theta_x\right)\right) + \\ & + \frac{1}{2}\left(v'^2 + w'^2 + \left(y^2 + z^2\right)\left(\theta_x'\right)^2\right) \end{aligned} \tag{3a}$$

$$\gamma_{xy} = 2\varepsilon_{xy} = \left(\frac{\partial \phi_S^P}{\partial y} - z\right)\theta_x' \qquad \gamma_{xz} = 2\varepsilon_{xz} = \left(\frac{\partial \phi_S^P}{\partial z} + y\right)\theta_x' \tag{3b,c}$$

Considering strains to be small, employing the second Piola – Kirchhoff stress tensor and assuming an isotropic and homogeneous material, the stress components are defined in terms of the strain ones as

$$\begin{Bmatrix} S_{xx} \\ S_{xy} \\ S_{xz} \end{Bmatrix} = \begin{bmatrix} E & 0 & 0 \\ 0 & G & 0 \\ 0 & 0 & G \end{bmatrix} \begin{Bmatrix} \varepsilon_{xx} \\ \gamma_{xy} \\ \gamma_{xz} \end{Bmatrix} \tag{4}$$

or employing eqns. (3) as

$$\begin{aligned} S_{xx} = E\Big[& u' + \left(z - z_C\right)\left(v'' \sin\theta_x - w'' \cos\theta_x\right) - \left(y - y_C\right)\left(v'' \cos\theta_x + w'' \sin\theta_x\right) + \\ & + \theta_x'' \phi_S^P - \theta_x' \left(z_C\left(v' \cos\theta_x + w' \sin\theta_x\right) + y_C\left(v' \sin\theta_x - w' \cos\theta_x\right)\right) + \\ & + \frac{1}{2}\left(v'^2 + w'^2 + \left(y^2 + z^2\right)\left(\theta_x'\right)^2\right)\Big] \end{aligned} \tag{5a}$$

$$S_{xy} = G \cdot \theta_x' \cdot \left(\frac{\partial \phi_S^P}{\partial y} - z\right) \qquad S_{xz} = G \cdot \theta_x' \cdot \left(\frac{\partial \phi_S^P}{\partial z} + y\right) \tag{5b,c}$$

In order to obtain the nonlinear equilibrium equations, the total potential energy variation

$$\delta\left(E_{int}-W_{ext}\right)=0 \tag{6}$$

expressed as a function of the stress resultants acting on the cross section of the beam in the deformed state is employed, where $\delta(\cdot)$ denotes variation quantities, E_{int} and W_{ext} are the strain energy and external load work, respectively given as

$$\delta E_{int}=\int_V\left(S_{xx}\delta\varepsilon_{xx}+S_{xy}\delta\gamma_{xy}+S_{xz}\delta\gamma_{xz}\right)dV \qquad \delta W_{ext}=\int_l\left(p_X\delta u_C+p_y\delta\tilde{v}+p_z\delta\tilde{w}\right)dx \tag{7a,b}$$

where u_C is the axial displacement of the centroid C and $\tilde{v}$, $\tilde{w}$ are the corresponding transverse displacements of the point at which p_y, p_z, respectively are applied.
Moreover, the stress resultants of the beam are given as

$$N=\int_\Omega S_{xx}d\Omega \qquad M_Y=\int_\Omega S_{xx}Zd\Omega \qquad M_Z=-\int_\Omega S_{xx}Yd\Omega \tag{8a,b,c}$$

$$M_t=\int_\Omega\left[S_{xy}\left(\frac{\partial\varphi_S^P}{\partial y}-z\right)+S_{xz}\left(\frac{\partial\varphi_S^P}{\partial z}+y\right)\right]d\Omega \qquad M_w=-\int_\Omega S_{xx}\varphi_S^P d\Omega \tag{8d,e}$$

$$M_R=\int_\Omega S_{xx}\left(y^2+z^2\right)d\Omega \tag{8f}$$

where M_t is the primary twisting moment [2] resulting from the primary shear stress distribution S_{xy}, S_{xz}, M_w is the warping moment due to torsional curvature and M_R is a higher order stress resultant. Substituting the expressions of the stress components (5) into equations (8a-8e), the stress resultants are obtained as

$$N=EA\left[u'+\frac{1}{2}\left(v'^2+w'^2+\frac{I_S}{A}\theta_x'^2\right)-\theta_x'\left(z_C\left(v'\cos\theta_x+w'\sin\theta_x\right)+y_C\left(v'\sin\theta_x-w'\cos\theta_x\right)\right)\right] \tag{9a}$$

$$M_Y=-EI_Y\left(k_Y\cos\theta_x-k_Z\sin\theta_x-\beta_Z\theta_x'^2\right) \qquad M_Z=EI_Z\left(k_Z\cos\theta_x+k_Y\sin\theta_x-\beta_Y\theta_x'^2\right) \tag{9b,c}$$

$$M_t^P=GI_t\theta_x' \qquad M_w=-EC_S\left(\theta_x''+\beta_\omega\theta_x'^2\right) \tag{9d,e}$$

$$\begin{aligned} M_R=&N\frac{I_S}{A}-2EI_Z\beta_Y\left(v''\cos\theta_x+w''\sin\theta_x\right)-2EI_Y\beta_Z\left(w''\cos\theta_x-v''\sin\theta_x\right)+\\ &+2EC_S\beta_\omega\theta x''+\frac{1}{2}E\left(I_R-\frac{I_S^2}{A}\right)\theta_x'^2 \end{aligned} \tag{9f}$$

where the area A, the polar moment of inertia I_S with respect to the shear center S, the principal moments of inertia I_Y, I_Z with respect to the cross section's centroid, the fourth moment of inertia I_R with respect to the shear center S, the torsion constant I_t and the warping constant C_S with respect to the shear center S are given as

$$A=\int_\Omega d\Omega \qquad I_S=\int_\Omega\left(y^2+z^2\right)d\Omega \qquad I_Y=\int_\Omega Z^2d\Omega \qquad I_Z=\int_\Omega Y^2d\Omega \tag{10a,b,c,d}$$

$$I_R=\int_\Omega\left(y^2+z^2\right)^2d\Omega \qquad C_S=\int_\Omega\left(\varphi_S^P\right)^2d\Omega \qquad I_t=\int_\Omega\left(y^2+z^2+y\frac{\partial\varphi_S^P}{\partial z}-z\frac{\partial\varphi_S^P}{\partial y}\right)d\Omega \tag{10e,f,g}$$

while the Wagner's coefficients β_Z, β_Y and β_ω are given as

$$\beta_Z = \frac{1}{2I_Y}\int_\Omega (z - z_C)\left((y - y_C)^2 + (z - z_C)^2\right) d\Omega + z_C \tag{11a}$$

$$\beta_Y = \frac{1}{2I_Z}\int_\Omega (y - y_C)\left((y - y_C)^2 + (z - z_C)^2\right) d\Omega + y_C \tag{11b}$$

$$\beta_\omega = \frac{1}{2C_S}\int_\Omega \left(y^2 + z^2\right)\varphi_S^P d\Omega \tag{11c}$$

In relations (9b-9c), the curvatures k_Y , k_Z exhibit their accurate expressions given as

$$k_Y = \frac{w''}{\sqrt{1 - w'^2}} \approx w''\left(1 + \frac{w'^2}{2}\right) \qquad k_Z = \frac{v''}{\sqrt{1 - v'^2}} \approx v''\left(1 + \frac{v'^2}{2}\right) \tag{12a,b}$$

Substituting the stress components given in eqns.(5) and the strain resultants given in equations (3a-3c) to the strain energy variation δE_{int} (eqn.7a) and employing equation (6), the equilibrium equations of the beam are derived as

$$-N' = p_X \tag{13a}$$

$$\begin{aligned} &\left(M_Z \cos\theta_x\right)'' + \left(M_Y \sin\theta_x\right)'' - N\left(v' - y_C\theta_x' \sin\theta_x - z_C\theta_x' \cos\theta_x\right)' = \\ &\quad = p_y - p_X\left(v' - y_C\theta_x' \sin\theta_x - z_C\theta_x' \cos\theta_x\right) \end{aligned} \tag{13b}$$

$$\begin{aligned} &-\left(M_Y \cos\theta_x\right)'' + \left(M_Z \sin\theta_x\right)'' - N\left(w' + y_C\theta_x' \cos\theta_x - z_C\theta_x' \sin\theta_x\right)' = \\ &\quad = p_z - p_X\left(w' + y_C\theta_x' \cos\theta_x - z_C\theta_x' \sin\theta_x\right) \end{aligned} \tag{13c}$$

$$\begin{aligned} &N\left(-y_C v'\theta_x' \cos\theta_x - y_C w'\theta_x' \sin\theta_x - z_C w'\theta_x' \cos\theta_x + z_C v'\theta_x' \sin\theta_x\right) + \\ &\quad + N\left(z_C\left(v' \cos\theta_x + w' \sin\theta_x\right)\right)' + N\left(y_C\left(v' \sin\theta_x - w' \cos\theta_x\right)\right)' + \\ &\quad + M_Y\left(w'' \sin\theta_x + v'' \cos\theta_x\right) + M_Z\left(w'' \cos\theta_x - v'' \sin\theta_x\right) - M_t' - M_w'' - \left(M_R\theta_x'\right)' = \\ &\quad p_X\left[z_C\left(v' \cos\theta_x + w' \sin\theta_x\right) + y_C\left(v' \sin\theta_x - w' \cos\theta_x\right)\right] - p_y y_p \sin\theta_x - p_z z_p \sin\theta_x \end{aligned} \tag{13d}$$

Equations (13) refer to a general case of loading and can be used for the nonlinear analysis of beams. They are rather complicated and definitely coupled. Therefore, they can be simplified if the approximate expressions

$$\cos\theta_x = 1 - \frac{\theta_x^{\,2}}{2} \qquad \sin\theta_x = \theta_x - \frac{\theta_x^{\,3}}{6} \tag{14a,b}$$

are employed. Thus, equations (13) of equilibrium after employing the expressions of the stress resultants (eqns.9), the curvature-displacement relations (eqns.12), the approximated expressions for trigonometric terms (eqns.14) and ignoring the nonlinear terms of the fourth or greater order can be written as

$$\begin{aligned} &-EA\left(u'' + w'w'' + v'v'' + \frac{I_S}{A}\theta_x'\theta_x'' - z_C\left(\theta x' w''\theta_x + \theta_x'' v' + \theta_x' v'' + \theta_x'^2 w' + \theta_x'' w'\theta_x\right) - \right. \\ &\quad \left. - y_C\left(\theta_x'' v'\theta_x - \theta_x'' w' - \theta_x' w'' + \theta_x' v''\theta_x + \theta_x'^2 v'\right)\right) = p_X \end{aligned} \tag{15a}$$

$$\begin{aligned}
& EI_Z\left(v'''' + 3v'v''v''' + v''^3 + \frac{1}{2}v''''v'^2\right) - N\left(-z_C\theta_x'' - y_C\left(\theta_x'^2 + \theta_x''\theta_x\right) + v''\right) + \\
& \quad + \left(EI_Z - EI_Y\right)\left(w''''\theta_x + 2w'''\theta_x' + w''\theta_x'' - v''''\theta_x^2 - 4v'''\theta_x\theta_x' - 2v''\theta_x\theta_x'' - 2v''\theta_x'^2\right) + \\
& \quad + EI_Z\left(-2\beta_Y\theta_x'\theta_x''' - 2\beta_Y\theta_x''^2\right) + EI_Y\left(2\beta_Z\theta_x'\theta_x'''\theta_x + 2\beta_Z\theta_x''^2\theta_x + 5\beta_Z\theta_x'^2\theta_x''\right) = \\
& \quad = p_y - p_X\left(v' - y_C\theta_x'\theta_x - z_C\theta_x'\right)
\end{aligned} \tag{15b}$$

$$\begin{aligned}
& EI_Y\left(w'''' + 3w'w''w''' + w''^3 + \frac{w''''w'^2}{2}\right) - N\left(w'' + y_C\theta_x'' - z_C\left(\theta_x'^2 + \theta_x\theta_x''\right)\right) + \\
& \quad + \left(EI_Z - EI_Y\right)\left(v''''\theta_x + 2v'''\theta_x' + v''\theta_x'' + w''''\theta_x^2 + 4w'''\theta_x\theta_x' + 2w''\theta_x\theta_x'' + 2w''\theta_x'^2\right) + \\
& \quad + EI_Z\left(-2\beta_Y\theta_x'\theta_x'''\theta_x - 5\beta_Y\theta_x'^2\theta_x'' - 2\beta_Y\theta_x''^2\theta_x\right) + EI_Y\left(-2\beta_Z\theta_x'\theta_x''' - 2\beta_Z\theta_x''^2\right) = \\
& \quad = p_z - p_X\left(w' + y_C\theta_x' - z_C\theta_x'\theta_x\right)
\end{aligned} \tag{15c}$$

$$\begin{aligned}
& EC_S\theta_x'''' - GI_t\theta_x'' - \frac{3}{2}E\left(I_R - \frac{I_S^2}{A}\right)\theta_x'^2\theta_x'' \\
& \quad - N\left(\frac{I_S}{A}\theta_x'' + y_C\left(w'' - v''\theta_x\right) - z_C\left(v'' + w''\theta_x\right)\right) + \\
& \quad + \left(EI_Z - EI_Y\right)\left(v''w'' - v''^2\theta_x + w''^2\theta_x\right) + \\
& \quad + EI_Z\beta_Y\left(2\theta_x''w''\theta_x + w''\theta_x'^2 + 2\theta_x'v''' + 2\theta_x''v'' + 2\theta_x'w'''\theta_x\right) + \\
& \quad + EI_Y\beta_Z\left(-2\theta_x''v''\theta_x + 2\theta_x''w'' + 2\theta_x'w''' - v''\theta_x'^2 - 2\theta_x'v'''\theta_x\right) = \\
& \quad = -p_X\left(\frac{I_S}{A}\theta_x' - y_Cv'\theta_x - z_Cw'\theta_x - z_Cv' + y_Cw'\right) - p_y y_p\theta_x - p_z z_p\theta_x
\end{aligned} \tag{15d}$$

The aforementioned governing differential equations are also subjected to the pertinent boundary conditions of the problem at hand, which are given as

$$a_1 u(x) + \alpha_2 N(x) = \alpha_3 \tag{16}$$

$$\beta_1 v(x) + \beta_2 V_y(x) = \beta_3 \qquad \bar{\beta}_1\theta_Z(x) + \bar{\beta}_2 M_Z(x) = \bar{\beta}_3 \tag{17a,b}$$

$$\gamma_1 w(x) + \gamma_2 V_z(x) = \gamma_3 \qquad \bar{\gamma}_1\theta_Y(x) + \bar{\gamma}_2 M_Y(x) = \bar{\gamma}_3 \tag{18a,b}$$

$$\delta_1\theta_x(x) + \delta_2 M_t(x) = \delta_3 \qquad \bar{\delta}_1\frac{d\theta_x(x)}{dx} + \bar{\delta}_2 M_w(x) = \bar{\delta}_3 \tag{19a,b}$$

at the beam ends $x = 0, l$, where N, V_y, V_z and M_Z, M_Y are the reactions and bending moments at the specific points with respect to X, y, z or to Y, Z axes, respectively, given by the following relations (ignoring again the nonlinear terms of the fourth or greater order)

$$N = EA\left(u' + \frac{1}{2}\left(v'^2 + w'^2 + \frac{I_S}{A}\theta_x'^2\right) - \theta_x'\left(z_C\left(v' + w'\theta_x\right) + y_C\left(v'\theta_x - w'\right)\right)\right) \tag{20a}$$

$$V_y = N\left(v' - z_C\theta_x' - y_C\theta_x\theta_x'\right) +$$
$$+ EI_Z\left(v'''\theta_x^2 - w''\theta_x' - w'''\theta_x - v''^2v' - \frac{v'''v'^2}{2} - v''' + 2v''\theta_x\theta_x' + 2\beta_Y\theta_x'\theta_x''\right) +$$
$$+ EI_Y\left(w'''\theta_x + w''\theta_x' - 2v''\theta_x\theta_x' - v'''\theta_x^2 - \beta_Z\theta_x'^3 - 2\beta_Z\theta_x'\theta_x''\theta_x\right) \tag{20b}$$

$$V_z = N\left(w' + y_C\theta_x' - z_C\theta_x'\theta_x\right) +$$
$$+ EI_Y\left(w'''\theta_x^2 - \frac{w'''w'^2}{2} + v'''\theta_x - w''^2w' - w''' + v''\theta_x' + 2w''\theta_x\theta_x' + 2\beta_Z\theta_x'\theta_x''\right) - \tag{20c}$$
$$- EI_Z\left(v''\theta_x' + w'''\theta_x^2 + v'''\theta_x + 2w''\theta_x\theta_x' - 2\beta_Y\theta_x'\theta_x''\theta_x - \beta_Y\theta_x'^3\right)$$

$$M_Z = EI_Z\left(w''\theta_x - \beta_Y\theta_x'^2 + v'' + \frac{v''v'^2}{2} - v''\theta_x^2\right) + EI_Y\left(-w''\theta_x + v''\theta_x^2 + \beta_Z\theta_x'^2\theta_x\right) \tag{20d}$$

$$M_Y = EI_Z\left(-w''\theta_x^2 + \beta_Y\theta_x'^2\theta_x - v''\theta_x\right) + EI_Y\left(\beta_Z\theta_x'^2 - w'' + w''\theta_x^2 - \frac{w''w'^2}{2} + v''\theta_x\right) \tag{20e}$$

while M_t and M_w are the torsional and warping moments at the boundary of the bar, respectively, given as

$$M_t = GI_t\theta_x' - EC_S\theta_x''' + N\left(-z_Cw'\theta_x + y_Cw' - y_Cv'\theta_x - z_Cv' + \frac{I_S}{A}\theta_x'\right) +$$
$$+ EI_Z\beta_Y\left(-2\theta_x'v'' - 2\theta_x'w''\theta_x\right) + EI_Y\beta_Z\left(-2\theta_x'w'' + 2\theta_x'v''\theta_x\right) + \frac{1}{2}E\left(I_R - \frac{I_S^2}{A}\right)\theta_x'^3 \tag{21a}$$

$$M_w = -EC_S\left(\theta_x'' + \beta_\omega\theta_x'^2\right) \tag{21b}$$

Finally, $\alpha_k, \bar{\alpha}_k, \beta_k, \bar{\beta}_k, \gamma_k, \bar{\gamma}_k, \delta_k, \bar{\delta}_k$ ($k = 1,2,3$) are functions specified at the beam ends $x = 0,l$. Eqs. (16)-(19) describe the most general boundary conditions associated with the problem at hand and can include elastic support or restraint. It is apparent that all types of the conventional boundary conditions (clamped, simply supported, free or guided edge) can be derived from these equations by specifying appropriately these functions (e.g. for a clamped edge it is $\alpha_1 = \beta_1 = \gamma_1 = \delta_1 = 1$, $\bar{\alpha}_1 = \bar{\beta}_1 = \bar{\gamma}_1 = \bar{\delta}_1 = 1$, $\alpha_2 = \alpha_3 = \beta_2 = \beta_3 = \gamma_2 = \gamma_3 = \delta_2 = \delta_3 = \bar{\alpha}_2 = \bar{\alpha}_3 = \bar{\beta}_2 = \bar{\beta}_3 = \ = \bar{\gamma}_2 = \bar{\gamma}_3 = \bar{\delta}_2 = \bar{\delta}_3 = 0$).

The differential equations of equilibrium (15) have been derived using the nonlinear relations (12) between bending moments and curvatures. In the case where the approximate expressions

$$k_Y \approx w'' \qquad\qquad k_Z \approx v'' \tag{22a,b}$$

are employed, the differential equations (15) are written as

$$-EA\left(u'' + w'w'' + v'v'' + \frac{I_S}{A}\theta_x'\theta_x'' - z_C\left(\theta x'w''\theta_x + \theta_x''v' + \theta_x'v'' + \theta_x'^2w' + \theta_x''w'\theta_x\right) -\right.$$
$$\left. - y_C\left(\theta_x''v'\theta_x - \theta_x''w' - \theta_x'w'' + \theta_x'v''\theta_x + \theta_x'^2v'\right)\right) = p_X \tag{23a}$$

$$\begin{aligned}
& EI_Z v'''' - N\left(-z_C\theta_x'' - y_C\left(\theta_x'^2 + \theta_x''\theta_x\right) + v''\right) + \\
& \quad + \left(EI_Z - EI_Y\right)\left(w''''\theta_x + 2w'''\theta_x' + w''\theta_x'' - v''''\theta_x^2 - 4v'''\theta_x\theta_x' - 2v''\theta_x\theta_x'' - 2v''\theta_x'^2\right) + \\
& \quad + EI_Z\left(-2\beta_Y\theta_x'\theta_x''' - 2\beta_Y\theta_x''^2\right) + EI_Y\left(2\beta_Z\theta_x'\theta_x'''\theta_x + 2\beta_Z\theta_x''^2\theta_x + 5\beta_Z\theta_x'^2\theta_x''\right) = \\
& \quad = p_y - p_X\left(v' - y_C\theta_x'\theta_x - z_C\theta_x'\right)
\end{aligned} \tag{23b}$$

$$\begin{aligned}
& EI_Y w'''' - N\left(w'' + y_C\theta_x'' - z_C\left(\theta_x'^2 + \theta_x\theta_x''\right)\right) + \\
& \quad + \left(EI_Z - EI_Y\right)\left(v''''\theta_x + 2v'''\theta_x' + v''\theta_x'' + w''''\theta_x^2 + 4w'''\theta_x\theta_x' + 2w''\theta_x\theta_x'' + 2w''\theta_x'^2\right) + \\
& \quad + EI_Z\left(-2\beta_Y\theta_x'\theta_x'''\theta_x - 5\beta_Y\theta_x'^2\theta_x'' - 2\beta_Y\theta_x''^2\theta_x\right) + EI_Y\left(-2\beta_Z\theta_x'\theta_x''' - 2\beta_Z\theta_x''^2\right) = \\
& \quad = p_z - p_X\left(w' + y_C\theta_x' - z_C\theta_x'\theta_x\right)
\end{aligned} \tag{23c}$$

$$\begin{aligned}
& EC_S\theta_x'''' - GI_t\theta_x'' - \frac{3}{2}E\left(I_R - \frac{I_S^2}{A}\right)\theta_x'^2\theta_x'' - N\left(\frac{I_S}{A}\theta_x'' + y_C\left(w'' - v''\theta_x\right) - z_C\left(v'' + w''\theta_x\right)\right) + \\
& \quad + \left(EI_Z - EI_Y\right)\left(v''w'' - v''^2\theta_x + w''^2\theta_x\right) + \\
& \quad + EI_Z\beta_Y\left(2\theta_x''w''\theta_x + w''\theta_x'^2 + 2\theta_x'v''' + 2\theta_x''v'' + 2\theta_x'w'''\theta_x\right) + \\
& \quad + EI_Y\beta_Z\left(-2\theta_x''v''\theta_x + 2\theta_x''w'' + 2\theta_x'w''' - v''\theta_x'^2 - 2\theta_x'v'''\theta_x\right) = \\
& \quad = -p_X\left(\frac{I_S}{A}\theta_x' - y_C v'\theta_x - z_C w'\theta_x - z_C v' + y_C w'\right) - p_y y_p\theta_x - p_z z_p\theta_x
\end{aligned} \tag{23d}$$

Lateral buckling analysis aims at finding the critical load where the behaviour of the beam changes from flexural to flexural-torsional. Therefore, for the rest of the analysis, taking into account that the external transverse loading causes only bending as it is passing through the shear center, it is assumed that during the prebuckling behaviour the beam is untwisted.

The instability criterion is based on the positive definiteness of the second variation of the total potential energy, which means that buckling occurs when the determinant of the tangential stiffness matrix becomes negative. During the following analysis, it is assumed that the pre-buckling behaviour of the beam is linear and the deflections until the critical load are taken into account. Therefore, the influence from the axial loading in the computation of the transverse displacements has to be negligible and can be ignored.

Thus, the aforementioned differential equations (15) for the pre-buckling deformation problem can be written as

$$-EAu'' = p_X \qquad EI_Z v'''' = p_y \qquad EI_Y w'''' = p_z \qquad EC_S\theta_x'''' - GI_t\theta_x'' = 0 \tag{24a,b,c,d}$$

under the boundary conditions (16)-(19), where N, V_y, V_z , M_Z, M_Y, M_t and M_w are given by the following relations

$$N = EAu' \qquad V_y = -EI_Z v''' \qquad V_z = -EI_Y w''' \tag{25a,b,c}$$

$$M_Z = EI_Z v'' \qquad M_Y = -EI_Y w'' \qquad M_t = GI_t\theta_x' - EC_S\theta_x''' \qquad M_w = -EC_S\theta_x'' \tag{25d,e,f,g}$$

3. Integral Representations – Numerical Solution

According to the precedent analysis, the lateral buckling analysis of beams of arbitrary cross section reduces in establishing the critical load for which the determinant of the tangential stiffness matrix becomes negative. The differential equations (15b), (15c), (15d) are highly coupled and an analytic solution of this problem is out of question. Therefore, the recourse to a numerical solution is inevitable. In this investigation, the Analog Equation method [1] is employed.

4. Numerical Examples

IPE	HEA
$I_Y = 8150\,cm^4$	$I_Y = 3556\,cm^4$
$I_Z = 602\,cm^4$	$I_Z = 1333\,cm^4$
$C_S = 125.93 \times 10^3\,cm^6$	$C_S = 108 \times 10^3\,cm^6$
$I_t = 15.7\,cm^4$	$I_t = 15\,cm^4$

Table 1. Geometric and inertia constants of the examined cross sections.

For comparison reasons, the special case of a simply supported beam ($E = 210GPa$, $G = 80.77GPa$) of length $l = 6.0\,m$ subjected to a uniformly distributed load p_z has been studied. Two cases of doubly symmetric cross sections have been analyzed, namely an IPE type and a HEA type. In Table 1, the properties of each of these cross sections are presented (the dimensions and geometric constants given in ref.[3] have been adopted here for comparison reasons), noting that the ratio $I_Y / I_Z = 13.54$ of the IPE type cross section is much larger than that ($I_Y / I_Z = 2.67$) of the HEA type one. Three different cases of the application point of the load p_z are examined, namely at the top flange, at the bottom flange and at the shear center. In Table 2 the values of the critical bending moment $M_{mid} = p_z l^2 / 8$ at the midpoint point of the examined beam, corresponding to the bifurcation point for the aforementioned cases of the loading point are presented as compared with those obtained from an analytic solution and a numerical solution [3] taking into account the pre-buckling deflections (as the proposed method) and from Eurocode 3 [4] ignoring these deflections. From this table both the accuracy of the results of the proposed method and the conservative character of the EC3 standard solutions for beam sections of equivalent bending resistance about the two principal axes are remarkable.

Case studied	AEM Present Study	Galerkin's method [3]		EC3 [4]
		Analytic	Numerical	
IPE cross section				
Load at top flange	72.88	72.82	73.0	70.75
Load at shear center	97.72	97.82	98.2	94.07
Load at bottom flange	130.93	131.42	132.2	125.06
HEA cross section				
Load at top flange	118.69	119.5	119.5	101.77
Load at shear center	169.72	170.09	169.6	134.47
Load at bottom flange	242.35	241.33	240.5	177.68

Table 2. Critical bending moments M_{mid} (kNm) at the midpoint point of the examined beams.

5. Concluding Remarks

The main conclusions that can be drawn from this investigation are

a. The numerical technique presented in this investigation is well suited for computer aided analysis for beams of arbitrary symmetric, monosymmetric or asymmetric thin or thick walled cross section, subjected to the combined action of arbitrarily distributed or concentrated transverse loading.

b. The proposed method can be employed to beams of various boundary conditions including elastic support or restraint.
c. The developed method can take into account nonlinear relationships between bending moments and curvatures.
d. The accuracy of the results of the proposed method for a small number of boundary elements and nodal points is remarkable.
e. The effect of the load height is demonstrated.
f. The proposed stability criterion takes into account the pre buckling deflections.
g. In some cases the discrepancy of the Eurocode 3 standard solutions is notified.
h. The results obtained from the proposed method are in good agreement with experimental results
i. The effect of warping in small values of beam length is remarkable.

Acknowledgements

This work has been funded by the project PENED 2003. The project is cofinanced 75% of public expenditure through EC - European Social Fund and 25% of public expenditure through Ministry of Development - General Secretariat of Research and Technology and through private sector, under measure 8.3 of OPERATIONAL PROGRAM "COMPETITIVENESS" in the 3rd Community Support Program.

References

[1] J.T.Katsikadelis The Analog Equation Method. A Boundary-Only Integral Equation Method for Nonlinear Static and Dynamic Problems in General Bodies, *Theoretical and Applied Mechanics*, **27**, 13-38, (2002).
[2] E.J.Sapountzakis and V.G.Mokos Warping Shear Stresses in Nonuniform Torsion by BEM, *Computational Mechanics,* **30**(2), 131-142, (2003).
[3] F.Mohri, L.Azrar and M.Potier-Ferry Lateral Post-Buckling Analysis of Thin-Walled Open Section Beams, *Thin-Walled Structures*, **40**, 1013–1036, (2002).
[4] Eurocode3, Design of steel structures, Part 1.1: General rules for buildings. European Committee for standardisation, Draft Document ENV 1993-1-1, Brussels, 1992.

Flexural - Torsional Nonlinear Analysis of Timoshenko Beams of Arbitrary Cross Section by BEM

E.J. Sapountzakis and J.A. Dourakopoulos

[1,2]School of Civil Engineering, National Technical University,
Zografou Campus, GR-157 80 Athens, Greece

Keywords: Flexural-Torsional Analysis; Timoshenko Beam; Shear center; Shear deformation coefficients; Nonlinear analysis; Boundary element method

Abstract. In this paper a boundary element method is developed for the nonlinear flexural – torsional analysis of Timoshenko beams of arbitrary simply or multiply connected constant cross section, undergoing moderate large deflections under general boundary conditions. The beam is subjected to the combined action of an arbitrarily distributed or concentrated axial and transverse loading as well as to bending and twisting moments. To account for shear deformations, the concept of shear deformation coefficients is used. Seven boundary value problems are formulated with respect to the transverse displacements, to the axial displacement, to the angle of twist (which is assumed to be small), to the primary warping function and to two stress functions and solved using the Analog Equation Method, a BEM based method. Application of the boundary element technique yields a system of nonlinear equations from which the transverse and axial displacements as well as the angle of twist are computed by an iterative process. The evaluation of the shear deformation coefficients is accomplished from the aforementioned stress functions using only boundary integration. Numerical examples with great practical interest are worked out to illustrate the efficiency, the accuracy and the range of applications of the developed method. The influence of both the shear deformation effect and the variableness of the axial loading are remarkable.

1. Introduction

In recent years, a need has been raised in the analysis of the components of plane and space frames or grid systems to take into account the influence of the action of axial, lateral forces and end moments on their deformed shape. Lateral loads and end moments generate deflection that is further amplified by axial compression loading. The aforementioned analysis becomes much more accurate and complex taking into account that the axial force is nonlinearly coupled with the transverse deflections. This non-linearity results from retaining the square of the slope in the strain–displacement relations (intermediate non-linear theory), avoiding in this way the inaccuracies arising from a linearized second – order analysis. Moreover, unless the beam is very “thin” the error incurred from the ignorance of the effect of shear deformation may be substantial, particularly in the case of heavy lateral loading.

In this paper, which is an extension of the aforementioned work of the first author, a boundary element method is developed for the nonlinear flexural – torsional analysis of Timoshenko beams of arbitrary simply or multiply connected constant cross section, undergoing moderate large deflections under general boundary conditions. The beam is subjected to the combined action of an arbitrarily distributed or concentrated axial and transverse loading as well as to bending and twisting moments. To account for shear deformations, the concept of shear deformation coefficients is used. Seven boundary value problems are formulated with respect to the transverse displacements, to the axial displacement, to the angle of twist (which is assumed to be small), to the primary warping function and to two stress functions and solved using the Analog Equation Method [1], a BEM based method. Application of the boundary element technique yields a system of nonlinear equations from which the transverse and axial displacements as well as the angle of twist are computed by an iterative process. The evaluation of the shear deformation coefficients is accomplished from the aforementioned stress functions using only boundary integration. The essential features and novel aspects of the present formulation compared with previous ones are summarized as follows.

i. The beam is subjected in an arbitrarily distributed or concentrated axial and transverse loading as well as to bending and twisting moments.
ii. The beam is supported by the most general boundary conditions including elastic support or restrain, while its cross section is an arbitrary one.

iii. For the first time in the literature, the present formulation is applicable to arbitrarily shaped thin or thick-walled cross sections occupying simple or multiple connected domains, taking into account shear deformation effect.
iv. The present formulation does not stand on the assumption of a thin-walled structure and therefore the cross section's torsional rigidity is evaluated exactly without using the so-called Saint –Venant's torsional constant.
v. The shear deformation coefficients are evaluated using an energy approach, instead of Timoshenko's and Cowper's definitions, for which several authors [2] have pointed out that one obtains unsatisfactory results or definitions given by other researchers, for which these factors take negative values.
vi. The effect of the material's Poisson ratio v is taken into account.
vii. The proposed method employs a pure BEM approach (requiring only boundary discretization) resulting in line or parabolic elements instead of area elements of the FEM solutions (requiring the whole cross section to be descretized into triangular or quadrilateral area elements), while a small number of line elements are required to achieve high accuracy.

Numerical examples are worked out to illustrate the efficiency, the accuracy and the range of applications of the developed method. The influence of the shear deformation effect is observed. The obtained numerical results are compared with those obtained from a 3-D FEM solution using solid elements.

2. Statement of the Problem

Let us consider a prismatic beam of length l (Fig.1), of constant arbitrary cross-section of area A. The homogeneous isotropic and linearly elastic material of the beam cross-section, with modulus of elasticity E, shear modulus G and Poisson's ratio v occupies the two dimensional multiply connected region Ω of the y,z plane and is bounded by the $\Gamma_j\left(j=1,2,...,K\right)$ boundary curves, which are piecewise smooth, i.e. they may have a finite number of corners. In Fig. 1a CYZ is the coordinate system through the cross section's centroid C, while y_C, z_C are its coordinates with respect to the Syz principal shear system of axes through the cross section's shear center S. The beam is subjected to the combined action of the arbitrarily distributed or concentrated axial loading $p_X=p_X(X)$, transverse loading $p_Y=p_Y\left(X\right)$, $p_Z=p_Z\left(X\right)$ acting in the Y and Z directions, respectively, bending moments $m_Y=m_Y\left(X\right)$, $m_Z=m_Z\left(X\right)$ along Y and Z axes, respectively and twisting moment $m_x=m_x\left(x\right)$ (Fig. 1b).

Under the action of the aforementioned loading, the displacement field of the beam, assuming small angle of twist θ_x, that is $\cos\theta_x\approx 1$, $\sin\theta_x\approx\theta_x$ and ignoring the resulting nonlinear terms of the small angle of twist, is given as

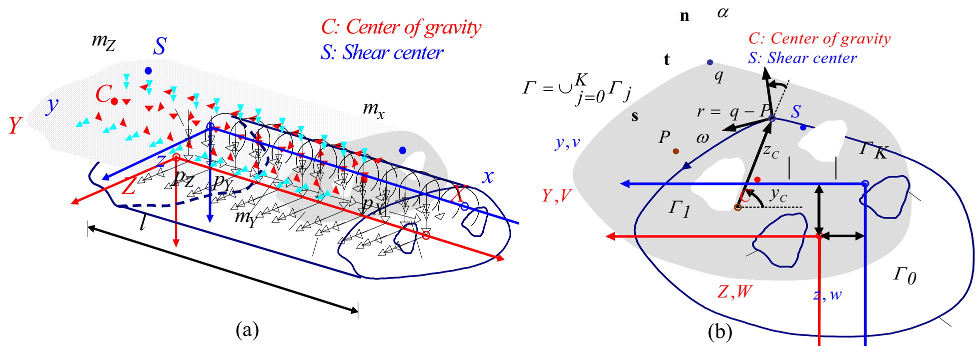

Fig.1. Prismatic beam in axial - flexural – torsional loading (a) with an arbitrary cross-section occupying the two dimensional region Ω (b).

$$\bar{u}\left(x,y,z\right)=u\left(x\right)-Y\theta_Z\left(x\right)+Z\theta_Y\left(x\right)+\theta_x'\left(x\right)\varphi_S^P\left(y,z\right) \tag{1a}$$

$$\bar{v}(x,z) = v(x) - z\theta_x(x) \tag{1b}$$
$$\bar{w}(x,y) = w(x) + y\theta_x(x) \tag{1c}$$

where $\bar{u}$, $\bar{v}$, $\bar{w}$ are the axial and transverse beam displacement components with respect to the Syz shear system of axes; $u = u(x)$, $v = v(x)$, $w = w(x)$ are the corresponding components of the shear center S; θ_Y, θ_Z are the angles of rotation due to bending of the cross-section with respect to its centroid; $\theta'_x(x)$ denotes the rate of change of the angle of twist θ_x regarded as the torsional curvature and ϕ_S^P is the primary warping function with respect to the shear center S [3].

Employing the strain-displacement relations of the three - dimensional elasticity for moderate displacements, the following strain components can be easily obtained

$$\varepsilon_{xx} = \frac{\partial \bar{u}}{\partial x} + \frac{1}{2}\left[\left(\frac{\partial \bar{v}}{\partial x}\right)^2 + \left(\frac{\partial \bar{w}}{\partial x}\right)^2\right] \qquad \gamma_{xz} = \frac{\partial \bar{w}}{\partial x} + \frac{\partial \bar{u}}{\partial z} \qquad \gamma_{xy} = \frac{\partial \bar{v}}{\partial x} + \frac{\partial \bar{u}}{\partial y} \qquad \varepsilon_{yy} = \varepsilon_{zz} = \gamma_{yz} = 0$$

(2a,b,c,d)

Moreover the angles of rotation of the cross-section due to bending taking into account shear deformation effect are obtained as

$$\theta_Y(x) = -\frac{dw}{dx} + \gamma_{xz} \qquad \theta_Z(x) = \frac{dv}{dx} - \gamma_{xy} \tag{3a,b}$$

Assuming small rotations, the total angles of rotation ω_y, ω_z and β_y, β_z (Fig.2) of the cross-section in the *x-z* and *x-y* planes of the beam, with respect to the Sx and CX axes, respectively, satisfy the following relations

$$\sin\omega_y \approx \omega_y = -\frac{dw}{dx} = \theta_Y - \gamma_{xz} \qquad \sin\omega_z \approx \omega_z = -\frac{dv}{dx} = -\theta_Z - \gamma_{xy} \tag{4a,b}$$

$$\cos\beta_y \approx 1 \qquad \cos\beta_z \approx 1 \qquad \sin\beta_y \simeq -\frac{dw_C}{dx} \qquad \sin\beta_z \simeq -\frac{dv_C}{dx} \tag{4c,d,e,f}$$

where $w_C = w_C(x)$, $v_C = v_C(x)$ are the transverse displacements of the cross section's centroid C with respect to the Syz shear system of axes, while the corresponding curvatures are given as

$$k_Y = \frac{d\theta_Y}{dx} = -\frac{d^2w}{dx^2} + \frac{d\gamma_{xz}}{dx} = -\frac{d^2w}{dx^2} + \frac{1}{GA_z}\frac{dQ_z}{dx} \tag{5a}$$

$$k_Z = \frac{d\theta_Z}{dx} = \frac{d^2v}{dx^2} - \frac{d\gamma_{xy}}{dx} = \frac{d^2v}{dx^2} - \frac{1}{GA_y}\frac{dQ_y}{dx} \tag{5b}$$

where γ_{xy}, γ_{xz} are the additional angles of rotation of the cross-section due to shear deformation and GA_y, GA_z are its shear rigidities of the Timoshenko's beam theory, where

$$A_z = \kappa_z A = \frac{1}{a_z}A \qquad A_y = \kappa_y A = \frac{1}{a_y}A \tag{6a,b}$$

are the shear areas with respect to y, z axes, respectively with κ_y, κ_z the shear correction factors, a_y, a_z the shear deformation coefficients and A the cross section area.

Noting that the direction of the axial force N is the tangential to the deformed centroidal axis and its normal in the *x-y* and *x-z* planes of the beam gives the direction of the shear forces Q_y, Q_z, respectively (Fig.2), the stress resultants R_x, R_y, R_z acting in the x, y, z directions (undeformed beam directions), respectively, are related to the axial N and shear Q_y, Q_z forces as

$$R_x = N\cos\beta + Q_z \sin\beta_y + Q_y \sin\beta_z \qquad R_y = -N\sin\beta_z + Q_y\cos\beta_z \qquad R_z = -N\sin\beta_y + Q_z\cos\beta_y \quad \text{(7a,b,c)}$$

which by virtue of eqns. (4) become

$$R_x = N - Q_z\frac{dw_C}{dx} - Q_y\frac{dv_C}{dx} \quad \text{(8a)}$$

$$R_y = N\frac{dv_C}{dx} + Q_y = N\left(\frac{dv}{dx} - z_C\frac{d\theta_x}{dx}\right) + Q_y \qquad R_z = N\frac{dw_C}{dx} + Q_z = N\left(\frac{dw}{dx} + y_C\frac{d\theta_x}{dx}\right) + Q_z \quad \text{(8b,c)}$$

The second and third terms in the right hand side of eqn. (8a), express the influence of the shear forces Q_y, Q_z on the horizontal stress resultant R_x. However, these terms can be neglected since $Q_z w_C'$ and $Q_y v_C'$ are much smaller than N and thus eqn. (8a) can be written as

$$R_x \approx N \quad \text{(9)}$$

Employing eqns.(1) to the strain – displacement equation (2a) of the three-dimensional elasticity, the normal strain component ε_x can be written as

$$\varepsilon_x = \frac{du}{dx} + \frac{d\theta_Y}{dx}Z - \frac{d\theta_Z}{dx}Y + \frac{d^2\theta_x}{dx^2}\phi_S^P + \frac{1}{2}\left(\left(\frac{dv}{dx}\right)^2 + \left(\frac{dw}{dx}\right)^2 + \left(y^2+z^2\right)\left(\frac{d\theta_x}{dx}\right)^2\right) - z\frac{dv}{dx}\frac{d\theta_x}{dx} + y\frac{dw}{dx}\frac{d\theta_x}{dx} \quad \text{(10)}$$

Employing eqn.(10), the arising bending moments M_Y, M_Z after ignoring the resulting nonlinear terms of the small angle of twist are given as

$$M_Y = \int_\Omega E\varepsilon_x Z d\Omega = EI_{YY}\frac{d\theta_Y}{dx} - EI_{YZ}\frac{d\theta_Z}{dx} \qquad M_Z = -\int_\Omega E\varepsilon_x Y d\Omega = EI_{ZZ}\frac{d\theta_Z}{dx} - EI_{YZ}\frac{d\theta_Y}{dx} \quad \text{(11a,b)}$$

where I_{YY}, I_{ZZ}, I_{YZ} are the moments and the product of inertia of the cross-section with respect to its centroid C. Substituting eqns.(3a,b) in eqns. (11a,b) the bending moments M_Y, M_Z can be written as

$$M_Y = EI_{YY}\left(\frac{1}{GA_z}\frac{dQ_z}{dx} - \frac{d^2w}{dx^2}\right) - EI_{YZ}\left(\frac{d^2v}{dx^2} - \frac{1}{GA_y}\frac{dQ_y}{dx}\right) \quad \text{(12a)}$$

$$M_Z = EI_{ZZ}\left(\frac{d^2v}{dx^2} - \frac{1}{GA_y}\frac{dQ_y}{dx}\right) - EI_{YZ}\left(\frac{1}{GA_z}\frac{dQ_z}{dx} - \frac{d^2w}{dx^2}\right) \quad \text{(12b)}$$

The governing equations of the problem at hand will be derived by considering the equilibrium of the deformed element. Thus, referring to Fig. 2 we obtain

$$\frac{dR_x}{dx} + p_X = 0 \quad \frac{dR_y}{dx} + p_Y = 0 \quad \frac{dR_z}{dx} + p_Z = 0 \quad \frac{dM_Y}{dx} - Q_z + m_Y = 0 \quad \frac{dM_Z}{dx} + Q_y + m_Z = 0 \quad \text{(13a,b,c,d,e)}$$

Eqns. (13a,b,c) after employing eqns. (9), (8b,c) can be written as

$$\frac{dN}{dx}=-p_X \tag{14a}$$

$$\frac{dQ_y}{dx}+\frac{dN}{dx}\left(\frac{dv}{dx}-z_C\frac{d\theta_x}{dx}\right)+N\left(\frac{d^2v}{dx^2}-z_C\frac{d^2\theta_x}{dx^2}\right)+p_Y=0 \tag{14b}$$

$$\frac{dQ_z}{dx}+\frac{dN}{dx}\left(\frac{dw}{dx}+y_C\frac{d\theta_x}{dx}\right)+N\left(\frac{d^2w}{dx^2}+y_C\frac{d^2\theta_x}{dx^2}\right)+p_Z=0 \tag{14c}$$

Substituting eqns (14b,c) into eqns (12a,b) the expressions of the bending moments M_Y, M_Z are obtained as

$$\begin{aligned}M_Y=&-EI_{YY}\frac{d^2w}{dx^2}-\alpha_z\frac{EI_{YY}}{GA}\left(p_Z-p_X\left(\frac{dw}{dx}+y_C\frac{d\theta_x}{dx}\right)+N\left(\frac{d^2w}{dx^2}+y_C\frac{d^2\theta_x}{dx^2}\right)\right)-\\&-EI_{YZ}\frac{d^2v}{dx^2}-\alpha_y\frac{EI_{YZ}}{GA}\left(p_Y-p_X\left(\frac{dv}{dx}-z_C\frac{d\theta_x}{dx}\right)+N\left(\frac{d^2v}{dx^2}-z_C\frac{d^2\theta_x}{dx^2}\right)\right)\end{aligned} \tag{15a}$$

$$\begin{aligned}M_Z=&EI_{ZZ}\frac{d^2v}{dx^2}+\alpha_y\frac{EI_{ZZ}}{GA}\left(p_Y-p_X\left(\frac{dv}{dx}-z_C\frac{d\theta_x}{dx}\right)+N\left(\frac{d^2v}{dx^2}-z_C\frac{d^2\theta_x}{dx^2}\right)\right)+\\&+EI_{YZ}\frac{d^2w}{dx^2}+\alpha_z\frac{EI_{YZ}}{GA}\left(p_Z-p_X\left(\frac{dw}{dx}+y_C\frac{d\theta_x}{dx}\right)+N\left(\frac{d^2w}{dx^2}+y_C\frac{d^2\theta_x}{dx^2}\right)\right)\end{aligned} \tag{15b}$$

while employing eqns.(15a,b) and (13d,e) the corresponding expressions of the shear forces Q_y, Q_z are written as

$$\begin{aligned}Q_y=&-EI_{ZZ}\frac{d^3v}{dx^3}-EI_{YZ}\frac{d^3w}{dx^3}-m_Z-\\&-\alpha_y\frac{EI_{ZZ}}{GA}\left(\frac{dp_Y}{dx}-\frac{dp_X}{dx}\left(\frac{dv}{dx}-z_C\frac{d\theta_x}{dx}\right)-2p_X\left(\frac{d^2v}{dx^2}-z_C\frac{d^2\theta_x}{dx^2}\right)+N\left(\frac{d^3v}{dx^3}-z_C\frac{d^3\theta_x}{dx^3}\right)\right)-\\&-\alpha_z\frac{EI_{YZ}}{GA}\left(\frac{dp_Z}{dx}-\frac{dp_X}{dx}\left(\frac{dw}{dx}+y_C\frac{d\theta_x}{dx}\right)-2p_X\left(\frac{d^2w}{dx^2}+y_C\frac{d^2\theta_x}{dx^2}\right)+N\left(\frac{d^3w}{dx^3}+y_C\frac{d^3\theta_x}{dx^3}\right)\right)\end{aligned} \tag{16a}$$

$$\begin{aligned}Q_z=&-EI_{YY}\frac{d^3w}{dx^3}-EI_{YZ}\frac{d^3v}{dx^3}+m_Y-\\&-\frac{EI_{YY}}{GA}\alpha_z\left(\frac{dp_Z}{dx}-\frac{dp_X}{dx}\left(\frac{dw}{dx}+y_C\frac{d\theta_x}{dx}\right)-2p_X\left(\frac{d^2w}{dx^2}+y_C\frac{d^2\theta_x}{dx^2}\right)+N\left(\frac{d^3w}{dx^3}+y_C\frac{d^3\theta_x}{dx^3}\right)\right)\\&-\alpha_y\frac{EI_{YZ}}{GA}\left(\frac{dp_Y}{dx}-\frac{dp_X}{dx}\left(\frac{dv}{dx}-z_C\frac{d\theta_x}{dx}\right)-2p_X\left(\frac{d^2v}{dx^2}-z_C\frac{d^2\theta_x}{dx^2}\right)+N\left(\frac{d^3v}{dx^3}-z_C\frac{d^3\theta_x}{dx^3}\right)\right)\end{aligned} \tag{16b}$$

Eliminating these forces from eqns (14b,c) the first two coupled partial differential equations of the problem of the beam under consideration, subjected to the combined action of axial, bending and torsional loading are obtained as

$$EI_{ZZ}\frac{d^4v}{dx^4}+EI_{YZ}\frac{d^4w}{dx^4}-p_Y+p_X\left(\frac{dv}{dx}-z_C\frac{d\theta_x}{dx}\right)-N\left(\frac{d^2v}{dx^2}-z_C\frac{d^2\theta_x}{dx^2}\right)+\frac{dm_Z}{dx}+$$
$$+\alpha_y\frac{EI_{ZZ}}{GA}\left[\frac{d^2p_Y}{dx^2}-\frac{d^2p_X}{dx^2}\left(\frac{dv}{dx}-z_C\frac{d\theta_x}{dx}\right)-3\frac{dp_X}{dx}\left(\frac{d^2v}{dx^2}-z_C\frac{d^2\theta_x}{dx^2}\right)-\right.$$
$$\left.-3p_X\left(\frac{d^3v}{dx^3}-z_C\frac{d^3\theta_x}{dx^3}\right)+N\left(\frac{d^4v}{dx^4}-z_C\frac{d^4\theta_x}{dx^4}\right)\right]+ \tag{17a}$$
$$+\alpha_z\frac{EI_{YZ}}{GA}\left[\frac{d^2p_Z}{dx^2}-\frac{d^2p_X}{dx^2}\left(\frac{dw}{dx}+y_C\frac{d\theta_x}{dx}\right)-3\frac{dp_X}{dx}\left(\frac{d^2w}{dx^2}+y_C\frac{d^2\theta_x}{dx^2}\right)-\right.$$
$$\left.-3p_X\left(\frac{d^3w}{dx^3}+y_C\frac{d^3\theta_x}{dx^3}\right)+N\left(\frac{d^4w}{dx^4}+y_C\frac{d^4\theta_x}{dx^4}\right)\right]=0$$

$$EI_{YY}\frac{d^4w}{dx^4}+EI_{YZ}\frac{d^4v}{dx^4}-p_Z+p_X\left(\frac{dw}{dx}+y_C\frac{d\theta_x}{dx}\right)-N\left(\frac{d^2w}{dx^2}+y_C\frac{d^2\theta_x}{dx^2}\right)-\frac{dm_Y}{dx}+$$
$$+\alpha_z\frac{EI_{YY}}{GA}\left[\frac{d^2p_Z}{dx^2}-\frac{d^2p_X}{dx^2}\left(\frac{dw}{dx}+y_C\frac{d\theta_x}{dx}\right)-3\frac{dp_X}{dx}\left(\frac{d^2w}{dx^2}+y_C\frac{d^2\theta_x}{dx^2}\right)-\right.$$
$$\left.-3p_X\left(\frac{d^3w}{dx^3}+y_C\frac{d^3\theta_x}{dx^3}\right)+N\left(\frac{d^4w}{dx^4}+y_C\frac{d^4\theta_x}{dx^4}\right)\right]+ \tag{17b}$$
$$+\alpha_y\frac{EI_{YZ}}{GA}\left[\frac{d^2p_Y}{dx^2}-\frac{d^2p_X}{dx^2}\left(\frac{dv}{dx}-z_C\frac{d\theta_x}{dx}\right)-3\frac{dp_X}{dx}\left(\frac{d^2v}{dx^2}-z_C\frac{d^2\theta_x}{dx^2}\right)-\right.$$
$$\left.-3p_X\left(\frac{d^3v}{dx^3}-z_C\frac{d^3\theta_x}{dx^3}\right)+N\left(\frac{d^4v}{dx^4}-z_C\frac{d^4\theta_x}{dx^4}\right)\right]=0$$

Finally, the angles of rotation of the cross-section due to bending θ_Y , θ_Z are given from eqns. (3a,b) as

$$\theta_Y=-\frac{dw}{dx}-\alpha_z\frac{EI_{YY}}{GA}\frac{d^3w}{dx^3}-\alpha_z\frac{EI_{YZ}}{GA}\frac{d^3v}{dx^3}+a_z\frac{m_Y}{GA}-$$
$$-\alpha_z^2\frac{EI_{YY}}{G^2A^2}\left[\frac{dp_Z}{dx}-\frac{dp_X}{dx}\left(\frac{dw}{dx}+y_C\frac{d\theta_x}{dx}\right)-2p_X\left(\frac{d^2w}{dx^2}+y_C\frac{d^2\theta_x}{dx^2}\right)+N\left(\frac{d^3w}{dx^3}+y_C\frac{d^3\theta_x}{dx^3}\right)\right]- \tag{18a}$$
$$-\alpha_y\alpha_z\frac{EI_{YZ}}{G^2A^2}\left[\frac{dp_Y}{dx}-\frac{dp_X}{dx}\left(\frac{dv}{dx}-z_C\frac{d\theta_x}{dx}\right)-2p_X\left(\frac{d^2v}{dx^2}-z_C\frac{d^2\theta_x}{dx^2}\right)+N\left(\frac{d^3v}{dx^3}-z_C\frac{d^3\theta_x}{dx^3}\right)\right]$$

$$\theta_Z=\frac{dv}{dx}+\alpha_y\frac{EI_{ZZ}}{GA}\frac{d^3v}{dx^3}+\alpha_y\frac{EI_{YZ}}{GA}\frac{d^3w}{dx^3}+a_y\frac{m_Z}{GA}+$$
$$+\alpha_y^2\frac{EI_{ZZ}}{G^2A^2}\left[\frac{dp_Y}{dx}-\frac{dp_X}{dx}\left(\frac{dv}{dx}-z_C\frac{d\theta_x}{dx}\right)-2p_X\left(\frac{d^2v}{dx^2}-z_C\frac{d^2\theta_x}{dx^2}\right)+N\left(\frac{d^3v}{dx^3}-z_C\frac{d^3\theta_x}{dx^3}\right)\right]+ \tag{18b}$$
$$+\alpha_z\alpha_y\frac{EI_{YZ}}{G^2A^2}\left[\frac{dp_Z}{dx}-\frac{dp_X}{dx}\left(\frac{dw}{dx}+y_C\frac{d\theta_x}{dx}\right)-2p_X\left(\frac{d^2w}{dx^2}+y_C\frac{d^2\theta_x}{dx^2}\right)+N\left(\frac{d^3w}{dx^3}+y_C\frac{d^3\theta_x}{dx^3}\right)\right]$$

Equilibrium of torsional moments along x axis of the beam element, after taking into account the additional shear stresses due to the presence of the axial force N, which employing eqns. (1) are written as

$$\tau_{xz} = \frac{N}{A}\left(\frac{\partial \bar{w}}{\partial x}\right) = \frac{N}{A}\left(\frac{dw}{dx} + y\frac{d\theta_x}{dx}\right) \qquad \tau_{xy} = \frac{N}{A}\left(\frac{\partial \bar{v}}{\partial x}\right) = \frac{N}{A}\left(\frac{dv}{dx} - z\frac{d\theta_x}{dx}\right) \tag{19a,b}$$

and the corresponding arising additional twisting moment

$$M_{t,add} = \int_\Omega \left(\tau_{xz} y - \tau_{xy} z\right) d\Omega = N y_C \frac{dw}{dx} - N z_C \frac{dv}{dx} + N\frac{I_S}{A}\frac{d\theta_x}{dx} \tag{20}$$

leads to the third (coupled with the previous two) partial differential equation of the problem of the beam under consideration as

$$EC_S \frac{d^4\theta_x}{dx^4} - GI_t \frac{d^2\theta_x}{dx^2} - N\left(y_C \frac{d^2 w}{dx^2} - z_C \frac{d^2 v}{dx^2} + \frac{I_S}{A}\frac{d^2\theta_x}{dx^2}\right) = m_x + p_Z y_C - p_Y z_C - p_X\left(y_C \frac{dw}{dx} - z_C \frac{dv}{dx}\right) - p_X \frac{I_S}{A}\frac{d\theta_x}{dx} \tag{21}$$

where I_S is the polar moment of inertia with respect to the shear center S, EC_S and GI_t are the cross section's warping and torsional rigidities, respectively, with C_S, I_t being its warping and torsion constants, respectively, given as [3]

$$C_S = \int_\Omega \left(\varphi_S^P\right)^2 d\Omega \tag{22}$$

$$I_t = \int_\Omega \left(y^2 + z^2 + y\frac{\partial \varphi_S^P}{\partial z} - z\frac{\partial \varphi_S^P}{\partial y}\right) d\Omega \tag{23}$$

It is worth here noting that the primary warping function $\varphi_S^P(y,z)$ can be established by solving independently the Neumann problem [3]

$$\nabla^2 \varphi_S^P = 0 \qquad \text{in } \Omega \tag{24}$$

$$\frac{\partial \varphi_S^P}{\partial n} = \frac{1}{2}\frac{\partial\left(r_S^2\right)}{\partial s} \qquad \text{on } \Gamma_j \;\; (j = 1,2,\ldots,K) \tag{25}$$

where $\nabla^2 = \partial^2/\partial y^2 + \partial^2/\partial z^2$ is the Laplace operator; $r_S = \sqrt{y^2 + z^2}$ is the distance of a point on the boundary Γ_j from the shear center S; $\partial/\partial n$ denotes the directional derivative normal to the boundary Γ_j and $\partial/\partial s$ denotes differentiation with respect to its arc length s.

The aforementioned governing differential equations are also subjected to the pertinent boundary conditions of the problem, which are given as

$$\alpha_1 v(x) + \alpha_2 V_y(x) = \alpha_3 \qquad \bar{\alpha}_1 \theta_Z(x) + \bar{\alpha}_2 M_Z(x) = \bar{\alpha}_3 \tag{26a,b}$$

$$\beta_1 w(x) + \beta_2 V_z(x) = \beta_3 \qquad \bar{\beta}_1 \theta_Y(x) + \bar{\beta}_2 M_Y(x) = \bar{\beta}_3 \tag{27a,b}$$

$$\gamma_1 \theta_x(x) + \gamma_2 M_t(x) = \gamma_3 \qquad \bar{\gamma}_1 \frac{d\theta_x(x)}{dx} + \bar{\gamma}_2 M_w(x) = \bar{\gamma}_3 \tag{28a,b}$$

at the beam ends $x = 0, l$, where V_y, V_z and M_Z, M_Y are the reactions and bending moments with respect to y and z axes, respectively, obtained from eqns (8b,c), (15a,b), (16a,b) as

$$V_y=-EI_{ZZ}\frac{d^3v}{dx^3}-\alpha_y\frac{EI_{ZZ}}{GA}N\left(\frac{d^3v}{dx^3}-z_C\frac{d^3\theta_x}{dx^3}\right)-EI_{YZ}\frac{d^3w}{dx^3}-\alpha_z\frac{EI_{YZ}}{GA}N\left(\frac{d^3w}{dx^3}+y_C\frac{d^3\theta_x}{dx^3}\right)+N\left(\frac{dv}{dx}-z_C\frac{d\theta_x}{dx}\right) \tag{29}$$

$$V_z=-EI_{YY}\frac{d^3w}{dx^3}-\alpha_z\frac{EI_{YY}}{GA}N\left(\frac{d^3w}{dx^3}+y_C\frac{d^3\theta_x}{dx^3}\right)-EI_{YZ}\frac{d^3v}{dx^3}-\alpha_y\frac{EI_{YZ}}{GA}N\left(\frac{d^3v}{dx^3}-z_C\frac{d^3\theta_x}{dx^3}\right)+N\left(\frac{dw}{dx}+y_C\frac{d\theta_x}{dx}\right) \tag{30}$$

$$M_Y=-EI_{YY}\frac{d^2w}{dx^2}-\alpha_z\frac{EI_{YY}}{GA}N\left(\frac{d^2w}{dx^2}+y_C\frac{d^2\theta_x}{dx^2}\right)-EI_{YZ}\frac{d^2v}{dx^2}-\alpha_y\frac{EI_{YZ}}{GA}N\left(\frac{d^2v}{dx^2}-z_C\frac{d^2\theta_x}{dx^2}\right) \tag{31}$$

$$M_Z=EI_{ZZ}\frac{d^2v}{dx^2}+\alpha_y\frac{EI_{ZZ}}{GA}N\left(\frac{d^2v}{dx^2}-z_C\frac{d^2\theta_x}{dx^2}\right)+EI_{YZ}\frac{d^2w}{dx^2}+\alpha_z\frac{EI_{YZ}}{GA}N\left(\frac{d^2w}{dx^2}+y_C\frac{d^2\theta_x}{dx^2}\right) \tag{32}$$

the angles of rotation due to bending θ_Y, θ_Z are evaluated from eqns (18) as

$$\theta_Y=-\frac{dw}{dx}-\alpha_z\frac{EI_{YY}}{GA}\frac{d^3w}{dx^3}-\alpha_z^2\frac{EI_{YY}}{G^2A^2}N\left(\frac{d^3w}{dx^3}+y_C\frac{d^3\theta_x}{dx^3}\right)-\alpha_z\frac{EI_{YZ}}{GA}\frac{d^3v}{dx^3}-\alpha_y\alpha_z\frac{EI_{YZ}}{G^2A^2}N\left(\frac{d^3v}{dx^3}-z_C\frac{d^3\theta_x}{dx^3}\right) \tag{33a}$$

$$\theta_Z=\frac{dv}{dx}+\alpha_y\frac{EI_{ZZ}}{GA}\frac{d^3v}{dx^3}+\alpha_y^2\frac{EI_{ZZ}}{G^2A^2}N\left(\frac{d^3v}{dx^3}-z_C\frac{d^3\theta_x}{dx^3}\right)+\alpha_y\frac{EI_{YZ}}{GA}\frac{d^3w}{dx^3}+\alpha_z\alpha_y\frac{EI_{YZ}}{G^2A^2}N\left(\frac{d^3w}{dx^3}+y_C\frac{d^3\theta_x}{dx^3}\right) \tag{33b}$$

while in eqns. (28) M_t and M_w are the torsional and warping moments at the boundary of the bar, respectively, given as

$$M_t=-EC_S\frac{d^3\theta_x}{dx^3}+GI_t\frac{d\theta_x}{dx}+N\left(y_C\frac{dw}{dx}-z_C\frac{dv}{dx}+\frac{I_S}{A}\frac{d\theta_x}{dx}\right) \qquad M_w=-EC_S\frac{d^2\theta_x}{dx^2} \tag{34a,b}$$

Finally, $\alpha_k,\bar{\alpha}_k,\beta_k,\bar{\beta}_k,\gamma_k,\bar{\gamma}_k$ $(k=1,2,3)$ are functions specified at the beam ends $x=0,l$. Eqs. (26)-(28) describe the most general linear boundary conditions associated with the problem at hand and can include elastic support or restraint. It is apparent that all types of the conventional boundary conditions (clamped, simply supported, free or guided edge) can be derived from these equations by specifying appropriately these functions (e.g. for a clamped edge it is $\alpha_1=\beta_1=\gamma_1=1$, $\bar{\alpha}_1=\bar{\beta}_1=\bar{\gamma}_1=1$, $\alpha_2=\alpha_3=\beta_2=\beta_3=\gamma_2=\gamma_3=\bar{\alpha}_2=\bar{\alpha}_3=\bar{\beta}_2=\bar{\beta}_3=\bar{\gamma}_2=\bar{\gamma}_3=0$).

In the aforementioned boundary value problem the axial force N inside the beam or at its boundary is given from the following relation

$$N=EA\left[\frac{du}{dx}+\frac{1}{2}\left(\frac{dw}{dx}\right)^2+\frac{1}{2}\left(\frac{dv}{dx}\right)^2\right] \tag{35}$$

where $u=u(x)$ is the bar axial displacement, which can be evaluated from the solution of the following boundary value problem

$$EA\left[\frac{d^2u}{dx^2}+\frac{d^2w}{dx^2}\frac{dw}{dx}+\frac{d^2v}{dx^2}\frac{dv}{dx}\right]=-p_x \qquad \text{inside the beam} \tag{36}$$

$$c_1u(x)+c_2N(x)=c_3 \qquad \text{at the beam ends } x=0,l \tag{37}$$

where c_i $(i=1,2,3)$ are given constants.

The solution of the boundary value problem given from eqns (17), (21), (36) subjected to the boundary conditions (26)-(28), (37) which represents the nonlinear flexural – torsional analysis of beams, presumes the evaluation of the shear deformation coefficients a_y, a_z, corresponding to the principal shear axes coordinate system Syz. These coefficients are established equating the approximate formula of the shear strain energy per unit length [2]

$$U_{appr.} = \frac{a_y Q_y^2}{2AG} + \frac{a_z Q_z^2}{2AG} \tag{38}$$

with the exact one given from

$$U_{exact} = \int_\Omega \frac{\left(\tau_{xz}\right)^2 + \left(\tau_{xy}\right)^2}{2G} d\Omega \tag{39}$$

and are obtained as [4]

$$a_y = \frac{1}{\kappa_y} = \frac{A}{\Delta^2}\int_\Omega \left[\left(\nabla\Theta\right) - \boldsymbol{e}\right]\cdot\left[\left(\nabla\Theta\right) - \boldsymbol{e}\right] d\Omega \qquad a_z = \frac{1}{\kappa_z} = \frac{A}{\Delta^2}\int_\Omega \left[\left(\nabla\Phi\right) - \boldsymbol{d}\right]\cdot\left[\left(\nabla\Phi\right) - \boldsymbol{d}\right] d\Omega \tag{40a,b}$$

where $\left(\tau_{xz}\right)_j, \left(\tau_{xy}\right)_j$ are the transverse (direct) shear stress components, $\left(\nabla\right) \equiv \boldsymbol{i_Y}\left(\partial/\partial Y\right) + \boldsymbol{i_Z}\left(\partial/\partial Z\right)$ is a symbolic vector with $\boldsymbol{i_Y}, \boldsymbol{i_Z}$ the unit vectors along Y and Z axes, respectively, Δ is given from

$$\Delta = 2\left(1+\nu\right)\left(I_{YY} I_{ZZ} - I_{YZ}^2\right) \tag{41}$$

ν is the Poisson ratio of the cross section material, $\boldsymbol{e}$ and $\boldsymbol{d}$ are vectors defined as

$$\boldsymbol{e} = \left[\nu\left(I_{YY}\frac{Y^2 - Z^2}{2} - I_{YZ} YZ\right)\right]\boldsymbol{i_Y} + \left[\nu\left(I_{YY} YZ + I_{YZ}\frac{Y^2 - Z^2}{2}\right)\right]\boldsymbol{i_Z} \tag{42}$$

$$\boldsymbol{d} = \left[\nu\left(I_{ZZ} YZ - I_{YZ}\frac{Y^2 - Z^2}{2}\right)\right]\boldsymbol{i_Y} + \left[-\nu\left(I_{ZZ}\frac{Y^2 - Z^2}{2} + I_{YZ} YZ\right)\right]\boldsymbol{i_Z} \tag{43}$$

and $\Theta\left(Y,Z\right)$, $\Phi\left(Y,Z\right)$ are stress functions, which are evaluated from the solution of the following Neumann type boundary value problems [4]

$$\nabla^2\Theta = 2\left(I_{YZ} Z - I_{YY} Y\right) \quad \text{in } \Omega \qquad \frac{\partial\Theta}{\partial n} = \boldsymbol{n}\cdot\boldsymbol{e} \quad \text{on } \Gamma = \bigcup_{j=1}^{K+1}\Gamma_j \tag{44a,b}$$

$$\nabla^2\Phi = 2\left(I_{YZ} Y - I_{ZZ} Z\right) \quad \text{in } \Omega \qquad \frac{\partial\Phi}{\partial n} = \boldsymbol{n}\cdot\boldsymbol{d} \quad \text{on } \Gamma = \bigcup_{j=1}^{K+1}\Gamma_j \tag{45a,b}$$

where $\boldsymbol{n}$ is the outward normal vector to the boundary Γ. In the case of negligible shear deformations $a_z = a_y = 0$. It is also worth here noting that the boundary conditions (25), (44b), (45b) have been derived from the physical consideration that the traction vector in the direction of the normal vector $\boldsymbol{n}$ vanishes on the free surface of the beam.

3. Integral Representations – Numerical Solution

According to the precedent analysis, the nonlinear flexural – torsional analysis of Timoshenko beams of arbitrary cross section, undergoing moderate large deflections reduces in establishing the displacement components $v(x)$, $w(x)$ and $\theta_x(x)$ having continuous derivatives up to the fourth order with respect to x and the axial displacement $u = u(x)$ having continuous derivatives up to the second order with respect to x satisfying the coupled governing equations (17), (21), (36) inside the beam and the boundary conditions (26)-(28), (37) at the beam ends $x = 0,l$. Eqns (17), (21), (36) are solved using the Analog Equation Method [1].

4. Numerical Examples

To demonstrate the range of applications of the proposed method, a cantilever beam of length $l = 2.50m$ (Fig.2a), of the non-symmetric cross section ($A = 0.01186m^2$, $E = 2.1\times 10^8 kN/m^2$, $\nu = 0.3$, $C_s = 5.232\times 10^{-7} m^6$, $I_t = 1.910\times 10^{-6} m^4$, $I_S = 2.517\times 10^{-4} m^4$) of Fig. 2b has been studied. Since the proposed method requires the coordinate system CYZ through the cross section's centroid C to have Y, Z axes parallel to the principal shear axes, in the first column of Table 1 the geometric, the inertia constants and the shear deformation coefficients of the examined cross section are given with respect to an original coordinate system $C\tilde{Y}\tilde{Z}$, followed by the evaluation of the angle of rotation θ^S [4] giving the final coordinate system CYZ and the new geometric, inertia constants and shear deformation coefficients given in the second column of the aforementioned table. In Table 2 the transverse deflection w at the free end of the cantilever beam, subjected to a gradually increasing concentrated at the same point axial $\mu P_{\tilde{X}}$ ($P_{\tilde{X}} = -120kN$) and uniformly distributed axial $\mu p_{\tilde{X}}$ and transverse $\mu p_{\tilde{Z}}$ ($p_{\tilde{X}} = -20kN/m$, $p_{\tilde{Z}} = -40kN/m$) load are presented taking into account or ignoring shear deformation effect, for various values of the loading factor μ. The significant influence of the nonlinear analysis effect is verified especially in the case of intense loading, while the discrepancy of the results due to the influence of the shear deformation effect necessitates its inclusion in the analysis.

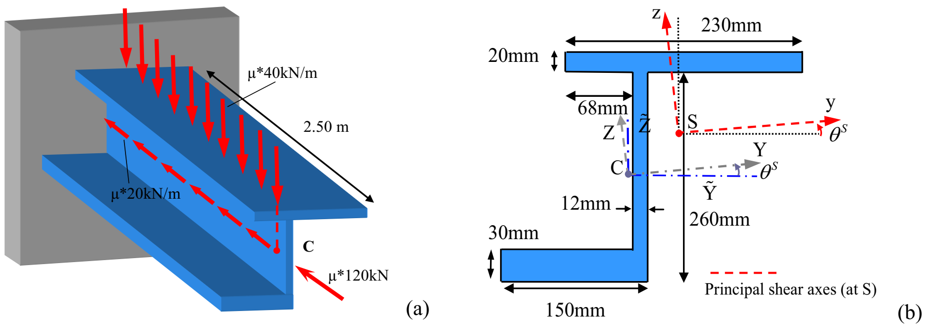

Fig. 2. 3-D view (a) and cross section (b) of the non-symmetric beam.

Coordinate system $C\tilde{Y}\tilde{Z}$		Coordinate system CYZ	
$I_{\tilde{Y}\tilde{Y}} = 1.606\times 10^{-4} m^4$	$\alpha_{\tilde{y}} = 1.741$ $\alpha_{\tilde{z}} = 3.902$	$I_{YY} = 1.545\times 10^{-4} m^4$	$\alpha_y = 1.736$ $\alpha_z = 3.907$
$I_{\tilde{Z}\tilde{Z}} = 5.665\times 10^{-5} m^4$	$\alpha_{\tilde{y}\tilde{z}} = -0.10$ $\theta^S = 0.046 rad$	$I_{ZZ} = 6.278\times 10^{-5} m^4$	$\alpha_{yz} = 0.0$
$I_{\tilde{Y}\tilde{Z}} = 6.384\times 10^{-5} m^4$	$\tilde{y}_C = -0.0384m$ $\tilde{z}_C = -0.0379m$	$I_{YZ} = 6.837\times 10^{-5} m^4$	$y_C = -0.0401m$ $z_C = -0.0361m$

Table 1. Geometric, inertia constants and shear deformation coefficients of the examined cross section.

Scale factor μ	Displacement w (cm)			
	Linear Analysis		Nonlinear Analysis	
	Ignoring Shear Deformation	With Shear Deformation ($a_z = 3.907$)	Ignoring Shear Deformation	With Shear Deformation ($a_z = 3.907$)
1	-1.10	-1.20	-1.15	-1.26
2	-2.20	-2.41	-2.42	-2.63
3	-3.31	-3.61	-3.83	-4.16
4	-4.41	-4.82	-5.41	-5.87
5	-5.51	-6.02	-7.21	-7.81
6	-6.61	-7.22	-9.29	-10.05
7	-7.72	-8.43	-11.75	-12.69
8	-8.82	-9.63	-14.72	-15.88
9	-9.92	-10.84	-18.42	-19.86
10	-11.02	-12.04	-23.23	-25.04

Table 2. Transverse deflection w at the free end of the cantilever beam for various values of factor μ.

5. Concluding remarks

The main conclusions that can be drawn from this investigation are

a. The numerical technique presented in this investigation is well suited for computer aided analysis for beams of arbitrary simply or multiply connected cross section.
b. The significant influence of geometrical nonlinear analysis in beam elements subjected in intense transverse loading is verified.
c. The discrepancy between the results of the linear and the nonlinear analysis demonstrates the significant influence of the axial loading.
d. In some cases the remarkable increment of all the deflections due to the influence of the shear deformation effect demonstrates its significant influence in nonlinear analysis.
e. The developed procedure retains the advantages of a BEM solution over a pure domain discretization method since it requires only boundary discretization.

Acknowledgments

This work has been funded by the project PENED 2003. The project is cofinanced 75% of public expenditure through EC - European Social Fund and 25% of public expenditure through Ministry of Development - General Secretariat of Research and Technology and through private sector, under measure 8.3 of OPERATIONAL PROGRAM "COMPETITIVENESS" in the 3rd Community Support Program.

References

[1] J.T.Katsikadelis, The Analog Equation Method. A Boundary-Only Integral Equation Method for Nonlinear Static and Dynamic Problems in General Bodies, *Theoretical and Applied Mechanics*, **27**, 13-38, (2002).
[2] U.Schramm, V. Rubenchik and W.D.Pilkey, Beam Stiffness Matrix Based on the Elasticity Equations, *International Journal for Numerical Methods in Engineering*, **40**, 211–232, (1997).
[3] E.J.Sapountzakis, and V.G.Mokos, Warping Shear Stresses in Nonuniform Torsion by BEM, *Computational Mechanics,* **30**(2), 131-142, (2003).
[4] E.J.Sapountzakis and V.G.Mokos, A BEM Solution to Transverse Shear Loading of Beams, *Computational Mechanics,* **36**, 384-397, (2005).

A Modified Boundary Integral Equation Method for Filtration Problem

S.Khabthani[1], A. Sellier[2], L.Elasmi[3], F.Feuillebois[4]
[1,3]LIM. Ecole Polytechnique de Tunisie,rue el Khawarezmi,BP 743,La Marsa,Tunisie
e-mail: sondes.khabthani@ept.rnu.tn
e-mail: assaad.elasmi@ept.rnu.tn
[2] LadHyx. Ecole Polytechnique, 91128 Palaiseau Cedex, France
e-mail: sellier@ladhyx.polytechnique.fr
[4]PMMH.Ecole Supérieure de Physique et de Chimie Industrielles de Paris, 10, rue Vauquelin - 75231 Paris Cedex 5, France
e-mail: feuilleb@pmmh.espci.fr

Keywords: Filtration problem, boundary-integral equations, Beavers and Joseph condition.

Abstract.
This work introduces a modified boundary-integral equation method for solving the filtration problem in case of arbitrary-shaped solid particles. The advocated approach is more interesting whenever the Green tensor is not symmetric and might therefore be employed in other fields as well. Here, the Green tensor fails to be symmetric because the Stokes equations in the fluid region and the Darcy's equations in the porous medium are coupled across the interface by a slip Beavers and Joseph type boundary condition.

Introduction

As sketched in Fig.1, we consider the motion of a solid particle with smooth surface S near a plane porous slab $\mathcal{P}$ with thickness e and plane and parallel boundaries Σ_0 and Σ_1.

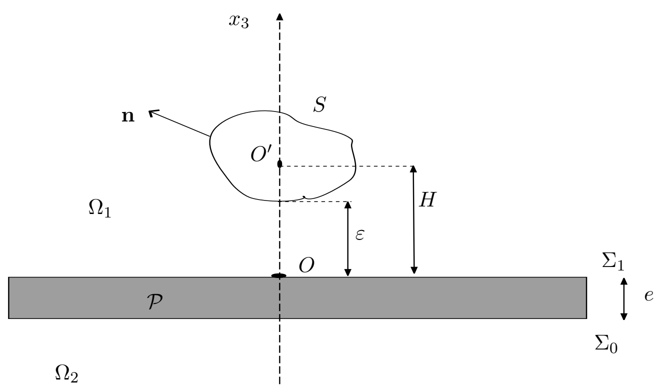

Figure 1: A solid particle with attached point O' immersed in a Newtonian liquid near a porous slab $\mathcal{P}$ with thickness e and parallel boundaries Σ_0 ($x_3 = -e$) and Σ_1 ($x_3 = 0$).

For convenience we henceforth employ the tensor summation notation in the Cartesian coordinates (O, x_1, x_2, x_3) with $\mathbf{OM} = x_i\mathbf{e}_i$. The flow is governed by the Stokes equations in the fluid domains Ω_1 ($x_3 > 0$), Ω_2 ($x_3 < -e$) and the Darcy's equations in the porous medium $\mathcal{P}$ ($-e < x_3 < 0$). These equations are coupled across the plane interfaces Σ_1 and Σ_0 by the slip boundary condition derived by Beavers and Joseph [1]. The associated Green tensor analytically obtained in [2] suggests using, at a first glance, the following usual integral representation [3] of each Cartesian component u_k of the fluid velocity in the upper liquid domain Ω_1:

$$u_k(\mathbf{x}) = \int_S T_{ij}(\mathbf{u}(\mathbf{y}))n_j G_i^k(\mathbf{y},\mathbf{x})dS(\mathbf{y}) + C_k(\mathbf{x},\Sigma_1) \text{ for } \mathbf{x}\in\Omega_1 \quad (1)$$

$$C_k(\mathbf{x},\Sigma_1) = \int_{\Sigma_1}[G_i^k(\boldsymbol{\eta},\mathbf{x})T_{ij}(\mathbf{u}(\boldsymbol{\eta})) - u_i(\boldsymbol{\eta})T_{ij}(\mathbf{G}^k(\boldsymbol{\eta},\mathbf{x}))]n_j dS\boldsymbol{\eta} \text{ for } \mathbf{x}\in\Omega_1 \quad (2)$$

with $T_{ij}\mathbf{e}_i\otimes\mathbf{e}_j$ the stress tensor and $\mathbf{n}$ the unit vector on $S\cup\Sigma_1$ directed into the liquid. Unfortunately, since each above term $C_k(\mathbf{x},\Sigma_1)$ involves an integral over the unbounded plane surface Σ_1 the formulation (1)-(2) is not suitable in practice. This work thus advocates a new and modified boundary-integral approach solely involving the particle's surface S. It also presents a few numerical results for a spherical particle.

Governing equations and associated Green tensor for the addressed filtration problem

We denote by $\mathbf{u}$ and p the velocity and pressure fields in each domains Ω_1, $\mathcal{P}$ and Ω_2. The liquid has uniform viscosity μ and the flow $(\mathbf{u},p)$ obeys the Darcy equations in the slab $\mathcal{P}$ and the Stokes equations elsewhere. In other words,

$$\mu\Delta\mathbf{u} = \nabla p \text{ and } \nabla.\mathbf{u} = 0 \text{ in } \Omega_1\cup\Omega_2, \quad (3)$$

$$\mathbf{u} = -\frac{K}{\mu}\nabla p \text{ and } \nabla.\mathbf{u} = 0 \text{ in } \mathcal{P}. \quad (4)$$

In (4) note that $K > 0$ designates the permeability of the porous medium. The particle has translational velocity $\mathbf{U}$ (the velocity of one attached point O') and angular velocity $\boldsymbol{\Omega}$. Each flow $(\mathbf{u},p)$ vanishes far from the particle and the equations (3)-(4) are supplemented with the boundary conditions:

$$u_3(\Sigma_i^+) = u_3(\Sigma_i^-) \text{ and } p(\Sigma_i^+) = p(\Sigma_i^-) \text{ for } i = 0,1; \quad (5)$$

$$\frac{\partial u_\beta}{\partial x_3}(\Sigma_1^+) = \frac{\sigma}{\sqrt{K}}(u_\beta(\Sigma_1^+) - u_\beta(\Sigma_1^-)) \text{ for } \beta = 1,2; \quad (6)$$

$$\frac{\partial u_\beta}{\partial x_3}(\Sigma_0^-) = -\frac{\sigma}{\sqrt{K}}(u_\beta(\Sigma_0^-) - u_\beta(\Sigma_0^+)) \text{ for } \beta = 1,2; \quad (7)$$

$$\mathbf{u} = \mathbf{U} + \boldsymbol{\Omega}\wedge\mathbf{O'M} \text{ for } M \text{ on } S \quad (8)$$

where (6)-(7) are the Beavers and Joseph boundary condition applied on Σ_1 and Σ_0 and σ is a dimensionless slip coefficient introduced in [1].
As obtained in [4] for less-complicated boundary conditions, the Green tensor associated with (3)-(8) consists of a Stokeslet and several images of singularities. Such a tensor has been analytically obtained in [2]. A source with strength $\mathbf{e}_k$ located at $\mathbf{y}$ in Ω_1 then produces at the observation point $\mathbf{x}$ in Ω_1 a velocity field $G_j^k(\mathbf{x},\mathbf{y})\mathbf{e}_j$. If δ_{kl} is the Kronecker delta function we introduce the tensor

$$J_{kl} = \delta_{k\alpha}\delta_{\alpha l} - \delta_{k3}\delta_{3l} \quad (9)$$

$\mathbf{y}'$ is the symmetric of $\mathbf{y}$ with respect to Σ_1, $\mathbf{R} = \mathbf{x}-\mathbf{y}$ and $\mathbf{R}' = \mathbf{x}-\mathbf{y}'$. Then one gets

$$\begin{aligned}\mu G_j^k(\mathbf{x},\mathbf{y}) &= \frac{1}{2}w_j^k\phi - \frac{1}{2}w_j^k\phi' - \delta_{3k}w_j^3\phi_1' - J_{kl}\frac{\partial}{\partial R_l'}w_j^3\phi_2' - \delta_{3k}\frac{\partial}{\partial R_3'}\mathbf{w}_j^3\phi_3' \\ &+ J_{kl}\frac{\partial}{\partial R_l'}\frac{\partial}{\partial R_j'}\phi_5' + \delta_{3k}\frac{\partial}{\partial R_j'}\frac{\partial}{\partial R_3'}\phi_6' + \delta_{3k}\frac{\partial}{\partial R_j'}\phi_7' - 2J_{kl}\frac{\partial}{\partial R_l'}\delta_{3j}\phi_4' + 2J_{kj}\frac{\partial}{\partial R_3'}\phi_4' \quad (10)\end{aligned}$$

with the following derivative tensor

$$w_j^k = R_k'\frac{\partial}{\partial R_j'} - \delta_{kj}$$

and functions ϕ, ϕ' and $\phi'_i = \mathcal{H}_0[f_i(\xi)\psi]$ for $i = 1, 7$ (expressed as the Hankel transform of complicated functions f_i) available in [2]. More precisely,

$$\mathcal{H}_0[g](\rho, R'_3) = \int_0^{+\infty} \xi g(\xi, R'_3) J_0(\xi\rho) d\xi, \tag{11}$$

$$\psi_1 = -\frac{e^{-\xi R_3}}{4\pi\xi} = \mathcal{H}_0(\phi),\ \phi = -\frac{1}{4\pi R} \text{ and } \psi_2 = -\frac{e^{-\xi R'_3}}{4\pi\xi} = \mathcal{H}_0(\phi'),\ \phi' = -\frac{1}{4\pi R'} \tag{12}$$

As the reader may check, the above Green function does not satisfy the symmetry property. In other words, one arrives for the filtration problem at:

$$G_i^k(\mathbf{x}, \mathbf{y}) \neq G_k^i(\mathbf{y}, \mathbf{x}) \tag{13}$$

This implies that the terms $C_k(\mathbf{x}, \Sigma_1)$ given by (2) do not vanish. This property makes then it difficult to solve our tangential filtration problem (3)-(8) by resorting to the standard integral equations derived from (1)-(2).

Modified boundary-integral equation

This section presents for one particle another method also valid for several particles. To avoid integrals on the surface Σ_1, we propose to calculate the velocity and pressure fields $(\mathbf{u}, p)$ in the liquid domain Ω_1 using the following integral representations:

$$u_j(\mathbf{x}) = \mathbf{u}(\mathbf{x}).\mathbf{e}_j = \int_S G_j^k(\mathbf{x}, \mathbf{y}) d_k(\mathbf{y}) dS(\mathbf{y}),\ \ p(\mathbf{x}) = \int_S H^k(\mathbf{x}, \mathbf{y}) d_k(\mathbf{y}) dS(\mathbf{y}) \ \text{ for } \ \mathbf{x} \in \Omega_1 \tag{14}$$

where H^k is the Green function for the pressure and $\mathbf{d}$ the unknown Stokeslets surface density here provided by enforcing on the particle's surface S the no-slip boundary condition (8). This latter provides for $\mathbf{d}$ the Fredholm boundary-integral equation of the first kind:

$$\int_S G_j^k(\mathbf{x}, \mathbf{y}) d_k(\mathbf{y}) dS(\mathbf{y}) = [\mathbf{U} + \mathbf{\Omega} \wedge \mathbf{O'M}].\mathbf{e}_j \text{ for } \mathbf{x} = \mathbf{OM} \text{ on } S. \tag{15}$$

It is emphasized that $\mathbf{d}$ is *not* the surface traction exerted on S by the liquid flow $(\mathbf{u}, p)$. However, considering our non-trivial Green tensor as the sum of the weakly singular Oseen-Burger Green tensor (in free space) and a regular additional tensor, the knowledge of this density $\mathbf{d}$ is sufficient to calculate the net force $\mathbf{F}$ and torque $\mathbf{\Gamma}$ (about O') applied by the flow $(\mathbf{u}, p)$ on S using the relations:

$$\mathbf{F} = -\int_S \mathbf{d}\, dS,\ \ \mathbf{\Gamma} = -\int_S [\mathbf{O'M} \wedge \mathbf{d}]\, dS. \tag{16}$$

Relation between $(\mathbf{F}, \mathbf{\Gamma})$ and $(\mathbf{U}, \mathbf{\Omega})$ for a particle without inertia

For a solid particle with negligible inertia and settling under the action of a prescribed uniform gravity field $\mathbf{g}$, one further requires that

$$\mathbf{F} + M\mathbf{g} = \mathbf{0}, \quad \mathbf{\Gamma} = \mathbf{0} \tag{17}$$

provided that O' is the particle center of mass and M is the particle mass.
Let us introduce six steady Stokes flows $(\mathbf{u}_T^i, p_T^i)$ and $(\mathbf{u}_R^i, p_R^i)$ for $i = 1, 2, 3$ associated respectively with translations and rotations of the particle and such that

$$\mathbf{u}_T^i = \mathbf{e}_i \ \text{ and } \ \mathbf{u}_R^i = \mathbf{e}_i \wedge \mathbf{O'M} \quad \text{on } \ S. \tag{18}$$

These flows exert on the particle net forces $\mathbf{F}_T^i, \mathbf{F}_R^i$ and net torques $\mathbf{\Gamma}_T^i, \mathbf{\Gamma}_R^i$ (about O'). Setting $U_j = \mathbf{U}.\mathbf{e}_j$ and $w_j = \mathbf{\Omega}.\mathbf{e}_j$, the net force $\mathbf{F}$ and torque $\mathbf{\Gamma}$ applied on the moving particle thus read:

$$\mathbf{F} = U_j \mathbf{F}_T^j + \omega_j \mathbf{F}_R^j,\ \ \mathbf{\Gamma} = U_j \mathbf{\Gamma}_T^j + \omega_j \mathbf{\Gamma}_R^j. \tag{19}$$

Accordingly, the relations (17) yield the following 6-equation well-posed linear system

$$U_j[\mathbf{F}_T^j.\mathbf{e}_i] + \omega_j[\mathbf{F}_R^j.\mathbf{e}_i] = -M\mathbf{g}.\mathbf{e}_i \tag{20}$$

$$U_j[\mathbf{\Gamma}_T^j.\mathbf{e}_i] + \omega_j[\mathbf{\Gamma}_R^j.\mathbf{e}_i] = 0 \tag{21}$$

The matrix of (20)-(21), termed the resistance matrix, is non-singular and thus the system (20)-(21) admits a unique solution $(\mathbf{U}, \mathbf{\Omega})$.

Numerical strategy

The boundary-integral equation (15) is discretized by using on S a N-node mesh consisting of 6-node triangular and curved boundary elements. Then (15) reduces to a 3N-equation linear system $AX = B$ for the 3N-component array X consisting of the Cartesian components of the unknown density $\mathbf{d}$ at the nodal points. The influence matrix is computed by employing standard techniques [5]. For instance, the weakly-singular behavior of each term $G_j^k(\mathbf{x}, \mathbf{y})$ is accurately handled by using local polar coordinates for the boundary elements to which the node $\mathbf{x}$ belongs to. Finally, the system $AX = B$ is numerically inverted by appealing to a LU factorization algorithm since its 3N-3N square matrix A is dense and not symmetric.

Numerical results and discussion for a spherical particle

This section defines the range of each parameter K,e and σ -respectively the permeability and thickness of the porous slab and dimensionless slip coefficient-for applications and gives numerical results for a spherical particle.

Selected parameters

Let us consider a spherical particle with center O' and radius a larger than the typical size $\sqrt{K}$ of the pore of the porous slab $\mathcal{P}$. Thus $\sqrt{K} < a$. In the case of micro-filtration problem, the permeability of the membrane is in the $0.1\mu m - 10\mu m$ range and for a low Reynolds number flow ($Re \ll 1$), the particle radius satisfies $0.01\mu m < a < 100\mu m$. Moreover the Darcy's equation is appropriate when the size of pore is less than the distance $\varepsilon = H - a$ with $H = \mathbf{OO'}.\mathbf{e}_3$. Thus, $\sqrt{K} < \varepsilon$. Introducing dimensionless quantities, one therefore has

$$\sqrt{K^*} = \frac{\sqrt{K}}{a},\ e^* = \frac{e}{a},\ \varepsilon^* = \frac{\varepsilon}{a},\ \lambda = \frac{\sqrt{K^*}}{\sigma} < e^* \tag{22}$$

where λ denotes the slip length.

Force exerted on a sphere translating parallel to the membrane

Consider the case of a spherical particle translating with velocity $\mathbf{U} = U_1\mathbf{e}_1$ along the direction x_1 parallel to the plane boundary Σ_1. The dimensionless drag force F_{11}^* exerted on the translating particle in the x_1-direction may be expressed as

$$F_{11}^* = -\frac{\mathbf{F}_T^1.\mathbf{e}_1}{6\pi\mu a U_1} \tag{23}$$

where $\mathbf{F}_T^1$ has been introduced after (18). The friction coefficient F_{11}^* is plotted in Fig.2 versus the sphere-slab dimensionless gap $\varepsilon^* = \frac{H}{a} - 1$ for different values of the parameter λ. As seen in these curves, the friction increases as λ or ε^* decreases. For λ large, one recovers the perfect slip case whereas small values of λ deal with the case of a pure no-slip condition. One should note that when translating parallel to the porous slab, the sphere also experiences a torque about its center O'. Such

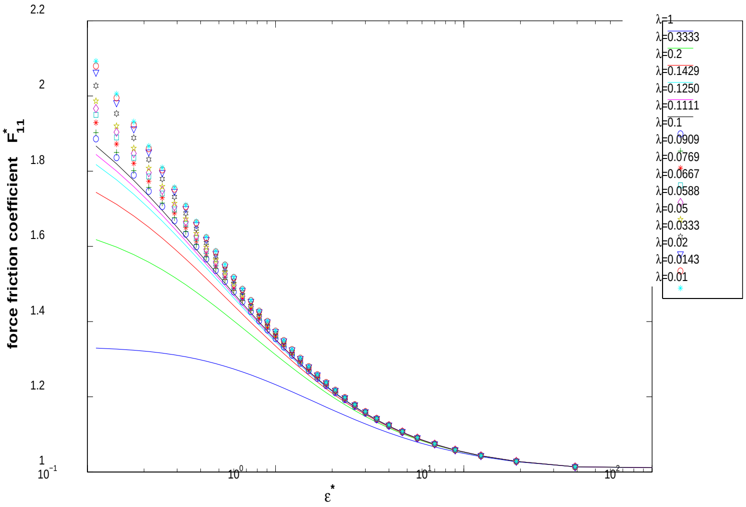

Figure 2: Force friction coefficient F^*_{11} for a sphere translating parallel to the membrane for $e^* = 1$ and $K^* = 10^{-2}$.

a torque is not plotted here for conciseness.

Torque experienced by a sphere rotating parallel to a slab

We turn to the case of a spherical particle rotating parallel to the porous slab with angular velocity $\mathbf{\Omega}$ aligned with $\mathbf{e}_2$. The sphere experiences a net torque $\mathbf{\Gamma}^2_R$ (recall definitions after (18)) parallel with $\mathbf{e}_2$ and this suggests introducing the following torque friction

$$\Gamma^*_{22} = -\frac{\mathbf{\Gamma}^2_R.\mathbf{e}_2}{8\pi\mu a^3}. \tag{24}$$

As seen in Fig.3, the coefficient Γ^*_{22} exhibits similar trends as the ones observed for F^*_{11} in Fig.2. This rotating motion also gives a force (not plotted here) directed along x_1-direction.

Motion of a sphere subject to a gravity aligned with $\mathbf{e}_3$

Finally we plot in Fig.4 the normalized velocity component u_3 of a sphere moving under a uniform gravity $\mathbf{g} = -g\mathbf{e}_3$ (i.e normal to porous slab $\mathcal{P}$). For a fluid with density ρ and a sphere with uniform density ρ_S, this velocity is defined as

$$u_3 = -\frac{9}{2}\frac{\mathbf{U}.\mathbf{e}_3}{(\rho_S - \rho)a^2} \tag{25}$$

The sedimentation velocity of the spherical particle in x_3-direction raises when the slip length scale λ increase. When the particle is close to the membrane, its movement is slowed down.

Conclusions

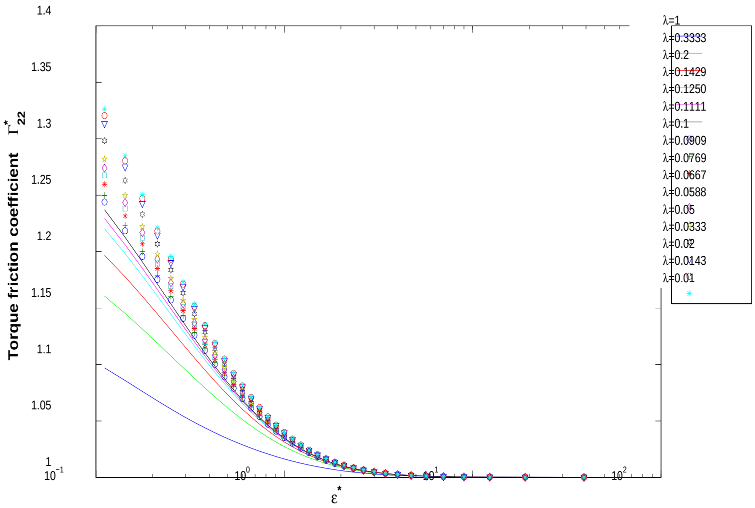

Figure 3: Torque friction coefficient Γ^*_{22} for a sphere rotating parallel to the membrane for $e^* = 1$ and $K^* = 10^{-2}$.

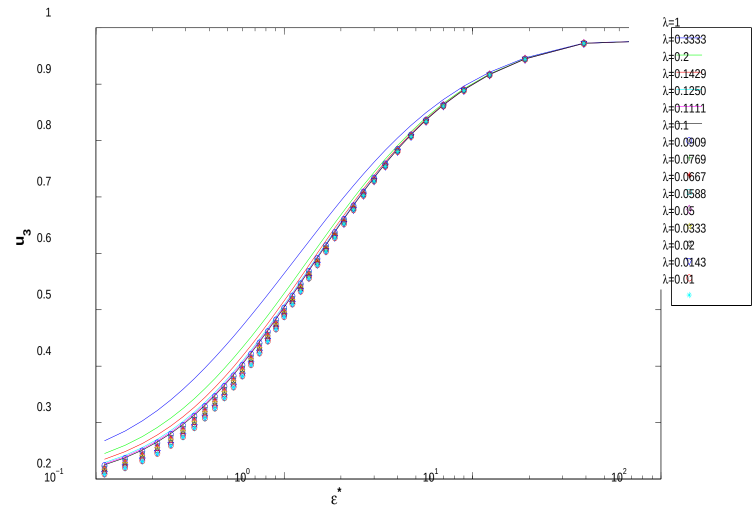

Figure 4: Normalized velocity u_3 of the sphere settling under the action of uniform gravity field $\mathbf{g} = -g\mathbf{e}_3$ for $e^* = 1$ and $K^* = 10^{-2}$.

A modified boundary-integral equation method has been proposed to deal with the filtration problem and the advocated approach is valid as well for a collection of arbitrary-shaped solid particles. The settling velocity of a solid sphere towards a porous slab is determined. Finally, preliminary results for the force and torque applied on the moving particle are presented and discussed.

References

[1] G.Beavers, D.Joseph Boundary conditions at a naturally permeable wall. *J.Fluid Mech.*, **30**, 197-207 (1967).

[2] S.Khabthani,L.Elasmi Etude des solutions élémentaires du problème de filtration tangentielle,18ème Congrès Français de Mécanique, Grenoble (2007).

[3] C. Pozrikidis *Boundary integral and singularity methods for linearized viscous flow*, Cambridge University Press, (1992).

[4] J. R. Blake A note on the image system for a Stokeslet in a no-slip boundary, Proc. Camb. Phil. Soc. **70**, 303-310, (1971).

[5] M. Bonnet *Boundary Integral Equation Methods for Solids and Fluids*, John Wiley & Sons Ltd, (1995).

Linear Bending Analysis of Stiffened Plates with Different Materials by the Bounary Element Method

Gabriela R. Fernandes

Civil Engineering Department, Federal University of Goiás (UFG) CAC – Campus Catalão, Av. Dr. Lamartine Pinto de Avelar, 1120, Setor UniversitárioCEP 75700-000 Catalão – GO Brazil,
email grezfernandes@itelefonica.com.br

Keywords: Plate bending, Boundary elements, Building floor structures, stiffened plates.

Abstract. In this work, is presented a boundary element method (BEM) formulation to perform linear bending analysis of building floor structures where the slabs and beams can be defined with different materials. The proposed formulation is based on Kirchhoff's hypothesis, being the building floor modeled by a zoned plate, where the beams are treated as thin sub-regions with larger rigidities. This composed structure is treated as a single body, being the equilibrium and compatibility conditions automatically taken into account. In the final integral equation the tractions are eliminated along the interfaces, reducing therefore the number of degrees of freedom. The displacements are approximated along the beam cross section, leading to a model where the values remain defined on the beam skeleton line instead of their boundaries. The accuracy of the proposed model is showed by comparing the numerical results with a well-known finite element code.

1. Introduction

The boundary element method (BEM) has already proved to be a suitable numerical tool to deal with plate bending problems. It is particularly recommended for the analysis of building floor structures where the combinations of slab, beam and column elements can be more accurately represented, considering that the method is very accurate to compute the effects of concentrated (in fact loads distributed over small areas) and line loads, as well to evaluate high gradient values as bending and twisting moments, and shear forces. Moreover, the same order of errors is expected when computing deflections, slopes, moments and shear forces, because the tractions are not obtained by differentiating approximation function as for other numerical techniques.

Recently several works about building floor analysis by the boundary element method (BEM) have been published. In [1-3] the BEM was coupled with FEM to develop the numerical model, where boundary elements have been chosen to model the plate behaviour, while beams and columns have been represented by finite elements. As usual, the different elements are combined together by enforcing equilibrium and compatibility conditions along the interfaces. However, for complex floor structures the number of degrees of freedom may increase rapidly diminishing the solution accuracy.

In [4-6] are proposed BEM formulations for analysing the bending problem of beam-stiffened elastic plates. Paiva & Aliabadi present in [7, 8] BEM formulations to analyse building floors structures which are modelled by a zoned plate with different thicknesses. In these works BEM is not coupled with FEM, therefore boundary elements are chosen to model both plate and beam elements.

An alternative scheme to reduce the number of degrees of freedom has been recently proposed by FERNANDES & VENTURINI [9] to perform simple bending analysis using only a BEM formulation based on Kirchhoff's hypothesis. In this work the building floor is modelled by a zoned plate where each sub-region defines a beam or a slab, being all of them represented by their middle surface. The beams are modelled as narrow sub-regions with larger thickness, being the tractions eliminated along the interfaces, reducing therefore the total number of unknowns. Then in order to reduce further the degrees of freedom, the displacements are approximated along the beam width, leading to a model where the bending values are defined only on the beams axis and on the plate boundary without beams. In [10] the authors have extended the formulation proposed in [9] in order to represent all sub-regions by a same reference surface, so that the eccentricity effects should be taken into account. It is important note that in the formulations proposed in [9] and [10] all sub-regions should have the same Poisson's ration and Young's modulus. More recently Fernandes and Konda [11] have modified the model proposed in [9] to consider the Reissner's theory instead of Kirchhoff's.

In this work the BEM formulation developed in [9] is extended to consider sub-regions with different values of Poisson's ration and Young's modulus. The accuracy of proposed model is confirmed by numerical examples whose results are compared with a well-known finite element code.

2. Basic Equations

Without loss of generality, let us consider the three sub-region plate depicted in Fig. (1), where t_1, t_2 and t_3 are the sub-regions thicknesses. The sub-regions are referred to a Cartesian system of co-ordinates with axes x_1, x_2 and x_3 defined in their middle plane (see Fig. 1b). The plate sub-domains assumed as isolated plates are denoted by Ω_1, Ω_2 and Ω_3, with boundaries Γ_1, Γ_2 and Γ_3, respectively. Alternatively, when the whole solid is considered, Γ gives the total external boundary, while Γ_{jk} represents interfaces, for which the subscripts denote the adjacent sub-regions (see Fig. 1a).

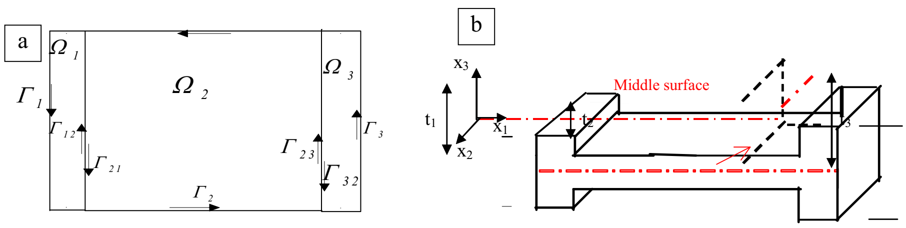

Figure 1: a) middle surface view; b) General zoned plate domain.

For a point placed at any of those plate sub-regions, the following equations can be defined:

- Equilibrium equations in terms of internal forces:

$$m_{ij},_j - q_i = 0 \tag{1}$$

$$q_i,_i + g = 0 \tag{2}$$

where g is the distributed load acting on the plate middle surface, m_{ij} are bending and twisting moments and q_i represents shear forces, with subscripts taken in the range $i,j=\{1, 2\}$.

- The plate bending differential equation,

$$m_{ij,ij} + g = 0 \tag{3}$$

or

$$w,_{iijj} = g / D \qquad (i,j = 1,2) \tag{4}$$

where $D = Et^3/(1-\nu^2)$ is the flexural rigidity and $w,_{iijj} = \nabla^4 w$, being ∇^4 the bi-harmonic operator.

- The generalised internal force × displacement relations,

$$m_{ij} = -D\left(\nu\delta_{ij} w,_{kk} + (1-\nu) w,_{ij}\right) \tag{5}$$

$$q_i = -Dw,_{jji} \tag{6}$$

- The effective shear force,

$$V_n = q_n + \partial m_{ns} / \partial s \tag{7}$$

where (n, s) are the local co-ordinate system, with n and s referred to the plate boundary normal and tangential directions, respectively.

The problem definition is then completed by assuming the following boundary conditions over Γ: $u_i = \bar{u}_i$ on Γ_1 (generalised displacements, deflections and rotations) and $p_i = \bar{p}_i$ on Γ_2 (generalised tractions, normal bending moment and effective shear forces), where $\Gamma_1 \cup \Gamma_2 = \Gamma$.

3. Integral Representations

In this section, we are going to derive the bending integral equations of a zoned plate where the thickness, Poisson's ratio and Young's modulus may vary from one sub-region to another, but must be constant over each sub-region. The equations will be derived by applying the reciprocity theorem to each sub-region and summing them to obtain the equation for the whole body. These integral equations will be used to model building floor structures, being each sub-region the representation of either a slab or a beam.

Let us consider initially a single sub-region Ω_m, for which the following reciprocity relation can be written in terms of moments and curvatures:

$$\int_{\Omega_m} w,_{ij}^{*(m)} m_{ij} d\Omega_S = \int_{\Omega_m} w,_{ij} m_{ij}^{*(m)} d\Omega_S \tag{8}$$

where $w,_{ij}^{m*}$ and m_{ij}^{m*} are fundamental solutions with the unit load acting in the x_3 direction (see Fig. 1b); no summation is implied on m.

Equation (8) can be modified by replacing the fundamental values of sub-region Ω_m, by the values referred to the sub-region where the load point is placed. This simplifies the formulation because allows to eliminate the tractions along the interfaces. Thus, denoting by D and $w,_{ij}^{*}$ the values related to the sub-region where the collocation point is placed the following relation can be defined:

$$w,_{ij}^{*(m)} = \frac{D}{D_m} w,_{ij}^{*} \tag{9}$$

Considering equation (9) the moment m_{ij}^{m*} can be written in terms of ν and m_{ij}^{*} referred to the sub-region where the load point is placed as follow:

$$m_{ij}^{*(m)} = \frac{\nu_m}{\nu} m_{ij}^{*} + D\left(\frac{\nu_m}{\nu} - 1\right) w,_{ij}^{*} \tag{10}$$

Replacing (9) and (10) into equation (8) one obtains:

$$\int_{\Omega_s} w,_{ij}^{*} m_{ij} d\Omega_s = \frac{D_s \nu_s}{D\nu} \int_{\Omega_S} w,_{ij} m_{ij}^{*} d\Omega_s + D_s\left(\frac{\nu_s}{\nu} - 1\right) \int_{\Omega_S} w,_{ij} w,_{ij}^{*} d\Omega_s \tag{11}$$

Note that in the case of having $\nu = 0$, eq. (11) can not be used. On the other hand one can demonstrate that if $\nu = 0$, eq. (8) results into the same equation presented in [9] related to the formulation where all sub-regions must have the same Poisson's ratio and Young's modulus. Applying eq. (11) for all sub-regions one obtains the bending reciprocity relation for the whole plate, as follows:

$$\int_{\Omega} w,_{ij}^{*}\, m_{ij} d\Omega = \sum_{m=1}^{N_S}\left[\frac{D_m \nu_m}{D\nu}\int_{\Omega_m} w,_{ij}\, m_{ij}^{*} d\Omega_m + D_m\left(\frac{\nu_m}{\nu}-1\right)\int_{\Omega_m} w,_{ij}\, w,_{ij}^{*} d\Omega_m\right] \tag{12}$$

where N_s is the sub-regions number.
Equation (12) can be integrated by parts to give the following representation of deflection:

$$\begin{aligned}
k(q)w(q) &= \sum_{m=1}^{N_S}\frac{D_m\nu_m}{D\nu}\int_{\Gamma_m}\left(M_n^*(q,P)w,_n(P)-V_n^*(q,P)w(P)\right)d\Gamma(P)+\\
&+\sum_{j=1}^{N_{int}}\int_{\Gamma_{ja}}\left(\frac{D_j\nu_j-D_a\nu_a}{D\nu}\right)\left(M_n^*(q,P)w,_n(P)-V_n^*(q,P)w(P)\right)d\Gamma_{ja}(P)+\\
&-\sum_{i=1}^{N_{c0}}\frac{D_i\nu_i}{D\nu}R_{ci}^*(q,P)w_{ci}(P)-\left(\frac{D_j\nu_j-D_a\nu_a}{D\nu}\right)\sum_{j=1}^{N_{c1}+N_{c2}}R_{cj}^*(q,P)w_{cj}(P)+\sum_{i=1}^{N_c}R_{ci}(P)w_{ci}^*(q,P)+\\
&+\int_{\Gamma}\left(V_n(P)w^*(q,P)-M_{nn}(P)w,_n^*(q,P)\right)d\Gamma(P)+\int_{\Omega_g}\left(g(p)w^*(q,p)\right)d\Omega_g(p)+\\
&+\sum_{m=1}^{N_S}D_m\left(\frac{\nu_m}{\nu}-1\right)\int_{\Gamma_m}\left(w,_n\, w,_{nn}^*+w\left(\frac{Q_n^*}{D}-\frac{\partial w,_{ns}^*}{\partial s}\right)\right)d\Gamma+\\
&+\sum_{j=1}^{N_{int}}\left[D_j\left(\frac{\nu_j}{\nu}-1\right)-D_a\left(\frac{\nu_a}{\nu}-1\right)\right]\int_{\Gamma_{ja}}\left(w,_n\, w,_{nn}^*+w\left(\frac{Q_n^*}{D}-\frac{\partial w,_{ns}^*}{\partial s}\right)\right)d\Gamma+\\
&\qquad-\sum_{i=1}^{Nc0}D_i\left(\frac{\nu_i}{\nu}-1\right)R_{ci}^{*\prime}w_{ci}-\sum_{i=1}^{Nc1+Nc2}\left[D_i\left(\frac{\nu_i}{\nu}-1\right)-D_a\left(\frac{\nu_a}{\nu}-1\right)\right]R_{ci}^{*\prime}w_{ci}
\end{aligned} \tag{13}$$

where N_c is the total number of corners, N_{int} is the interfaces number, no summation is implied on n and s that are local normal and shear direction co-ordinates, respectively; Γ_m is the external boundary of sub-region Ω_m, Γ_{ja} represents an interface, being the subscript a referred to the adjacent sub-region to Ω_j N_{c0}, N_{c1} and N_{c2} are numbers of corners between boundary elements, between interface elements and between interface and boundary elements, respectively (see [9]); Ω_g is the plate loaded area and $R_{ci}^{*\prime} = w,_{ns}^{*(+)} - w,_{ns}^{*(-)}$, being $w,_{ns}^{*(+)}$ the value of the curvature $w,_{ns}^{*}$ after the corner i and $w,_{ns}^{*(-)}$ the value of $w,_{ns}^{*}$ before the corner i.

In eq. (13) the free term $K(q)$ can assume several values depending on the position of the collocation point as follows: $K(q)=1$, $K(Q)=1/2$ and $K(Q)=(1+D_a/D)/2$ for internal points, boundary points and interface points, respectively. For the free term value on the corners see [9].

Note that in the case of having $\nu = 0$, the integral representation of deflection is the same presented in [9] where are adopted the same Poisson's ratio and Young's modulus for all sub-regions. Equation (13) is the exact representation of deflection of a zoned plate bending problem. The interface values V_n and M_n were eliminated, remaining therefore the displacements w and $w,_n$ along interfaces, while on the external boundary the usual four values are maintained: w; $w,_n$; M_n and V_n.

Observe that differentiating eq. (13) once one can obtain the integral representation of deflection derivative. One has to differentiate once more eq. (13) to obtain the curvature integral representations at internal points. Then, bending and twisting moment integral representations are obtained by simply applying the definition given in eq. (5). To obtain the shear force integral representation, completing the internal force values at internal points, one can differentiate the deflection derivative equation twice to apply the definition given in eq.(6).

Equation (13) can be used for solving the bending problem of stiffened plates. In this case the interface collocation points are adopted on the interfaces. However we have considered some approximations for the displacements over the beam cross sections in order to translate the displacement components related to the beam interfaces to its axis. In this model instead of having interface collocations points we have collocations points placed along the beams axis. Thus the number of degrees of freedom is strongly reduced (for more details see [9]). After introducing these approximations we have the deflections w and the deflections derivative $w,_n$ defined on the beams axis, while along the external boundary the usual four values are maintained: w; $w,_n$; M_n and V_n. It is important to stress that despite of having all values referred to nodes defined along the beam axis the integrals are still performed along the interfaces. Thus, no singular or hyper-singular term is found when transforming the integrals representations into algebraic ones.

4. Integral Representations

As usual for any BEM formulation, the integral representations (13) are transformed into algebraic expressions after discretizing the boundary and interfaces into geometrically linear elements, where quadratic shape functions were adopted to approximate the variables.

After writing the required number of algebraic equations, one can get the set of equations to solve the problem in terms of boundary and beam axis values. The boundary nodal values remained in the algebraic system are: one deflection w and its normal derivative $w,_n$, being the counterpart values given by the moment M_n normal to the boundary and the effective shear force V_n. Along the beams axis we have defined only the displacements w and $w,_n$. Besides on the corners is defined the deflection w and its counterpart value given by the corner reaction R_c. Thus two algebraic equations have to be written for each boundary node and other two relations for each beam axis node. For each boundary node we define two outside collocation points very near to the boundary, where the deflection representation (13) is written. For each beam axis node is defined one collocation point where are written two algebraic equations: one of the deflection and another one of the deflection normal derivative. The beam axis collocations points are coincident with the node when variable continuity is assumed or defined at skeleton element internal point when variable discontinuity is required. Besides, for both, boundary and interface corners, one extra equation of deflection must be written.

After selecting the recommended collocation points and writing the corresponding algebraic relation for all of them, one obtains the standard set of equations given as usual by the following expression:

$$\mathbf{HU} = \mathbf{GP} + \mathbf{T} \tag{14}$$

where **U** contains the generalized displacement nodal values defined along the boundary and along the skeleton lines, **P** contains only boundary nodal tractions, and **T** is the independent vector due to the applied loads.

5. Numerical Application - Plate reinforced by two external beams

The stiffened plate depicted in Fig. (2) is now shown to demonstrate the performance of the proposed formulation. The results are compared to a well-known finite element code (ANSYS, version 9), where shell elements have been used to discretize all floor slabs as well as the beams. Observe also that in the proposed model the elements placed at external beams ends, in the direction of the beam width, are automatically generated by the code, so that there is no need of defining them.

The plate to be analysed is reinforced by two boundary beams, increasing the stiffness of the structural system mainly in the x_1 direction, as shown in Fig. (2). A distributed load g of $0.04kN/cm^2$ is applied over all surface of the stiffened plate. The side defined by the coordinate $x_1 = -100cm$ (see Fig. 2) is considered fixed ($w=w,_n=0.0$), while the remaining three sides are assumed free ($V_n=M_n=0.0$). For this analysis thickness $t_p=10.0cm$, Poisson's ratio $\nu_p=0.2$ and Young's modulus $E_p=3x10^3kN/cm^2$ were adopted for the plate, while $t_b=25cm$, $\nu_b=0.0$ and $E_b=2.7x10^4kN/cm^2$ were assumed for the beams.

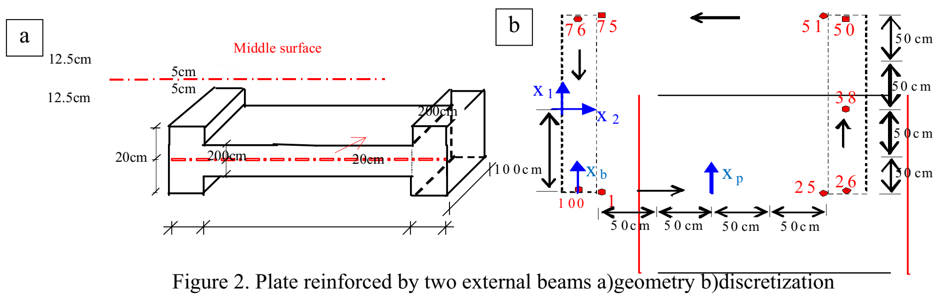

Figure 2. Plate reinforced by two external beams a)geometry b)discretization

The adopted discretization is shown in Fig. (2b), where each plate side without beams as well as each beam axis was discretized by *12* quadratic elements, giving the total amount of 48 elements and 100 nodes.

Deflections obtained in the plate middle axes x_2 (defined for x_1=0.0) and x_p (defined for x_2=120cm) are displayed, respectively, in Fig. (3) and (4). Figures (5) and (6) show, respectively, the deflections and the bending moments along the beam axis x_b (defined for x_2=10.0cm). As can be seen the numerical results compare very well with the ones obtained by ANSYS.

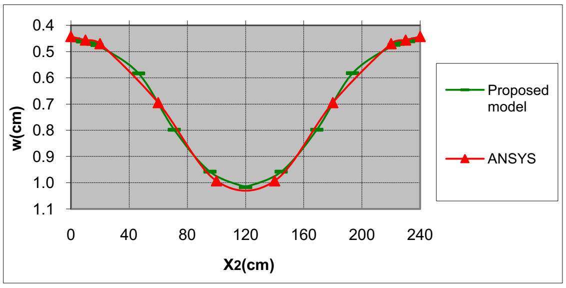

Figure 3 – Deflections on the plate middle axis x_2

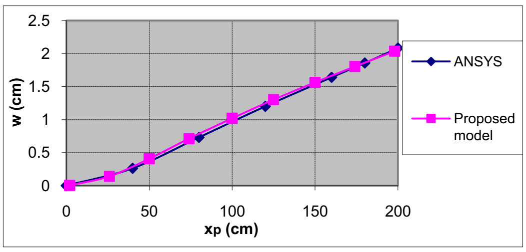

Figure 4 – Deflections on the plate middle axis x_p

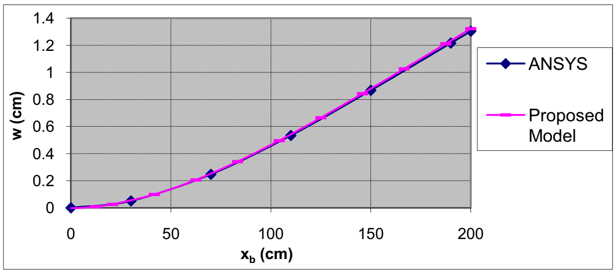

Figure 5 – Deflections on the beam axis x_b

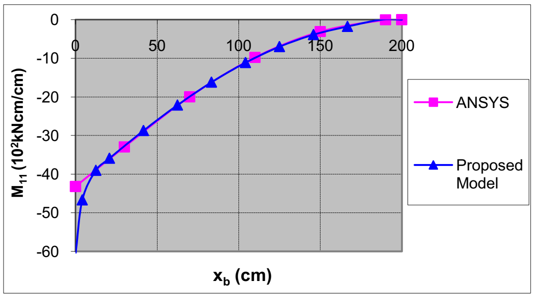

Figure 6 – Moments M_{11} on the beam axis x_b

6. CONCLUSIONS

A BEM formulation based on Kirchhoff's hypothesis for performing bending analysing of plates reinforced by beams has been extended to deal with reinforced plates composed by beams and slabs of different materials. So that different values of thickness, Young's modulus and Poisson's ratio can be defined for each plate sub-region. The beams are assumed as narrow sub-regions, without dividing the reinforced plate into beam and plate elements. Therefore this composed structure is treated as a single body, where equilibrium and compatibility conditions are automatically guaranteed by the global integral equations. In order to reduce the number of degrees of freedom some approximations are considered for the displacements along the beam cross section, leading to a model where the problem values are defined on the beam axis and on the plate boundary without beams. The performance of the proposed formulation has been confirmed by comparing the results with a well-known finite element code.

Acknowledgements:
The author wish to thank FAPESP (São Paulo State Foundation for Scientific Research) as well as for CNPQ (Conselho Nacional de Desenvolvimento Científico e Tecnológico) for the financial support.

References

[1] Hu, C. & Hartley, G.A., Elastic analysis of thin plates with beam supports. *Engineering Analysis with Boundary Elements*, **13**: 229-238, 1994.
[2] Hartley, G.A., Development of plate bending elements for frame analysis. *Engineering Analysis with Boundary Elements*, **17**: 93-104, 1996.
[3] Tanaka, M. & Bercin, A.N., A boundary Element Method applied to the elastic bending problems of stiffened plates. In: *Boundary Element Method XIX*, Eds. C.A. Brebbia et al., CMP, Southampton, 1997.
[4] Sapountzakis, E.J. & Katsikadelis, J.T., Analysis of plates reinforced with beams. *Computational Mechanics*, **26**: 66-74, 2000.

[5] Sapountzakis, E.J. & Katsikadelis, J.T., Elastic deformation of ribbed plates under static, transverse and inplane loading. *Computers & Structures*, **74**: 571-581, 2000
[6] Tanaka, M., Matsumoto, T. and Oida*, S.,* A boundary element method applied to the elastostatic bending problem of beam-stiffened plate*. Engineering Analysis with Boundary Elements,* **24**:751-758, 2000.
[7] Paiva, J. B. and Aliabadi, M. H., Boundary element analysis of zoned plates in bending*. Computational Mechanicss,* ***25****: 560-566, 2000.*
[8] Paiva, J. B. and Aliabadi, M. H., Bending moments at interfaces of thin zoned plates with discrete thickness by the boundary element method*. Engineering Analysis with Boundary Elements,* **28**: 747-751, 2004.
[9] Fernandes, G.R and Venturini, W.S., Stiffened plate bending analysis by the boundary element method. *Computational Mechanics*, **28**: 275-281, 2002.
[10] Fernandes, G.R. and Venturini, W. S., Building floor analysis by the Boundary element method. *Computational Mechanics,* **35**:277-291, 2005.
[11] Fernandes, Gabriela R., Konda, Danilo H.A BEM formulation based on Reissner¿s theory to perform simple bending analysis of plates reinforced by rectangular beams. Computational Mechanics. , v.42, p.671 - 683, 2008

Dynamics of free hexagons based on BEM

P.Prochazka

Society of Science, Research and Advisory, Czech Association of Civil Engineers
Prague, Czech Republic
petr.proch@gmail.com

Keywords: Geodynamics, discrete element method – free hexagons, boundary elements, bumps in deep mines, longwall mining

Abstract. Geodynamical problems are often solved by discrete element methods, which can describe possible damage in rock. The assessment of bumps occurrence in deep mines, which can occur during longwall mining, for example, belongs to the most serious tasks for mining engineers since its consequences are commonly fatal. Describing the problem in early stage of bumps (small displacements are considered) this is a stability assessment, as ones the wall loses its stability, the next movement of rock particles is not decisive. If gas explosion occurs in the rock, for example, discrete element method – hexagonal particles – can be applied in combination with boundary elements involving dynamical effects. Eigenparameters simulate the explosion.

1. Introduction

In this work interface between static, [1], and dynamical states before and at the moment of bumps is characterized. First the main idea is mentioned and basic formulas are derived, and then some applications to rock bumps are presented. Time-dependent problem with the D'Alembert forces, which are caused by very fast movement of the particles, leads to a simplification that the body of the rock and coal seam are substituted by hexagons, which are, or are not in a mutual contact. The material properties along the interfaces of adjacent hexagons are determined from the stress state, transformed to the contact tractions. The hexagons represent a possible shape of the grains the earth consists of. The most natural contact conditions obeying Generalized Mohr-Coulomb hypotheses may be simply introduced and, after imposing all such contact conditions, the localized damage, or "cracking" can be found out. The stability then depends on the "measure" of the touched zones. Mechanical behavior inside each element is either linear or non-linear (plastic, viscoelastic, viscoplastic, etc) and is expressed in terms of boundary elements. The effect of eigenparameters appears in our conception either in characterization of the plastic behavior or in expressing the gas exlosion in appended examples. In any case the uniform eigenparameters are used inside of the hexagon elements, so that integration of volume integrals is dropped out.

2. Equilibrium in one element

Principal ideas of discrete elements (DEM) are adopted here: the domain defining the continuum (both mine and surrounding rock) is covered by non overlapping elements (grains) of hexagonal shape (generally various shapes of hexagons may be taken into account), see Fig. 1. In this paper, generalized Hooke's law is used and non-linear behavior appears on the interfacial boundary due to Mohr-Coulomb hypotheses. Hence, the free hexagon element method presented here fulfills elastic material properties involving eigenparameters being assigned to the particles and other geotechnical material parameters (the angle of internal friction, the shear strength or cohesion, the tensile strength) are allocated on the interfacial boundary of the elements. As said above, the shapes of hexagonal elements can be diversified. On the other hand, considering the most particles are of the same shape leads to very powerful iteration procedures, as the stiffness matrix can be stored in the internal memory of computers only ones, and during the iteration process only unknown displacements, spring stiffnesses and tractions along the interfaces change.

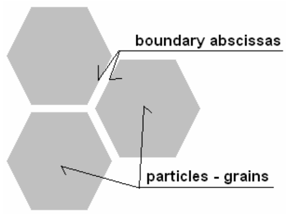

Figure 1: Adjacent grains set up.

Let us consider a typical hexagonal element from the set $\Omega_s, s = 1,...,n$, where n is the number of elements covering the original domain describing the system coal seam - rock overburden, with abscissa-shaped boundaries $\Gamma_{sl}, l = 1,...,6$. In undeformed state the domain Ω_s is equipped with a local coordinate system $0x_1x_2$ (the problem is solved as two-dimensional). Elasticity being assumed in each hexagonal element is described by a well-known set of 8 equations for eight unknowns displacements $\boldsymbol{u}^s(\boldsymbol{x},t) \equiv \{u_1^s(\boldsymbol{x},t), u_2^s(\boldsymbol{x},t)\}$, strains $\boldsymbol{\varepsilon}^s(\boldsymbol{x},t) \equiv \{\varepsilon_{11}^s(\boldsymbol{x},t), \varepsilon_{12}^s(\boldsymbol{x},t), \varepsilon_{22}^s(\boldsymbol{x},t)\}$ and stresses $\boldsymbol{\sigma}^s(\boldsymbol{x},t) \equiv \{\sigma_{11}^s(\boldsymbol{x},t), \sigma_{12}^s(\boldsymbol{x},t), \sigma_{22}^s(\boldsymbol{x},t)\}$, all being dependent on position $\boldsymbol{x} \in \Omega_s$ and time t. In the sequel the index s is dropped out for simplicity.

Generalized Hooke's law relates strains and stresses as:

$$\sigma_{ij}(\boldsymbol{x},t) = L_{ij\alpha\beta}[\varepsilon_{\alpha\beta}(\boldsymbol{x},t) - \mu_{\alpha\beta}(t)],\ \ \sigma_{ij}(\boldsymbol{x},t) = L_{ij\alpha\beta}\varepsilon_{\alpha\beta}(\boldsymbol{x},t) + \lambda_{ij}(t), \qquad i,j,\alpha,\beta = 1,2 \tag{1}$$

and the dynamical equilibrium is expressed as:

$$\frac{\partial\sigma_{ij}(\boldsymbol{x},t)}{\partial x_j} = \rho\frac{\partial^2 u_i(\boldsymbol{x},t)}{\partial t^2} \tag{2}$$

In (1) $L_{ij\alpha\beta}$ is the elastic material stiffness tensor, $\mu_{\alpha\beta}$ is the eigenstrain tensor and λ_{ij} is the eigenstress tensor, both being constant inside of each hexagonal element. In our case they describe sudden change of volume due to the underground gas blasting. Note that relation $\lambda_{ij} = -L_{ij\alpha\beta}\mu_{\alpha\beta}$ holds valid, and the eigenparameters can generally stand for plastic strain, relaxation stress, change of temperature, they can express hereditary problems, etc, which property may be used for more complicated problems. Moreover, the volume weight vector is neglected and ρ is the mass density being assumed to be constant in the entire element.

Integral equations will formulate an equivalent problem to (2): Consider a single hexagonal element (described by the domain Ω_s with its boundary Γ_{sl}), being in a current state. In each hexagonal element the elastic material properties are taken into account, i.e., the element behaves linearly. This makes it possible to introduce only elastic material stiffness matrix, which is considered homogeneous and isotropic, and we get well-known integral equations being valid along the boundary abscissas of the hexagons:

$$c_{ij}(\xi)u_j(\xi,T) = \int_{\Gamma_{sl}} p_i(\boldsymbol{x},T)u^*_{ij}(\boldsymbol{x};\xi)\,\mathrm{d}\boldsymbol{x} - \int_{\Gamma_{sl}} u_i(\boldsymbol{x},T)p^*_{ij}(\boldsymbol{x};\xi)\,\mathrm{d}\boldsymbol{x} + \\ + \int_{\Omega_s} \rho\frac{\partial^2 u_i(\boldsymbol{x},T)}{\partial t^2}u^*_{ij}(\boldsymbol{x},\xi)\,\mathrm{d}\boldsymbol{x} + \int_{\Omega_s} \mu_{i\alpha}(T)\sigma^*_{ij\alpha}(\boldsymbol{x};\xi)\,\mathrm{d}\boldsymbol{x} \tag{3}$$

where $\boldsymbol{\xi}$ is the point of observation, $\boldsymbol{x}$ is the integration point, c_{ij} is a matrix its values depends on a position of the point of observation, and the subscript l identifies the pertinence of the displacements and tractions to the element number s (this index does not appear at the variables, again for simplicity), $\frac{\partial^2 u_i(\boldsymbol{x},T)}{\partial t^2} = \frac{\partial^2 u_i(\boldsymbol{x},t)}{\partial t^2}/_{t=T}$. For example, if uniform distribution of displacements and stresses is considered, $c_{ij} = \frac{1}{2}\delta_{ij}$, where δ_{ij} is the Kronecker symbol. If linear and regular distribution of hexagons is assumed (the vertex angles are 120^0), then $c_{ij} = \frac{1}{3}\delta_{ij}$. The quantities with asterisks are given kernels.

The solution of the problem of elasticity in each hexagonal element Ω_s is realized by the simplest approximation. The positioning of DOFs can be carried out either at the middle of the boundary abscissas (uniform distribution of displacements and stresses - tractions) or at the vertices of the hexagons - then the distribution of boundary displacements and tractions is linear.

Without loss of generality, assuming the uniform distribution of boundary quantities (displacements $u_i(\boldsymbol{x},T)$ and tractions $p_i(\boldsymbol{x},T)$, $i = 1,2$), and uniformly distributed eigenstrains $\mu_{i\alpha}(T)$ in the domain Ω_s, and, furthermore, placing the points of observation $\boldsymbol{\xi}$ successively at the points $\boldsymbol{\xi}_l$, which are centered at the boundary abscissas of the hexagonal elements, the integral equation (3) turns to:

$$\frac{1}{2}u^l_j(T) = p^l_i(T)\int_{\Gamma_{sl}} u^*_{ij}(\boldsymbol{x};\xi_l)\,\mathrm{d}\boldsymbol{x} - u^l_i(T)\int_{\Gamma_{sl}} p^*_{ij}(\boldsymbol{x};\xi_l)\,\mathrm{d}\boldsymbol{x} + \\ + \rho(T)\ddot{u}^l_i(T)\int_{\Omega_s} u^*_{ij}(\boldsymbol{x};\xi_l)\,\mathrm{d}\boldsymbol{x} + \mu_{i\alpha}(T)\int_{\Omega_s} \sigma^*_{ij\alpha}(\boldsymbol{x};\xi_l)\,\mathrm{d}\boldsymbol{x},\ j = 1,2, l = 1,...,6 \tag{4}$$

where $u^l_i(T)$, $p^l_i(T)$, and $b^l_i(T)$ are values of the relevant quantities positioned at the $\boldsymbol{x}_l, l = 1,...,6$, i.e. $u^l_i(T) = u_i(\boldsymbol{x}_l,T)$, and $p^l_i(T) = p_i(\boldsymbol{x}_l,T)$. Point out again that the density ρ is considered uniform inside of each element, and $\ddot{u}^l_i(T) = \frac{\partial^2 u_i(\boldsymbol{x}_l,t)}{\partial t^2}\Big/_{t=T}$.

Note that if uniform distribution of eigenparameters is assumed inside of the particles the integrals of kernels belonging to the eigenstains in (5) can easily be calculated using Eshelby's forces. Knowing the form of kernels and substituting the approximations for boundary displacements and tractions, for the volume weight and eigenstrains matrix, the following equations are obtained:

$$\boldsymbol{Au} = \boldsymbol{f} + \boldsymbol{q}, \qquad \boldsymbol{Ku} = \boldsymbol{F} + \boldsymbol{Q}, \qquad \boldsymbol{K} = \boldsymbol{B}^{-1}\boldsymbol{A}, \qquad \boldsymbol{F} = \boldsymbol{B}^{-1}\boldsymbol{f}, \qquad \boldsymbol{Q} = \boldsymbol{B}^{-1}\boldsymbol{q}, \tag{5}$$

where $\boldsymbol{A}, \boldsymbol{B}$, and $\boldsymbol{K}$ are square matrices (12 * 12), $\boldsymbol{u}$ is the vector of displacement approximations, $\boldsymbol{f}$ and $\boldsymbol{F}$ are the vectors of approximating tractions, $\boldsymbol{V}$ involve the influences of the inertia forces while $\boldsymbol{q}$ and $\boldsymbol{Q}$ are the vectors of effects of the eigenstrains. The latter are vectors (12*1). Note that the stiffness matrix $\boldsymbol{K}$ is different from that arising in applications of finite elements (here it is prevailingly non-symmetric square matrix).

For the next purpose write the matrix equation (5) as:

$$K_{ij}^{11}u_1^j + K_{ij}^{12}u_2^j = F_1^i + V_1^i + Q_1^i, \qquad K_{ij}^{21}u_1^j + K_{ij}^{22}u_2^j = F_2^i + V_2^i + Q_2^i, \quad i,j = 1,...,6$$

or

$$\begin{vmatrix} \boldsymbol{K}^{11} & \boldsymbol{K}^{12} \\ \boldsymbol{K}^{21} & \boldsymbol{K}^{22} \end{vmatrix} \begin{vmatrix} \boldsymbol{u}_1 \\ \boldsymbol{u}_2 \end{vmatrix} = \begin{vmatrix} \boldsymbol{F}_1 \\ \boldsymbol{F}_2 \end{vmatrix} + \begin{vmatrix} \boldsymbol{V}_1 \\ \boldsymbol{V}_2 \end{vmatrix} + \begin{vmatrix} \boldsymbol{Q}_1 \\ \boldsymbol{Q}_2 \end{vmatrix} \tag{6}$$

Index i denotes the number of row and index j stands for the number of slope in the above matrix notation. $\boldsymbol{K}^{11}, \boldsymbol{K}^{12}, \boldsymbol{K}^{21}$ and $\boldsymbol{K}^{22}$ are matrices (6*6) and the other quantities in (6) are vectors (6*1). Subscript 1 denotes the quantities in x_1-direction and index 2 describes quantities in x_2-direction.

3. Current equilibrium inside the particle with fixed neighborhood

If each hexagonal element is considered small enough, lump mass dynamical problem can be formulated. Suppose the only element s can move while the others in the neighborhood remain stable. Now we are able to fill in the distinctive terms in (6). The unknowns in the formulation of the problem will be displacements along the boundaries of elements in x_1 and x_2 directions, which create interfaces between adjacent elements. In the element s the interfacial forces act (formulations for general approximation, not only for uniformly distributes displacements and tractions along the boundaries):

In x_1 - direction:

$$F_1^{sj} = k_{11}^{sj}[u_1^{js} - u_1^{sj}] + k_{12}^{sj}[u_2^{js} - u_2^{sj}] = k_{11}^{sj}[u]_1^{js} + k_{12}^{sj}[u]_2^{js},$$

$$V_1^{sj} = -\rho_s \int_{\Omega_s} \frac{\partial^2 u_1^s(\boldsymbol{x})}{\partial t^2} u_{11}^*(\boldsymbol{x};\boldsymbol{\xi}_j)\mathrm{d}\boldsymbol{x} - \int_{\Omega_s} \rho_s \frac{\partial^2 u_2^s(\boldsymbol{x})}{\partial t^2} u_{21}^*(\boldsymbol{x};\boldsymbol{\xi}_j)\mathrm{d}\boldsymbol{x}, \tag{7}$$

$$Q_1^{sj} = -\int_{\Omega_s} [\mu_{11}^s \sigma_{111}^*(\boldsymbol{x};\boldsymbol{\xi}_j) + \mu_{22}^s \sigma_{212}^*(\boldsymbol{x};\boldsymbol{\xi}_j)]\mathrm{d}\boldsymbol{x}, \quad j = 1,...,6$$

and similarly in x_2-direction. Vector $\boldsymbol{V}^{sj} \equiv \{V_1^{sj}, V_2^{sj}\}$ is the term expressing the influence of the dynamical forces.

As the eigenparameters stand here for description of explosion no shear components are considered in (7). This means that the rotation of particles is suppressed, as this is mostly caused by irregular shape of the particles, so that this assumption is versatile. Since the internal equilibrium has to be fulfilled, for the force resultants it inevitably holds

$$H_s = \sum_{j=1}^{6}(F_1^{sj} + V_1^{sj} + Q_1^{sj}); \qquad V_s = \sum_{j=1}^{6}(F_2^{sj} + V_2^{sj} + Q_2^{sj}). \tag{8}$$

Decoding the latter equations yields using (6) yields

$$\begin{aligned} &\sum_{j=1}^{6}(K_{ij}^{s11} + k_{11}^{sj}\delta_{ij})u_1^{sj} + (K_{ij}^{s12} + k_{12}^{sj}\delta_{ij})u_2^{sj} = k_{11}^{si}u_1^{is} + k_{12}^{si}u_2^{is} + V_1^{si} + Q_1^{si}, \\ &\sum_{j=1}^{6}(K_{ij}^{s21} + k_{21}^{sj}\delta_{ij})u_1^{sj} + (K_{ij}^{s22} + k_{22}^{sj}\delta_{ij})u_2^{sj} = k_{21}^{si}u_1^{is} + k_{22}^{si}u_2^{is} + V_2^{si} + Q_2^{si} \end{aligned} \qquad i=1,\ldots,6 \tag{17}$$

which is a system of 12 equations for 12 unknowns displacements, six in x_1 direction and six in x_2 direction. This system is always solved in an iteration step, in which the neighboring elements are considered fixed and the values of displacements are taken from the previous step.

4. Example

Hereinafter study on a longwall mining after gas explosion loading is carried out. Before tackling the concrete problems, some simplifications will be introduced. First the volume weight forces b_i can be neglected, as only a small part of the rock mechanically cooperates with the coal seam. The effect of overburden (mostly several hundreds of meters) is simulated as loading along the upper part of the domain describing the whole system rock – coal seam. There is no aim to delve into details concerning the description of the time development steps, which are based on finite differences. The formulas for that are exactly the same as those used for PFC and other distinct element codes, see [2].

The domain describing the problem is a rectangle of 26 m x 9.5 m, the coal seam is 4.75 m high. Regular distribution of hexagons is considered, internal radius of each hexagon is 0.25 m, the adit has the width 3 m. Number of particles is 1532. Material parameters of the rock mass have the following values: the elastic modulus E = 50 GPa, the shear modulus G = 20 GPa, the angle of internal friction is 25 degrees, the shear strength c = 1 MPa and the tensile strength p_n^+ = 100 kPa. The coal seam is characterized by E = 5 GPa, G = 2 GPa, the angle of internal friction and the shear strength vary. The load due to the volume weight γ = 25 kN/m^3 is given by the overburden. Depth of the mine is considered as 1000 m. In Fig. 2 setting of hexagonal elements is seen, shaded part describes the coal seam and the upper part the overburden. Also boundary conditions are simulated by rollers along the outer boundary. The zone of explosion 10 m x 4 m is also marked. The boundary of the blast of gas is 10 m far from the face of opening. In the following pictures each particular hexagonal element is drawn in undeformed shape (regular hexagons), although they undertake a local deformation (described by movement of centers of gravity of deformed elements). The reason is that the accumulation and fictitious overlapping of particles underlines a concentration of stresses.

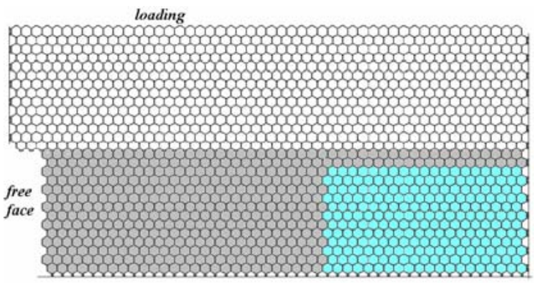

Figure 2: The region of gas explosion in the coal seam

The explosion of the gas is simulated by eigenstrains, which are applied inside of the coal seam and do not change during the development of time dependent deformation in the system rock - coal. Affect of the blast magnitudes on the face stability are solved.

The damage caused by the blast the magnitude of which attains 10 MPa is seen in Figs. 3 and 4. Vertical disconnections in a large band along the upper part of the coal seam are obviously seen in the pictures. In this band the largest nucleation of cracks is concentrated and according to various material properties the behavior in this band is slightly different. It seems remarkable that the face deforms very similarly for all cases of material properties. The most different changes are observed right ahead and even above the center of explosion.

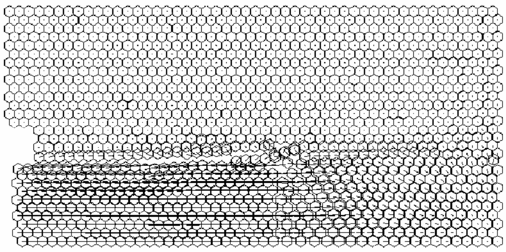

Figure 3: Movements for p_n^+ = 10 kPa, c = 150 kPa, gas pressure = 10 MPa.

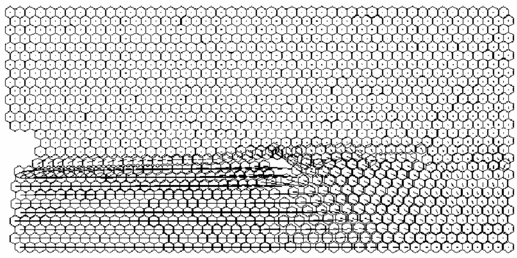

Figure 4: Movements for p_n^+ = 40 kPa, c = 250 kPa, gas pressure = 10 MPa.

5. Conclusions

Dynamical behavior in a coal seam due to a gas explosion at the moment of rock burst and closely after it is studied in this paper. In comparison with classical DEM, for instant with the PFC, we start with different shape of particles to have possibility to obtain also stresses in the particles and between them and with static equilibrium in the state when no inertia forces may occur. If dynamic origin of loading is expected the kinetics of the moved particles is employed. The inertia part of the governing equations starts to prevail and becomes active. Generally, in contradiction with the PFC dynamical equilibrium is taken into consideration after sufficient differences in movements of the hexagonal elements. Regular distribution of elements speeds up the iteration and also better overview on behavior of particles is provided by the pictures.

Acknowledgment: This paper was prepared under financial support of GAČR, project No. 103/08/0922. Financial support of Ministry of Education and Sport of the Czech Republic, project numbers MSM 6840770001 is also acknowledged.

References

[1] P.P. Procházka: Application of discrete element methods to fracture mechanics of rock bursts. Engng Fract Mech 71,(2004);71: p. 601-618.

[2] P.A. Cundall: A computer model for simulation progressive large scale movements of blocky rock systems. Symposium of the international society of rock mechanics, 1971, p. 132-150.

Analysis of Radial Basis Functions in BEM-AEM for non-homogeneous bodies

M.A. Riveiro[1] and Rafael Gallego[2]

[1] Dept. Structural Mechanics, University of Granada, Ed. Politécnico de Fuentenueva, 18071 Granada, Spain, mriveiro@ugr.es

[2] Dept. Structural Mechanics, University of Granada, Ed. Politécnico de Fuentenueva, 18071 Granada, Spain, gallego@ugr.es

Keywords: Non-homogenous materials, Functionally Graded Materials, Analog Equation Methods, Radial Basis Functions

Abstract. A study of the application of Boundary Element Methods to problems involving non-homogeneous materials like Functionally Graded Materials (FGMs) is presented. The Analogue Equation Method (AEM) is used to transform the original problem into a new problem with unknown forcing term but known fundamental solution. By means of this transformation an undetermined system of Boundary Integral Equations (BIEs) can be obtained combining standard boundary element discretization and Radial Basis Functions (RBFs) approximation for the residual term. The application of the original differential operator to the displacement BIE provides the extra equations to compute the unknown forcing term. The boundary character of the method is maintained since the integrals involved in the equations are limited only to the boundary if radial basis functions are selected in such a way that the corresponding analogue equation could be solved analytically. A performance analysis of several radial approximations is presented according to different types of radial functions and the number and distribution of radial source points. In the same way the application of the method to wave propagation problems in frequency domain is studied for different wave lengths.

Introduction

The Boundary Element Method (*Brebbia and Domínguez* [1]) (BEM) has been used successfully for solving many engineering problems governed by systems of partial differential equations. The key feature of the method is that only boundary discretization is required in order to solve the problem. Nevertheless a fundamental solution is needed in analytical form or with low computational cost. In practice, this condiction often limits the application of the BEM to constant coefficient systems. The introduction of new materials including functionally graded materials (FGMs) has increased the interest in boundary methods capable of dealig with materials exhibing heterogeneous composition.

Several techniques has been used to avoid these problems including change of variable ([2, 3]) that despite the advantage that the fundamental solution is obtained in analytical form, the application fields is strongly limited to a small range of variation of properties. Other approaches including Localized Boundary Element Method ([4, 5]) and Dual Reciprocity Method (DRM) [6–8] has been tested for this type of materials. To simplify and automate these methods a combination of analog equation Method (AEM) and DRM approaches has been used [9] to make the choice of the fundamental solution independent of the problem.

The accuracy of this approaches are strongly dependent on the function used in the approximation [10, 11]. A variety of interpolation functions will be tested in this work for the solution of 2D problems using the AEM-BEM.

Problem Statement and Solution Method

The response of a nonhomogeneous body is governed by the boundary value problem:

$$L_{ij}(u_j) + b_i(\mathbf{x}) = 0 \quad \text{en } \mathbf{x} \in \Omega \tag{1}$$

$$G_{ij}(u_j) + h_i(\mathbf{x}) = 0 \quad \text{en } \mathbf{x} \in \Gamma \tag{2}$$

Where $u_i = u_i(\mathbf{x})$ is the response of the body, i represents the problem dimension, L_{ij} are a general second-order elliptic operators defined in Ω and G_{ij} are general linear firs order operators defined in Γ.
Conventional BEM approach demands to obtain the fundamental solution for L_{ij} operators. At present time there is no formulation for solving a general case in closed analytical form. According to AEM [9], for a problem well-posedness in the Hadamard with $\mathbf{u}(\mathbf{x})$ solution we can re-write the previous equations to obtain:

$$\overset{0}{L}_{ij}(u_j) + \hat{b}_i(\mathbf{x}) = 0 \quad \text{en } \mathbf{x} \in \Omega \tag{3}$$

$$G_{ij}(u_j) + h_i(\mathbf{x}) = 0 \quad \text{en } \mathbf{x} \in \Gamma \tag{4}$$

For the above system displacement BIE can be written as:

$$\begin{aligned} c_i^m(\mathbf{z})\Big[u_i(\mathbf{z}) - \sum_j \alpha_j \hat{u}_i(\mathbf{z};\mathbf{y}^j)\Big] + \int_\Gamma \Big[u_i(\mathbf{x}) - \sum_j \alpha_j \hat{u}_i(\mathbf{x};\mathbf{y}^j)\Big] \overset{0}{Q}{}_i^m(\mathbf{x};\mathbf{z}) \mathrm{d}\Gamma(\mathbf{x}) \\ = \int_\Gamma \Big[q_i(\mathbf{x}) - \sum_j \alpha_j \hat{q}_i(\mathbf{x};\mathbf{y}^j)\Big] \overset{0}{U}{}_i^m(\mathbf{x};\mathbf{z}) \mathrm{d}\Gamma(\mathbf{x}) \end{aligned} \tag{5}$$

Where the unknownn forcing has been transferred to the boundary using DRM techniques [6]. This step is always possible if we select the appropiate $\overset{0}{L}_{ij}$ operator. Due to $\hat{b}_i(\mathbf{x})$ is unknown new equations are needed, so following Katsikadelis [12] we apply the original differential operator to the previous equation obtaining:

$$\begin{aligned} -b_k(\mathbf{z}) - \sum_j \alpha_j L_{km}\Big[\hat{u}_m(\mathbf{z};\mathbf{y}^j)\Big] + \int_\Gamma \Big[u_i(\mathbf{x}) - \sum_j \alpha_j \hat{u}_i(\mathbf{x};\mathbf{y}^j)\Big] L_{km}\Big[\overset{0}{U}{}_i^m(\mathbf{x};\mathbf{z})\Big] \mathrm{d}\Gamma(\mathbf{x}) \\ = \int_\Gamma \Big[q_i(\mathbf{x}) - \sum_j \alpha_j \hat{q}_i(\mathbf{x};\mathbf{y}^j)\Big] L_{km}\Big[\overset{0}{Q}{}_i^m(\mathbf{x};\mathbf{z})\Big] \mathrm{d}\Gamma(\mathbf{x}) \end{aligned} \tag{6}$$

In order to close the problem, for a general set of boundary conditions defined by (2) a new equation derived from (5) must be built:

$$\begin{aligned} -d_k^l(\mathbf{z})\Big\{h_l(\mathbf{z}) - \sum_j \alpha_j G_{lm}\Big[\hat{u}_m(\mathbf{z};\mathbf{y}^j)\Big]\Big\} + \int_\Gamma \Big[u_i(\mathbf{x}) - \sum_j \alpha_j \hat{u}_i(\mathbf{x};\mathbf{y}^j)\Big] G_{km}\Big[\overset{0}{U}{}_i^m(\mathbf{x};\mathbf{z})\Big] \mathrm{d}\Gamma(\mathbf{x}) \\ = \int_\Gamma \Big[q_i(\mathbf{x}) - \sum_j \alpha_j \hat{q}_i(\mathbf{x};\mathbf{y}^j)\Big] G_{km}\Big[\overset{0}{Q}{}_i^m(\mathbf{x};\mathbf{z})\Big] \mathrm{d}\Gamma(\mathbf{x}) \end{aligned} \tag{7}$$

Many times the equation (7) can be simplified or even not used according to the type of problem, $\overset{0}{L}_{ij}$ operator, or the selected discretization. In this work Laplace operator will be used as auxiliary operator and scalar problems with "flux" (type $\frac{\partial u}{\partial n}$) boundary conditions will be tested so the boundary conditions will be imposed directly and equation (7) will not be used.

Interpolation Functions

Performance of AEM-BEM approach for 2D scalar problems will be tested using the following RBFs :

- Interpolation type $f(r) = c + r$:

  This (with $c = 1$) was the most popular choice for these methods until the 90s[13]. The parameter allows the inclusion of a new equation for energy minimization or equivalence condtitions.

- Interpolation type $f(r) = \sqrt{c^2 + r^2}$:

  Multiquadrics was one of the first improves in order to achieve more accurate results [12].

- Interpolation type ATPS:

  Golberg [14] proposed the use of augmented thin plate splines (ATPS) for building systems with better conditioning which in $\mathbb{R}^2$ and in $\mathbb{R}^3$ are represented with:

$$
\begin{aligned}
&\mathbb{R}^2 \rightarrow b(\mathbf{x}) \approx \sum_{j}^{M} \alpha_j r_j^2 \mathrm{Log}(r_j) + a_1 x_1 + a_2 x_2 + a_0 \\
&\mathbb{R}^3 \rightarrow b(\mathbf{x}) \approx \sum_{j}^{M} \alpha_j r_j + a_1 x_1 + a_2 x_2 + a_0 \\
&\text{Where} \quad \sum_{j=1}^{M} \alpha_j = \sum_{j=1}^{M} \alpha_j x_1(\mathbf{x}_j) = \sum_{j=1}^{M} \alpha_j x_2(\mathbf{x}_j) = 0
\end{aligned}
$$

- Interpolation type Supported Spline:

  This supported type approximation [15, 16] uses functions with local nature allowing interpolation independence among different zones of the domain.

$$
\begin{aligned}
&b(\mathbf{x}) \approx \sum_{j}^{M} \alpha_j f(r_j) + a_1 x_1 + a_2 x_2 + a_0 \\
&f(r_j) = \begin{cases} 1 - 6\left(\frac{r_j}{s}\right)^2 + 8\left(\frac{r_j}{s}\right)^3 - 3\left(\frac{r_j}{s}\right)^4 & 0 \leqslant r_j \leqslant s \\ 0 & r_j \geqslant s \end{cases} \\
&\text{Where} \quad \sum_{j=1}^{M} \alpha_j = \sum_{j=1}^{M} \alpha_j x_1(\mathbf{x}_j) = \sum_{j=1}^{M} \alpha_j x_2(\mathbf{x}_j) = 0
\end{aligned}
$$

Numerical Examples

As stated before scalar 2D problems will be tested. Constant element discretization has been selected for simplicity. Only interior points will be used for interpolation functions but improvements are expected extending this to the boundary. A minimum distance from interior points to the boundary for avoiding explosive divergences has been set to 1.5 element length.

Example 1: The first problem considered will be the thermal distribution in a plane body with mixed boundary conditions (See Figure 2) governed by

$$\nabla \bullet \{K(\mathbf{x})\nabla T\} = 0 \quad \text{in} \quad \Omega \tag{8}$$

$$\text{Where} \quad K(\mathbf{x}) = (2x + y + 2)^2$$

The following solution of the diferential operator will be used with its respective boundary values:

$$T(\mathbf{x}) = 100 + \frac{6x^2 - 6y^2 + 20xy + 30}{2x + y + 2} \tag{9}$$

This case has been selected because by means of a variable transform [2] it can be turned into a conventional Laplace problem so we can easily pose a comparition in terms of accuracy. In Figure 1 is presented the evolution of the mean error (percentage) of the calculated T in the boundary versus the number of equations for 100 interpolation functions. The behaviour for interior points, boundary flux as well as an increase of interpolation functions is similar, so the graph is representative in terms of trends. The only exception is multiquadrics.

Instabilities are more marked with the increase of interpolation functions and calculations at interior points or for derivative variables.

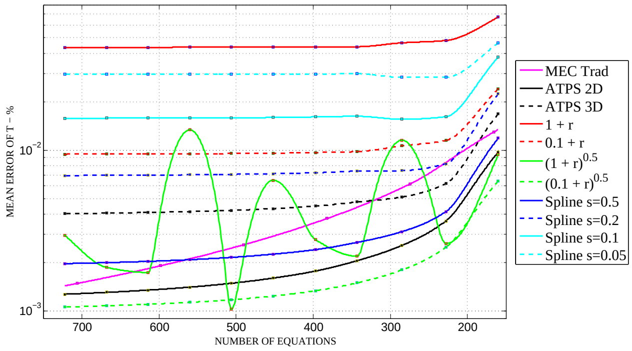

Figure 1: T Mean Error - B.E. Variation - NI = 100

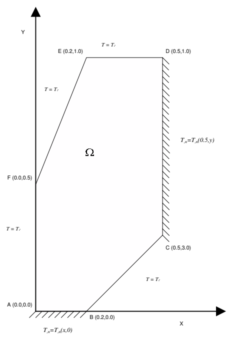

Figure 2: Boundary Conditions

Example 2: The next problem considered will be a general second order operator applied to the same plane boby.

$$y^2u_{xx} + 2x^2u_{yy} + 2xyu_{xy} + xu_x - yu_y + u = e^x\{[10 + 7\mathrm{sen}(2y)][1 + x - 7x^2] + [14\mathrm{cos}(2y)][2xy - y]\} \tag{10}$$

The following solution of the differential operator will be used with its respective boundary values:

$$u = e^x[10 + 7\mathrm{sen}(2y)] \tag{11}$$

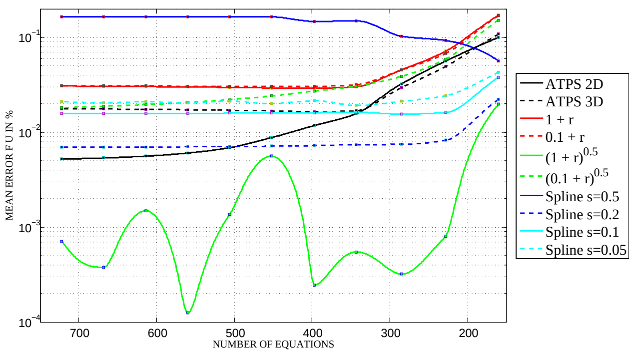

Figure 3: U Mean Error - B.E. Variation - NI = 100

In the Figure 3 is presented the evolution of the mean error (percentage) of the calculated U in the boundary versus the number of equations for 100 interpolation functions. Again, conditioning problems are present for multiquadrics. The convergence speed is lower than in the previous case and a increase of the number of internal nodes above 2-3 times boundary elements means small improves in terms of accurcy.

Example 3: Next the plane body will be a 1x1 square with mixed boundary conditions under:

$$\nabla^2 u - \frac{2}{1+x+y}u_x - \frac{2}{1+x+y}u_y + \left[2w^2 + \frac{4}{(1+x+y)^2}\right]u = 0 \tag{12}$$

The following solution of the differential operator will be used with its respective boundary values:

$$u = [1 + x + y]\mathrm{sen}(wx)\mathrm{sen}(wy) \tag{13}$$

Interpolation Type	NI	U Mean Error	Q Mean Error
Multiquadrics c=1	900	-	-
	1600	-	-
Multiquadrics c=0.1	900	0.186	1.22
	1600	0.192	1.19
ATPS 2D	900	4.08	2.60
	1600	1.30	1.33
ATPS 3D	900	55.4	22.4
	1600	20.6	10.1
Spline s=0.5	900	0.701	0.939
	1600	1.09	1.48
Spline s=0.2	625	0.659	0.767
	900	0.140	0.270
	1600	0.0594	0.184
Spline s=0.1	900	0.910	0.655
	1600	0.230	0.224
Spline s=0.05	900	76.6	27.1
	1600	26.5	13.7

Table 1: Mean Error in Boundary - U, q

In this example case $w = 20$ will be studied. This example is selected in comparision to the previous cases to check a problem with a high number of cycles of variation inside the domain. This type of problems entails a greater number of internal nodes to achieve accurate results. It's interesting to point out that the shape of the field solution is captured by the algorithm and the difference between exact and calculated solution adopts the form of an attenuation. Since a relative small number of equations is necessary to identify the shape of the solution, this information can be used for an adaptative algorithm to obtain improved results.

Conclusions

The main objective of this work was to test the sensitivity of the implementation of the AEM-BEM approach to the choice of radial basis functions (RBFs). We have found that in problems with "soft" variations of the residual term (mainly steady problems) the AEM-BEM is an accurate approach with a relative small number of internal nodes and a proportion of 25-50% (internal nodes - total equations) seems to be the best combination for not wasting numerical efforts.
In terms of stability ATPS and augmented Splines has the best behaviour due to they are designed to produce positive defined matrix in the direct problem. In the opposite side multiquadrics as shown instabilities and lack of convergence. In terms of accuracy ATPS 2D has generally shown the best results. Splines has achieved the highest accuracy in problems with many cycles of variation. However, when using these functions, a new variable is introduced: the size of the support, and there is no rigorous guideline on how to choose it, which affects largely the accuracy and the convergence of the code.

References

[1] Brebbia C.A. y Dominguez J. *Boundary elements, an introductory course*. McGraw-Hill, New York, 1992.

[2] Shaw, R. P. Green's functions for heterogeneous media potential problems. *Engineering Analysis with Boundary Elements*, 13:219–221, 1994.

[3] Chan Y.S., Gray L.J. , Kaplan T. y Paulino G.H. Green's function for a two-dimensional exponentially graded elastic medium. *Proceedings of the Royal Society of London A: Mathematical, Physical and Engineering Sciences*, pages 1689–1706, 2004.

[4] Sladek V., Sladek V., Zhang Ch. y Krivaceck J. Local biem for transient heat conduction analysis in 3-d axisymmetricfunctionally graded solids. *Computational Mechanics*, 2003.

[5] Mikhailov S.E. Localized direct boundarydomain integrodifferential formulations for scalar nonlinear boundary value problems with *Journal of Engineering Mathematics*, 2006.

[6] Partridge P.W., Brebbia C.A. y Wrobel L.C. *The Dual Reciprocity Boundary Element Method*. Computational Mechanics Publications, Southampton, 1992.

[7] L. Marin, L. Elliott, P.J. Heggs, D.B. Ingham, D. Lesnic, and X. Wen. Dual reciprocity boundary element method solution of the cauchy problem for helmholtz-type equations with variable coefficients. *Journal of Sound and Vibration*, 2006.

[8] Ang W.T., Clements D.L. y Vahdati N. A dual-reciprocity boundary element method for a class of elliptic boundary value problems for non-homogeneous anisotropic media. *Engineering Analysis with Boundary Elements*, 2003.

[9] Katsikadelis J.T. The analog equation method - a powerful bem-based solution technique for solving linear and nonlinear engineering problems. *Computational Mechanics Publications - Boundary Element Method XVI*, 1994.

[10] Golberg M. A. , Chenb C. S. y Bowman, H. Some recent results and proposals for the use of radial basis functions in the bem. *Engineering Analysis with Boundary Elements*, 23(4):285–296, 1999.

[11] Buhmann M. *Radial Basis Functions: Theory and Implementations*. Cambridge University Press, Cambridge, 2003.

[12] Katsikadelis J. T. The bem for non homogeneous bodies. *Archive of Applied Mechanics*, 74:780–789, 2005.

[13] Partridge P.W., Brebbia C.A. y Wrobel L.C. *The Dual Reciprocity Boundary Element Method*. Computational Mechanics Publications: Southampton and Elsevier Applied Science, New York, 1992.

[14] Golberg M.A. The numerical evaluation of particular solutions in the bem:a review. *Archive of Applied Mechanics*, 6:99–106, 2005.

[15] Atluri S.N. y Shen S. *The Meshless Local Petrov-Galerkin (MLPG) Method*. Tech Science Press, Stuttgart, 2002.

[16] Gao X.W., Zhang Ch. y Guo L. Boundary-only element solutions of 2d and 3d nonlinear and nonhomogeneous elastic problems. *Engineering Analysis with Boundary Elements*, 31(12):974–982, 2007. Kluwer Academic Publishers.